Molecular Characterization and Investigation of Pathomechanisms of Methylmalonic Aciduria: towards Novel Therapies

---

Dissertation

zur

Erlangung der naturwissenschaftlichen Doktorwürde

(Dr. sc. nat.)

vorgelegt der

Mathematisch-naturwissenschaftlichen Fakultät

der

Universität Zürich

von

Patrick Forny

von

Hohtenn VS

Promotionskommission

Prof. Dr. Olivier Devuyst (Vorsitz)

Prof. Dr. Matthias Baumgartner (Leitung der Dissertation)

Prof. Dr. Wyatt Yue

Prof. Dr. Stefan Kölker

Prof. Dr. Hanns Ulrich Zeilhofer

Zürich, 2016

DECLARATION

I hereby declare that this dissertation is the result of my own work and effort. Wherever contributions of others have been involved or other sources of information have been used, they are acknowledged.

This work was carried out under the supervision of Prof. Matthias Baumgartner at the Division of Metabolism, University Children's Hospital, Zurich, Switzerland from January 2012 to February 2016.

Peer-reviewed publications represented in this work:

1. **Functional characterization and categorization of missense mutations that cause methylmalonyl-CoA mutase (MUT) deficiency**

   Patrick Forny, D Sean Froese, Terttu Suormala, Wyatt W Yue, Matthias R Baumgartner

   Human Mutation 2014 December; 35(12):1449-58.

2. **Molecular genetic characterization of 151 *mut*-type methylmalonic aciduria patients and identification of 41 novel mutations in *MUT***

   Patrick Forny, Anne-Sophie Schnellmann, Celine Buerer, Seraina Lutz, Brian Fowler, D Sean Froese, Matthias R Baumgartner

   Submitted to Human Mutation, February 2016.

3. **Novel mouse models of methylmalonic aciduria recapitulate phenotypic traits with a genetic dosage effect**

   Patrick Forny, Anke Schumann, Merima Mustedanagic, Deborah Mathis, Marie-Angela Wulf, Claus-Dieter Langhans, Assem Zhakupova, Joerg Heeren, Ludger Scheja, Ralph Fingerhut, Heidi L Peters, Thorsten Hornemann, Beat Thony, Stefan Koelker, Patricie Burda, D Sean Froese, Olivier Devuyst, Matthias R Baumgartner

   Submission to Human Molecular Genetics planned in March 2016.

ACKNOWLEDGMENTS

I thank Matthias Baumgartner for supporting me in every way possible during my thesis, for his generosity and inspiration, for his outstanding ability to introduce me to all aspects of the metabolic field, and for his friendship.

I am grateful to Sean Froese, who taught me science from the very beginning with a keen eye on always using the right controls and who encouraged me to think and experiment independently.

I would like to thank all the former and present members of the Kispi lab, including Alexander Lämmle, Angelika Schwarze, Anke Schumann, Anne-Sophie Schnellmann, Beat Thöny, Brian Fowler, Carmen Diez, Cecilia Giunta, Céline Bürer, Claudio Gemperle, David Coelho, Déborah Mathis, Gabriella Allegri, Hiu Man Viecelli, Johannes Häberle, Liyan Hu, Lorena Gallego Villar, Luke Simmons, Marianne Rohrbach, Marie Lucienne, Martin Hersberger, Mattia Schmid, Merima Mustedanagic, Micha Tobler, Michele Frapolli, Mirka Epskamp, Patricie Burda, Ralph Fingerhut and the newborn screening team, Saskia Karg, Seraina Lutz, Tanja Plessl, Tanja Scherer, Terttu Suormala, Tuyet Trinh Lu, Uschi Lindert, Vanja Danilovic, Véronique Rüfenacht, Victoria Fettelschoss. They were always there for fruitful discussions and created a supportive and excited working environment – thanks for the Apéros!

Separate mention goes to our collaborators: to Wyatt Yue at the University of Oxford for his exceptional enthusiasm regarding my project; to Wasim Kiyani for creating a great lab atmosphere including musical intermezzos; to Aurora Martinez, Jarl Underhaug and Ming Ying for an intriguing time at the University of Bergen; to Angela Wulf and Adriano Aguzzi for support with brain histology; to Stefan Kölker, Claus-Dieter Langhans and Sven Sauer for scientific input and metabolite measurements; to Olivier Devuyst, Erica Faccin and Nadine Nägele for helping me with kidney related questions; to Uli Zeilhofer and Dietmar Benke for allowing me to learn primary neuron cell culture in their lab.

I am grateful to the members of my thesis committee (all mentioned above) for their helpful advice and scientific input; to Felix Sennhauser for supporting my initial intentions to pursue a physician-scientist education; to the national and local MD-PhD programs for initiating platforms to get to know other scientists and share crucial experiences, scientifically and personally; and to the Swiss National Science Foundation for generous financial support (grant no. 323530_145248).

Finally, I thank my family for their endless and unconditional love and for their support of my endeavours in science and outside of the lab.

This is dedicated to M.

TABLE OF CONTENTS

LIST OF ABBREVIATIONS AND ACRONYMS

2-MC	2-methylcitrate
AdoCbl	5'-deoxyadenosylcobalamin, adenosylcobalamin
Ala	alanine
Arg	arginine
Asn	asparagine
Asp	aspartic acid
C2	acetylcarnitine
C3	propionylcarnitine
Cbl	cobalamin
CCs	chemical chaperones
CNS	central nervous system
CoA	coenzyme A
Cys	cysteine
DMSO	dimethyl sulfoxide
DSF	differential scanning fluorimetry
ERT	enzyme replacement therapy
Gln	glutamine
Glu	glutamic acid
Gly	glycine
GSD	glycogen storage disorder
HC	homocystinuria
HGMD	human gene mutation database (www.hgmd.org)
HGVS	human genome variation society
His	histidine
HPLC	high performance liquid chromatography
IEM	inborn error of metabolism
Ile	isoleucine
IVA	isovaleric aciduria
Leu	leucine
LSD	lysosomal storage disease
Lys	lysine
MCoA	malonyl-CoA
Met	methionine

MetCbl	methylcobalamin
MIM	mendelian inhertiance in man (www.omim.org)
MMA	methylmalonic acid
MMAuria	methylmalonic aciduria
MS	methionine synthase
MSUD	maple syrup urine disease
MUT	methylmalonyl-CoA mutase
NBS	newborn screening
NCBI	national center for biotechnology information
OHCbl	hydroxocobalamin
PA	propionic aciduria
PCR	polymerase chain reaction
PCs	pharmacological chaperones
Phe	phenylalanine
PI	propionate incorporation
PKU	phenylketonuria
Pro	proline
RT-PCR	reverse transcription polymerase chain reaction
RT-qPCR	quantitative real-time polymerase chain reaction
SDS-PAGE	sodium dodecyl sulfate polyacrylamide gel electrophoresis
Ser	serine
SPR	surface plasmon resonance
SRT	substrate reduction therapy
TCA cycle	tricarboxylic acid cycle, Krebs cycle, citric acid cycle
Thr	threonine
Trp	tryptophan
Tyr	tyrosine
Val	valine
wt	wild-type

ABSTRACT IN ENGLISH

Methylmalonic acidurias represent a group of rare inborn errors of metabolism caused by deficient activity of the mitochondrial enzyme methylmalonyl-CoA mutase (MUT). Deficiency of MUT results either from defects of the MUT apoenzyme itself, which is encoded by the *MUT* gene, or from defects of the intracellular synthesis of its cofactor, 5-deoxyadenosylcobalamin, and leads to the accumulation of methylmalonic acid and other toxic metabolites. Methylmalonic aciduria (MMAuria) typically presents in early infancy with life-threatening metabolic decompensations. Most surviving patients show failure to thrive and develop chronic renal failure linked to tubulointerstitial nephritis. Moreover, approximately half of them suffer from severe neurological impairment such as an extrapyramidal movement disorder. Although the symptoms observed in MMAuria are thought to be the result of the accumulation of toxic intermediary products, knowledge concerning pathomechanisms is scarce, and the evidence base and efficacy of current treatment strategies is not satisfactory. A fundamental limitation for pathophysiological studies is that durable animal models of MMAuria have not been established, *i.e.* full knockout mice display neonatal lethality.

Given the severe phenotypic and pathological outcomes of MMAuria there is an imminent need to explore the pathomechanisms of MMAuria and search for novel therapeutic approaches. In this PhD thesis, this problem is tackled by 1) characterizing a cohort of MMAuria patients regarding their mutations and biochemical properties; 2) investigating functional consequences of *MUT* missense mutations on enzyme activity, cofactor binding, structural protein integrity, and thermal stability; 3) investigating the effect of the cobalamin cofactor of MUT and of screening-derived small molecule chaperones on MUT protein stability and enzymatic activity; and 4) validation and characterization of novel conditional *Mut* knock-out and constitutive *Mut* knock-in mice in order to study the recapitulation of MMAuria in these models.

The analysis of MMAuria patients revealed a very diverse cohort with regard to mutations and mutation types, enzymatic and biochemical properties, and clinical phenotype. Further detailed analysis of 23 missense mutations derived from this cohort, allowed an in-depth categorization of these mutations into various classes of biochemical defects, identifying specific missense mutations which were judged to be of value in pursuing the aims of two follow-up studies:

i. Identification of missense mutations that produce an unstable protein allowed addition of MMAuria to the list of misfolding disorders. We established MUT as a suitable candidate for pharmacological chaperone screening in which identified small molecules that can rescue unstable MUT protein via stabilization.

ii. A missense allele which correlates to low residual enzyme activity and to an intermediate MMAuria clinical phenotype was selected in order to generate a novel knock-in mouse model which was successfully validated as an accurate model recapitulating human MMAuria and which may be further utilized as a tool in future studies on pathomechanisms and treatment of MMAuria.

ABSTRACT IN GERMAN

Methylmalonazidurien bilden eine Gruppe im Bereich der seltenen angeborenen Stoffwechselstörungen und sind durch einen Mangel des mitochondrialen Enzyms Methylmalonyl-CoA Mutase (MUT; codiert durch das *MUT* Gen) verursacht. Die Defizienz dieses Enzyms rührt entweder von einem Defekt im Apoenzym MUT selbst oder von einem Defekt in der intrazellulären Synthese des essenziellen Kofaktors Adenosylcobalamin her. Durch die Fehlfunktion des MUT-Enzyms kommt es zur Akkumulation von Methylmalonsäure und anderen Metaboliten, welche sich toxisch auf den Organismus auswirken. Methylmalonazidurien präsentieren sich typischerweise im Säuglingsalter mit lebensbedrohlichen metabolischen Entgleisungen. Die meisten Patienten, welche diese initiale Krise überleben, leiden unter Gedeihstörungen und entwickeln basierend auf einer tubulo-interstitiellen Nephritis ein chronisches Nierenversagen. Bei der Hälfte der überlebenden Patienten entwickeln sich zudem schwere neurologische Defekte mit extrapyramidalen Bewegungsstörungen. Obwohl vermutet wird, dass die Akkumulation von toxischen Stoffwechselzwischenprodukten zu den schweren Krankheitsfolgen führt, mangelt es an präzisem, evidenzbasiertem Wissen bezüglich der Pathomechanismen und die heutigen Therapieansätze zeitigen nur unbefriedigende Ergebnisse. Eine fundamentale Limitation der Erforschung der Methylmalonazidurie stellen dabei fehlende Tiermodelle dar, welche eine Langzeituntersuchung von phänotypischen Krankheitsaspekten erlauben würden.

Angesichts des schweren Krankheitsbildes der Methylmalonazidurie besteht dringender Bedarf an Forschungsprojekten, welche die Grundlage zur Entwicklung von neuartigen Therapien legen. In dieser Dissertation verfolgen verschiedene Subprojekte dieses Ziel: 1) Charakterisierung einer Kohorte von Methylmalonazidurie-Patienten hinblicklich des Genotyps und biochemischer Eckdaten; 2) Untersuchung der funktionalen Konsequenzen von *MUT* missense Mutationen auf die Enzymaktivität, Kofaktoraffinität, Proteinstabilität und Thermostabilität der Genprodukte; 3) Bestimmung des Effekts des Cobalamin-Kofaktors und anderer Chaperonmoleküle auf die Enzymaktivität und Stabilität von MUT; 4) Validierung und Charakterisierung von neuen konditionalen *Mut* knock-out und konstitutiven *Mut* knock-in Mausmodellen.

Die Analyse der Patienten-Kohorte ergab ein diverses Portfolio von verschiedenen *MUT* Mutationen mit unterschiedlichen Auswirkungen auf die biochemischen Eigenschaften des Enzyms. Die detaillierte Untersuchung von 23 missense Mutationen erlaubte deren Verwendung in weiterführenden Studien:

i. Aufgrund der Beschreibung von instabilen missense Mutanten, konnte die Methylmalonazidurie als Fehlfaltungs-Krankheit kategorisiert werden. Dies erlaubte ein spezifisches Screening nach Chaperonmolekülen und deren Validierung als Stabilisatoren von MUT.

ii. Die Identifikation einer mittelschweren missense Mutation erlaubte die Entwicklung eines überlebungsfähigen Mausmodells, welches zahlreiche Aspekte der menschlichen Methylmalonazidurie rekapituliert und sich als wertvollen Forschungsgegenstand zukünftiger Studien im Bereich der Pathomechanismen und Therapieformen der Methylmalonazidurie anbietet.

1 INTRODUCTION

1.1 MUTATION IS THE ORIGIN OF GENETIC DISEASE

Variation in the genomic sequence occurs within and among populations. In *Homo sapiens sapiens* the similarity among all individuals regarding their DNA sequence has always thought to be around 99.9%. Recently, this number has been corrected and lowered to 99.5% (Redon, et al., 2006). A number which is actually surprisingly low, when considering the similarity between the DNA sequences from chimps (*Pan troglodytes*) and humans, which accounts for about 98% depending on the comparison method (Britten, 2002; Chimpanzee-Sequencing-Consortium, 2005; Wildman, et al., 2003). The overall similarity to mice was found to be around 90% (Church, et al., 2009; Gunter and Dhand, 2002). When it comes to the coding part of the DNA, the genes, it is even more surprising how similar organisms from different species are at the genetic level. As a matter of fact, it is estimated that all life forms on our planet share about 50% of their genes – a phenomenon explained by universal common ancestry (Theobald, 2010). On the one hand it is striking that life on earth is based on such similar genetic material, on the other hand individuals from the same species are, genetically spoken, surprisingly different from each other.

Traits of individuals are influenced by environmental factors and their genetic background. This is why genetic variation plays an important role in life. During evolution stochastic changes in the DNA of organisms were crucial for the development of all life forms. The new variants were subjected to selection processes, which lead to the evolution of the genetic material and subsequently to the genesis of new traits and finally novel species. The reasons why variation in DNA occurs are not discussed here. But this process of random genetic changes is not limited to ancient times – it is still ongoing and the human genome is still evolving. Genetic changes are partly responsible for phenotypic variation but go unnoticed in many cases. However, in some cases a variant can cause a malfunction of a gene which is relevant to the health of the organism. In other words, certain variants can occasionally cause disease in humans. In this case, the variants are referred to as mutations.

Mutations and their nomenclature are complex. There are not only simple base pair exchanges, but rather several different ways how DNA can be changed, modified, and rearranged. They are extensively discussed in this thesis. Often traits are only partially influenced by a single DNA change and a combination of many changes in different genes are required to make an individual more vulnerable to be affected by a specific disease, *e.g.* diabetes type II. Several genetic factors have been identified in diabetes type II (such as TCF7L2 (Gloyn, et al., 2009) or ABCC8 (Thomas, et al., 1995)), which makes it a polygenetic disorder. Often polygenetic diseases are also influenced by environmental factors

such as toxins or lifestyle. By contrast, a class of completely different disorders, which are solely determined by one single gene, exists.

Mutations in genes, which are of vital important to the integrity of a specific pathway in the organism, can directly cause disease. In this case, mutations in other genes or the presence of certain environmental factors play a subordinate role and are usually not necessary at all. Such diseases are known as single-gene disorders and are accordingly inherited in a Mendelian manner. If these genes are part of a metabolic pathway this group of disorders is referred to as the inborn errors of metabolism (IEMs).

1.2 Inborn Errors of Metabolism

IEMs constitute a group of diseases which are characterized by the deficiency of function of a single gene and the consequences of this malfunction on the metabolism of a patient. These consequences can be very various depending on the affected gene and the clinical phenotype can vary with different organs or organ systems being affected. The difference of the affected genes themselves and additionally their distinct expression in different cell types and tissues provide an explanation for the heterogeneity of IEMs. This chapter tries to summarize general aspects of IEMs related to clinical phenotype, diagnosis and treatment without asserting to claim complete coverage of this topic.

1.2.1 Background

Single IEMs are often rare and only found in very few patients. This might be due to the high number of genes (estimate of the total number of genes in *Homo sapiens*: 21,000 (Pennisi, 2012)) which can be affected; with each defective gene resulting in a specific disease. In countries without high rates of consanguinity, another important factor contributing to the rarity of IEMs is the autosomal recessive inheritance pattern. Also the low likelihood that a random mutation actually has a deleterious effect on the function of the gene product contributes to the low prevalence of single IEMs. The rarity of these disorders hinders the formation of large stakeholder groups and public awareness of IEMs is sparse. As a consequence, public funds are only seldom allocated to the research of rare diseases. In addition, the scientific community is faced with many new disorders, which are currently discovered at a high frequency, making those novel disorders so far mostly unexplored. Also metabolic clinicians become aware of new metabolic diseases since patients survive with acute and supportive care which improved significantly over the last few decades. Together, the novelty of many IEMs and the financial limitation of research efforts leads to numerous open questions in the understanding of these disorders.

Unsolved problems related to IEMs remain a challenge, especially in the view of the prevalence of all IEMs together. It is estimated that overall IEM incidence accounts to about 1:2,000 (Applegarth, et al., 2000; Hutchesson, et al., 1998) which is comparable to diabetes type II incidence in adolescents (D'Adamo and Caprio, 2011). This indicates that the sum of IEMs is very relevant to the public health system, impacting on quality of life of many patients and also causing considerable healthcare costs.

1.2.2 Pathophysiological mechanisms

At the beginning of the early 20th century Archibald Garrod fomulated the term inborn error of metabolism during his work on the inherited disease alkaptonuria (Garrod, 1902). Based on Garrod's studies George Beadle and Edward Tatum developed the "one gene-one enzyme" concept, in which each gene produces one enzyme which is in turn responsible for a specific step in a metabolic pathway (Beadle and Tatum, 1941). From a present-day perspective this seems to be an oversimplification to describe the relation of genes and proteins, but it was the first scientific endeavour into a field which is today known as molecular biology (Horowitz, et al., 2004).

This simplified concept can be used to summarize the pathophysiology in different IEMs. According to Saudubray et al. (Saudubray, et al., 2012) there are three pathophysiological groups which are useful from a diagnostic perspective:

i. Disorders that give rise to **intoxication**. This group of disorders is characterized by a metabolic reaction which is massively reduced in its throughput which consequently leads to the accumulation of intermediary metabolites of the affected pathway. The accumulating metabolites cause intoxication-like clinical characteristics, such as vomiting and lethargy at onset. Usually these metabolites have been identified but their molecular mode of action of how they harmfully interfere with the normal metabolism of the cell is often not known. Typically, disorders of this group (organic acidurias, urea cycle defects, amino acid disorders etc.) are characterized by unproblematic intrauterine development and a symptom-free interval after birth.

ii. Disorders involving **energy metabolism**. Deficiencies in energy production or utilization can be caused by cytoplasmic and mitochondrial defects, with the latter being more severe. Processes involving glycolysis, gluconeogenesis, glycogen metabolism, mitochondrial respiratory chain, mitochondrial transporters, fatty acid oxidation and several others can be affected in this group of disorders. Diagnosis is very difficult and requires specialized biochemical as well as genetic investigations.

iii. Disorders involving **complex molecules**. In this group the synthesis or catabolism of complex molecules of different kinds are impaired. Examples are lysosomal storage disorders,

peroxisomal disorders, congenital disorders of glycosylation, disorders of cholesterol synthesis and several others. Many of these diseases are usually detectable on the genetic level and are mostly not amenable to treatment in the acute phase.

1.2.3 Clinical picture

IEMs show a great variation of clinical symptoms with regard to timing and characteristics. Therefore, this section only summarizes some general clinical aspects of IEMs and groups them in three forms of early-onset, late-onset with acute crisis, and chronic/progressive (Saudubray, et al., 2012).

Striking early symptoms can entail antenatal and neonatal malformations, dysplasias and functional manifestations such as growth retardation. But it needs to be born in mind, that most often these specific symptoms are not present and the detection of a metabolic disorder in a neonate is challenging. This is due to the general and unspecific nature of the symptoms such as respiratory distress, hypotonia, poor suckling reflex, vomiting, diarrhoea, dehydration, lethargy and seizures. Often neurological symptoms and poor feeding are the very first signs. High ammonia levels (hyperammonemia) can give rise to hypotonia and encephalopathy with subsequent seizures. Cardiac and liver focused diseases can present with hepatomegaly and hypertrophic cardiomyopathy with cardiac failure. Previous siblings having died during the neonatal period may give rise to the suspicion of an IEM.

Later onset forms of IEMs often manifest with an acute crisis often precipitated by an intercurrent infection which can reoccur during later exacerbations of the disease. An acute crisis can present with striking symptoms depending on the underlying disorder. Vomiting, acidosis, and neurological symptoms (*e.g.* lethargy, coma, metabolic stroke, attacks of ataxia) are seen in crises of organic acidurias. Even acute psychiatric symptoms can be observed, *e.g.* in mild forms of ornithine transcarbamylase deficiency.

Chronic and progressive forms of IEM often present with symptoms which worsen over time and are very difficult to treat. These disorders often show neurological features which lead to very severe clinical pictures, making the patient completely dependent on community or home care. Symptoms may include developmental delay, mental retardation, neurological deterioration and psychiatric signs. Often the situation is complicated by episodes of epileptic seizures.

1.2.4 Diagnostic methods

The suspicion of an IEM should lead to initial laboratory investigations to determine the diagnosis as soon as possible since specific treatment based on the diagnosis may be required in the acute phase. Laboratory support of the diagnosis is often essential because many IEMs show only general clinical

symptoms. Since IEMs cause disturbed metabolism, many traces of the impaired metabolic processes, such as increased or decreased metabolite levels, can be detected in body fluids of patients. A specific metabolic pattern often points to a concrete disease or at least a disease group, which can be further evaluated by biochemical methods, often including enzymatic assays. Genetic tests are mostly used as a final confirmation of the defective gene although in some cases, genetic analysis is even applied in parallel to first-line diagnostics. Additionally, more general measurements, such as ketone bodies, blood gases, blood pH, anion gap, ammonia, lactate etc., are also needed in order to help decisions regarding acute patient management.

Newborn screening (NBS) allows early detection of diseases. In most parts of the world, where NBS is in place, the vast majority of the diseases included in NBS belong to the group of IEMs. This diagnostic tool is very helpful to detect disorders before they manifest with an acute clinical crisis. Even though the Wilson's criteria provide useful guidelines (Wilson and Jungner, 1968), it is hotly debated which diseases should be included in these screenings and the number of diseases included in newborn screening programs varies greatly between countries. Recently, the possibility of complementing this metabolic screening by genetic methods such as whole genome or exome sequencing has been discussed (Ross, et al., 2013). This brings into play more ethical considerations regarding the collection of information which is not completely understood, in many cases not clinically relevant, and for which no informed consent of the neonate exists (Mayer, et al., 2011). Many of the available diagnostic tools can also be applied to the unborn child during prenatal diagnosis, implying similar ethical issues.

1.2.5 Classical treatment

Different inborn errors of metabolism are treated in very specific ways and the vast number of different diseases complicates a uniform summary of treatment approaches. Therefore, this section is limited to a few basic principles which apply to the treatment of IEMs.

1.2.5.1 Supportive/symptomatic treatment

In the acute phase, nearly all IEMs require supportive care even if there is an established disease-specific treatment procedure available. Supportive treatment includes ventilator or cardiac support as well as correction of hydration and electrolyte status (Saudubray, et al., 2012).

1.2.5.2 Dietary treatment

Since many metabolites derive from food intake, the modulation of the latter can influence the throughput of certain metabolic pathways. For example in the case of intoxication-type disorders, where toxic metabolites accumulate, it is desirable to minimize the substrate of this pathway in order

to maintain levels of toxic metabolites as low as possible. This is possible via a reduction of the intake of specific diet components, *e.g.* a reduction of protein in the diet of patients suffering from an amino acid disorder. Also an increase of some nutrients (often the products of the deficient enzymes) may be necessary, *e.g.* as in the case of glycogen-storage disorder where hypoglycaemia is prevented by frequent intake of carbohydrates.

More importantly, dietary management should prevent catabolism by aggressive promotion of anabolism. This is especially crucial in the acute phase, when an increased breakdown (catabolism) of protein leads to metabolic decompensation as observed in organic acidurias. High glucose infusions combined with insulin under continuous monitoring of blood glucose and lactate levels are used to promote sufficient anabolism (Baumgartner, et al., 2014). As soon as the clinical condition of the patient allows it, enteral feeding should be reinitiated to provide energy to meet metabolic demands and maintain an anabolic state.

1.2.5.3 Detoxification of metabolites

In the acute phase of certain IEMs accumulating metabolites reach levels which are exceeding normal ranges by far. These high concentrations of metabolites can be lowered by applying scavenger molecules. These carrier molecules are capable of binding accumulating metabolites and makinkg them innocuous. Subsequently the carrier is excreted together with the toxic metabolite. One example is carnitine which can bind accumulating propionyl-coenzyme A (propionyl-CoA) in methylmalonic aciduria. In this case, carnitine is not only given to scavenge propionyl-CoA but also to replenish the carnitine levels. Other examples are benzoate and phenylbutyrate in urea cycle disorders to scavenge amino acids in order to lower ammonia levels. Benzoate is conjugated with glycine to generate hippurate; phenylbutyrate is converted to phenylacetate which then conjugates with glutamine to generate phenylacetylglutamine (Haberle, et al., 2012). Both conjugate products are excreted in the urine.

In the acute phase, toxic metabolites can be lowered not only by scavengers but also by applying methods of hemofiltration. Veno-venous hemodiafiltration is recommended for children and infants, while haemodialysis should be employed in adults for extracorporeal detoxification (Baumgartner, et al., 2014).

1.2.5.4 Enzyme replacement therapy

IEMs are usually caused by a gene defect which leads to the production of a dysfunctional protein or even no protein at all. The missing or dysfunctional protein can be replaced via different methods in the application of enzyme replacement therapy (ERT). This approach has shown recent success for lysosomal storage diseases (LSDs) (Ohashi, 2012; Parenti, et al., 2013) such as Gaucher disease, Fabry

disease, Pompe disease, and for some types of mucopolysaccharidosis. In ERT recombinantly produced enzymes are supplemented mostly via the intravenous route. The main issue of this conceptwise simple method is the limited possibility of treating neurological symptoms since the blood-brain barrier prevents the recombinant enzyme crossing into and subsequently fulfilling its function in the brain. This drawback of ERT has recently been circumvented by intrathecal application of the recombinant protein, but only with partial success (Dickson, et al., 2007). In general, ERT is more successful in slowing down the progression of symptoms when started early in the disease course and in patients with mild disease limited to organs that are well accessible to the intravenously applied enzyme. The results in more severely affected patients or patients, which have a disease which is far progressed, are often discouraging, suggesting that commencement of ERT intervention should be at as young an age as possible (Harmatz, 2015). However, the efficacy of ERT is debated since long-term outcome studies are still lacking and measures to monitor outcome (surrogate markers) are controversial.

Although recombinant protein production is a routine procedure nowadays, it remains a sophisticated task to purify protein of high quality. The process requires numerous purification steps in order to achieve a high yield and concentration of the protein of interest and also to avoid contamination with other substances. For clinical application of recombinant proteins, the product has to meet a catalogue of requirements, making this process complex and intricate. Therefore, great investments in research and development of these drugs are required. The exceptionally big proportion of development costs over the number of potential patients, which is very low for all IEMs, may explain the expensive prices of these drugs. Hence, despite some clinical improvements, which have been observed in LSD patients under ERT, this innovative approach still suffers from pitfalls regarding costs and efficacy.

1.2.5.5 Organ and hematopoietic cell transplantation

The approach of ERT is based on the idea to substitute the dysfunctional mutant protein, encoded by a defective gene, with functional wild-type protein. Since ERT has its inherent problems, other solutions are needed. It is possible to not only substitute the enzyme itself but also to replace a complete organ in order to supply the patient with cells of sufficient protein (often enzyme) function to cope with the demand of the defective metabolic pathway. Often the liver or the hematopoietic system is transplanted in order to achieve higher levels of enzyme activity. However, this treatment strategy also has its drawbacks: If the defective enzyme is also expressed in the brain, metabolites which accumulate within the brain and cannot cross the blood-brain barrier will not be processed by the enzyme in the transplanted organ and remain trapped in the brain. Also immunosuppressive

therapy, which is required after transplantation, has its intrinsic problems and may negatively influence the quality of life of patients.

1.2.5.6 Substrate reduction

Substrate reduction therapy (SRT) is currently used in glycogen-storage disorders and LSDs. In this approach small molecules inhibit crucial steps in the production of toxic metabolites which would otherwise accumulate. Consequently, the concentration of these toxic metabolites can be lowered in the patient's body fluids and tissues. SRT small molecules can cross the blood-brain barrier but they are considered to be less effective than ERT and can show significant neurological side effects, *e.g.* as observed in miglustat treatment (Machaczka, et al., 2012).

1.2.5.7 Protein enhancement with chaperones

Mutations, especially of the missense type, can cause a structurally unstable protein. After aggregation, the protein is consequently degraded by the proteasomal degradation system. In addition to the naturally occurring chaperone proteins, such as Hsp60, Hsp70 and Hsp90, there is a growing number of drugs which mimic this chaperone function in order to improve the stability and function of mutant proteins in various ways. These molecules are known as pharmacological chaperones (PCs) in the case of small molecules, or chemical chaperones which are usually osmolytes. These compounds have the purpose of interfering with the degradation process of the mutant proteins in the following ways:

i. Chaperones can support the folding process of a mutant proteins.

ii. Chaperones can stabilize mutant protein and protect it from being degraded.

iii. Chaperones can support the disposal of already degraded and aggregated mutant proteins.

Studies on the famous mutant protein ΔPhe508 cystic fibrosis transmembrane conductance regulator show that the application of osmolytes can be successful and can support the stabilization of the protein and promote the trafficking of the transmembrane channel to the cell membrane (Welch and Brown, 1996). Even before that, glycerol was known to stabilize protein confirmations *in vitro* (Gekko and Timasheff, 1981). Although successful, these chemical chaperone molecules are not ideal candidates for clinical application. This is due to the high concentration at which they need to be applied and their unspecific mode of action of stabilization of proteins. As a consequence, harmful effects on other protein (off-target) are possible and raise the concern of side effects.

Therefore, more specific molecules are needed. These compounds are known as pharmacological chaperones (PCs) and are small, target-specific small molecules which exert a stabilizing effect on the protein of interest. This allows the application of lower dosages and minimization of off-target

effects. In the search for PCs, *in vitro* screening approaches are applied (Pey, et al., 2008). In the clinical context, these molecules have been most successfully tested in LSDs (Boyd, et al., 2013; Fan, 2008; Parenti, et al., 2014).

More information on chaperone therapy in MMAuria, is considered in chapter 5 of this thesis.

1.3 Branched-chain Organic Acidurias

The branched-chain amino acids are leucine, isoleucine, and valine, all characterized by the eponymic branched side chain. Other amino acids, which also have a branched side chain, exist but are not proteogenic. In the breakdown of these amino acids, specific enzymes can be defective, leading to different types of IEMs. Still, these diseases are quite similar to each other, not only regarding their biochemical background but also their clinical signs. They can present with early-onset, late-onset with recurrent crises or in a chronic/progressive form. Because of their common features and due to the accumulation of characteristic organic acids in the urine they are categorized within the group of organic acidurias. Diagnosis can be accomplished by the analysis of acylcarnitine and organic acid profiles. The most commonly encountered organic acidurias are maple syrup urine disease (MSUD), isovaleric aciduria (IVA), propionic aciduria (PA), and methylmalonic aciduria (MMAuria).

1.3.1 Maple syrup urine disease, isovaleric aciduria, propionic aciduria

MSUD is known for the characteristic maple syrup odour of the urine of the patients and shows a prevalence of 1:225,000 (Carleton, et al., 2010). The amino acids valine, isoleucine, leucine and alloisoleucine are elevated in plasma caused by a deficiency of the branched-chain alpha-keto acid dehydrogenase complex. In comparison to other organic acidurias, no activated CoA compounds are generated, hence the acylcarnitine profile is usually not changed. There is usually a less severe acidosis and degree of hyperammonemia, key traits of many organic acidurias, possibly attributable to the absence of accumulating CoA molecules. The molecular background of MSUD is quite complex and involves a number of proteins encoded by four genes which are all inherited in a recessive manner. Involved proteins comprising the branched-chain alpha-keto acid dehydrogenase complex are the subunits $E_1\alpha$, $E_1\beta$, E_2, and E_3, which are encoded by the genes *BCKDHA*, *BCKDHB*, *DBT*, and *DLD*. In addition, the deficiency of E_3 leads to a malfunction of pyruvate dehydrogenase complex which converts pyruvate to acetyl-CoA. The clinical aspects of the disease include progressive encephalopathy in the acute phase of severe forms starting a few days after birth or a developmental delay with various neurological symptoms in milder forms. The acute treatment involves glucose and insulin administration in order to promote protein anabolism. The long-term treatment focuses on diet modification with a reduced intake of protein to control the plasma values of leucine, isoleucine and valine.

IVA is the rarest organic aciduria discussed in this section with an incidence of about 1:250,000 in the United States. Deficiency of isovaleryl-CoA dehydrogenase is the cause of IVA and leads to the accumulation of isovaleryl-CoA derivatives, including free isovaleric acid. The enzyme is expressed in the mitochondrion and it transfers electrons to the respiratory chain via the electron transfer flavoprotein. While accumulating isovaleryl-CoA conjugates with carnitine to build isovalerylcarnitine, alternative pathways are activated which leads to the accumulation of 3-hydroxyisovaleric acid and *N*-isovalerylgylcine. Since the reaction catalysed by isovaleryl-CoA dehydrogenase represents an early step in leucine metabolism, no other amino acid pathways are affected in IVA. The underlying gene is *IVD*, mutations of which are inherited in an autosomal recessive manner. The clinical course can be acute with onset in the neonatal period (Newman, et al., 1967) or chronic intermittent with recurrent crises (Tanaka, et al., 1966). Treatment is based on carnitine supplementation and glycine medication, since glycine can conjugate with isovaleric acid with subsequent excretion of the conjugate. In addition, the diet is modified in order to lower the leucine intake.

PA is caused by a deficiency of propionyl-CoA carboxylase which contains two different subunits encoded by *PCCA* and *PCCB* and requires the cofactor biotin for proper function. It catalyses the carboxylation reaction which produces methylmalonyl-CoA from propionyl-CoA. PA is caused in ~40% of the cases by mutations in the *PCCA* gene and in ~60% by mutations in the *PCCB* gene (Perez, et al., 2003; Yang, et al., 2004). The prevalence of PA varies depending on the cohort tested. It is estimated to be found in 1 of 100,000 live births worldwide; but a higher prevalence is observed, *e.g.* in Saudi Arabia or Greenland (Ravn, et al., 2000). PA is inherited in an autosomal-recessive manner. Propionyl-CoA carboxylase is involved in the catabolism of amino acids (methionine, isoleucine, valine, threonine), odd-chain fatty acids, cholesterol and propionate produced by bacteria in the gut. Its deficient activity leads to the accumulation of propionic acid in urine and blood. Also other metabolites accumulate such as propionylcarnitine (acylation of propionyl-CoA to carnitine), methylcitrate (condensation of propionyl-CoA with oxaloacetate) (Saudubray, et al., 2012) and hydroxypropionate (by β- or ω-oxidation of propionyl-CoA) (Ando, et al., 1972). Clinical characteristics are recurrent metabolic crises and long-term complications including growth retardation, intellectual disability, seizures, pancreatitis and cardiomyopathy. Treatment options are very similar to MMAuria (see next section).

1.3.2 Methylmalonic aciduria

Isolated MMAurias are a group of rare inborn errors of metabolism caused by a deficiency of the isomerase methylmalonyl-CoA mutase (MUT), which catalyses L-methylmalonyl-CoA to succinyl-CoA providing anaplerotic substrate to the tricarboxylic acid cycle (TCA cycle). MUT deficiency can

be caused by a defect in the apoenzyme itself or in the production of its essential cofactor 5'-deoxyadenosylcobalamin (AdoCbl). The disease was first characterized in 1967 as an autosomal recessive IEM (Oberholzer, et al., 1967) and named after the name-giving metabolite methylmalonic acid (MMA) which is found elevated in urine of MMAuria patients. The estimated frequency in the population is estimated at 1:50,000 (Chace, et al., 2001; Shigematsu, et al., 2002; Sniderman, et al., 1999).

Isolated MMAurias have to be differentiated from combined forms of MMAurias with homocystinuria (HC). These disease entities are intertwined because they share a common pathway – the intracellular cobalamin (Cbl) pathway. In humans Cbl must be converted into two coenzyme forms, methylcobalamin (MetCbl) and AdoCbl, in order to assure the function of the two target enzymes of Cbl (MUT and methionine synthase (MS)), which are responsible for the homeostasis of MMA and homocysteine (Jusufi, et al., 2014).

MS is located in the cytosol where it utilizes Cbl in the form of MetCbl to convert homocysteine to methionine. Deficiencies of MS itself (encoded by the *MTR* gene, *cblG* complementation group), methionine synthase reductase (encoded by the *MTRR* gene, *cblE* complementation group), and methylmalonic aciduria and homocystinuria type D protein (MMADHC, encoded by the *MMADHC* gene, *cblD*-HC complementation group) all lead to isolated forms of HC, with the latter two proteins being involved in the production of MetCbl.

Since Cbl synthesis and trafficking of MetCbl and AdoCbl have a common pathway after the Cbl molecule is taken up into the cell via endocytosis, the productions of both cofactors can be defective at the same time (Coelho, et al., 2008). Proteins involved at this step are the lysosomal protein LMBRD1 (encoded by the *LMBRD1* gene, *cblF* complementation group) (Rutsch, et al., 2009) and the transmembrane protein with ATPase function ABCD4 (encoded by the *ABCD4* gene, *cblJ* complementation group) (Coelho, et al., 2012), which probably interact (Deme, et al., 2014) in order to extract Cbl from the lysosome and feed it into further processing steps in the cytosol. In the cytosol the proteins MMACHC (encoded by the *MMACHC* gene, *cblC* complementation group) (Lerner-Ellis, et al., 2006) and MMADHC (*cblD*-MMA/HC complementation group) are further involved. Deficiencies of these proteins lead to a combined form of MMAuria and HC. A special case is the MMADHC protein which can cause isolated MMAuria, isolated HC or combined forms of both, depending on the location and type of the defect in the protein (Stucki, et al., 2012).

The products of the genes *MMADHC*, *MMAA*, *MMAB*, *MCEE*, and *MUT* are involved in production and utilization of AdoCbl and are further introduced in the next section. Mutations in these genes can lead to isolated MMAuria.

1.3.2.1 Molecular basis

Isolated MMAurias are caused by a defective MUT enzyme or by defects in the pathway exclusive to mitochondrial delivery and modification of AdoCbl. Proteins involved in this pathway are MMADHC (*cblD*-MMA complementation group), MMAA (encoded by the *MMAA* gene, *cblA* complementation group) (Dobson, et al., 2002b) and the cob(I)alamin adenosyltransferase MMAB (encoded by the *MMAB* gene, *cblB* complementation group) (Dobson, et al., 2002a). Deficiencies of these proteins lead to an insufficient supply of the MUT enzyme with its cofactor AdoCbl. The *MMAA* gene encodes a protein which belongs to the G3E family of GTP-binding proteins. The most common mutated allele detected is the c.433C>D (p.R145X) point mutation (Saudubray, et al., 2012). In the *MMAB* gene most mutations were detected at the active site of the adenosyltransferase MMAB that it encodes. The gene *MCEE* encodes methylmalonyl-CoA epimerase which converts (R)-methylmalonyl-CoA to (S)-methylmalonyl-CoA. Mutations in this gene have been found to be associated with mild MMAuria, but the clinical relevance is not certain (Bikker, et al., 2006; Dobson, et al., 2006).

Most commonly isolated MMAuria is caused by a defect in the apoenzyme MUT itself due to mutations in the *MUT* gene (*mut* complementation group) (Ledley, et al., 1988a; Ledley, et al., 1988b). Depending on the degree of incorporation of radioactively labelled propionate into fibroblast cell proteins of a patient or control cell line (PI assay), *mut*-type MMAuria can be further subdivided in the two classes mut^- and mut^0. The assay is performed in cell culture, with medium supplemented with hydroxocobalamin (OHCbl) or not. A ratio of >1.5 (absolute propionate incorporation under OHCbl-supplemented conditions over propionate incorporation without supplementation) assigns a patient cell line to the mut^- subclass, whereas a ratio of ≤1.5 allocates the cell line and the corresponding patient into the mut^0 subclass.

1.3.2.2 Clinical presentation

As with most intoxication-type IEMs, MMAuria patients show normal embryo-foetal development with no manifestations of disease during pregnancy. After a non-complicated delivery, no dysmorphic features are present that might trigger the suspicion of an inherited metabolic disorder. MMAuria patients show a typical symptom-free interval after birth. Depending on the severity of the defect, patients can start to develop a sepsis-like clinical picture on day 2-4 of life which manifests with poor feeding, lethargy and neurological symptoms as first symptoms. Neonates with MMAuria present with hypotonia which is correlated with hyperammonemia. Seizures and further deterioration of the general condition occur, if no treatment is initiated at this point. Other MMAuria patients with a less severe defect, may present later in life. Often the disease becomes clinically manifest when the throughput of the propionate pathway is unusually high, *e.g.* due to febrile illness which usually induces a catabolic state with increased protein breakdown. The symptoms during these

metabolic crises are the same as found in early-onset patients described above. These patients often suffer from life-threatening recurrent crises.

Long-term survivors with isolated MMAuria invariably show chronic kidney damage (tubulo-interstitial nephritis) which subsequently leads to end stage renal failure. Early sings of the development of kidney damage can be renal tubular acidosis and hyperuricemia. Over time the glomerular filtration rate will be reduced and dialysis and kidney transplantation is often required before the age of 20 years (Leonard, 1995; Leonard, et al., 2001).

The second important long-term complication observed in MMAuria patients affects the central nervous system (CNS) and is very comparable to the symptoms observed in PA patients. Damage in this organ may manifest as progressive extrapyramidal syndrome due to lesions in the basal ganglia, especially in the area of the globus pallidus (Baker, et al., 2014). These specific lesions may derive from chronic basal ganglia injury or acute crises during which patients may experience the phenomenon of a "metabolic stroke" – an acute injury of brain tissue not due to a haemorrhage or a vascular occlusion. The pathomechanisms describing how an acute metabolic crisis leads to stroke-like lesions in the basal ganglia of MMAuria patients are debated (Kolker, et al., 2008; Kolker, et al., 2006). Most patients affected by a metabolic stroke suffer from a disabling movement disorder with paresis and choreoathetosis. In addition to these findings, optic atrophy with visual impairment evolves as another long-term complication (Traber, et al., 2011; Williams, et al., 2009). Finally, brain MRI of MMAuria patients can reveal cerebral atrophy and delayed myelination (Brismar and Ozand, 1994; Chemelli, et al., 2000), while patients show variable mild intellectual impairment.

Prediction of the clinical outcome is very difficult. Based on the assignment of the complementation group, the patients show different severity of disease, *e.g.* patients of the *cblB* and *mut*^{0} complementation group tend to show an earlier onset of disease and a higher frequency of complications and deaths compared to patients belonging to the groups *cblA* and *mut*$^-$ (Horster, et al., 2007). *In vitro* parameters such as residual enzyme activity and the response to cobalamin (PI assay) may help to stratify the patients into more severe and milder prognosis groups (Horster, et al., 2009). Chapter 1 of this thesis elucidates information on genotype-phenotype correlations in *mut*-type MMAuria patients with regard to their clinical outcome.

1.3.2.3 Diagnosis of methylmalonic aciduria

Analysis of organic acids in plasma and/or urine by gas-liquid chromatography and mass spectrometry and measurement of acylcarnitines in tandem mass spectrometry may elevated levels of propionylcarnitine, MMA, 2-methylcitrate and hydroxypropionate. These parameters allow a diagnosis of unclassified form of MMAuria. Further laboratory investigations, such as PI (Willard, et al., 1976) and

MUT enzyme assay (Forny, et al., 2014) together with cobalamin distribution assays, are needed to delineate the exact defect in the pathway. Complementation analysis allow the assignment to a complementation group (Gravel, et al., 1975). Finally, mutational analysis is performed to confirm the defect in the specific gene and to verify the carrier status of the parents of the patient.

1.3.2.4 Treatment in methylmalonic aciduria

Treatment in MMAuria aims at detoxification of accumulated metabolites in the acute phase and metabolic control in the long-term therapy. The acute exacerbation in MMAuria is usually caused by an increased load of the propionate pathway due to a catabolic state (*e.g.* fasting or febrile illness) or increased protein intake. Critical patients in an acute metabolic crisis need stabilization by restoration of volume and promotion of anabolism. Protein intake needs to be reduced or stopped immediately in order to avoid further build-up of toxic metabolites. The application of glucose infusions combined with insulin helps to stop further protein catabolism and restore anabolism. During this phase careful monitoring of electrolytes, ammonia, pH and blood gases is required. In very severe cases hemofiltration has to be performed in order to accelerate the detoxification process.

Long-term treatment includes diet modification which aims at limiting amino acids that lead to production of propionic acid by giving a low protein diet that may be supplemented by a precursor-free amino acid mixture. Vitamin B_{12} responsive patients should be given intramuscular OHCbl injections. It is known that most patients of the *cblA* complementation group respond to this treatment, while only some *cblB* patients display responsiveness (Matsui, et al., 1983a). Also *mut*$^-$ show a higher response rate than *mut*^{0} patients (Horster, et al., 2007). Responsiveness should be evaluated according to proposed protocols (Fowler, et al., 2008). Additional therapy consists of carnitine supplementation and metronidazole (or other antibiotics) which reduce the production of gut bacteria-derived propionate. To avoid intermittent crises, infections should be prevented or treated aggressively immediately after occurrence.

Liver has the highest amount of propionate conversion, therefore replacement of this organ could contribute enzyme activity to the organism's demand. A liver with normal expression of wild-type MUT has a high capacity to turn over most of the propionyl-CoA which is produced by the entire body. This concept proved to be partially valid, since transplanted patients are protected against metabolic crises, but still display elevated metabolites. Although acute events are prevented, long-term complications cannot be avoided as shown in several cases of MMAuria patients who were transplanted and still suffered from metabolic stroke events (Chakrapani, et al., 2002; Nyhan, et al., 2002; Vernon, et al., 2014). Possibly very early transplantation may be beneficial to patients as shown in recent studies which show improved techniques and outcome of liver transplantation in MMAuria

patients (Spada, et al., 2015), but timing remains very difficult to evaluate (Sloan, et al., 2015). Alternatively, kidney transplantation can be combined with liver transplantation or performed as a single-organ transplantation with the same intention of increasing the enzymatic activity of this tissues, and also to replace a potentially damaged kidney (Brassier, et al., 2013; Clothier, et al., 2011; Lubrano, et al., 2007; Lubrano, et al., 2001; Van Calcar, et al., 1998).

1.3.2.5 Current mouse models of MMAuria

Mouse models allow posing of scientific questions regarding the whole organism or organ systems, which would otherwise not be feasible to be solved. In MMAuria research the absence of such models contributed to the persistence of a lack of knowledge on pathomechanisms and therefore the development of novel therapies was hindered. This hurdle still needs to be overcome since the available treatment options for MMAuria patients are not satisfying. Even classical treatment procedures cannot be tested in animal models, although this would be especially useful in MMAuria, since the small number of patients suffering from this disease only allows very small group sizes in clinical studies. Since the 2000's there have been efforts to fill the gap of a lacking animal model by attempting to generate a mouse model of MMAuria.

The first MMAuria mouse model was developed in 2003. A Mut knock-out (ko) model was generated by a deletion of exon 3 of the *Mut* gene which leads to a frameshift and therefore to a null function of the Mut enzyme (Peters, et al., 2003). Newborn pups of the homozygous ko/ko genotype only survived the first 24 hours of life and perished soon after, most likely due to acute metabolic decompensation. It was clear before that the Mut pathway exists in mice, but its relevance was proved for the first time with this model: Similar to the human situation, a null mutation led to very severe metabolic decompensation with potentially lethal outcome. Nevertheless, this model was not useful for further long-term studies and had to be modified in order to achieve a surviving model. Applying the same principle of a deleted exon 3 of the *Mut* gene (Chandler, et al., 2007), Chandler et al. started to modify the background of the mice, aiming at a surviving model. They succeeded in 2009 and started to study mitochondrial dysfunction in MMAuria with the help of this model (Chandler, et al., 2009). In addition, the same group generated an MMAuria mouse model by implementing stable transgenic *Mut* expression in the liver in order to constitute residual enzyme activity. This led to the rescue from neonatal lethality in these mice which enabled the first mouse model studies of kidney dysfunction in MMAuria (Manoli, et al., 2013). A similar study showed AAV-mediated rescue of the *Mut*-ko mice (Chandler and Venditti, 2008; Chandler and Venditti, 2010), successfully demonstrating gene therapy in these models.

1.3.2.6 Pitfalls of current models and novel approaches

Although these mouse models of MMAuria allowed the study of certain aspects of the disease, they exhibit some significant pitfalls:

i. The first model (Peters, et al., 2003) showed neonatal lethality which prevents long-term studies on the chronic course of MMAuria.

ii. Background modification as shown in (Chandler, et al., 2009) is a common method to rescue ko mice from neonatal lethality. However, the mechanism or phenomenon underlying a specific case of rescue remains unclear (Montagutelli, 2000). This uncertainty complicates the usage of this model since it remains unknown if the modified background affected relevant metabolic pathways which may directly interfere with the Mut pathway of interest. If this might be true, any conclusions drawn under these circumstances can be misleading with regard to comparing results from the mouse models with the human patient situation.

iii. Partial rescue models as presented in the previous chapter (Chandler and Venditti, 2010; Manoli, et al., 2013) suffer from inaccurate representation of the patient situation where the deficient Mut enzyme is constitutively expressed in all cells of the organism.

2 PROJECT AIMS

The PhD project is divided into five main parts. All of them address different aspects of MMAuria and try to answer various questions which are relevant for a better understanding of the disease. The gathered knowledge should help to enable the development of novel therapeutic approaches in the future.

2.1 MUTATIONAL CHARACTERIZATION OF THE ZURICH/BASEL MMAURIA PATIENT COHORT

The first project deals with MMAuria patients, fibroblasts or DNA of which were referred to the metabolic institutions in Basel and Zurich for diagnostic purpose from the years 1977 to 2015. This cohort of patients with isolated MMAuria, caused by mutations in the *MUT* gene, will be analysed in order to better understand the landscape of disease-causing mutations in this gene of interest. The study aims to stratify the cohort by pursuing the following aims:

i. Compilation of a list of all patients and corresponding genotypes, biochemical data (propionate incorporation and mutase assay), *mut* subclass and age of onset.

ii. Analysis of all detected variants regarding distribution within the *MUT* gene, frequency, mutation type and structural location.

iii. Investigation of protein stability by Western blot in crude cell homogenates of a selection of patient cell lines (all cell lines homozygous for a missense mutation or compound heterozygous for a missense mutation and a null mutation).

iv. Analysis of possible correlations between *mut* subclass assignment and other features such as mutation type or age of onset.

v. Evaluation of *in silico* prediction tools in the missense mutations of the cohort.

2.2 MOLECULAR CHARACTERIZATION AND MECHANISMS IN MUT DEFICIENCY

To better understand the nature of defects which are caused by specific mutations found in the *MUT* gene, 23 missense mutants will be investigated in more detail by pursuing the following aims:

i. Large scale production, purification and characterization of MUT wild-type and mutants in an *E. coli* expression system.

ii. Expression of wild-type and mutant MUT in a mammalian expression system.

iii. Characterization of mutants regarding protein stability, enzyme activity, cofactor affinity, and thermal stability.

iv. Investigation of the effect of the cobalamin cofactor and other chaperones on protein folding/stability.

2.3 Pharmacological Chaperones for MUT

Many missense mutations can cause a functional but unstable enzyme. Despite the intact active site, the protein is directed to the degradation pathway due to its instability, resulting in a severe reduction of protein function and therefore leading to disease in patients carrying these mutations. Diseases, which show this phenomenon of instability due to misfolding, have been classified as misfolding disorders (Gersting, et al., 2008; Leandro, et al., 2011b; Muntau and Gersting, 2010), and ideas to treat these diseases with stabilizing molecules have evolved (Chaudhuri and Paul, 2006; Santos-Sierra, et al., 2012). Some of these molecules have already passed the clinical translation phase and are currently in use (Parenti, et al., 2015). As previously shown, library screening by differential scanning fluorimetry (DSF) can be a successful approach in the search of protein-stabilizing small molecules (Jorge-Finnigan, et al., 2013; Pey, et al., 2008). In our case, we are interested in pharmacological chaperones (PCs) which can stabilize the MUT protein in order to find pilot compounds which can be further developed for clinical application. This project is restricted to the initial screening and subsequent characterization of hit compounds. The aims are structured as follows:

i. Establishment of differential scanning fluorimetry for the MUT protein.

ii. Evaluation of the binding of endogenous ligands (AdoCbl and malonyl-CoA, a substrate analogue) and the stabilization conferred by them.

iii. High throughput screening of a library of small molecules to search for stabilizing compounds.

iv. Evaluation of hit compounds regarding their effect on MUT wild-type and mutant stability and activity by *E. coli* and mammalian fibroblast cell culture techniques.

2.4 Introduction of New MMAuria Mouse Models

As mentioned above currently available mouse models of MMAuria are plagued by important pitfalls (see introduction). Hence, we aim to generate mouse models which avoid the disadvantages of previous models by applying two different approaches.

First, the neonatal lethality of a full *Mut* knock-out mouse will be circumvented by deleting the *Mut* gene only in selected organs such as the brain in order to generate a so called conditional knock-out

model. This allows us to study the influence of a *Mut* knock-out specifically in the brain or the kidney which is of specific interest in MMAuria.

Second, we aim to generate a mouse model which survives and mimics the patient situation as close as possible. For this approach a missense mutation is selected which is known from MMAuria patients that show an intermediate phenotype of MMAuria. This should allow us to generate a surviving model which still shows clear features of MMAuria.

2.4.1 *Mut*$^{flox/flox}$;Nes-Cre model

It is known that MMAuria patients may suffer from a severe neurological phenotype, especially as a long-term complication (Nicolaides, et al., 1998). The brain is generally affected by white matter loss, but also specific lesions in the basal ganglia as a result of metabolic stroke or optic atrophy may be found. So far, no studies have investigated the brain phenotype in MMAuria patients at the molecular and mechanistic level. Studies on the blood-brain barrier have been undertaken in order to investigate the particular vulnerability of the CNS in other organic acidurias (Sauer, et al., 2006). It has been hypothesized that metabolites which are produced by cells within the brain compartment are trapped since they cannot cross the blood-brain barrier and are then exerting their toxic effects on the CNS (Morath, et al., 2008).

To answer questions related to the neurological phenotype of MMAuria patients, a novel mouse model is generated with a brain-specific knock-out of *Mut*. This novel model allows the study of the CNS phenotype of MMAuria but also the investigation of the "trapping hypothesis". In this thesis I present the initial characterization and evaluate the validity of this novel model with the following specific aims:

i. Validation of downregulation of Mut in the brain tissue at the transcript and protein level.

ii. Determination of enzymatic activity in brain tissue.

iii. Consequences of the genetic knock-down in the brain on MMA and 2-MC metabolite levels.

2.4.2 *Mut*$^{ki/ki}$ and *Mut*$^{ko/ki}$ models

In order to generate a mouse model which closely mimics the patient situation, a missense mutation is selected based on the studies presented in chapters 1 and 2. The mutation of interest has to show an intermediate phenotype in patients in order to be found suitable for the generation of a knock-in mouse model. We cross the created knock-in allele with a knock-out allele from a mouse model which was previously introduced (Peters, et al., 2003). In order to evaluate these new models for signs of human MMAuria, the following aims are pursued:

i. Selection of a feasible mutation to generate a knock-in mouse model based on a previous study (Forny, et al., 2014) and characterization of this mutant by enzymatic *in vitro* assays.

ii. Cross-breeding of homozygous *Mut*$^{ki/ki}$ mice with *Mut*$^{ko/wt}$ to generate *Mut*$^{ko/ki}$ mice and monitoring of survival in both new models.

iii. Basic characterization of the biochemical and clinical phenotype of new mouse models.

iv. Initial study of the renal and neurological phenotype.

v. Analysis of the impact of modified diets (high protein, enriched precursor diet) on the new mouse models.

vi. Evaluation of the treatment potential of classical cobalamin therapy.

3 CHAPTER I: THE ZURICH/BASEL *MUT*-TYPE MMAURIA COHORT FROM 1977-2015

This section represents an article which has been submitted for publication (February 2016). Citations in this chapter correlate to the bibliography at the end of the thesis. Figure and table numbering is only applicable to this section of the thesis.

MOLECULAR GENETIC CHARACTERIZATION OF 151 *MUT*-TYPE METHYLMALONIC ACIDURIA PATIENTS AND IDENTIFICATION OF 41 NOVEL MUTATIONS IN *MUT*

Patrick Forny[1, 2, 3], Anne-Sophie Schnellmann[1], Celine Buerer[1], Seraina Lutz[1], Brian Fowler[1], D Sean Froese[1, 2], Matthias R Baumgartner[1, 2, 3, *]

[1] Division of Metabolism and Children's Research Center, University Children's Hospital, CH-8032 Zurich, Switzerland

[2] radiz – Rare Disease Initiative Zurich, Clinical Research Priority Program for Rare Diseases, University of Zurich, Switzerland

[3] Zurich Center for Integrative Human Physiology, University of Zurich, Switzerland

[*] To whom correspondence may be addressed:

Matthias R Baumgartner, matthias.baumgartner@kispi.uzh.ch

The authors declare no conflict of interest.

3.1 ABSTRACT

Isolated methylmalonic aciduria (MMAuria) is an autosomal recessive disorder of propionate metabolism in many cases caused by mutations in the methylmalonyl-CoA mutase (*MUT*) gene (*mut*-type MMAuria). Here, we report a complete list of mutations identified in patients referred for diagnostic testing to the Basel and Zurich laboratories from 1977 to 2015. From 151 referred patients, 114 were classified as mut^0 and 32 as mut^- (5 not defined). We identified 110 different mutations of which 41 were novel. Forty-seven mutations were identified only once, suggesting many patients carry private mutations. Investigation of the missense mutations revealed that the mutations p.Asn219Tyr, p.Arg369His and p.Arg694Trp recur in >10 alleles. Only one missense mutation was found in the inter-domain linker region, implying this region is tolerant to substitution. Deficient alleles in the mut^- subclass were mostly caused by missense mutations. On the contrary, only half of the mut^0 mutations were of the missense type. Western blot analysis revealed reduced MUT protein for all 34 cell lines (27 mut^0, 7 mut^-) tested, suggesting protein instability as a major mechanism of deficiency in *mut*-type MMAuria. This large scale evaluation helps to characterize the landscape of *MUT* mutations and dysfunction.

3.2 KEY WORDS

methylmalonyl-CoA mutase; MUT; methylmalonic aciduria; missense mutations; genotype-phenotype correlation

3.3 INTRODUCTION

The mitochondrial enzyme methylmalonyl-CoA mutase (MUT, MIM #609058, EC 5.4.9.22) catalyzes the isomerization of L-methylmalonyl-CoA to succinyl-CoA. This chemical reaction represents an important step in propionate metabolism, funneling metabolites from the breakdown of amino acids (valine, isoleucine, methionine, and threonine), odd-chain fatty acids, and the side chain of cholesterol into the tricarboxylic acid cycle (Fowler, et al., 2008). Deficiency of the MUT apoenzyme is the underlying cause of *mut*-class methylmalonic aciduria (MMAuria, MIM #251000), an autosomal recessive inborn error of propionate metabolism. The disease is biochemically characterized by low incorporation of propionate (PI) into cell proteins and low or absent MUT enzyme activity, which leads to abnormally high levels of hallmark metabolites such as methylmalonic acid and propionylcarnitine (Fowler, et al., 2008). *mut* patients show normal intrauterine development, but may develop severe metabolic crisis almost immediately after birth (early-onset) or may present later either with intermittent metabolic decompensations or with chronic progression manifesting as failure to thrive and developmental delay (late-onset) (Baumgartner, et al., 2014). First signs after a symptom

free interval include severe ketoacidosis, feeding difficulties, lethargy and hypotonia. The acute symptoms may deteriorate into a comatose state including cerebral edema, apneas, and seizure-like episodes. Long-term survivors suffer from chronic renal failure and neurological complications (Horster, et al., 2007; Nicolaides, et al., 1998; Zsengeller, et al., 2014).

The *MUT* gene, which encodes the MUT enzyme, lies on chromosome 6p12.3 (Ledley, et al., 1988b). It consists of 13 exons with the first exon non-coding, resulting in a polypeptide chain of 750 amino acids. The folded enzyme is composed of two domains. The N-terminal domain harbors the binding site for the substrate methylmalonyl-CoA while the C-terminal domain binds the essential cofactor 5'-deoxyadenosylcobalamin (AdoCbl) (Froese, et al., 2010b). Both domains are interconnected by a linker region spanning amino acid positions 482 to 585. Human MUT assembles as a homodimer and has been structurally captured in three different states: the *apo* form, the *holo* form with the bound cofactor AdoCbl, and a *ternary* complex with both binding pockets occupied by AdoCbl and the substrate analogue malonyl-CoA (Froese, et al., 2010b).

Since the MUT enzyme requires AdoCbl as cofactor for proper function, isolated MMAuria can also be caused by a deficiency of other proteins involved in the generation of AdoCbl. The malfunction of the methylmalonic aciduria type B protein (MMAB, MIM #607568; MMA *cblB* type, MIM #251110), the methylmalonic aciduria type A protein (MMAA, MIM #607481; MMA *cblA* type, MIM #251100), or the methylmalonic aciduria and homocystinuria type D protein (MMADHC, MIM #611935; MMA *cblD* type variant 2, MIM #277410) all lead to isolated MMAuria due to a defect in AdoCbl production. Patient cell lines can be assigned to the complementation groups *mut*, *cblA*, *cblB*, or *cblD-MMA* by complementation analysis of fibroblast heterokaryons (Gravel, et al., 1975; Willard, et al., 1978b). In this study, we focus only on *mut*-type MMAuria, which can be further subdivided into the *mut*$^-$ and *mut*^{0} subclasses. Fibroblasts from *mut*$^-$ patients show a response in the PI assay to supplementation with hydroxocobalamin (OHCbl) and display residual MUT activity usually with a K_M for AdoCbl approximately 200 to 5000 times higher than wild-type control, and normal K_M for the substrate methylmalonyl-CoA (Morrow, et al., 1978; Willard and Rosenberg, 1977). Enzyme from this subclass often shows increased thermolability relative to wild-type enzyme (Forny, et al., 2014; Willard and Rosenberg, 1980). In addition, *mut*$^-$ patients usually present with a milder phenotype compared to *mut*^{0}, with lower occurrence of mortality, morbidity and long-term complications (Horster, et al., 2007). By contrast, patients are assigned to the *mut*^{0} subclass if their cells are not responsive to OHCbl supplementation in the PI assay and no residual mutase activity is detectable even when assayed in the presence of highly saturating AdoCbl concentrations (Morrow, et al., 1975; Willard and Rosenberg, 1977; Willard and Rosenberg, 1980).

255 mutations have been described thus far in the *MUT* gene ("The Human Gene Mutation Database" (HGMD) version 2015.3 as of November 2015, www.hgmd.org). While almost half of all mutations are private, some are recurrently found (Fowler, et al., 2008). For example, c.655A>T (p.Asn219Tyr) (Acquaviva, et al., 2001) and c.1106G>A (p.Arg369His) (Worgan, et al., 2006) have been repeatedly found in mut^0 patients, c.2080C>T (p.Arg694Trp) (Lempp, et al., 2007) in mut^- patients, c.322C>T (p.Arg108Cys) in patients of Mexican/Hispanic origin (Worgan, et al., 2006) and c.2150G>T (p.Gly717Val) in patients of African origin (Worgan, et al., 2006). With the work presented here we significantly expand the mutational spectrum of *MUT* based on our entire patient cohort from the years 1977 to 2015, representing a large European cohort.

3.4 VARIANTS

Analysis of 151 patients (145 families) in our cohort revealed 110 different mutations in the *MUT* gene (Fig. 1, Table 1) almost all of which were confirmed enzymatically or were previously identified (except for c.415G>A, c.467A>T, c.1853T>C and c.1975C>T). The missense type was detected in the majority of cases and was represented by 62 different single amino acid exchanges in our cohort (Fig. 2A). Other mutations detected were insertions/deletions (23), nonsense (16), those that primarily affected splicing (8) and one start codon mutation (Fig. 2A). Forty-one of the 110 mutations (37%) are presented here for the first time.

The p.Asn219Tyr (c.655A>T) mutation was the most frequently found mutation in our cohort and was detected in 24 alleles (17 patients, 17 families) (Table 1, Fig. 2B). N-terminal to p.Asn219, the residue p.Gln218 changed to histidine (p.Gln218His, c.654A>C) was found 7 times, suggesting an important role for this protein region, which is found within the substrate binding channel (Forny, et al., 2014). p.Arg369His (c.1106G>A) was the second most commonly detected disease allele (23 alleles, 16 patients, 15 families). Thus, the two most frequent mutations found in our cohort correspond to previous studies which show a high frequency of these two disease alleles (Acquaviva, et al., 2001; Worgan, et al., 2006). The third most frequently identified mutation was p.Arg694Trp (c.2080C>T) (11 alleles, 7 patients, 7 families) (Fig. 2B), a residue which was alternatively found to be mutated to leucine in three cases (p.Arg694Leu, c.2081G>T). Other common missense mutations were p.Leu328Phe (c.982C>T) and p.Pro615Thr (c.1843C>A), which were both detected in 9 alleles (both in 5 patients, 5 families) with the latter residue also found to be mutated to leucine in 4 alleles (p.Pro615Leu, c.1844C>T), while p.Ala191Glu (c.572C>A) and p.Gly203Arg (c.607G>A) (both in 6 alleles) were also more frequently identified (Table 1, Fig. 2B).

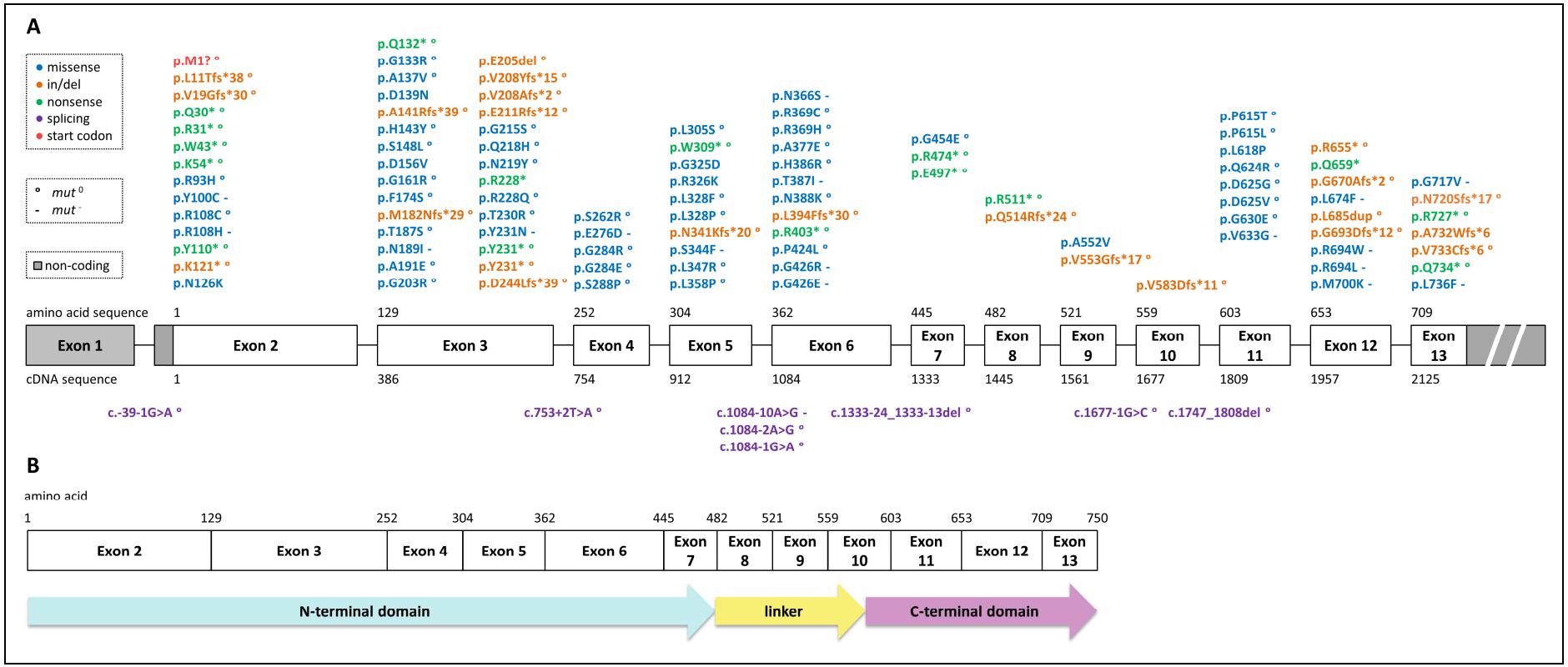

Figure 1. Schematic representation (not to scale) of the *MUT* gene and location of the presented sequence variants associated with *mut*-type MMAuria. A. Exons (boxes) and introns (lines) represent the structure of the human *MUT* gene. Greyed areas (exon 1, start of exon 2 and end of exon 13) depict untranslated (non-coding) regions. Exon sizes are proportional to each other, except for exon 13 which is longer than represented (indicated by white double-strike). The numbering of exons is according to NG_007100.1. The size of introns is not to scale and not proportional. cDNA numbering below exons is according to NM_000255.3, amino acid numbering above exons is according to NP_000246.2. Mutations are written above the exon or below the intron, where they occurred. Mutation types are color coded: blue, missense; orange, insertion/deletion; green, nonsense; purple, splicing; red, start codon. The *mut* subclass associated with each mutation is indicated by a circle "°" for mut^0 and a minus "-" for mut^-. **B.** Protein schematic of MUT. Below the boxes which represent the exons, the three domains are colored similar to (Forny, et al., 2014; Froese, et al., 2010b): light blue, N-terminal substrate binding domain; yellow, linker region; magenta, C-terminal cofactor binding domain. Amino acid numbers are indicated above exons

The two most frequently identified nonsense mutations were p.Arg403* (c.1207C>T, 10 alleles in 8 patients, 7 families) and p.Arg727* (c.2179C>T, 10 alleles in 7 patients, 6 families), both the result of C to T mutations causing a stop codon (Fig. 2B). Slightly less frequent, p.Tyr231* was 6 times (in 3 patients, 3 families) caused by the duplication mutation c.692dup and twice by the nonsense mutation c.693C>G. Finally, three nonsense mutations (p.Arg31*, c.91C>T; p.Trp43*, c.129G>A; p.Arg511*, c.1531C>T) were detected 5 times (Table 1, Fig. 2B). All other mutations were detected less than 5 times and almost half of all mutations (43%) were identified only once, indicating that many mutations are private. Splicing mutations were rare, accounting for only 7.3% of all mutations found (Fig. 2A).

Although mutations were found in every exon – except for the non-coding exon 1 – the distribution is not equal (Fig. 1A and 2C). While the DNA sequences encoding the substrate binding N-terminal domain and the cofactor binding C-terminal domain show comparable mutation rates, the region in between, corresponding to exons 8 to 10, is less often affected by mutations (Fig. 2C). This region only carries 5.5% of all mutations but covers 16% of the coding sequence. The amino acids encoded by this region correspond almost fully to the protein linker region, represented by amino acids 482 to 585 (Fig. 1B), which does not contribute residues to either the catalytic center or the ligand binding pockets (Froese, et al., 2010b). When amino acid conservation is examined, the linker region shows a mean conservation score of 0.70, whereas the adjacent N-terminal and C-terminal domains (amino acids 1 to 481 and 586 to 750) show conservation scores of 0.79 and 0.75, respectively (Fig. 2D). Further, we found only one missense mutation (p.Ala552Val, c.1655C>T) in the linker region, which lies on an unusually conserved and buried residue (Supp. Fig. S1). The significantly lower conservation and the structural property of this region can help explain the lower frequency of deleterious mutations found, and suggest that this region is more tolerant to sequence alterations.

Exon 3 shows the highest relative rate of mutations per base pair (Fig. 2C), and its corresponding amino acid sequence (residues 129 to 251) has the highest mean conservation score of all encoded exons (data not shown). Moreover, in our cohort 4 out of the 8 most common missense mutations map to exon 3, further underlining the importance of this genomic segment. The residues encoded by exon 3 provide important contributions to the architecture of the substrate binding channel (Supp. Fig. S2), a fact which may supply a structural rationalization for the over-proportional representation of mutations encoded by this exon.

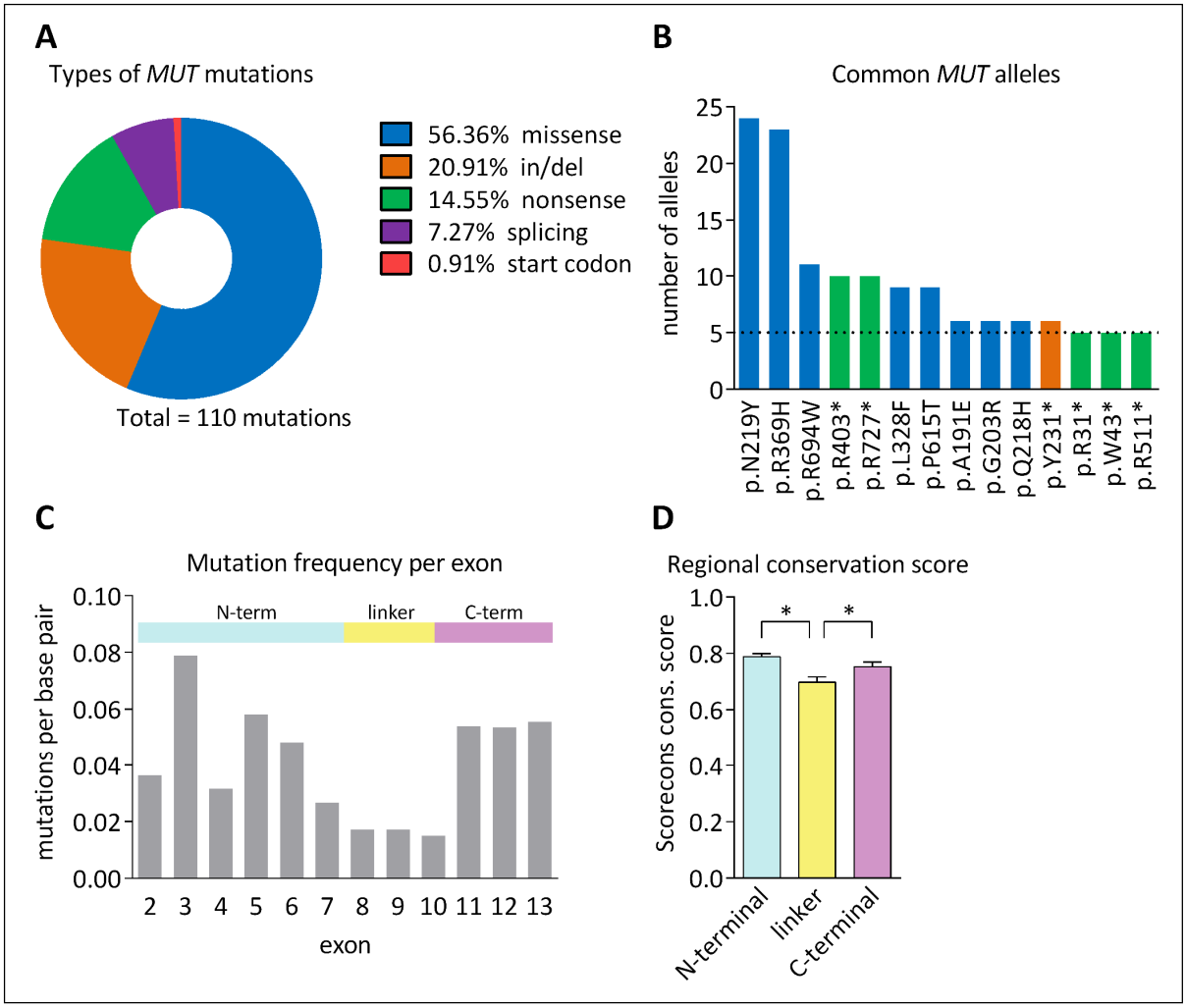

Figure 2. Frequency of variant types and alleles and their distribution. Coloring as in Fig. 1. **A.** Pie chart summarizing the types of *MUT* mutations found. Insertions, deletions, duplications and indels are condensed in the category "in/del" (orange). **B.** Frequency of the alleles which occurred at least 5 times in the presented cohort. See also Table 1. **C.** The relative mutation frequency for each individual exon (no exon 1, since it is non-coding; only the coding region of exons 2 and 13 were calculated). **D.** Conservation score of the three MUT protein domains. Bars represent mean values of all scores of the residues in the respective region, error bars are SEM, *: $p < 0.05$ (as determined by a Student's t-test). A multiple sequence alignment (MSA) file was created with the ConSurf server (Ashkenazy, et al., 2010): PDB code, 2XIQ; 150 homologues. The MSA was used to score each individual residue with the Scorecons server (Valdar, 2002). Amino acids at the N- and C-termini (1-30, 739-750) were excluded from the analysis since they represent particularly un-conserved residues (see Supp. Fig. S1).

We found eight mutations whose primary defect was suspected to be via altered splicing (Table 1). Following analysis by the "Human Splice Finder" (HSF 3.0; http://www.umd.be/HSF3/) (Desmet, et al., 2009), seven of these mutations were predicted to alter splicing; c.-39-1G>A could not be analyzed. RT-PCR analysis of the intronic mutation c.1084-10A>G demonstrated activation of a cryptic splice site in intron 5, leading to the insertion (between exon 5 and 6) of the 9 last nucleotides of intron 5

in the transcript, resulting in the mRNA r.1084-1_1084ins1084-9_1084-1 and predicted protein sequence p.Gln361_Asn362insIlePhe*. We also analyzed the intronic deletion mutation c.1333-24_1333-13del by RT-PCR, which showed the generation of an alternative splice site in intron 6. As a consequence, the last 12 nucleotides of intron six are inserted between exon 6 and 7, resulting in r.1333-1_1333ins1333-12_1333-1 and the predicted protein change p.Lys444_Leu445insPheSerPhe*. An interesting case was found in the mutation c.1808G>A which lies on the last nucleotide of exon 10. RT-PCR analysis confirmed that the major defect detected on the cDNA level was actually splicing as shown previously (Martinez, et al., 2005). The activation of an alternative splice site in the middle of exon 10 leads to the deletion of the last 62 nucleotides of exon 10, resulting in r.1747_1808del and the predicted protein change p.Val583Glyfs*3.

Sixteen out of the 110 mutations (14.5%) identified occurred on 13 different arginine residues, although arginine residues account for only 5.6% of all amino acids in the MUT protein sequence. This disproportion may be explained by the fact that 14 out of 16 mutated arginines were found to exist on CpG dinucleotides (except c.977G>A and c.1962_1963del), which are known to be highly mutable (Cooper and Youssoufian, 1988). By contrast, alanine, the most common amino acid in MUT (9.2% of all amino acids), was only found to be mutated six times (5.5% of all mutations).

3.5 Database

All unpublished variants in Table 1 were submitted to the freely accessible NCBI ClinVar database *http://www.ncbi.nlm.nih.gov/clinvar/* using the standard HGVS nomenclature.

3.6 Biological Significance

Mutations may exert their harmful effect on protein function via different mechanisms, one of which is impaired structural integrity leading to an unstable protein, which is then degraded by the proteasomal degradation system. Misfolding mutations (usually missense mutations), which result in these "unstable" mutants, represent a significant proportion of mutations in *MUT* (Forny, et al., 2014). In the present study, we selected 34 patient cell lines to investigate if the mutant MUT proteins expressed therein displayed altered protein levels, which can be used as a surrogate marker of protein destabilization. Cell lines were selected based on their availability and genotypic configuration: missense alleles in a homozygous state or compound heterozygous missense alleles in conjunction with a CRIM-negative mutation allowed a conclusion about the respective mutant allele. As controls homozygous truncation mutations were used.

Compared to MUT from wild-type fibroblasts, MUT protein levels from patient fibroblasts containing at least one missense mutation were mostly low or absent (Fig. 3). However, some missense mutations resulted in residual protein levels above 25% of wild-type. Of these, the most striking pattern of high residual protein level was induced by six mutations near the C-terminus (Fig. 3): four homozygous (p.Gln624Arg, p.Asp625Val, p.Asp625Gly, p.Leu674Phe) and two heterozygous mutations (p.Gly630Glu together with the truncation mutation p.Arg403*, p.Val633Gly with the *mut*^{0} mutant p.Asn219Tyr). These results suggest the primary biochemical defect caused by these mutations is something other than protein misfolding, *e.g.* thermolability, impaired catalytic activity or K_M defect for AdoCbl (Forny, et al., 2014). Structural investigation of all five strictly conserved residues (Supp. Fig. S1) revealed that they are located in the C-terminal domain poised next to the active site (Supp. Fig. S3). Due to the crucial location and potential for disturbance to the substrate-cofactor interaction, these mutations are likely to cause impaired catalytic activity. Four of the six cell lines (not no. 18 and 87) are classified as *mut*^{0}, suggesting a complete abrogation of catalytic activity. However, both cell lines from patients no. 18 and 87 showed a clear response to OHCbl supplementation in the PI assay (Table 2) and were therefore classified as *mut*$^-$. Additionally, cell line no. 18 harbors a known *mut*^{0} mutation (p.Asn219Tyr, c.655A>T) in conjunction with p.Val633Gly (c.1898T>G), which has been repeatedly reported as *mut*$^-$ (Acquaviva, et al., 2005; Adjalla, et al., 1998; Lempp, et al., 2007; Worgan, et al., 2006). Thus, although located at the active site, this latter mutation likely induces a K_M defect for AdoCbl, as previously described *in vitro* (Forny, et al., 2014).

Cell lines carrying homozygous mutations which caused a premature stop codon showed almost completely absent MUT protein (Fig. 3, truncations). As expected, these truncating mutations are all classified as *mut*^{0} mutations.

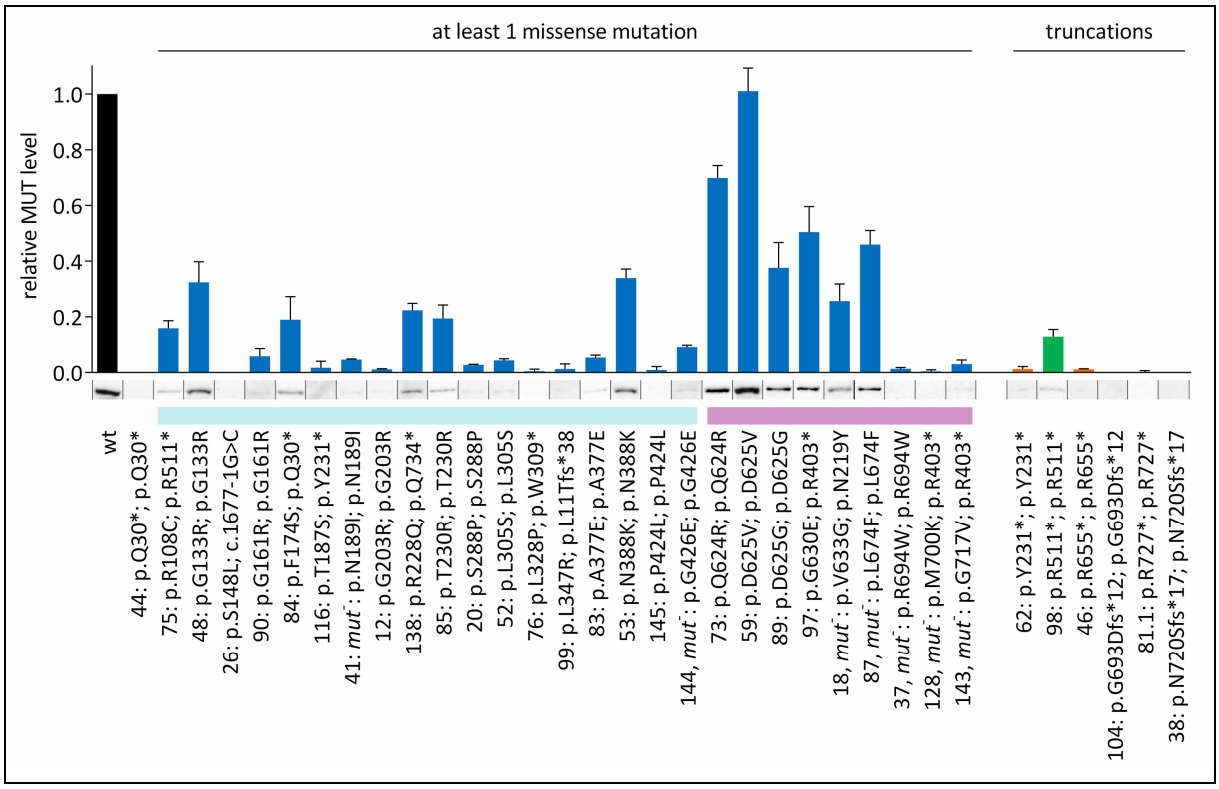

Figure 3. Western blot analysis and quantification of MUT expression from patient cell lines. The wild-type (*wt*) control bar is colored in black. **Left**: Blue bars represent the quantification of Western blot of cell lines carrying at least one missense mutation. **Right**: Quantification of Western blot of cell lines with homozygous truncating mutations; orange, insertion/deletion mutations; green, nonsense mutations. Relative MUT levels were determined by normalization to internal beta-actin controls. Representative MUT bands of a minimum of $n = 2$ experiments (error bars depict SEM) below the bar chart. Missense mutations are from different protein regions, indicated by the light blue (N-terminal domain) and magenta (C-terminal domain) coloring. Patient cell lines are designated with the patient number (Table 2), *mut* class (empty for *mut*^{0}), and mutations on protein level. Western blot was performed according to (Forny, et al., 2014).

3.7 Clinical Significance

The presented cohort consists of 151 patients from 145 families, all of whom were confirmed to suffer from *mut*-type MMAuria either by enzymatic testing (PI or mutase assay) or by mutation analysis (Table 2). Patients 1 to 35 (Table 2) have been published in (Lempp, et al., 2007). In all, 84 (55.6%) patients carried homozygous mutations, 66 (43.7%) patients were found to have compound heterozygous variants, while for 1 patient (0.3%) only one mutation could be identified (Table 2, patient no. 11). For the latter patient deficiency of MUT was confirmed by PI and mutase assay. Patients were assigned to the *mut* subclass based on their known mutations or on the ratio in the PI assay. If the ratio was >1.5 (ratio of activity with OHCbl versus that without OHCbl supplemented in the culture medium) the patients were classified as *mut*$^-$; the criterion for the *mut*^{0} class was no response in the PI assay (ratio ≤1.5), as described in (Lempp, et al., 2007). As the basis for evaluating the nature of the

clinical course in the *mut*^{0} and *mut*$^-$ patients of our cohort, we compared mutation type, residual enzyme activity and age of onset in the two subclasses.

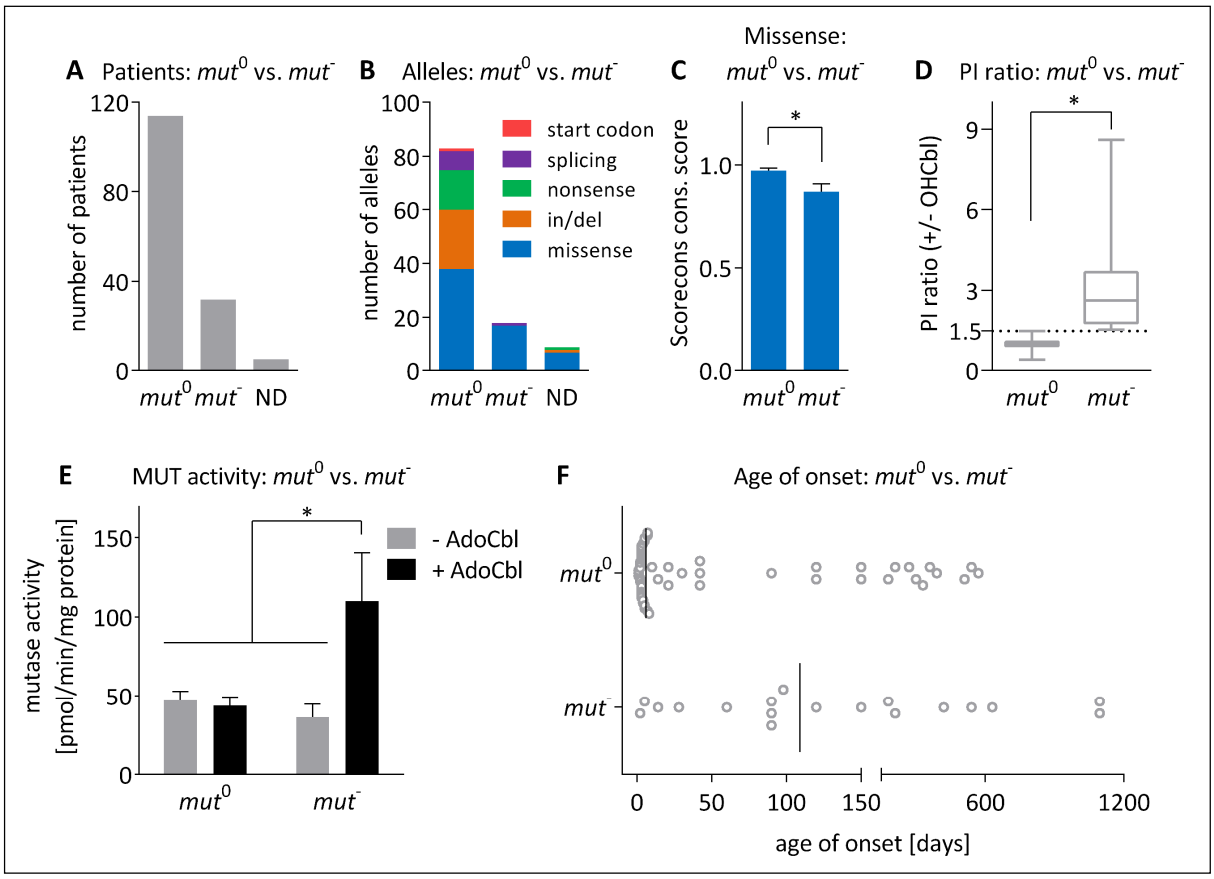

Figure 4. *mut*^{0} versus *mut*$^-$. A. Number of patients that were classified as *mut*^{0}, *mut*$^-$ or not defined (ND). **B.** Number of alleles for each subclass shown as a proportion of mutation type. For explanation of allele subclass classification see footnote in Table 1. **C.** Conservation score of residues, which carried a missense mutation, for each *mut* subclass. Bars represent mean values of scores, error bars depict SEM, *: $p = 0.001$ (by Student's t-test). For generation of scores see Fig. 2. **D.** PI ratios of each subclass (Table 2) shown as box plot, horizontal line in the box indicates median, whiskers represent minimum and maximum, *: $p < 0.0001$ (by Student's t-test). **E.** Bar chart of mean MUT activities with and without AdoCbl supplementation for bot *mut* subclasses, *: $p < 0.002$ (by two-way ANOVA, Sidak's multiple comparisons test). **F.** Age of onset of all patients with available data is shown. The vertical line depicts the median value. For clarity, the highest value in the *mut*$^-$ class is not shown (5475 days).

114 patients (83 alleles) belonged to the *mut*^{0} subclass, 32 (18 alleles) to *mut*$^-$ and for 5 patients (9 alleles) enzymatic data was lacking and therefore designated "not defined" (ND) (Fig. 4A and B). Thus, *mut*^{0} patients account for more than three quarters of all patients in our cohort (Fig. 4A). Nearly all nonsense and insertion/deletion mutations were associated with *mut*^{0} alleles (c.1975C>T, p.Gln659* and c.2194_2197delinsTGGAA, p.Ala732Trpfs*6 were classified as "not defined" due to a lack of biochemical data), suggesting that these mutation types usually lead to a completely dysfunctional enzyme. Within the *mut*$^-$ class, 17 of the 18 mutations were of the missense type (Fig. 4B). Comparison of these 17 *mut*$^-$ missense mutations with the 38 missense mutations that produced a *mut*^{0} allele reveals that the *mut*^{0} amino acid exchanges took place at residues with a higher overall conservation score (Fig. 4C), providing a possible rationalization for their more severe impact.

As expected, fibroblasts taken from *mut*^{0} patients in our cohort had a lower PI ratio than those from *mut*$^-$ (by definition, Fig. 4D). Interestingly, this is in line with enzymatic activity which more than doubled in *mut*$^-$ cells upon AdoCbl supplementation, while activity in *mut*^{0} cells stayed the same (Fig. 4E). This is further evidence that *mut*$^-$ mutations specifically interfere with utilization of the cofactor and, *in vitro* at least, benefit from bolstered AdoCbl levels.

For more than half of the patients in our cohort the age of onset was well documented (Table 2). These patients showed a very broad onset range, from day 1 to 15 years of life; while some patients detected in newborn screening were asymptomatic at the time of diagnosis (Table 2). Overall, the *mut*$^-$ subclass patients showed a later age of onset (mean age of onset: 273 days; median: 109 days) than *mut*^{0} patients (mean age of onset: 86 days; median: 6 days) (Fig. 4F), which is consistent with previous findings (Matsui, et al., 1983b).

To further investigate the stratification of the missense mutations into the *mut*^{0} and *mut*$^-$ subclasses, we mapped them onto the MUT protein structure (Fig. 5). Missense mutations of the *mut*^{0} class were clearly more present in the N-terminal domain, as 84% of all *mut*^{0} missense mutations were found there. Therefore, 68% of all missense mutations in this region were of the *mut*^{0} subclass. Since the N-terminal domain harbors the substrate binding site, we hypothesize that the missense mutations found in this region caused mainly severe *mut*^{0} alleles either via specific interference with the configuration required for substrate binding, or by general loss of protein stability (Fig. 3). The proportion of *mut*$^-$ subclass causing missense mutations was higher in the C-terminal domain (50% of all missense mutations) than in in the N-terminal domain (21%). This is consistent with the AdoCbl binding function of this domain, disturbance of which can lead to inhibited AdoCbl binding, as reflected in the higher PI ratio and response to AdoCbl supplementation in the MUT activity assay in *mut*$^-$ fibroblasts (Fig. 4D and E).

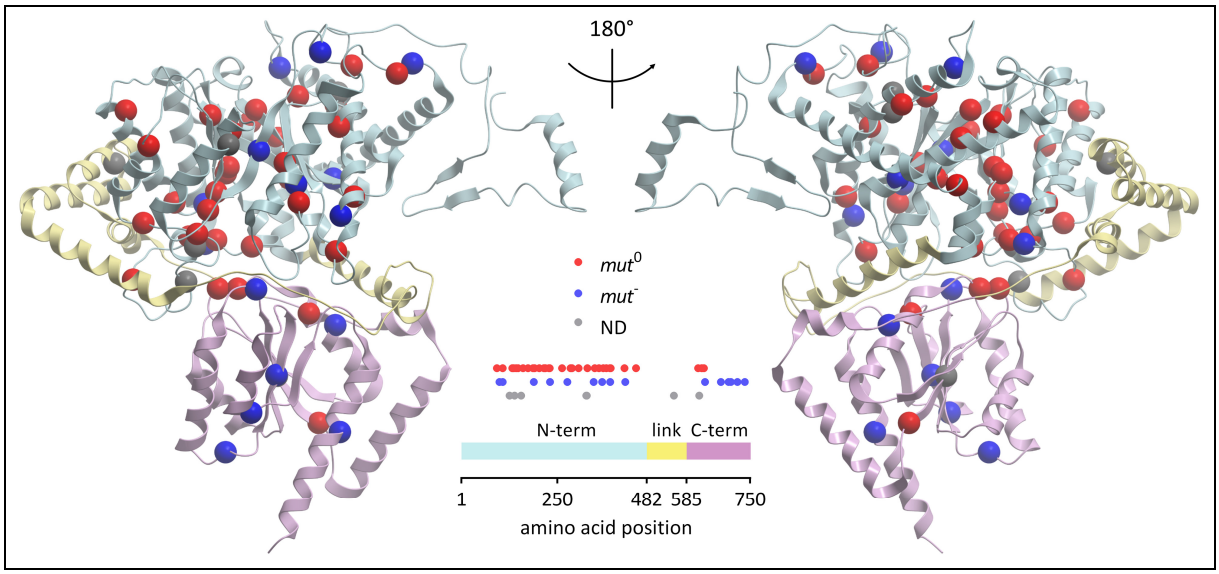

Figure 5. Structural mapping of missense mutations on the MUT protein. The MUT structure according to PDB code 2XIQ, colored as in Fig. 1B: light blue, N-terminal domain; yellow, inter-domain linker; magenta, C-terminal domain. Missense mutations (Table 1) are shown as circles in red (*mut*^{0}), blue (*mut*$^-$) or grey (ND: not defined). Between the two monomers a schematic protein representation shows the relative distribution of missense mutations in the 2D polypeptide chain.

3.8 Diagnostic Relevance

In a clinical setting, general symptoms such as lethargy or even coma combined with vomiting and severe ketoacidosis can be the first signs which trigger the suspicion of MMAuria. The initial metabolic differential diagnosis at this step involves – among other diseases – organic acidurias which can closely imitate MMAuria, such as maple syrup urine disease, isovaleric aciduria, and propionic aciduria. Identification of characteristic changes in the organic acid and acylcarnitine profile, especially elevated urine and/or blood methylmalonic acid and elevated propionylcarnitine level (Baumgartner, et al., 2014) allows the diagnosis of unclassified MMAuria and initiation of acute phase treatment. However, optimized long-term treatment and prognosis depend on knowledge of the exact defect. A reliable and well-established systematic approach to achieve this involves performance of PI assay followed by direct assay of mutase activity and complementary mutation analysis.

First-line mutation analysis may be appropriate in cases of prenatal diagnosis, known siblings with the disorder, or in special populations. However, this study highlights pitfalls in using this approach in other situations. The high number of private mutations (here we present 18 novel missense mutations, in total 186 missense mutations are known according to HGMD version 2015.3), together with the large number of known SNPs (414 according to dbSNP, NCBI as of November 2015), makes it difficult to differentiate whether a novel variant indeed causes disease. This is particularly relevant for non-synonymous point mutations resulting in missense changes.

We tested all of our missense mutations *in silico* with three different variant severity prediction programs (see footnote Table 1). From these, a total of four mutations were designated as "benign" or "neutral". One mutation (p.Arg603Lys) was predicted to be non-detrimental by all three algorithms, implying that the predicted protein change might not be the main/only defect conferred by this mutation. This hypothesis is supported by the detection of an alternative transcript detected by RT-PCR (Table 1, c.1747_1808del), indicating that this mutation causes altered splicing. Further, 3 mutations (p.Gly203Arg, p.Ser288Pro, p.Met700Lys) were predicted to be non-damaging by PROVEAN and PolyPhen-2 even though there is clear evidence that they are disease-causing. The mutations p.Gly203Arg (in patient no. 12 and 95) and p.Ser288Pro (in patients no. 20) were both detected in a homozygous state and analysis of the patient cells showed clear enzymatic evidence of MMAuria (Table 2). In addition, p.Met700Lys was independently expressed and displayed a catalytic defect in a previous study (Forny, et al., 2014). This data demonstrates that these *in silico* programs can be applied as a guide in diagnostic practice, but should not be used as confirmation of a defect. Hence, biochemical testing by PI or mutase assay remains crucial for the diagnosis of *mut*-type MMAuria.

3.9 Future Prospects

This study underpins our understanding of a number of mechanistic questions and points to further studies regarding the link between mutations and disease in this important disorder.

First, knowledge of the *mut* class is important for prognosis of the future development of the disease, where mut^0 patients show a more severe course of the disorder (Horster, et al., 2007). Supporting this, in our cohort mut^0 patients presented earlier than mut^-. Future studies should evaluate detailed follow-up data on clinical course in relation to *mut* class. In some cases, these investigations will need to be combined with expression of particular mutations. However, it needs to be born in mind that the prognosis of the clinical course of MMAuria in a single patient, solely based on the biochemical *mut* class assignment, is uncertain.

Second, establishment of the patient's response to cobalamin supplementation therapy is crucial for a proper treatment regimen and should be tested using a standardized protocol (Baumgartner, et al., 2014; Fowler, et al., 2008). Most *cblA* patients improve upon this therapy and about one third of *cblB* patients respond to cobalamin treatment (Matsui, et al., 1983b; Rosenberg, et al., 1968). However, *mut* patients have only been assessed under non-standardized protocols (Horster, et al., 2007; Matsui, et al., 1983b) and results can sometimes be confusing, since methylmalonic acid urine levels are influenced by factors (*e.g.* undetected infection) which are difficult to control. As indicated by our data, *in vitro* studies can provide valuable help in assessing the likelihood of an *in vivo* response. A high PI ratio and increase of mutase activity in the assay upon AdoCbl supplementation can indicate

a response to cobalamin. We also show that missense mutations, which are localized in the C-terminal domain, are more likely to belong to the *mut*$^{-}$ class and therefore be responsive to cobalamin *in vitro*. Nevertheless, further study of the biochemical mechanisms behind cobalamin responsiveness is needed in order to better understand the molecular behaviour of cofactor binding and its disruption.

Third, this study shows that out of all the missense mutations only about one third are associated with response to cobalamin *in vitro*, indicating a cofactor binding defect. As exemplified by our Western blot analysis (Fig. 3), a large proportion of the other missense mutations appear to cause protein destabilization. This feature may render these mutations candidates for protein stabilization therapy, *e.g.* by pharmacological chaperones or by inhibition of the proteasomal protein degradation machinery (Cohen and Kelly, 2003; Muntau, et al., 2014), facilitating an individualized, mutation-tailored treatment approach in the future.

3.10 Funding

This work was supported by the Rare Disease Initiative Zurich (radiz), a clinical research priority program for rare diseases of the University of Zurich, Switzerland and the Swiss National Science Foundation (SNSF 31003A_138521). P.F. was supported by an SNSF MD-PhD fellowship (SNSF 323530_145248).

3.11 Tables

For better readability tables are presented in landscape mode.

Table 1. Summary of mutant alleles found in *MUT* and their consequences

Nucleotide change [a]	Predicted protein change [b]	Exon/ Intron	*mut* class [c]	No. of alleles	No. of patients	No. of families	PROVEAN score [d]	SIFT score [e]	Poly-Phen-2 score [f]	Literature Reference
c.-39-1G>A	splice site [g]	Intron 1	mut^0	1	1	1				This study
c.2T>C	p.(Met1?)	Exon 2	mut^0	1	1	1				This study
c.30dup	p.(Leu11Thrfs*38)	Exon 2	mut^0	1	1	1				This study
c.55dup	p.(Val19Glyfs*30)	Exon 2	mut^0	2	1	1				This study
c.88C>T	p.(Gln30*)	Exon 2	mut^0	3	2	2				This study
c.91C>T	p.(Arg31*)	Exon 2	mut^0	5	4	4				(Worgan, et al., 2006)
c.129G>A	p.(Trp43*)	Exon 2	mut^0	5	3	2				This study
c.160A>T	p.(Lys54*)	Exon 2	mut^0	2	1	1				(Fuchshuber, et al., 2000)
c.278G>A	p.(Arg93His)	Exon 2	mut^0	2	1	1	-4.94	0	1	(Raff, et al., 1991)
c.299A>G	p.(Tyr100Cys)	Exon 2	mut^-	2	1	1	-8.89	0	1	(Lempp, et al., 2007)
c.322C>T	p.(Arg108Cys)	Exon 2	mut^0	1	1	1	-7.91	0	1	(Worgan, et al., 2006)
c.323G>A	p.(Arg108His)	Exon 2	mut^-	1	1	1	-7.91	0	1	(Acquaviva, et al., 2005)
c.330T>G	p.(Tyr110*)	Exon 2	mut^0	1	1	1				This study
c.360dup	p.(Lys121*)	Exon 2	mut^0	1	1	1				(Acquaviva, et al., 2005)
c.378C>A	p.(Asn126Lys)	Exon 2	ND	2	2	1	-4.63	0.003	0.998	This study
c.394C>T	p.(Gln132*)	Exon 3	mut^0	1	1	1				(Dundar, et al., 2012)
c.397G>A	p.(Gly133Arg)	Exon 3	mut^0	2	1	1	-7.97	0	1	This study
c.410C>T	p.(Ala137Val)	Exon 3	mut^0	1	1	1	-3.99	0	1	(Lempp, et al., 2007)
c.415G>A	p.(Asp139Asn)	Exon 3	ND	1	1	1	-4.98	0	1	This study
c.421del	p.(Ala141Argfs*39)	Exon 3	mut^0	2	1	1				(Peters, et al., 2002)
c.427C>T	p.(His143Tyr)	Exon 3	mut^0	1	1	1	-5.98	0	1	(Lempp, et al., 2007)
c.443C>T	p.(Ser148Leu)	Exon 3	mut^0	1	1	1	-5.97	0	1	(Acquaviva, et al., 2005)
c.467A>T	p.(Asp156Val)	Exon 3	ND	2	1	1	-8.98	0	1	This study
c.481G>A	p.(Gly161Arg)	Exon 3	mut^0	2	1	1	-7.99	0	1	(Filippi, et al., 2009)
c.521T>C	p.(Phe174Ser)	Exon 3	mut^0	1	1	1	-7.99	0	1	(Fuchshuber, et al., 2000)
c.544dup	p.(Met182Asnfs*29)	Exon 3	mut^0	2	1	1				(Fuchshuber, et al., 2000)
c.560C>G	p.(Thr187Ser)	Exon 3	mut^0	1	1	1	-3.99	0	1	This study
c.566A>T	p.(Asn189Ile)	Exon 3	mut^-	2	1	1	-8.98	0	1	This study

c.572C>A	p.(Ala191Glu)	Exon 3	*mut*^{0}	6	5	5	-4.99	0	1	(Acquaviva, et al., 2005)
c.607G>A	p.(Gly203Arg)	Exon 3	*mut*^{0}	6	4	4	**-2.43**	0	0.999	(Fuchshuber, et al., 2000)
c.613_615del	p.(Glu205del)	Exon 3	*mut*^{0}	1	1	1				This study
c.622del	p.(Val208Tyrfs*15)	Exon 3	*mut*^{0}	1	1	1				(Peters, et al., 2002)
c.623_624del	p.(Val208Alafs*2)	Exon 3	*mut*^{0}	1	1	1				(Ostergaard, et al., 2005)
c.630del	p.(Glu211Argfs*12)	Exon 3	*mut*^{0}	1	1	1				This study
c.643G>A	p.(Gly215Ser)	Exon 3	*mut*^{0}	2	2	2	-5.98	0	1	(Acquaviva, et al., 2005)
c.654A>C	p.(Gln218His)	Exon 3	*mut*^{0}	6	5	5	-4.99	0	1	(Fuchshuber, et al., 2000)
c.655A>T	p.(Asn219Tyr)	Exon 3	*mut*^{0}	24	17	17	-7.98	0	1	(Acquaviva, et al., 2005)
c.682C>T	p.(Arg228*)	Exon 3	*mut*^{0}	1	1	1				(Acquaviva, et al., 2005)
c.683G>A	p.(Arg228Gln)	Exon 3	*mut*^{0}	1	1	1	-3.99	0	1	(Adjalla, et al., 1998)
c.689C>G	p.(Thr230Arg)	Exon 3	*mut*^{0}	4	2	2	-5.99	0	1	This study
c.691T>A	p.(Tyr231Asn)	Exon 3	*mut*$^-$	1	1	1	-8.48	0	1	(Janata, et al., 1997)
c.692dup	p.(Tyr231*)	Exon 3	*mut*^{0}	6	3	3				This study
c.693C>G	p.(Tyr231*)	Exon 3	*mut*^{0}	2	2	2				This study
c.729_730insTT	p.(Asp244Leufs*39)	Exon 3	*mut*^{0}	4	2	2				(Worgan, et al., 2006)
c.753+2T>A	splice site [g]	Intron 3	*mut*^{0}	2	2	2				(Worgan, et al., 2006)
c.786T>G	p.(Ser262Arg)	Exon 4	*mut*^{0}	1	1	1	-4.99	0	1	(Yi, et al., 2011)
c.828G>C	p.(Glu276Asp)	Exon 4	*mut*$^-$	1	1	1	-2.99	0.001	1	This study
c.850G>A	p.(Gly284Arg)	Exon 4	*mut*^{0}	1	1	1	-7.99	0	1	This study
c.851G>A	p.(Gly284Glu)	Exon 4	*mut*^{0}	1	1	1	-7.99	0	1	This study
c.862T>C	p.(Ser288Pro)	Exon 4	*mut*^{0}	3	2	2	**-1.1**	0.003	**0.012**	(Lempp, et al., 2007)
c.914T>C	p.(Leu305Ser)	Exon 5	*mut*^{0}	2	1	1	-5.75	0	1	(Worgan, et al., 2006)
c.927G>A	p.(Trp309*)	Exon 5	*mut*^{0}	1	1	1				This study
c.974G>A	p.(Gly325Asp)	Exon 5	ND	2	2	1	-2.65	0	0.998	This study
c.977G>A	p.(Arg326Lys)	Exon 5	ND	1	1	1	-3	0	1	This study
c.982C>T	p.(Leu328Phe)	Exon 5	*mut*^{0}	9	5	5	-3.89	0.001	1	(Acquaviva, et al., 2005)
c.983T>C	p.(Leu328Pro)	Exon 5	*mut*^{0}	1	1	1	-6.87	0	1	(Martinez, et al., 2005)
c.1022dup	p.(Asn341Lysfs*20)	Exon 5	*mut*^{0}	1	1	1				(Worgan, et al., 2006)
c.1031C>T	p.(Ser344Phe)	Exon 5	*mut*$^-$	1	1	1	-5.96	0	1	(Lempp, et al., 2007)
c.1040T>G	p.(Leu347Arg)	Exon 5	*mut*^{0}	1	1	1	-5.99	0	1	(Worgan, et al., 2006)
c.1073T>C	p.(Leu358Pro)	Exon 5	*mut*^{0}	1	1	1	-6.53	0	1	(Merinero, et al., 2008)
c.1084-10A>G [h]	p.(Gln361_Asp362insIlePhe*)	Intron 5	*mut*$^-$	2	1	1				(Liu, et al., 2012)
c.1084-1G>A	splice site [g]	Intron 5	*mut*^{0}	2	1	1				This study

c.1084-2A>G	splice site [g]	Intron 5	*mut*^{0}	1	1	1				This study
c.1097A>G	p.(Asn366Ser)	Exon 6	*mut*$^-$	2	2	1	-4.95	0	1	(Lempp, et al., 2007)
c.1105C>T	p.(Arg369Cys)	Exon 6	*mut*^{0}	2	2	2	-7.92	0	1	(Jung, et al., 2005)
c.1106G>A	p.(Arg369His)	Exon 6	*mut*^{0}	23	16	15	-4.95	0	1	(Janata, et al., 1997)
c.1130C>A	p.(Ala377Glu) [j]	Exon 6	*mut*^{0}	2	1	1	-4.53	0	1	(Jansen and Ledley, 1990)
c.1157A>G	p.(His386Arg)	Exon 6	*mut*^{0}	1	1	1	-7.92	0	1	(Worgan, et al., 2006)
c.1160C>T	p.(Thr387Ile)	Exon 6	*mut*$^-$	4	2	1	-5.94	0	1	(Dundar, et al., 2012)
c.1164T>A	p.(Asn388Lys)	Exon 6	*mut*^{0}	2	1	1	-5.94	0	1	This study
c.1181dup	p.(Leu394Phefs*30)	Exon 6	*mut*^{0}	1	1	1				This study
c.1207C>T	p.(Arg403*)	Exon 6	*mut*^{0}	10	8	7				(Peters, et al., 2002)
c.1271C>T	p.(Pro424Leu)	Exon 6	*mut*^{0}	2	1	1	-9.9	0.005	1	This study
c.1276G>A	p.(Gly426Arg)	Exon 6	*mut*$^-$	1	1	1	-5.68	0	1	(Worgan, et al., 2006)
c.1277G>A	p.(Gly426Glu)	Exon 6	*mut*$^-$	2	1	1	-5.68	0	1	This study
c.1333-24_1333-13del [h]	p.(Lys444_Leu445insPheSerPhe*)	Intron 6	*mut*^{0}	2	1	1				This study
c.1361G>A	p.(Gly454Glu)	Exon 7	*mut*^{0}	1	1	1	-7.93	0	1	(Lempp, et al., 2007)
c.1420C>T [k]	p.(Arg474*)	Exon 7	*mut*^{0}	4	3	3				(Acquaviva, et al., 2005)
c.1489G>T	p.(Glu497*)	Exon 7	*mut*^{0}	1	1	1				This study
c.1531C>T	p.(Arg511*)	Exon 8	*mut*^{0}	5	3	3				(Acquaviva, et al., 2005)
c.1541del	p.(Gln514Argfs*24)	Exon 8	*mut*^{0}	1	1	1				(Worgan, et al., 2006)
c.1655C>T	p.(Ala552Val)	Exon 9	ND	1	1	1	-3.61	0.003	0.98	This study
c.1658del	p.(Val553Glyfs*17)	Exon 9	*mut*^{0}	2	1	1				(Acquaviva, et al., 2005)
c.1677-1G>C	splice site [g]	Intron 9	*mut*^{0}	4	4	4				(Acquaviva, et al., 2005)
c.1677_1747dup [m]	p.(Val583Aspfs*11)	Exon 10	*mut*^{0}	1	1	1				This study
c.1747_1808del [n] (c.1808G>A)	p.(Val583Glyfs*3) (p.(Arg603Lys))	Exon 10	*mut*^{0}	2	1	1	**(-0.25)**	**(0.915)**	**(0.002)**	(Martinez, et al., 2005)
c.1843C>A	p.(Pro615Thr)	Exon 11	*mut*^{0}	9	5	5	-7.82	0	0.998	(Peters, et al., 2002)
c.1844C>T	p.(Pro615Leu)	Exon 11	*mut*^{0}	4	3	3	-9.78	0.013	0.981	(Dundar, et al., 2012)
c.1853T>C	p.(Leu618Pro)	Exon 11	ND	1	1	1	-6.32	0	1	This study
c.1871A>G	p.(Gln624Arg)	Exon 11	*mut*^{0}	2	1	1	-3.85	0.001	0.999	(Acquaviva, et al., 2005)
c.1874A>T	p.(Asp625Val)	Exon 11	*mut*^{0}	2	1	1	-8.82	0	1	(Dundar, et al., 2012)
c.1874A>G	p.(Asp625Gly)	Exon 11	*mut*^{0}	2	1	1	-6.86	0	1	This study
c.1889G>A	p.(Gly630Glu)	Exon 11	*mut*^{0}	4	4	4	-7.84	0	1	(Crane and Ledley, 1994)
c.1898T>G	p.(Val633Gly)	Exon 11	*mut*$^-$	1	1	1	-6.8	0	1	(Adjalla, et al., 1998)

c.1962_1963del	p.(Arg655*)	Exon 12	*mut*^{0}	4	2	2				(Dundar, et al., 2012)
c.1975C>T	p.(Gln659*)	Exon 12	ND	2	1	1				This study
c.2009del	p.(Gly670Alafs*2)	Exon 12	*mut*^{0}	1	1	1				(Fuchshuber, et al., 2000)
c.2020C>T	p.(Leu674Phe)	Exon 12	*mut*$^-$	2	1	1	-2.98	0.003	1	(Dundar, et al., 2012)
c.2053_2055dup	p.(Leu685dup)	Exon 12	*mut*^{0}	2	2	2				(Adjalla, et al., 1998)
c.2078del	p.(Gly693Aspfs*12)	Exon 12	*mut*^{0}	2	1	1				This study
c.2080C>T	p.(Arg694Trp)	Exon 12	*mut*$^-$	11	7	7	-5.15	0.001	1	(Crane and Ledley, 1994)
c.2081G>T	p.(Arg694L)	Exon 12	*mut*$^-$	3	2	2	-4.09	0.007	0.938	(Lempp, et al., 2007)
c.2099T>A	p.(Met700Lys)	Exon 12	*mut*$^-$	3	3	3	-3.36	0	**0.146**	(Acquaviva, et al., 2005)
c.2150G>T	p.(Gly717Val)	Exon 13	*mut*$^-$	2	2	2	-8.82	0	1	(Crane, et al., 1992)
c.2159_2160del	p.(Asn720Serfs*17) [l]	Exon 13	*mut*^{0}	2	1	1				(Worgan, et al., 2006)
c.2179C>T	p.(Arg727*)	Exon 13	*mut*^{0}	10	7	6				(Worgan, et al., 2006)
c.2193_2196dup	p.(Val733Cysfs*6)	Exon 13	*mut*^{0}	1	1	1				This study
c.2194_2197delinsTGGAA	p.(Ala732Trpfs*6)	Exon 13	ND	2	2	2				This study
c.2200C>T	p.(Gln734*)	Exon 13	*mut*^{0}	1	1	1				This study
c.2206C>T	p.(Leu736Phe)	Exon 13	*mut*$^-$	1	1	1	-2.82	0.001	0.786	(Forny, et al., 2014)

Table Footnotes:

[a] According to cDNA sequence NM_000255.3. Sequencing of mutations was performed according to (Lempp, et al., 2007).

[b] According to amino acid sequence NP_000246.2.

[c] Since in patient cells the two present alleles cannot be tested individually but only in combination, we assigned in our study the *mut* subclass to the alleles as follows: 1) In homozygous cell lines both alleles were assigned the same subtype as the tested patient cell line; 2) in a heterozygous mut^0 cell line, both alleles were assigned mut^0; 3) in a heterozygous mut^- cell line, the first allele was assigned mut^-, if the second one was a known mut^0 allele; 4) previously determined alleles were assigned the same *mut* class in all patient cell lines. ND, not defined.

[d] Protein Variation Effect Analyzer (PROVEAN) scores of missense mutations were calculated on http://provean.jcvi.org/. If the PROVEAN score is equal to or below a threshold of -2.5, the protein variant is predicted to have a "deleterious" effect. If the PROVEAN score is above the threshold, the variant is predicted to have a "neutral" effect (in bold) (Choi and Chan, 2015).

[e] SIFT scores (0-0.05 corresponds to amino acid changes that likely affect protein function, "benign" changes have a score of >0.05 and are in bold) of missense changes were calculated on the server http://sift.jcvi.org/ (Kumar, et al., 2009).

[f] PolyPhen-2 scores of missense changes were calculated on http://genetics.bwh.harvard.edu/pph2/. Scores above 0.432 are categorized as "probably damaging", scores below predict the variant as "benign" (in bold) (Adzhubei, et al., 2010).

[g] RT-PCR investigations did not reveal the effect of the mutation on transcript level.

[h] For splicing effect see text.

[j] Reported as p.(Ala378Glu) in reference.

[k] Reported as c.1423C>T in reference.

[l] Reported as p.(Asn720Serfs*14) in reference.

[m] This mutation in patient no. 141 was identified at the cDNA level, but was not confirmed at the genomic level.

[n] The major defect conferred by this variant was found to be splicing as detected on cDNA level (c.1747_1808del). The genomic mutation and its predicted protein change are given in brackets. For details see text.

Table 2. Summary of the patient cohort reports age of onset, biochemical data, *mut* class and genotype

Patient ID [a]	Age of onset (days) [b]	Propionate incorporation [c] (nmol/mg protein/10 or 16 h)			MUT activity [d] (pmol/min/mg protein)		Mutations	
		Medium -OHCbl	Medium +OHCbl	PI ratio (+OHCbl/ -OHCbl)	Assay -AdoCbl	Assay +AdoCbl	Nucleotide change [e]	Predicted protein change [f]
Patients classified as *mut*$^-$ in this study [a]								
18	5475	0.23	2.01	8.62	22*	182*	c.655A>T c.1898T>G	p.(Asn219Tyr) p.(Val633Gly)
128	n.r.	0.73	6.01	8.21	0	71	c.1207C>T c.2099T>A	p.(Arg403*) p.(Met700Lys)
125	NBS	0.79	5.71	7.22	15	352	c.655A>T c.828G>C	p.(Asn219Tyr) p.(Glu276Asp)
13	90	0.88	5.22	5.97	98*	142*	c.299A>G (hom)	p.(Tyr100Cys)
22	14	1.45	6.66	4.59	55*	88*	c.2099T>A c.623_624del	p.(Met700Lys) p.(Val208Alafs*2)
31	180	0.47	1.77	3.75	15*	36*	c.572C>A c.2099T>A	p.(Ala191Glu) p.(Met700Lys)
74	n.r.	1.46	5.43	3.72	32	105	c.1276G>A c.1655C>T	p.(Gly426Arg) p.(Ala552Val)
144	n.r.	0.73	2.65	3.64	9	35	c.1277G>A (hom)	p.(Gly426Glu)
121.1	5	0.70	2.51	3.61	16	18	c.1160C>T (hom)	p.(Thr387Ile)
16	630	1.49	5.22	3.51	84*	163*	c.2081G>T c.1207C>T	p.(Arg694L) p.(Arg403*)
67	n.r.	2.54	8.23	3.24	50	199	c.753+2T>A c.2206C>T	splice site p.(Leu736Phe)
41	1095	2.03	6.28	3.09	20	63	c.566A>T (hom)	p.(Asn189Ile)
87	2	0.30	0.85	2.81	5	0	c.2020C>T (hom)	p.(Leu674Phe)
15.2	60	0.37	1.05	2.80	3*	2*	c.1097A>G c.1106G>A	p.(Asn366Ser) p.(Arg369His)

17	90	0.29	0.76	2.63	4*	8*	c.91C>T c.323G>A	p.(Arg31*) p.(Arg108His)
15.1	150	0.36	0.89	2.49	37*	87*	c.1097A>G c.1106G>A	p.(Asn366Ser) p.(Arg369His)
137	n.r.	4.62	10.59	2.29	205	159	c.977G>A c.2194_2197delinsTGGAA	p.(Arg326Lys) p.(Ala732Trpfs*6)
143	n.r.	0.50	1.13	2.27	33	832	c.1207C>T c.2150G>T	p.(Arg403*) p.(Gly717Val)
54.1	NBS	0.88	1.98	2.25	0	3	c.378C>A c.974G>A	p.(Asn126Lys) p.(Gly325Asp)
49	98	1.35	2.78	2.05	107	140	c.1084-10A>G (hom)	p.(Gln361_Asp362insIlePhe*)
36	NBS	2.74	5.53	2.02	24	37	c.572C>A (hom)	p.(Ala191Glu)
1	540	0.84	1.52	1.85	44*	80*	c.2080C>T (hom)	p.(Arg694Trp)
2	28	0.48	0.83	1.75	3*	34*	c.654A>C c.1106G>A	p.(Gln218His) p.(Arg369His)
37	n.r.	1.17	1.97	1.68	49	75	c.2080C>T (hom)	p.(Arg694Trp)
131	120	0.71	1.20	1.68			c.1022dup c.2150G>T	p.(Asn341Lysfs*20) p.(Gly717Val)
4	n.r.	0.83	1.43	1.67	26*	49*	c.2080C>T (hom)	p.(Arg694Trp)
9	210	1.59	2.61	1.66	11*	62*	c.1106G>A c.691T>A	p.(Arg369His) p.(Tyr231Asn)
21	90	0.75	1.25	1.63	30*	28*	c.2080C>T (hom)	p.(Arg694Trp)
11	1095	0.58	0.88	1.55	19*	29*	c.1031C>T [g]	p.(Ser344Phe)
54.2	n.r.						c.378C>A c.974G>A	p.(Asn126Lys) p.(Gly325Asp)
121.2	n.r.						c.1160C>T (hom)	p.(Thr387Ile)
140	420						c.2081G>T (hom)	p.(Arg694Leu)
Patients classified as *mut*^{0} in this study [a]								
130 [h]	270	1.06	1.67	1.57	5*	11*	c.1531C>T (hom)	p.(Arg511*)
76	510	0.13	0.20	1.50	5*	10*	c.927G>A c.983T>C	p.(Trp309*) p.(Leu328Pro)
101	n.r.	0.77	1.12	1.45	0*	17*	c.654A>C c.1106G>A	p.(Gln218His) p.(Arg369His)

154	n.r.	0.71	0.95	1.34	86	69	c.2T>C c.850G>A	p.(Met1?) p.(Gly284Arg)
73	n.r.	0.91	1.22	1.34	29	45	c.1871A>G (hom)	p.(Gln624Arg)
142	4	1.06	1.40	1.33	49	24	c.1658del (hom)	p.(Val553Glyfs*17)
145	n.r.	0.61	0.81	1.33	5	0	c.1271C>T (hom)	p.(Pro424Leu)
89	n.r.	0.83	1.09	1.32	35	1	c.1874A>G (hom)	p.(Asp625Gly)
45	300	0.25	0.32	1.27	0	4	c.654A>C (hom)	p.(Gln218His)
80	NBS	0.54	0.68	1.26	1*	20*	c.1106G>A (hom)	p.(Arg369His)
152	n.r.	0.51	0.64	1.26	0	0	c.654A>C c.655A>T	p.(Gln218His) p.(Asn219Tyr)
149	n.r.	0.61	0.76	1.25	7	6	c.91C>T c.2080C>T	p.(Arg31*) p.(Arg694Trp)
63	n.r.	0.76	0.94	1.24	0	0	c.982C>T (hom)	p.(Leu328Phe)
153	n.r.	0.33	0.40	1.23	0	6	c.862T>C c.1157A>G	p.(Ser288Pro) p.(His386Arg)
141	n.r.	0.82	0.99	1.21	59	52	c.129G>A c.1677_1747dup	p.(Trp43*) p.(Val583Aspfs*11)
48	n.r.	0.58	0.70	1.21	251	219	c.397G>A (hom)	p.(Gly133Arg)
47	210	0.36	0.43	1.19	125	96	c.689C>G (hom)	p.(Thr230Arg)
34	2	0.34	0.40	1.16	40*	37*	c.1106G>A c.2009del	p.(Arg369His) p.(Gly670Alafs*2)
102	21	0.57	0.66	1.16	12*	11*	c.394C>T c.655A>T	p.(Gln132*) p.(Asn219Tyr)
39	n.r.	1.41	1.62	1.15	65*	37*	c.655A>T (hom)	p.(Asn219Lys)
50	n.r.	0.58	0.67	1.14	172	177	c.786T>G c.1889G>A	p.(Ser262Arg) p.(Gly630Glu)
65	540	0.94	1.07	1.14	0	0	c.91C>T c.2053_2055dup	p.(Arg31*) p.(Leu685dup)
14	42	0.89	1.01	1.14	14*	5*	c.1361G>A c.427C>T	p.(Gly454Glu) p.(His143Tyr)
139	3	0.49	0.56	1.13			c.729_730insTT (hom)	p.(Asp244Leufs*39)
126	n.r.	1.94	2.16	1.11			c.91C>T (hom)	p.(Arg31*)
129	n.r.	0.61	0.67	1.10	113	42	c.160A>T (hom)	p.(Lys54*)
60	n.r.	0.72	0.80	1.10	120	116	c.421del (hom)	p.(Ala141Argfs*39)

122	n.r.	0.58	0.63	1.09	0	2	c.692dup (hom)	p.(Tyr231*)
66	5	1.17	1.26	1.08	0	0	c.1106G>A (hom)	p.(Arg369His)
136	n.r.	0.74	0.80	1.08			c.544dup (hom)	p.(Met182Asnfs*29)
68	n.r.	0.73	0.79	1.08			c.692dup (hom)	p.(Tyr231*)
8	1	1.83	1.97	1.08	0*	21*	c.982C>T (hom)	p.(Leu328Phe)
38	5	0.44	0.48	1.07	22*	27*	c.2159_2160del (hom)	p.(Asn720Serfs*17)
88	n.r.	0.24	0.25	1.07	2*	12*	c.1843C>A (hom)	p.(Pro615Thr)
5	42	0.49	0.52	1.06	118*	139*	c.2080C>T c.1677-1G>C	p.(Arg694Trp) splice site
32	150	0.76	0.81	1.06	38*	26*	c.655A>T (hom)	p.(Asn219Tyr)
150	n.r.	0.72	0.76	1.06	41	23	c.682C>T c.1181dup	p.(Arg228*) p.(Leu394Phefs*30)
83	n.r.	0.62	0.65	1.06	126	90	c.1130C>A (hom)	p.(A377Glu)
84	n.r.	0.72	0.76	1.05	24	14	c.88C>T c.521T>C	p.(Gln30*) p.(Phe174Ser)
116	3	2.45	2.58	1.05	0	18	c.560C>G (hom)	p.(Thr187Ser)
113	n.r.	0.91	0.95	1.05	85	84	c.1843C>A (hom)	p.(Pro615Thr)
71	n.r.	0.65	0.67	1.04	263	264	c.1489G>T c.2193_2196dup	p.(Glu497*) p.(Val733Cysfs*6)
99	3	0.49	0.51	1.04	3	3	c.30dup c.1040T>G	p.(Leu11Thrfs*38) p.(Leu347Arg)
91	n.r.	0.99	1.02	1.03	75	71	c.1106G>A (hom)	p.(Arg369His)
25	3	2.08	2.11	1.03	28*	0*	c.655A>T c.1420C>T	p.(Asn219Tyr) p.(Arg474*)
96	7	0.41	0.42	1.02	11	32	c.278G>A (hom)	p.(Arg93His)
75	21	1.30	1.33	1.02	22	29	c.322C>T c.1531C>T	p.(Arg108Cys) p.(Arg511*)
92	n.r.	0.29	0.29	1.02	6*	11*	c.982C>T (hom)	p.(Leu328Phe)
155	n.r.	0.92	0.94	1.02	91	86	c.360dup c.2179C>T	p.(Lys121*) p.(Arg727*)
19	3	1.06	1.08	1.02	39*	62*	c.2080C>T c.1677-1G>C	p.(Arg694Trp) splice site
61	n.r.	0.57	0.57	1.01	10	5	c.1843C>A c.2179C>T	p.(Pro615Thr) p.(Arg727*)

133	n.r.	0.41	0.42	1.01	20	24	c.655A>T c.1889G>A	p.(Asn219Tyr) p.(Gly630Glu)
7	3	0.22	0.22	1.00	64*	69*	c.607G>A c.1106G>A	p.(Gly203Arg) p.(Arg369His)
108	n.r.	0.49	0.49	0.99			c.330T>G c.630del	p.(Tyr110*) p.(Glu211Argfs*12)
138	2	0.57	0.57	0.99	139	134	c.683G>A c.2200C>T	p.(Arg228Gln) p.(Gln734*)
51	n.r.	0.53	0.53	0.99	190	159	c.-39-1G>A (hom)	splice site
64	n.r.	0.85	0.84	0.99	0	2	c.982C>T (hom)	p.(Leu328Phe)
132	n.r.	0.74	0.73	0.99	7*	7*	c.1962_1963del (hom)	p.(Arg655*)
117	10	0.90	0.89	0.98	89	89	c.1084-1G>A (hom)	splice site
35	2	0.64	0.62	0.98	17*	15*	c.654A>C c.1677-1G>C	p.(Gln218His) splice site
90	n.r.	0.92	0.90	0.98	138	91	c.481G>A (hom)	p.(Gly161Arg)
26	3	0.39	0.39	0.98	34*	10*	c.443C>T c.1677-1G>C	p.(Ser148Leu) splice site
86	n.r.	1.18	1.15	0.98	6*	13*	c.693C>G c.1106G>A	p.(Tyr231*) p.(Arg369His)
10	390	1.05	1.03	0.98	30*	0*	c.1106G>A (hom)	p.(Arg369His)
46	2	0.30	0.29	0.97	160	145	c.1962_1963del (hom)	p.(Arg655*)
12	42	2.19	2.12	0.97	0*	0*	c.607G>A (hom)	p.(Gly203Arg)
58	7	0.51	0.49	0.96	2	0	c.572C>A c.1541del	p.(Ala191Glu) p.(Gln514Argfs*24)
123	5	0.88	0.84	0.96			c.655A>T (hom)	p.(Asn219Tyr)
27	3	1.60	1.54	0.96	4*	19*	c.655A>T (hom)	p.(Asn219Tyr)
52	150	0.35	0.34	0.96	135	130	c.914T>C (hom)	p.(Leu305Ser)
56	7	0.81	0.78	0.96	22	30	c.55dup (hom)	p.(Val19Glyfs*30)
3	1	1.61	1.54	0.96	12*	0*	c.1106G>A (hom)	p.(Arg369His)
55	n.r.	0.77	0.74	0.96	145	156	c.2179C>T (hom)	p.(Arg727*)
115	120	3.39	3.23	0.95	34	23	c.729_730insTT (hom)	p.(Asp244Leufs*39)
97	330	0.66	0.63	0.95	6	1	c.1207C>T c.1889G>A	p.(Arg403*) p.(Gly630Glu)

6	3	0.32	0.29	0.95	77*	4*	c.410C>T c.655A>T	p.(Ala137Val) p.(Asn219Tyr)
72	n.r.	0.91	0.85	0.94	6*	12*	c.1420C>T (hom)	p.(Arg474*)
40	1	0.24	0.22	0.92	34	24	c.1747_1808del (hom) (c.1808G>A)	p.(Val583Glyfs*3) (p.(Arg603Lys))
44	3	0.16	0.15	0.92	0	0	c.88C>T (hom)	p.(Gln30*)
148.1	n.r.	0.66	0.61	0.92	16	102	c.1207C>T (hom)	p.(Arg403*)
82	n.r.	1.00	0.91	0.92	7*	14*	c.622del c.2053_2055dup	p.(Val208Tyrfs*15) p.(Leu685dup)
28	5	0.66	0.60	0.91	8*	0*	c.1843C>A (hom)	p.(Pro615Thr)
85	4	0.60	0.55	0.91	16	9	c.689C>G (hom)	p.(Thr230Arg)
53	n.r.	0.76	0.69	0.91	94	64	c.1164T>A (hom)	p.(Asn388Lys)
81.1	n.r.	1.61	1.45	0.90	1*	65*	c.2179C>T (hom)	p.(Arg727*)
57	30	0.58	0.50	0.87	39	61	c.851G>A c.982C>T	p.(Gly284Glu) p.(Leu328Phe)
98	n.r.	0.40	0.33	0.83	42	29	c.1531C>T (hom)	p.(Arg511*)
59	4	0.71	0.59	0.83	124	117	c.1874A>T (hom)	p.(Asp625Val)
119	3	0.41	0.34	0.83	87	83	c.613_615del c.1420C>T	p.(Glu205del) p.(Arg474*)
95	8	0.76	0.62	0.81	30*	25*	c.607G>A (hom)	p.(Gly203Arg)
93	570	1.82	1.46	0.81	12*	23*	c.1084-10A>G c.1333-24_1333-13del	p.(Gln361_Asn362insIlePhe*) p.(Lys444_Leu445insPheSer-Phe*)
151	n.r.	1.23	0.98	0.80			c.753+2T>A c.1084-2A>G	splice site splice site
147	2	0.67	0.52	0.78			c.1106G>A (hom)	p.(Arg369His)
33	120	1.13	0.86	0.76	85*	25*	c.655A>T c.1889G>A	p.(Asn219Tyr) p.(Gly630Glu)
94	90	0.33	0.24	0.72	16*	12*	c.607G>A c.1105C>T	p.(Gly203Arg) p.(Arg369Cys)
24	180	0.13	0.09	0.68	16*	13*	c.655A>T (hom)	p.(Asn219Tyr)
20	n.r.	0.25	0.12	0.50	37*	67*	c.862T>C (hom)	p.(Ser288Pro)
104	14	0.31	0.12	0.40	27*	18*	c.2078del (hom)	p.(Gly693Aspfs*12)
62	n.r.				48	63	c.692dup (hom)	p.(Tyr231*)

78	n.r.						c.1843C>A (hom)	p.(Pro615Thr)
79	n.r.						c.1105C>T c.1207C>T	p.(Arg369Cys) p.(Arg403*)
81.2	n.r.						c.2179C>T (hom)	p.(Arg727*)
105	n.r.						c.643G>A c.2179C>T	p.(Gly215Ser) p.(Arg727*)
106	n.r.						c.655A>T c.1106G>A	p.(Asn219Tyr) p.(Arg369His)
107	n.r.						c.1073T>C c.1844C>T	p.(Leu358Pro) p.(Pro615Leu)
110	n.r.						c.1844C>T (hom)	p.(Pro615Leu)
111	n.r.						c.572C>A c.1207C>T	p.Ala191Glu) p.(Arg403*)
114	n.r.						c.655A>T (hom)	p.(Asn219Tyr)
120.1	3						c.129G>A (hom)	p.(Trp43*)
120.2	n.r.						c.129G>A (hom)	p.(Trp43*)
127	360						c.655A>T (hom)	p.(Asn219Tyr)
134	n.r.						c.643G>A c.2179C>T	p.(Gly215Ser) p.(Arg727*)
148.2	n.r.						c.1207C>T (hom)	p.(Arg403*)
156	n.r.						c.1106G>A (hom)	p.(Arg369His)
Patients with undefined *mut* subclass in this study [a]								
109	n.r.						c.655A>T c.2194_2197delinsTGGAA	p.(Asn219Tyr) p.(Ala732Trpfs*6)
112	n.r.						c.1844C>T c.1853T>C	p.(Pro615Leu) p.(Leu618Pro)
118	n.r.						c.415G>A c.572C>A	p.(Asp139Asn) p.(Ala191Glu)
124	2						c.467A>T (hom)	p.(Asp156Val)
135	n.r.						c.1975C>T (hom)	p.(Gln659*)

Table Footnotes:

[a] Patients are listed according to decreasing PI ratio, separated into the *mut* subclasses as follows: Patients were assigned to the *mut*$^-$ class when the PI assay showed a ratio of >1.5 and to the *mut*^{0} class when the ratio was ≤1.5. Five patients had an undefined *mut* subclass. Patient ID numbers are not incremental. If there are siblings, the index patient is indicated by the suffix .1. Patients 1-35 correspond to (Lempp, et al., 2007), where patient 15.1. is 15 and 15.2 is 15.1.

[b] Some patients were detected during newborn screening (NBS) without being symptomatic. "n. r." means the age of onset was not reported.

[c] Results from PI assay are given as absolute values and ratio of incorporation of ^{14}C-propionate in patient fibroblasts cultured in supplemented (1 or 10 mg OHCbl (+OHCbl)) and un-supplemented medium (-OHCbl). Numbers represent means of duplicate values from 1-4 replicate experiments. Control values (mean ±SD from *n* = 110 experiments) in wild-type fibroblasts from healthy controls are: -OHCbl, 9.25 ±3.43; +OHCbl, 10.90 ±4.19; ratio, 1.19 ±0.17. For patients 5, 7, 19, 20, 31, 34 and 35 at least one experiment has the control values (mean ±SD from *n* = 32 experiments): -OHCbl, 3.54 ±1.71; +OHCbl, 3.64 ±1.80; ratio, 1.03 ±0.09.

[d] Methylmalonyl-CoA mutase activity was assayed with (+AdoCbl) and without AdoCbl (-AdoCbl) in crude homogenates of patient fibroblasts, which were grown for one passage in medium supplemented with 1 mg of OHCbl (except for patients no. 62 and 86, where no OHCbl was added to the medium). Numbers represent means of duplicate values from one or two experiments. Empty fields mean no data available. Most values were generated by the method described in (Forny, et al., 2014) and correspond to the following control values (mean ±SD from *n* = 49 experiments): -AdoCbl, 1058 ±381; +AdoCbl, 2569 ±782. Values which were generated by the method described in (Baumgartner, 1983) are indicated by asterisks (*) and have the following controls (mean ±SD from *n* = 48 experiments): -AdoCbl, 454 ±229; +AdoCbl, 1085 ±516.

[e] According to cDNA sequence NM_000255.3. For heterozygous patients both mutations are given. Homozygous patients are indicated by "hom".

[f] According to amino acid sequence NP_000246.2.

[g] Only one mutation identified.

[h] This patient carries a known *mut*^{0} mutation in a homozygous state and was therefore classified as *mut*^{0}.

3.12 Supplementary Figures

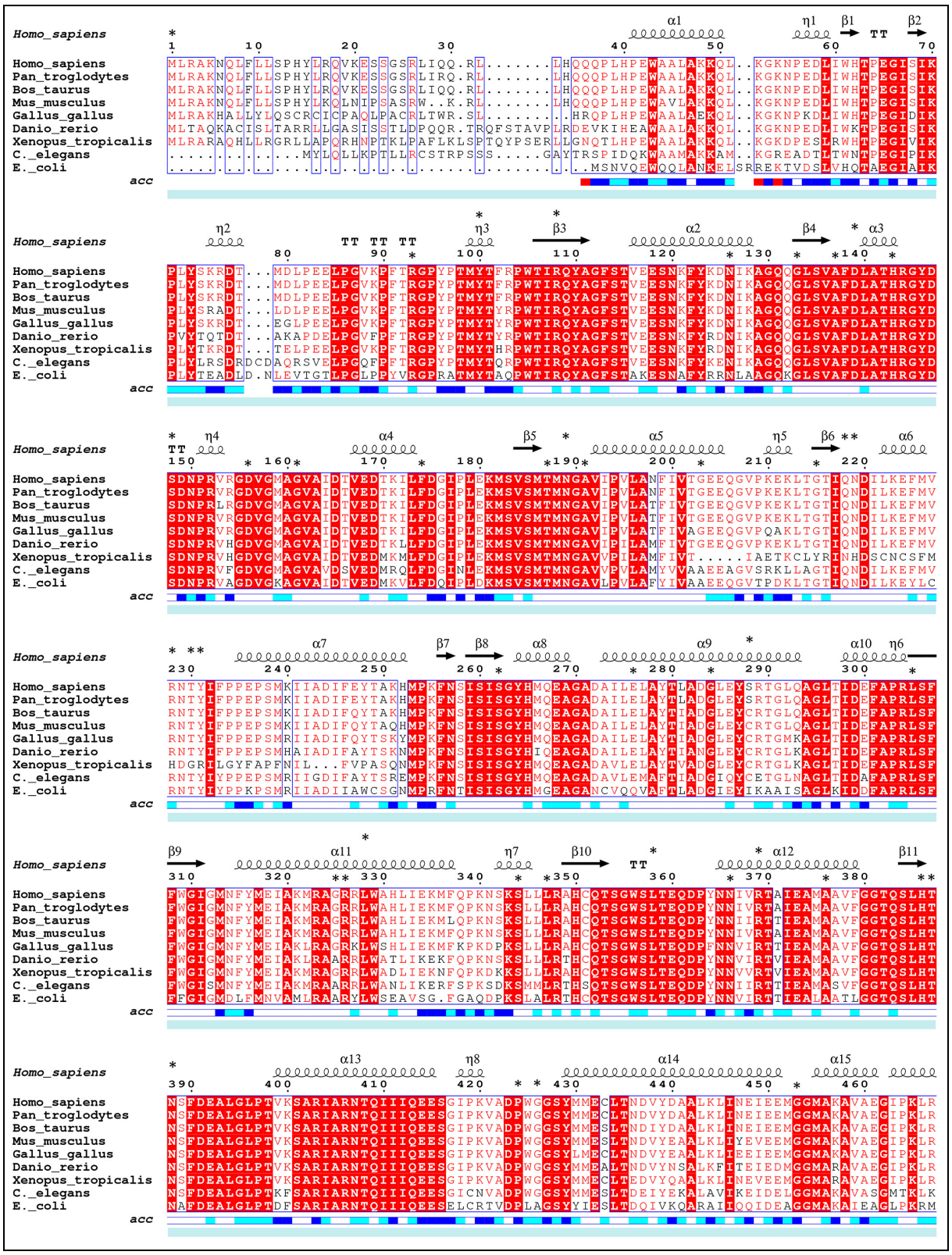

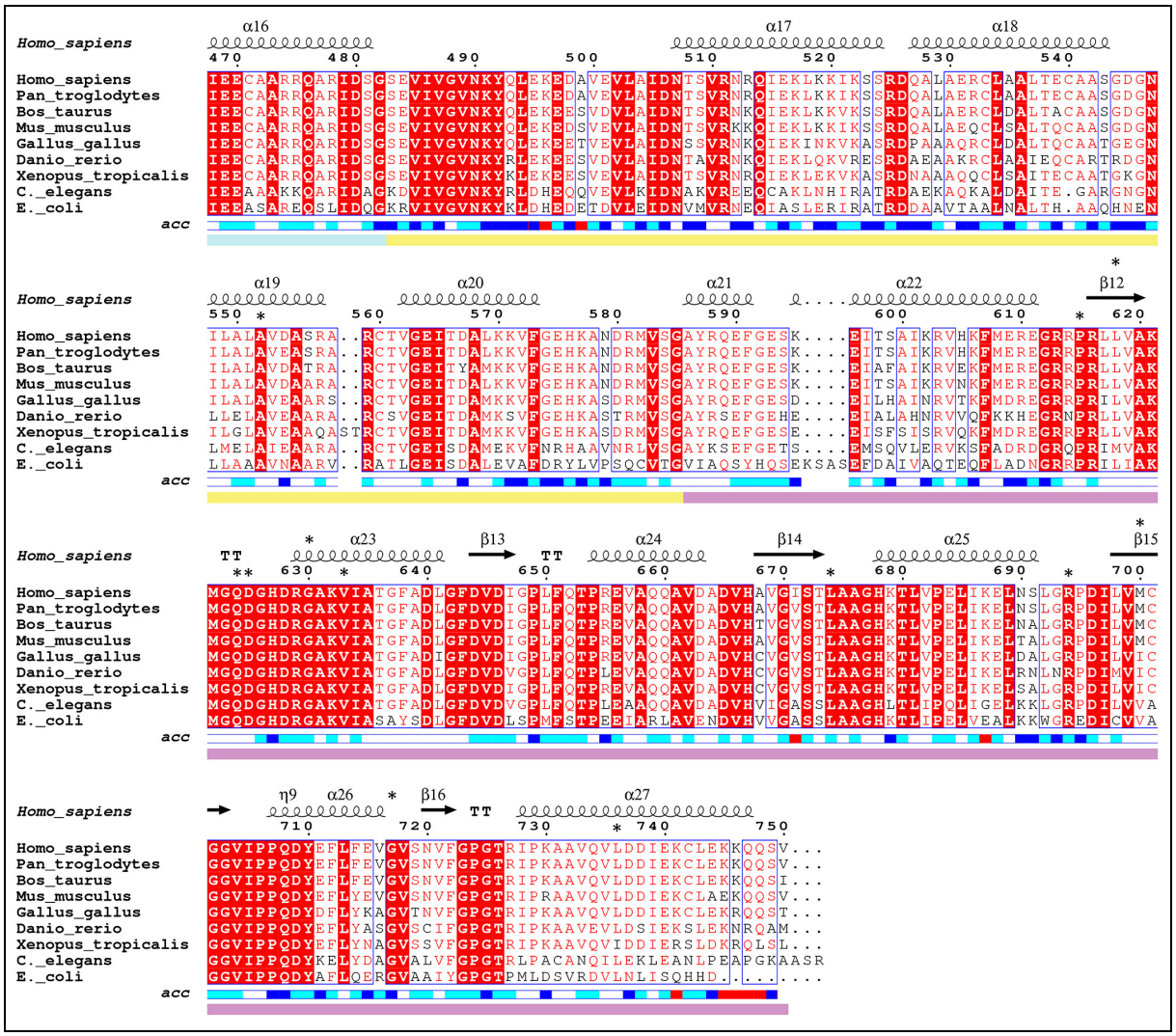

Supp. Figure S1. Sequence alignment of MUT from human to *E. coli*. Protein sequences of *Homo sapiens* (Homo_sapiens, NP_000246.2), *Pan troglodytes* (Pan_troglodytes, XP_001146876.1), *Bos taurus* (Bos_taurus, NP_776364.2), *Mus musculus* (Mus_musculus, NP_032676.2), *Gallus gallus* (Gallus_gallus, XP_420055.1), *Danio rerio* (Danio_rerio, NP_001092696.1), *Xenopus tropicalis* (Xenopus_tropicalis, XP_002933609.2), *Caenorhabditis elegans* (C._elegans, NP_497786.2), *Escherichia coli* (E._coli, WP_000073223.1) were used to create a multiple sequence alignment created by multalin (Corpet, 1988) and visualized by usage of the ESPript 3.0 server (Robert and Gouet, 2014). Strictly conserved residues are marked in red shading, well conserved residues in red font. Missense mutations are marked by black asterisks. Secondary structure elements from the human MUT structure (PDB ID: 2XIQ) are indicated at the top of the alignment: α- and 3_{10}-helices (represented by the η symbol) are displayed as squiggles, β-strands are rendered as arrows, strict β-turns as TT letters. The relative surface accessibility of each residue is indicated by the color in the row "acc": blue, accessible; cyan, intermediate; white, buried; red, accessibility is not predicted. Schematic protein domains are colored according to Fig. 1B: light blue, N-terminal domain; yellow, inter-domain linker; magenta, C-terminal domain.

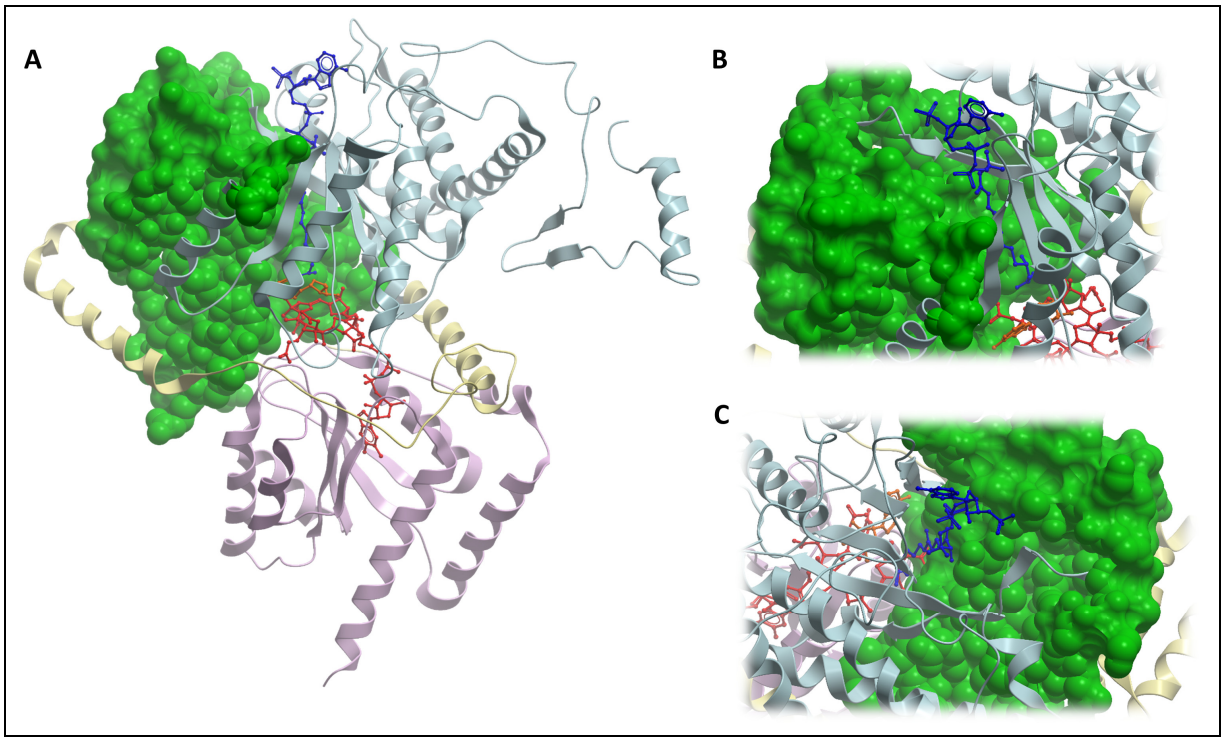

Supp. Figure S2. MUT structure with highlighted region which corresponds to exon 3. A. Human MUT structure with coloring according to domains: light blue, N-terminal domain; yellow, inter-domain linker; magenta, C-terminal domain. Ligands are in sticks: dark blue, malonyl-CoA (substrate analogue); red, cobalamin; orange, adenosyl moiety. The green space fill region represents the segment of the polypeptide chain which corresponds to the area of exon 3. **B.** and **C.** A magnified view onto the malonyl-CoA ligand reveals that one side of the binding channel for the substrate is built by amino acids encoded by exon 3.

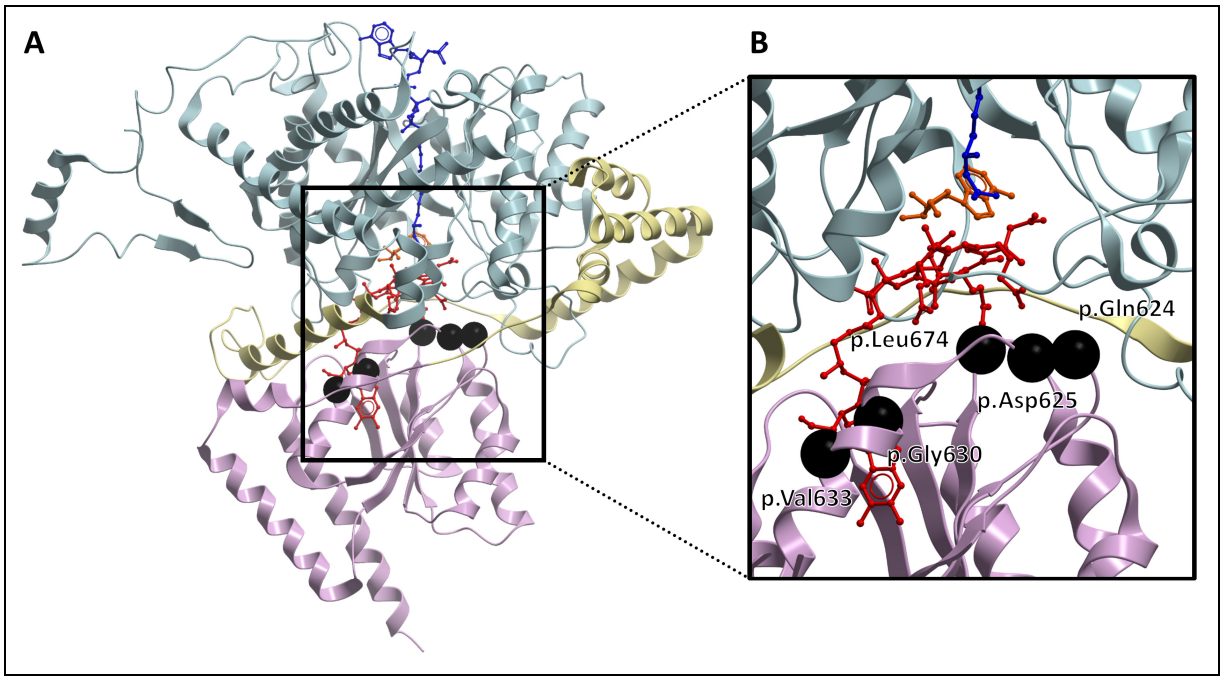

Supp. Figure S3. Structural mapping of *mut*⁻ missense mutations which show high MUT protein levels in Western blot quantification. A. MUT structure in complex with malonyl-CoA (dark blue) in the N-terminal domain (light blue) and cobalamin (red) with adenosyl moiety (orange) in the C-terminal domain (magenta). Linker domain in yellow. Black balls represent residues of missense mutations, which were found to have high residual MUT levels in Fig. 3 and are discussed in the section "Biological Significance". From left to right (on residue p.Asp625 two mutations were found): p.Val633, p.Gly630, p.Leu674, p.Asp625, p.Gln624. **B.** Magnified region of the five residues. The parts of the protein structure, which block the view onto the area of interest, are clipped off.

4 CHAPTER II: MOLECULAR CHARACTERIZATION OF MISSENSE MUTATIONS IN MUT

This section represents an article which was published in 2014 during the PhD project (Forny, et al., 2014). Citations in this chapter correlate to the bibliography section at the end of the thesis. Figure and table numbering is only applicable to this section of the thesis.

FUNCTIONAL CHARACTERIZATION AND CATEGORIZATION OF MISSENSE MUTATIONS THAT CAUSE METHYLMALONYL-COA MUTASE (MUT) DEFICIENCY

Patrick Forny[1,2,*], D Sean Froese[1,3,*], Terttu Suormala[1], Wyatt W Yue[3,#], Matthias R Baumgartner[1,2,#]

[1] Division of Metabolism and Children's Research Center, University Children's Hospital, Zurich, Switzerland CH-8032

[2] Zurich Center for Integrative Human Physiology, University of Zurich, Switzerland

[3] Structural Genomics Consortium, University of Oxford, UK OX3 7DQ

[*] P.F. and D.S.F. contributed equally to this work.

[#] To whom correspondence may be addressed:

Matthias R Baumgartner, matthias.baumgartner@kispi.uzh.ch

Wyatt W Yue, wyatt.yue@sgc.ox.ac.uk

The authors declare no conflict of interest.

4.1 ABSTRACT

Methylmalonyl-CoA mutase (MUT) is an essential enzyme in propionate catabolism that requires adenosylcobalamin as cofactor. Almost 250 inherited mutations in the *MUT* gene are known to cause the devastating disorder methylmalonic aciduria; however, the mechanism of dysfunction of these mutations, more than half of which are missense changes, has not been thoroughly investigated. Here, we examined 23 patient missense mutations covering a spectrum of exonic/structural regions, clinical phenotypes and ethnic populations in order to determine their influence on *protein stability*, using two recombinant expression systems and a thermostability assay; and *enzymatic function*, by measuring MUT activity and affinity for its cofactor and substrate. Our data stratify MUT missense mutations into categories of biochemical defects, including: (i) reduced protein level due to misfolding, (ii) increased thermolability, (iii) impaired enzyme activity, and (iv) reduced cofactor response in substrate turnover. We further demonstrate the stabilization of wild-type and thermolabile mutants by chemical chaperones *in vitro* and in bacterial cells. This in-depth mutation study illustrates the tools available for MUT enzyme characterization, guides future categorization of further missense mutations and supports the development of alternative, chaperone-based therapy for patients not responding to current treatment.

4.2 KEY WORDS

inborn errors of metabolism, methylmalonic aciduria, methylmalonyl-CoA mutase (MUT), cobalamin, missense mutations, thermolability

4.3 INTRODUCTION

Mitochondrial methylmalonyl-CoA mutase (MUT, EC 5.4.99.2) catalyzes the reversible isomerisation of L-methylmalonyl-CoA to succinyl-CoA, requiring vitamin B_{12} (cobalamin) in the form of adenosylcobalamin (AdoCbl) as cofactor. In humans, this reaction represents an important step in propionate catabolism, funnelling metabolites from the breakdown of amino acids (valine, isoleucine, methionine and threonine), odd-chain fatty acids, and the side chain of cholesterol into the tricarboxylic acid cycle (TCA cycle). The MUT enzyme is highly conserved from bacteria to human, and is well studied at the enzymatic (Banerjee and Ragsdale, 2003; Fenton, et al., 1982) and structural (Froese, et al., 2010b; Mancia, et al., 1996) level. The importance of the MUT-catalyzed reaction is further underlined by the metabolic disorder methylmalonic aciduria (MMAuria) which is caused by a genetic defect in the MUT enzyme itself (MIM# 251000, MMA *mut* type), or in one of several proteins (MMAA, MMAB, MMADHC,) involved in the uptake, modification and delivery of AdoCbl to the MUT enzyme

for its activity (MMA *cblA* type, MIM# 251100; MMA *cblB* type, MIM# 251110; MMA *cblD-variant 2* MIM# 277410) (Fowler, et al., 2008).

The human *MUT* gene (OMIM: 609058; chromosome location 6p12-21.2) (Ledley, et al., 1988a; Ledley, et al., 1988b) is the site of almost 250 deleterious mutations reported to cause MMAuria (Froese and Gravel, 2010) (human gene mutation database, HMGD Professional version as of December 2013, *hgmd.org*). Patient cell lines can be assigned to the *mut* type MMAuria by complementation analysis of fibroblast heterokaryons (Gravel, et al., 1975; Willard, et al., 1978a). Further biochemical characterization, applying MUT activity assay and propionate fixation, allows *mut* classification into two subtypes. Mutants with residual mutase activity in cell homogenates under saturating concentrations of AdoCbl, and whose ability to incorporate [1-^{14}C]propionate into acid precipitable material in intact skin fibroblasts is responsive to supplementation of the culture medium with hydroxocobalamin, are designated *mut*$^{-}$; mutants with no residual MUT activity and no response of propionate incorporation to hydroxocobalamin, are designated *mut*^{0} (Willard and Rosenberg, 1980). *mut*^{0} patients often present in the newborn period with ketoacidosis, lethargy, repeated vomiting, coma or even death, and suffer from severe long-term complications such as renal failure and neurological impairments. On the contrary, *mut*$^{-}$ patients have a lower occurrence of mortality, morbidity and long-term complications (Horster, et al., 2007). Dietary interventions, carnitine supplementation and symptom management are the mainstay of current treatment, although pharmacological doses of hydroxocobalamin are given to some MUT deficient patients (Horster, et al., 2007). While some *mut*$^{-}$ patients seem to respond to this treatment, others – including most if not all *mut*^{0} patients – do not (Horster, et al., 2007). Alternative therapeutic approaches should therefore be investigated, evaluating therapeutic potential on the basis of a systematic characterization of individual *mut*^{0} and *mut*$^{-}$ alleles. Nevertheless, the sheer quantity of mutations in the *MUT* gene – most of which are private and rare (Acquaviva, et al., 2005; Fowler, et al., 2008; Lempp, et al., 2007; Worgan, et al., 2006) – means that such a large-scale analysis has not been forthcoming, with previous reports of *in vitro* MUT characterization on only a handful of mutations, *e.g.* (Crane and Ledley, 1994; Janata, et al., 1997).

Common to many other metabolic disorders (*e.g.* phenylketonuria, PKU (Mitchell, et al., 2011); ornithine transcarbamylase deficiency (Shchelochkov, et al., 2009)), the largest proportion of *MUT* mutations are missense changes (131 out of 243, 54%; *hgmd.org*) whose effects on the protein are difficult to predict *a priori* (Froese and Gravel, 2010; Yue, et al., 2014). MUT is therefore an attractive target to interrogate the genotype-specific biochemical penalties for missense mutations at the protein level, an approach adopted for other metabolic enzymes (Pekkala, et al., 2010; Pey, et al., 2007; Shi, et al., 2012). With this in mind, we have chosen 7 *mut*^{0} and 16 *mut*$^{-}$ missense mutations for an in-depth analysis. Based on recombinant expression (*E. coli* and human fibroblasts), thermal denaturation and enzyme assays, we catalogue each mutation as defective in stability, activity or both, and further

define subcategories in each. To the best of our knowledge, this work represents the first large scale biochemical categorization of MUT mutations and sets the stage for exploring the potential of small molecule therapeutics, an approach that is gaining wide interest to augment mutant enzyme activity (Gomes, 2012).

4.4 Materials & Methods

4.4.1 Cloning

For expression in *E. coli* we used a previously described construct of MUT (called hMUT in (Froese, et al., 2010b)). For expression in fibroblasts, the MUT cDNA sequence was purchased from GeneCopoeia (Construct ID: E0205; RefSeq NM_000255.3) and subsequently subcloned into pTracer-CMV2 (Invitrogen) via *EcoRV* and *NotI* restriction sites by PCR, using the following primers: ACATA-GATATCCACGCTGTTTTGA (*EcoRV* site underlined) and AGTGGTTGATCGCGTGCATG (*NotI* site is part of the original GeneCopoeia plasmid), respectively. All single-site missense mutations were generated using the QuikChange site-directed mutagenesis kit (Stratagene) following manufacturer's instructions, using forward and reverse primers (Microsynth) described in Supp. Table S2, and confirmed by Sanger sequencing.

4.4.2 Bacterial expression and purification

MUT was expressed in *E. coli*, and purified as previously described (Froese, et al., 2010b) with minor modifications. For small scale purification, cells were grown in a total of 50 ml, induced with 0.1 mM IPTG at 18°C overnight, harvested by centrifugation at 4000 x*g*, lysed by sonication and purified by affinity (Ni-NTA; Qiagen) chromatography. Where applicable, chemical chaperones were added concurrently with the IPTG. Samples from total cell lysate (1 µl of 2 ml total) ('L'), including all cellular proteins both soluble and insoluble, and affinity eluants (15 µl of 250 µl total) ('E'), including those soluble proteins eluted from the nickel affinity column, were analyzed by SDS-PAGE and stained with Coomassie blue (Expedion). For large scale purification, cells were grown in a total of 6 l, harvested by centrifugation at 5000 x*g*, lysed with an Emulsiflex C3 homogenizer, and purified by affinity (Ni-NTA, Qiagen), size-exclusion (Superdex 200; GE Healthcare), cleavage with His-tagged TEV protease and reverse-affinity chromatography (Ni-NTA). Purification buffers are detailed in the webpage *http://www.thesgc.org/structures/details?pdbid=2XIQ*.

4.4.3 Transfection and expression in fibroblasts

Fibroblasts of a *mut*^{0} patient homozygous for the mutation p.Q30* were immortalized by transfection with pRNS1 (Litzkas, et al., 1984) using electroporation (Baumgartner, et al., 2001) and grown in

Dulbecco's Modified Eagle Medium (Gibco) supplemented with 10% fetal bovine serum (Gibco) and antibiotics (PAA), as previously described (Suormala, et al., 2004). pTracer-MUT *wt* and mutant constructs were transiently transfected into the immortalized fibroblasts by electroporation with a transfection efficiency of 6-24%, as determined by FACS measuring the proportion of cells co-expressing the green fluorescent protein from the pTracer construct. This is comparable to previous observations (Coelho, et al., 2008). Cells were harvested 48 hours after electroporation by trypsinization, washed twice with phosphate buffered saline and stored frozen at -80°C until assayed for MUT activity or used for Western blotting.

4.4.4 Western blot

Fibroblast lysates were obtained by sonication (details under MUT activity assay). Crude cell lysates (25 µg of protein per sample) were mixed with 2x Laemmli Sample Buffer (Bio-Rad) and heated to 96°C for 6 minutes. Proteins were separated by 10% SDS-PAGE, transferred to a Protran BA85 nitrocellulose membrane (Whatman), blocked at room temperature for 1 h with Buffer A (5% skimmed milk, 1.2% w/v Tris-Base, 9% w/v NaCl, 0.2% Tween 20, pH 7.6), incubated with polyclonal mouse anti-human MUT (Abcam) (1:1000 in Buffer A), or â-actin (Sigma-Aldrich) (1:4000 in Buffer A) overnight, detected by incubation with goat anti-mouse antibody coupled to horseradish peroxidase (Santa Cruz) (1:5000 in Buffer A) for one hour, and visualized with ECL Western Blotting Detection Reagents (GE Healthcare Life Sciences) on a Gel Logic 6000 Pro (Carestream).

4.4.5 MUT activity assay

MUT activity was assayed in crude cell lysates by measuring the production of [^{14}C]succinate from [^{14}C]methylmalonyl-CoA by a modification of earlier described methods (Baumgartner, 1983; Causey and Bartlett, 1984). All operations were performed in a dark room illuminated with a 15W red Safelight bulb (Dr. Fischer). Cell lysates were prepared by pipetting 5 mM potassium phosphate buffer (pH 7.4) on frozen cells and disrupting the pellet by sonicating twice for 15 seconds using the microprobe of an XL-2000 sonicator (Microson) at amplitude 1.5. Specific activities were measured in 50 µl reaction mixture containing 0.1 M potassium phosphate buffer (pH 7.4), 1 mM DL-2-[methyl-^{14}C]methylmalonyl-CoA (ARC; specific activity 7.03 MBq/mmol in assay) and 50 – 100 µg cell proteins without (*holo*-MUT activity) and with (total MUT activity) 50 µM AdoCbl. To estimate K_M for AdoCbl, its concentration was varied between 0.0025 µM and 50 µM. To estimate K_M for methylmalonyl-CoA, its concentration was varied between 0.01 and 1.0 mM in the presence of 50 µM AdoCbl. Reactions were initiated by addition of cell lysate, allowed to proceed for 30 min at 37°C and terminated by addition of 6 µl 5N KOH (Merck). Samples were re-incubated for 15 min at 37°C to hydrolyze CoA derivatives, neutralized by adding 5 µl 5N perchloric acid (Merck) and spiked with 5 µl of 1% solution

(w/v) of succinic acid (Merck) in order to visualize succinate during high performance liquid chromatography (HPLC) separation. Samples were centrifuged to remove precipitate, 50 µl of the supernatant were injected into an Amimex HPX-87H Ion Exclusion column (300 mm x 7.8 mm. H-form, 9 µm, Biorad) and [^{14}C]succinate was separated from [^{14}C]methylmalonate by elution with 0.5 mM H_2SO_4 at 30°C using a flow rate of 0.4 ml/min. Succinate (retention time 17 min) and methylmalonate (11 min) peaks were visualized at 210 nm using an UV detector, 0.2 ml fractions covering the succinate peak were collected and [^{14}C]succinate was quantitated in a Tri-Carb C1 900TR scintillation spectrometer (Packard) with Optiphase Higsafe 2 counting cocktail (PerkinElmer). Protein in cell lysates was determined by the Lowry method. MUT activity was expressed as nmol succinate formed per min and mg protein. K_M values for AdoCbl were determined using Eadie-Hofstee plot.

4.4.6 Differential scanning fluorimetry

Purified homodimeric MUT was assayed for shifts in melting temperature (T_m), which is the midpoint transition from a folded to an unfolded state, as previously described (Froese, et al., 2010a; Niesen, et al., 2007). Each mutant and *wt* protein was assayed in the *apo* state, or with pre-incubation of 50 µM AdoCbl (Sigma-Aldrich), or a combination of 50 µM AdoCbl and 500 µM malonyl-CoA (MCoA) (Sigma-Aldrich). MCoA was used as a substrate analogue because it has been confirmed to bind to the substrate pocket (PDB: 2XIQ) (Froese, et al., 2010b). For chemical osmolyte screening, various concentrations of betaine and TMAO (up to 1200 mM) and glyercol (up to 40%) were pre-incubated with protein before analysis.

4.5 RESULTS

4.5.1 Rationale for mutation selection

From the repertoire of known *MUT* missense mutations, we selected 23 for this study (Table 1) with the rationale that they (i) cover both phenotypically severe *mut*^{0} (*n*=7) and milder *mut*$^-$ (*n*=16) subtypes, (ii) are widely distributed across the gene (exons 2-13), and (iii) include representative mutations prevalent in different ethnic populations, *e.g.* African Americans (p.G717V, c.2150G>T) (Worgan, et al., 2006), Caucasians (p.N219Y, c.655A>T; p.R369H, c. 1106G>A; p.R694W, c.2080C>T) (Acquaviva, et al., 2005; Lempp, et al., 2007), and Turkish Asians (p.P615T, c.1843C>A) (Dundar, et al., 2012). These 23 mutations, reported in both homozygous and heterozygous states, are found in highly-conserved residues, and their amino acid substitutions are predicted to be largely untolerated according to *SIFT* prediction (Table 1B). All selected mutations have been reported (Table 1A, references therein) with the exception of p.L736F, c.2206C>T, a novel mutation that exists in a compound heterozygous state with the splice site mutation c.753+2T>A (Worgan, et al., 2006) in an MMAuria

patient diagnosed in our lab. Propionate fixation and MUT activity assays on cells from this patient are consistent with the *mut*$^-$ subtype.

We mapped the missense mutations onto the human MUT crystal structure (Froese, et al., 2010b) to understand their local structural environments (Supp. Figure S1; an interactive version is available at *www.thesgc.org/MUT*). These mutations are located across the entire polypeptide, including the N-terminal substrate binding domain (*n*=13), C-terminal cofactor binding domain (*n*=9), and inter-domain linker (*n*=1) (Figure 1A). A number of them contribute to the binding regions of the substrate (*e.g.* p.Y100C) and cofactor (*e.g.* p.M700K) (Figure 1B), while four residues are buried at, or located near, the MUT dimer interface (p.P86L, p.Y316C, p.R369H, p.G426R) (Table 1B, Figure 1B). Compatible with the large proportion of private mutations, no hot spot regions are found for the above, or other known MUT mutations.

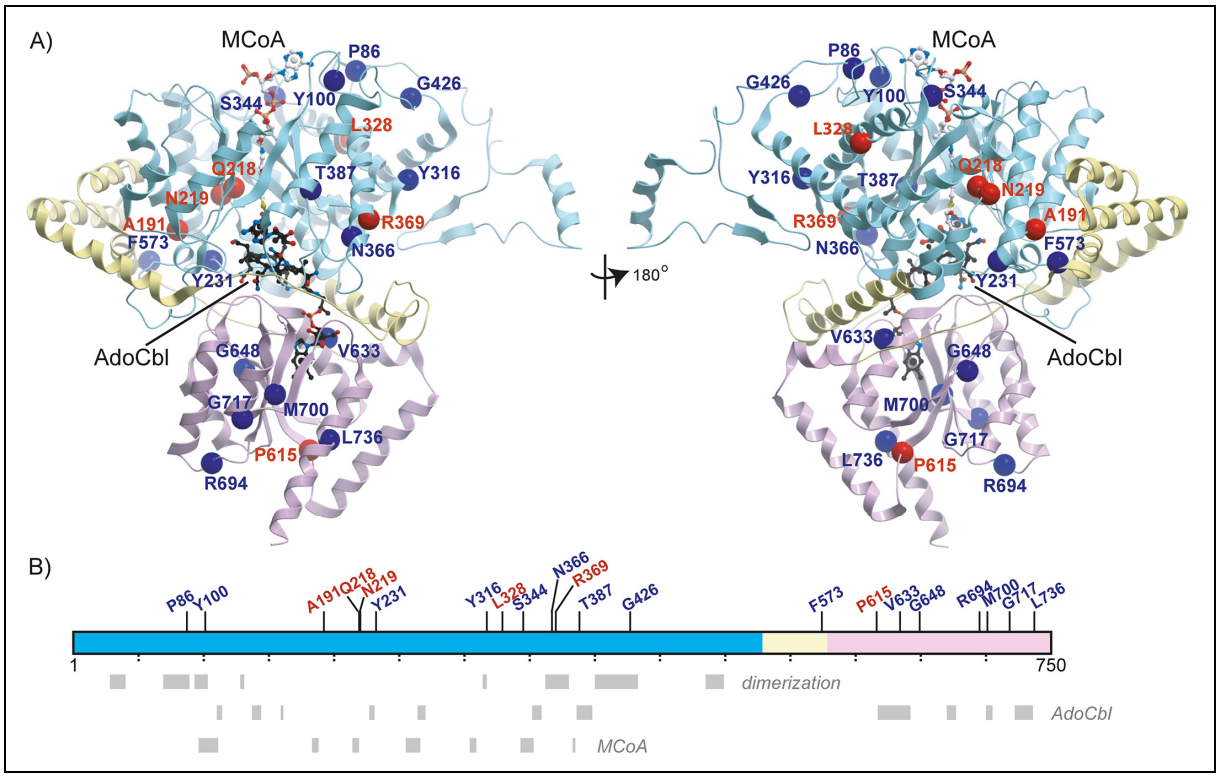

Figure 1. Structural mapping of MUT missense mutations. **A.** The human MUT structure in complex with MCoA and AdoCbl (PDB code 2XIQ) is coloured according to domains, *i.e.* N-terminal substrate binding domain cyan, C-terminal cofactor binding domain magenta, inter-domain linker yellow. Mutations in this study are shown as red circles (*mut*^{0}) or blue circles (*mut*$^-$). Ligands are in stick representation, coloured white for MCoA and black for AdoCbl. **B.** Domain organization of MUT highlighting locations of the studied mutations, dimerization interface, and binding regions for MCoA and AdoCbl in the polypeptide. An interactive version of this structural representation is available online at *www.thesgc.org/MUT*.

4.5.2 Effects on protein integrity in two expression systems

The diverse structural locations of the 23 missense mutations, many of which are distant from the catalytic centre, suggest some mutations may impact on non-catalytic properties such as the stability of translated polypeptides. To investigate this, we reconstructed these alleles in two recombinant expression systems, *E. coli* and human fibroblasts (Figure 2A, B), both of which have been used to produce MUT previously (Froese, et al., 2010b; Janata, et al., 1997; Wilkemeyer, et al., 1991). For *E. coli* expression, the mutant proteins (*n*=21, excluding p.N219Y and p.Y316C which we were unable to clone) were assessed on their (i) expression level relative to wild-type (*wt*) protein, as judged by protein amount in total cell lysate, and (ii) solubility, as judged by protein amount after affinity purification. We first tested several post-induction growth temperatures (37/26/18/12°C) for *wt* MUT, and observed the highest solubility level with 18°C overnight growth (data not shown). While all 21 mutants are expressed in *E. coli* at this temperature (Figure 2A, lanes 'L'), a number of them have poor solubility compared to *wt*, resulting in no (p.A191E and p.L328F) or reduced (p.S344F, p.F573S, p.P615T/L) protein recovery from the affinity eluant (lanes 'E'). This observation, unchanged by a lower post-induction temperature (12°C; data not shown), indicates insoluble mutant protein expression likely due to a global folding defect. In addition to *E. coli*, we expressed MUT mutants using an immortalized MUT-deficient patient fibroblast cell-line. Western blot (Figure 2B) of the expressed mutants detected very low protein levels for p.P615T/L, which agrees with bacterial expression. However, the p.A191E and p.L328F proteins, insoluble in *E. coli*, have near-*wt* expression levels in human fibroblasts, suggesting that additional factors exclusive to eukaryotes may assist in the proper folding for certain mutant proteins.

construct	vector	*wt*	p.P86L	p.Y100C	p.A191E	p.Q218H	p.Y231N	p.L328F	p.S344F	p.N366S	p.R369H	p.T387I	p.N219Y
mut class	-	-	*mut*$^-$	*mut*$^-$	*mut*^{0}	*mut*^{0}	*mut*$^-$	*mut*^{0}	*mut*$^-$	*mut*$^-$	*mut*^{0}	*mut*$^-$	*mut*^{0}
bacterial system kDa A) affinity purification 125 93 MUT → 57 31 24		L E											
mammalian system MUT B) Western blot β-actin													
C) total MUT activity (% wt)	0.0	100	79	60	0.8	0.4	60	0.2	3.1	2.9	1.3	9.1	1.2
D) K_M for AdoCbl (times wt)	-	1	636	770	-	-	1270	-	8	46	-	14	-
E) ΔT_m (mutant vs wt in °C)	-	0.0	-8.7	0.2	-	-1.7	-2.7	-	-	0.3	-0.6	1.6	-

construct	vector	p.G426R	p.F573S	p.P615T	p.P615L	p.V633G	p.G648D	p.R694W	p.R694L	p.M700K	p.G717V	p.L736F	p.Y316C
mut class	-	*mut*$^-$	*mut*$^-$	*mut*^{0}	*mut*^{0}	*mut*$^-$	*mut*$^-$	*mut*$^-$	*mut*$^-$	*mut*$^-$	*mut*$^-$	*mut*$^-$	*mut*$^-$
bacterial system kDa A) affinity purification 125 93 MUT → 57 31 24													
mammalian system MUT B) Western blot β-actin													
C) total MUT activity (% wt)	0.0	13	6.0	1.1	0.4	51	85	3.6	2.7	3.3	27	13	18
D) K_M for AdoCbl (times wt)	-	1954	5	-	-	214	1395	10	18	79	1790	47	4
E) ΔT_m (mutant vs wt in °C)	-	-7.8	-0.1	-	-	0.0	-1.7	-2.5	-4.2	-1.3	-3.3	-	-

Figure 2. MUT missense mutations confer different effects on stability and activity. **A.** Coomassie staining of SDS-PAGE following small-scale bacterial expression and affinity purification. For each mutation lanes for total cell lysate ('L', left) and eluant after purification ('E', right) are shown. **B.** Western blot following expression of each mutation in a MUT deficient patient cell line. Vector, empty vector. **C.** Total MUT activity (assay with 50 µM AdoCbl) of each mutation expressed as percent of mean *wt* activity. **D.** K_M for AdoCbl, expressed as times the mean *wt* value. **E.** ΔT_m of *apo* mutant compared to *apo-wt* protein (see Figure 3). '–', not applicable.

4.5.3 Effects on enzymatic function

MUT catalyzes the isomerization of methylmalonyl-CoA to succinyl-CoA via reactive radical intermediates generated from a homolytic bond cleavage of AdoCbl (Banerjee and Ragsdale, 2003). To investigate if and how each mutation affects MUT enzymatic function, we determined catalytic activity

and ligand affinity for *wt* and mutant MUT expressed in MUT-deficient human fibroblasts. Under saturating AdoCbl levels (50 µM), *wt* MUT exhibited a mean substrate turnover of 20.2 nmol/min/mg protein (Supp. Table S1). All 23 mutants showed decreased enzyme activity, ranging from 0.2-85 % of *wt* values (Figure 2C; Supp. Table S1). They can be broadly described as having *high* (> 50% of *wt*, *n*=5), *intermediate* (5-50% of *wt*, *n*=6) and *low* (< 5% of *wt*, *n*=12) levels of residual enzyme activity (Supp. Figure S2). All mut^0 mutants studied were near the assay detection limit (< 2% of *wt*), consistent with their reported clinical severity, while the mut^- mutants (2.7-85% of *wt*) are distributed into all three levels of activity. The more substantial residual activity of mut^- mutations allowed us to further determine their K_M values for AdoCbl and methylmalonyl-CoA. *wt* MUT had a mean K_M for AdoCbl of 4.7 nM (Supp. Table S1), similar to published values (Morrow, et al., 1978). All characterized mutants exhibited higher K_M values than *wt*, to varying degrees (Figure 2D). Seven proteins had a K_M of > 200-times *wt* levels, of which four (p.Y231N, p.G426R, p.G648D and p.G717V) are at least three orders of magnitude higher, indicating a strong K_M defect. On the contrary, five proteins had near-*wt* K_M (*e.g.* Y316C and p.F573S, < 5-times *wt*), suggesting their catalytic impairment is not primarily due to reduced cofactor affinity. No mutants showed large increases in K_M for methylmalonyl-CoA (data not shown), suggesting substrate binding was not defective in these mutants, as has been shown previously (Willard and Rosenberg, 1980).

4.5.4 Effects on protein thermolability

To test whether the catalytic impairment of certain MUT mutants relates to changes in their structural integrity, we expressed and purified in large-scale those mutants that were sufficiently soluble in *E. coli* (Figure 2A, *n*=15). They had similar retention volumes in size exclusion chromatography as *wt* MUT (Froese, et al., 2010b), with no detection of higher-order aggregates (data not shown), indicating a native-like homodimer devoid of global folding defects. To identify any subtle stability changes, we applied a differential scanning fluorimetry (DSF) assay (Vedadi, et al., 2006) to follow temperature induced protein unfolding in order to measure the melting temperature (T_m) of each purified protein. As proof of principle, we first interrogated the stability effect of physiological ligands (cofactor AdoCbl, substrate analogue malonyl-CoA (MCoA)) on the T_m of *wt* MUT, with the rationale that binding of the cognate ligands should stabilize MUT thereby increasing its T_m. Consistent with this, *wt* MUT (at 1 µM) exhibits a T_m of 58.2°C in the *apo* form, which increases in a dose-dependent manner upon addition of the native-like ligands (Supp. Figure S3A, B), reaching T_m values of 60.8°C (ΔT_m = 2.6°C) with AdoCbl (50 µM), and 73.7°C (ΔT_m = 15.5°C) with both AdoCbl (50 µM) and MCoA (500 µM) (Figure 3 inset). The extent of these 'T_m shifts' corroborates previous structural observations (Froese, et al., 2010b), in that the smaller ΔT_m by binding AdoCbl alone is consistent with a modest rearrangement in the MUT C-terminal domain (Supp. Figure S4A), while the larger ΔT_m with

AdoCbl+MCoA is associated with a substantial conformational change in the N-terminal domain (Supp. Figure S4B). Notably, MCoA alone (500 µM) did not increase the T_m of MUT beyond *apo* levels (data not shown), suggesting an ordered binding mechanism of AdoCbl cofactor first, followed by substrate, in the ternary complex.

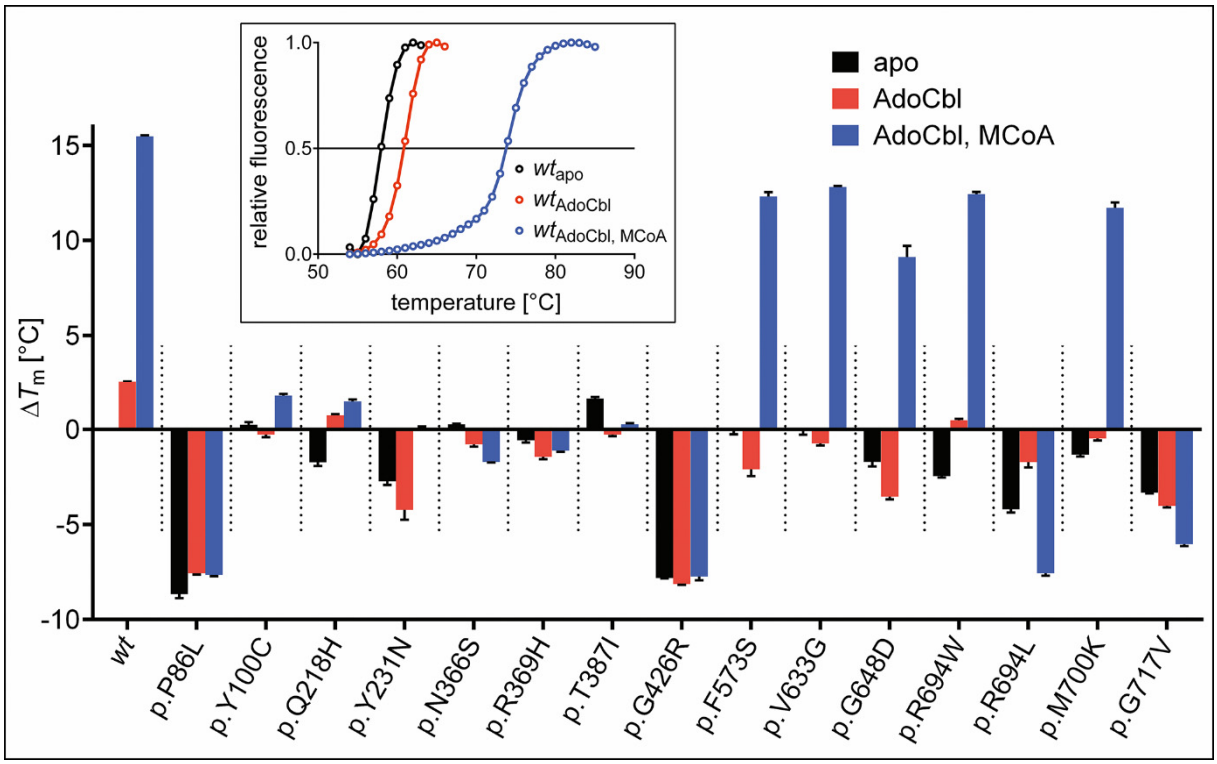

Figure 3. Thermolability of MUT mutations. The change in T_m values (ΔT_m, compared to *apo wt*) for each mutant MUT in the *apo* state, or following addition of AdoCbl alone or with AdoCbl and MCoA, are shown. Black, *apo* protein; red, with 50 µM AdoCbl; blue, with 50 µM AdoCbl and 500 µM MCoA. Error bars depict SEM from at least 3 measurements. **Inset.** Representative DSF melting curves of *wt* MUT in the *apo* form (black), with 50 µM AdoCbl (red) and with 50 µM AdoCbl and 500 µM MCoA (blue).

We subsequently measured the T_m values of purified mutant proteins in the *apo*, AdoCbl bound, and AdoCbl+MCoA bound states (Figure 3), to determine if they had a lower T_m than *wt*, an indicator of protein destabilization (Leandro, et al., 2011a). For clarity, the ΔT_m of *apo*-mutants compared to *apo-wt* is given in Figure 2E. Six out of 15 proteins exhibited near-*wt* T_m in their *apo* forms, indicating intact protein integrity. Of these, two (p.F573S, p.V633G) responded to AdoCbl+MCoA stabilization with similar T_m shifts as *wt*, while four (p.Y100C, p.N366S, p.R369H, p.T387I) did not, suggesting that the latter mutants lost the capacity for native ligand stabilization. In particular, p.T387I showed a concentration-dependent decrease of T_m when adding AdoCbl alone (Supp. Figure S3C). The other nine proteins, however, were more thermolabile than *wt* in their *apo* forms. While five (p.Q218H,

p.Y231N, p.G648D, p.R694W, p.M700K) had slightly lower T_m than *wt* (ΔT_m range -2.7 to -1.3) and responded to AdoCbl+MCoA stabilization, four (p.P86L, p.G426R, p.R694L, p.G717V) were substantially more thermolabile than *wt* (maximum destabilization: p.P86L, ΔT_m -8.7°C) and did not respond to ligand supplementation.

4.5.5 Stabilization of MUT mutants by osmolytes

The insolubility and thermolability of a number of MUT mutants, compared to *wt*, implicate protein destabilization as a biochemical defect and prompted us to investigate the potential for post-translational stabilization of mutant proteins by six different osmolytes using DSF and bacterial expression (Figure 4; Supp. Figure S5, S6). When applied in high-mM concentrations, these uncharged, low molecular weight compounds function as 'chemical chaperones' and have been shown to stabilize a number of disease-associated proteins prone to misfolding, an effect likely mediated by osmotic changes in the milieu (Majtan, et al., 2010; Nascimento, et al., 2008). The two most thermolabile MUT mutants in our study, p.P86L and p.G426R, showed T_m increases at high osmolyte concentrations (10% glycerol, 600 mM others), with the efficacy of stabilization dependent on the osmolyte used (Figure 4A, B). These osmolytes confer a non-saturating dose response, and the effect appears non-selective, as *wt* and all mutant proteins tested demonstrate stabilization in their *apo* forms to similar degrees (Supp. Figure S5). To determine if osmolytes could also stabilize proteins co-translationally, we expressed several mutants with varying levels of solubility in *E coli*, and supplemented their growth (Supp. Figure S6). Compared to no supplement control, soluble protein yield was improved with glycerol (at 1% concentration: p.A191E and p.G426R; 5%: p.R694W), TMAO (100 mM: p.P615T and p.R694W), and to a lesser extent betaine (100mM: p.R694W). No improvement for p.L328F was seen, while *wt* protein was very soluble under all conditions, suggesting the rescue could be mutant specific. Together, our data demonstrate the amenability of small exogenous molecules to modulate MUT stability, and support the notion to develop target-specific 'pharmacological chaperones'.

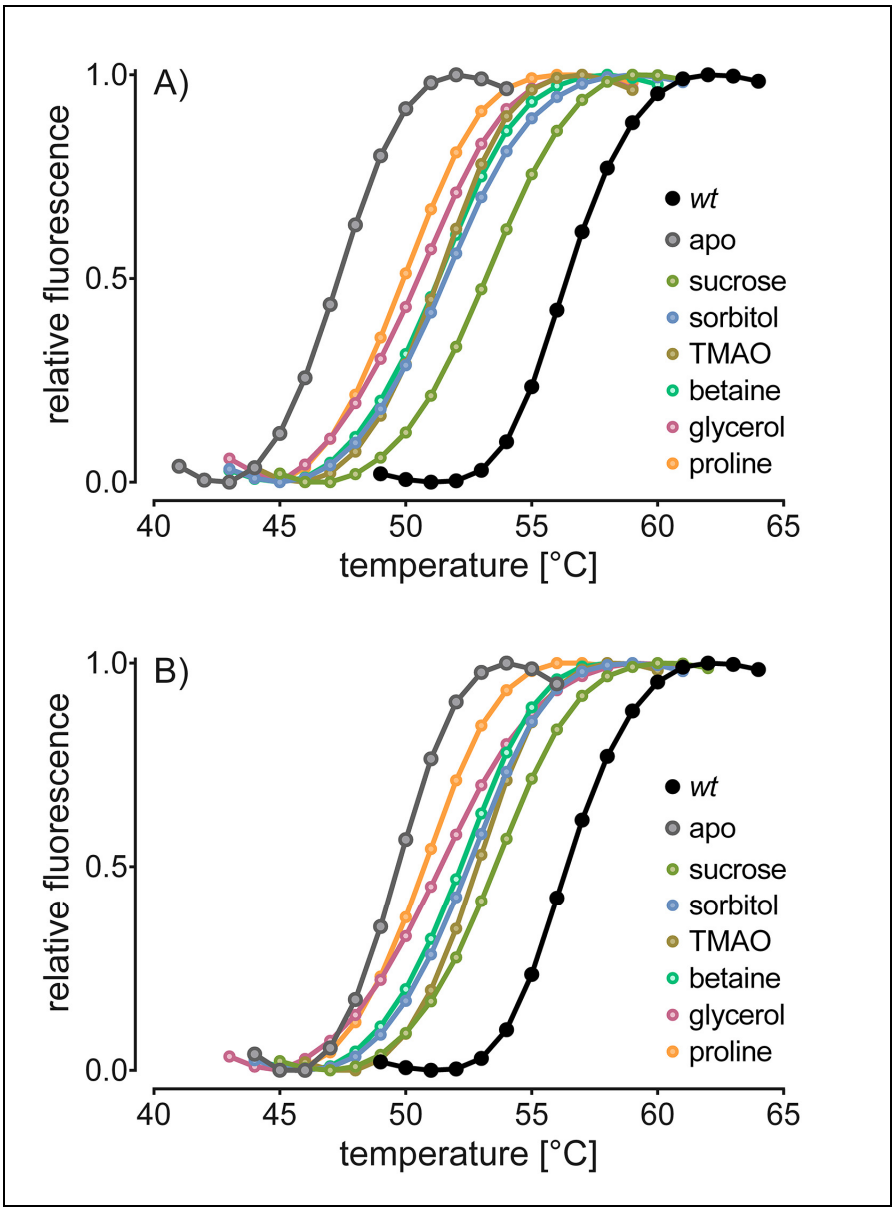

Figure 4. Stabilization of mutant MUT by osmolytes. Representative DSF melting curves for p.P86L (**A**) and p.G426R (**B**) mutants in the *apo* form (grey) and in the presence of osmolytes (colours) are shown along with MUT-wt (black).

4.6 Discussion

Our study aimed to establish a genotype-phenotype correlation by characterizing the biochemistry associated with a set of *MUT* missense mutations. Earlier small scale studies have tested the activity and expression of MUT missense mutants, for example using the lower eukaryote *S. cerevisiae* (5 mutations) (Crane and Ledley, 1994) and *E. coli* (4 mutations) (Janata, et al., 1997) as recombinant hosts. Our selected set of 23 mutants, five of which overlap with those previous studies (p.Y231N, p.R369H, p.G648D, p.R694W, p.G717V), constitutes to our knowledge the largest biochemical analysis of MUT mutations to date.

4.6.1 A catalogue of biochemical defects in MUT mutants

Traditionally, MMAuria phenotypes are broadly classified into *mut*^{0} and *mut*$^-$ subtypes based on the response of a patient cell line to hydroxocobalamin in propionate incorporation (Lempp, et al., 2007). In order to understand the molecular mechanism(s) governing the *mut*^{0}/*mut*$^-$ subtypes and catalogue the associated biochemical defects, we have further assessed MUT mutations based on stability and catalytic properties as summarized in Table 1B.

We evaluated mutants on two stability criteria, *'folding'* and *'thermolability'*. *'Folding'* defects refer to the aggregation or degradation of translated polypeptides, thereby reducing the steady state protein. These mutants displayed drastically reduced soluble protein yield, as exemplified by p.P615T/L. Four other mutants, two from each *mut* subtype (*mut*^{0}: p.A191E, p.L328F; *mut*$^-$: p.S344F, p.F573S), also fit this category, having reduced detectable protein in one of the two expression systems. A few mutants displayed only slightly decreased soluble *E. coli* expression, such as p.G717V and p.R694W, consistent with a previous report (Crane and Ledley, 1994), and were not included in the '*folding*' category. *'Thermolabile'* mutants had near-*wt* levels of recombinant expression and solubility, reflecting near-native folding, but increased temperature sensitivity. Four mutations in this study fell into the *'thermolabile'* category (p.P86L, p.G426R, p.R694L, p.G717V).

Inspection of the MUT crystal structure shows that both *'folding'* and *'thermolabile'* mutants involve amino acid changes that (i) remove a conformationally-restricted proline residue (*e.g.* p.P86L, p.P615L/T); (ii) cause steric clashes with a bulky side-chain (*e.g.* p.L328F, p.S344F); or (iii) disrupt the natively charged/polar (*e.g.* p.R694L) or non-polar (*e.g.* p.A191E) environment. Furthermore, stability mutations are distributed across the entire polypeptide, indicating that all domains of the protein contribute to its intrinsic stability.

In addition to stability mutants, we also identified direct kinetic impairment, which we termed *'catalytic'* and *'K_M'* mutants. *'Catalytic'* mutants had low residual activity (< 5% of *wt*) despite detectable eukaryotic expression, and constituted the largest category of mutants (10 in this study, Table 1B). Of particular note, two *'catalytic'* mutants, p.Q218H and p.A219E, involve structurally adjacent residues lining the substrate binding channel (Figure 1A; Supp. Figure S1d, e), where p.Q218 has been implicated in transition state stabilization (Loferer, et al., 2003). *'K_M'* mutants exhibited > 200-fold increased K_M for AdoCbl compared to *wt*. Among the seven '*K_M*' mutants identified (Table 1B), only three (p.V633G, p.G648D and p.G717V) are buried within the C-terminal cobalamin binding domain (Figure 1A; Supp. Figure S1p, q, t). The other four are towards the N-terminal end: p.Y231N is situated at the inter-domain interface, within a loop that contacts the cobalamin corrin ring (Supp. Figure S1f); p.G426R is situated at the dimeric interface; and p.P86L and p.Y100C are located near the N-terminal substrate binding channel, distant from any obvious involvement in cobalamin binding.

Further investigation is therefore warranted to understand how the K_M effect of these mutations is mediated.

It is of note that our classification scheme is not aimed at '*pigeonholing'* mutant alleles into disparate, mutually exclusive categories; on the contrary, there is a high degree of interdependence between various stability and catalytic properties that together contribute to proper enzyme function. This is clearly exemplified with seven mutants fitting multiple criteria. Three of them had a significantly increased K_M but were also thermolabile (p.P86L, p.G426R, p.G717V), one was *'thermolabile'* with a *'catalytic'* dysfunction (p.R694L), and three met the criteria of *'folding'* and *'catalytic'* defects (p.A191E, p.L328F, p.S344F). In addition, three mutations were termed *'unclear'* (p.Y316C, p.T387I and p.L736F), since in our assays they lack definitive aberration in stability and enzyme kinetics, showed detectable protein by Western blot, intermediate enzyme activity and only moderate K_M change.

Future studies should aim to address the lesser characterized biochemical aspects of MUT and possible mutational effects, which are beyond the scope of this study. These include: (i) possible allostery between substrate and cofactor binding, which could potentially explain the T_m shift from MCoA+AdoCbl but not MCoA alone; (ii) potential formation of a supramolecular complex with the GTPase MMAA and adenosyltransferase MMAB (Froese and Gravel, 2010), required for the proper assembly of AdoCbl onto the MUT enzyme; and (iii) inter-allelic rescue of certain MUT disease alleles (*e.g.* p.R93H and p.G717V), (Worgan, et al., 2006).

4.6.2 Clinical utility and implications of *in vitro* characterization

A clinical application for our biochemical categorization of *MUT* genotypes is to help prognosticate the course of the disease. As expected the characterized *mut*^{0} mutants harbour *'folding'* or *'catalytic'* defects, resulting in very low or undetectable residual enzyme activities consistent with their predominance in neonatal onset patients with severe long-term complications. On the contrary, the characterized *mut*$^-$ mutants can present in any one, or combinations, of the four biochemical defects defined here. We postulate that mutations that do not interfere with protein stability and have less of a catalytic penalty would result in milder disease (*e.g.* p.P86L or p.G426R). Similar to other metabolic diseases where an activity threshold of ~5-10% of *wt* is sufficient to ameliorate disease (Leinekugel, et al., 1992; Suzuki, 2013), *mut*$^-$ patients often show a later onset and less long-term complications, presumably due to the intermediate level of residual MUT activity.

Whether any MUT deficient patient, including those of the *mut*$^-$ subtype, benefit from treatment with high doses of hydroxocobalamin is controversial. Early publications documented no response (Matsui, et al., 1983a; Wilcken, et al., 1977) and recent documentation of a possible response has relied on retrospective reviews (Horster, et al., 2007), while up to now, no controlled studies clearly

demonstrating response to hydroxocobalamin have been published. This picture is very different from PKU, where > 40% patients respond clinically to the cognate cofactor tetrahydropterin (BH_4) of PAH (Zurfluh, et al., 2008). For *mut* type MMAuria, a clinical response to treatment is usually defined as reduced plasma or urinary concentration of methylmalonic acid. While difficult to measure because of its broad variation in body fluids (Fowler, et al., 2008; Horster, et al., 2007; Thompson and Chalmers, 1990), and clinical improvement even more difficult to determine reliably, lower methylmalonic acid levels are thought to reflect a higher residual enzyme activity protecting patients from severe long-term complications (*e.g.* chronic renal failure and neurological complications) (Cosson, et al., 2009; Horster, et al., 2007; Thompson and Chalmers, 1990). Therefore, careful evaluation of potential responsiveness to hydroxocobalamin treatment in all MMAuria patients is warranted, and a protocol has been proposed (Fowler, et al., 2008). Our thermal denaturation data offer a molecular explanation to a possible mechanism of cobalamin treatment by revealing AdoCbl-induced stability improvement in certain mutants, in a ligand-specific manner similar to that of BH_4 on mutant PAH. Our results also predict that patients harbouring a *'K_M'* defect (*e.g.* p.G648D) are more likely to benefit from cobalamin treatment, on the assumption that increased hydroxocobalamin plasma levels result in increased cellular AdoCbl production, since in our enzyme assay these mutants exhibited high activity levels in the presence of high AdoCbl concentration. Nevertheless, hydroxocobalamin treatment may only benefit a small subset of patients with intermediate to high residual activity, if any, outlining an imperative to search for alternative therapies.

4.6.3 Small molecule chaperones as alternative therapy?

Our stability data add MUT to the growing list of metabolic enzymes in which mutation-induced protein destabilization is widely believed to play a causative role in disease pathogenesis (Gregersen, 2006). In this model, mutant polypeptides tend to misfold, aggregate and be degraded by protein quality control in the cell. Chemical or pharmacologic approaches to partially correct misfolding, divert the mutant polypeptide from degradation/aggregation pathways, and deliver it to the native subcellular destination may therefore allow a sufficient recovery of physiological function. This small molecule 'chaperoning' approach has been proposed as a viable treatment for a number of protein misfolding diseases (Gomes, 2012; Pey, et al., 2008). We provide proof of principle for MUT chaperone therapy by showing *in vitro* and in cell stabilization of several mutant proteins using chemical osmolytes. These small organic solutes enhance protein stability via a non-selective, non-target-specific mode of preferential exclusion from the protein's surface (Arakawa and Timasheff, 1985), although necessitating high effective concentrations (in mM range) that may be toxic to the cell - restricting their therapeutic utility.

Alternatively, target-specific pharmacological chaperones (PCs) could be developed for MUT which, unlike chemical chaperones, exert a direct stabilization effect by binding to the affected protein, potentially allowing lower, clinically tolerable dosage concentrations. PCs have shown promise in several lysosomal storage diseases, entering early-stage clinical trials for Gaucher, Tay-Sachs and Fabry diseases (Boyd, et al., 2013). In the case of MUT, we anticipate that an effective PC molecule need only stabilize the mutant protein 'long enough' to be delivered to mitochondria, where it can be further stabilized by its native ligands and protein interaction partners (MMAA, MMAB). Such a PC molecule may increase the residual enzyme activity of the mutant protein to a sufficient level that copes with the cellular demands of propionate catabolism. Therefore PC therapy is likely to rescue mild stability defects (*i.e.* alleles that give rise to destabilized protein and partial loss-of-function; *e.g.* p.G426R, p.M700K, p.G717V), either to be administered alone, or as a complement to the existing diet/hydroxocobalamin treatment. Other '*catalytic*', 'K_M' mutations, without stability defects, may also benefit from PCs that potentially increase residual activity, acting as 'enzymatic activators'. Altogether, the stage is set for a systematic, non-biased screening regime in the search for PC molecules targeting MUT, and our established DSF assay may provide a good starting point for this screening.

4.7 Acknowledgments

This work was supported by the Rare Disease Initiative Zurich (radiz), a clinical research priority program for rare diseases of the University of Zurich, Switzerland and the Swiss National Science Foundation (SNSF 31003A_138521). P.F. was supported by an SNSF MD-PhD fellowship (SNSF 323530_145248) and an EMBO Short-Term Fellowship.

The Structural Genomics Consortium is a registered charity (number 1097737) that receives funds from AbbVie, Boehringer Ingelheim, the Canada Foundation for Innovation, the Canadian Institutes for Health Research, Genome Canada, GlaxoSmithKline, Janssen, Lilly Canada, the Novartis Research Foundation, the Ontario Ministry of Economic Development and Innovation, Pfizer, Takeda, and the Wellcome Trust [092809/Z/10/Z].

4.8 Table

To improve readability, the table is presented in landscape mode.

Table 1. Selection of mutations in the *MUT* gene and study results.

A. pre-study data					**B. study results**			
amino acid change	**nucleotide change[&]**	**genomic location**	***mut* sub-type**	**references**	**category of biochemical defect**	**conservation score***	**buried surface at dimer[#]**	**SIFT tolerance[¶]**
p.P86L	c.257C>T	exon 2	*mut*$^-$	(Worgan, et al., 2006)	thermolabile, K_M	0.705	100%	0.00
p.Y100C	c.299A>G	exon 2	*mut*$^-$	(Lempp, et al., 2007)	K_M	0.953	0%	0.00
p.A191E	c.572C>A	exon 3	*mut*^{0}	(Acquaviva, et al., 2005; Worgan, et al., 2006)	folding, catalytic	0.936	0%	0.00
p.Q218H	c.654A>C	exon 3	*mut*^{0}	(Worgan, et al., 2006)	catalytic	1.000	0%	0.00
p.N219Y	c.655A>T	exon 3	*mut*^{0}	(Acquaviva, et al., 2005; Lempp, et al., 2007; Worgan, et al., 2006)	catalytic	1.000	0%	0.00
p.Y231N	c.691T>A	exon 3	*mut*$^-$	(Lempp, et al., 2007; Worgan, et al., 2006)	K_M	0.951	0%	0.00
p.Y316C	c.947A>G	exon 5	*mut*$^-$	(Worgan, et al., 2006)	unclear	0.817	97%	0.00
p.L328F	c.982C>T	exon 5	*mut*^{0}	(Acquaviva, et al., 2005; Lempp, et al., 2007)	folding, catalytic	0.901	0%	0.01
p.S344F	c.1031C>T	exon 5	*mut*$^-$	(Lempp, et al., 2007)	folding, catalytic	0.944	0%	0.00
p.N366S	c.1097A>G	exon 6	*mut*$^-$	(Lempp, et al., 2007)	catalytic	1.000	0%	0.00
p.R369H	c.1106G>A	exon 6	*mut*^{0}	(Lempp, et al., 2007; Worgan, et al., 2006)	catalytic	1.000	99%	0.00
p.T387I	c.1160C>T	exon 6	*mut*$^-$	(Dundar, et al., 2012)	unclear	1.000	0%	0.00
p.G426R	c.1276G>A	exon 6	*mut*$^-$	(Worgan, et al., 2006)	thermolabile, K_M	0.702	98%	0.00
p.F573S	c.1718T>C	exon 10	*mut*$^-$	(Worgan, et al., 2006)	folding	0.586	0%	0.03
p.P615T	c.1843C>A	exon 11	*mut*^{0}	(Acquaviva, et al., 2005; Lempp, et al., 2007)	folding	0.862	0%	0.00
p.P615L	c.1844C>T	exon 11	*mut*^{0}	(Dundar, et al., 2012)	folding	0.862	0%	0.00
p.V633G	c.1898T>G	exon 11	*mut*$^-$	(Lempp, et al., 2007; Worgan, et al., 2006)	K_M	0.794	0%	0.00
p.G648D	c.1943G>A	exon 11	*mut*$^-$	(Ledley and Rosenblatt, 1997)	K_M	0.729	0%	0.00
p.R694W	c.2080C>T	exon 12	*mut*$^-$	(Acquaviva, et al., 2005; Lempp, et al., 2007)	catalytic	0.549	0%	0.00

p.R694L	c.2081G>T	exon 12	*mut*$^-$	(Lempp, et al., 2007)	thermolabile, catalytic	0.549	0%	0.08
p.M700K	c.2099T>A	exon 12	*mut*$^-$	(Acquaviva, et al., 2005; Lempp, et al., 2007; Worgan, et al., 2006)	catalytic	0.570	0%	0.00
p.G717V	c.2150G>T	exon 13	*mut*$^-$	(Worgan, et al., 2006)	thermolabile, K_M	0.840	0%	0.00
p.L736F	c.2206C>T	exon 13	*mut*$^-$	**this study**[ς]	unclear	0.625	0%	0.02

Table Footnotes:

[&] Nucleotide numbering uses +1 as the A of the ATG translation initiation codon in the reference sequence (NM_000255.3), with the initiation codon as codon 1.

* The conservation score (0 = unconserved; 1 = strictly conserved) was calculated using Scorecons server (*http://www.ebi.ac.uk/thornton-srv/databases/cgi-bin/valdar/scorecons_server.pl*, as of June 2014) (Valdar, 2002), based on a multiple sequence alignment of 146 MUT homologues from different phyla, generated from the CONSURF server (*http://consurf.tau.ac.il/*, as of June 2014) (Ashkenazy, et al., 2010).

[#] Percentage of the amino acid total surface that is buried in the human MUT dimer, calculated from the PISA server v1.48 (*http://www.ebi.ac.uk/pdbe/pisa/*) (Krissinel and Henrick, 2007).

[¶] SIFT tolerance score (0-0.05 correspond to amino acid changes that likely affect protein function) was calculated using the SIFT server (*http://sift.jcvi.org/*, as of June 2014) (Kumar, et al., 2009).

[ç] The new variant has been submitted to dbSNP (*http://www.ncbi.nlm.nih.gov/SNP/*).

4.9 Supplementary Material

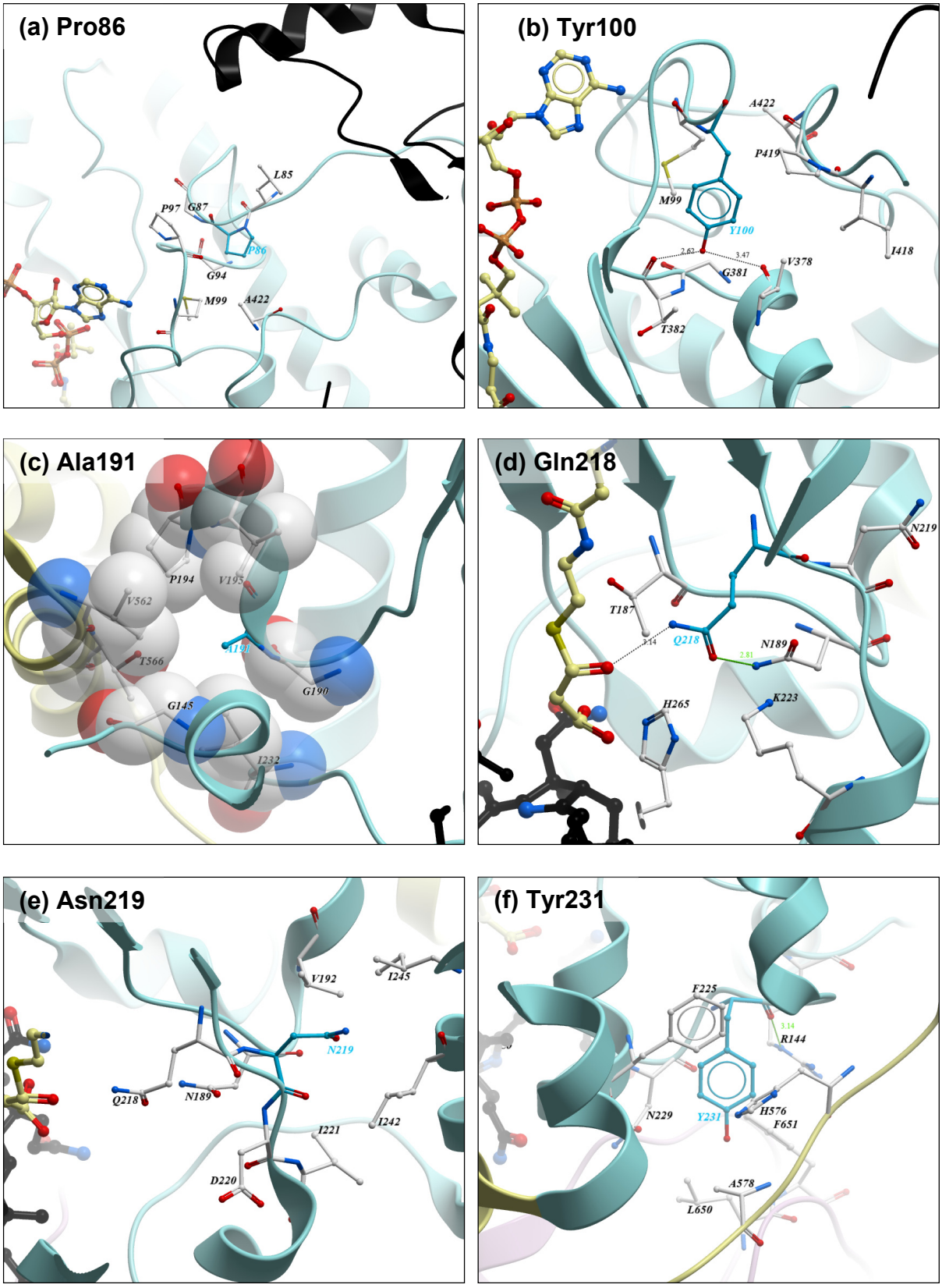

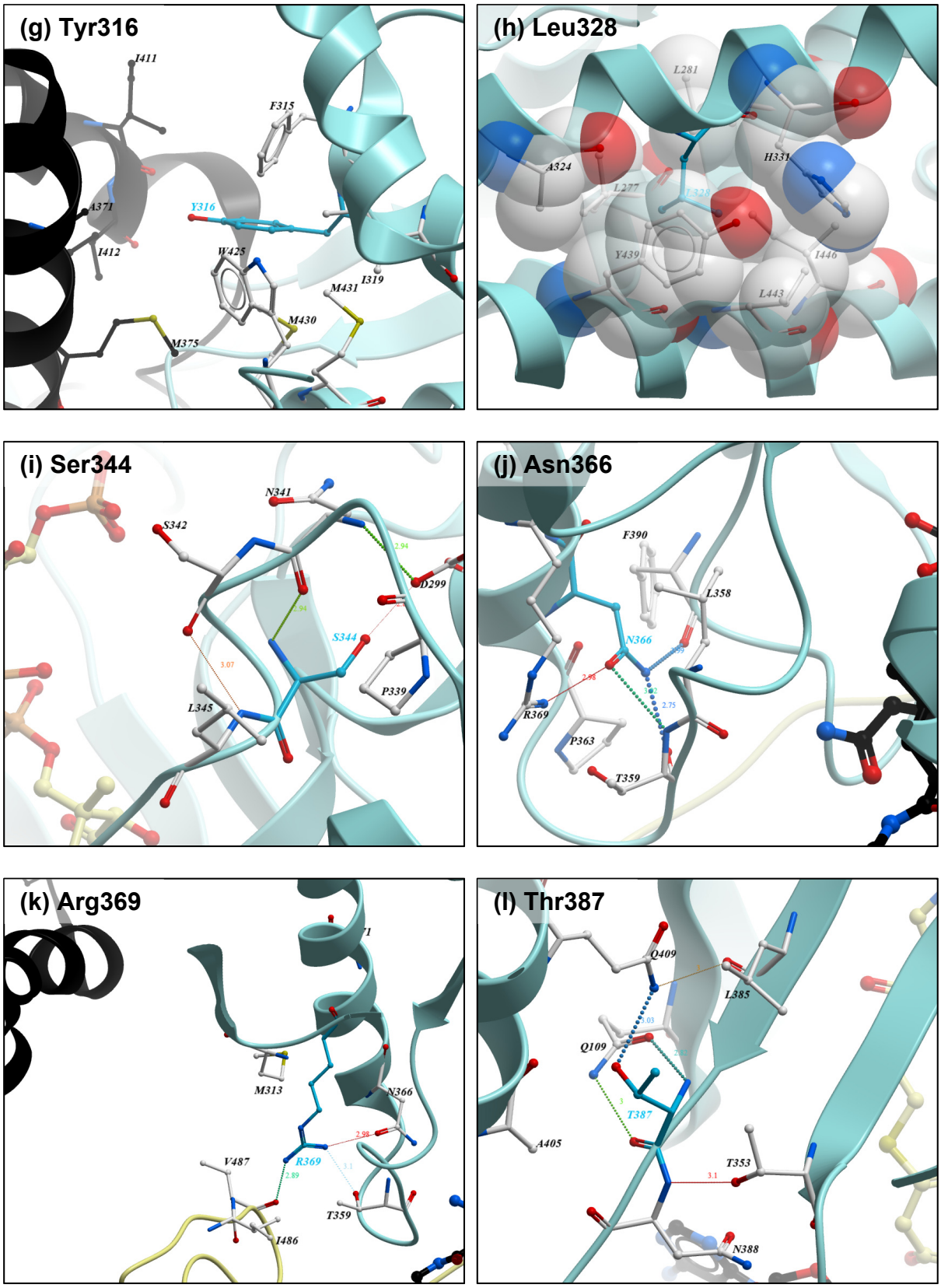
(g) Tyr316
I411
F315
A371
Y316
I412
W425
I319
M431
M430
M375
(h) Leu328
L281
A324
H331
L277
L328
Y439
I446
L443
(i) Ser344
N341
S342
D299
S344
P339
L345
(j) Asn366
F390
L358
N366
R369
P363
T359
(k) Arg369
M313
N366
V487
R369
T359
I486
(l) Thr387
Q409
L385
Q109
T387
A405
T353
N388

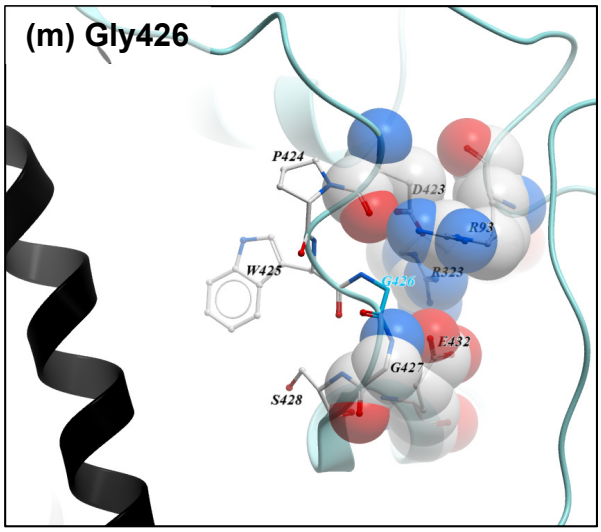
(m) Gly426
P424
D423
R93
W425
R323
G426
E432
G427
S428

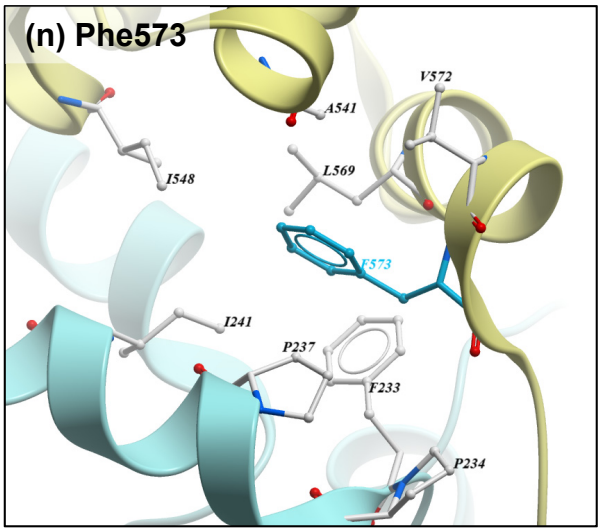
(n) Phe573
V572
A541
I548
L569
F573
I241
P237
F233
P234

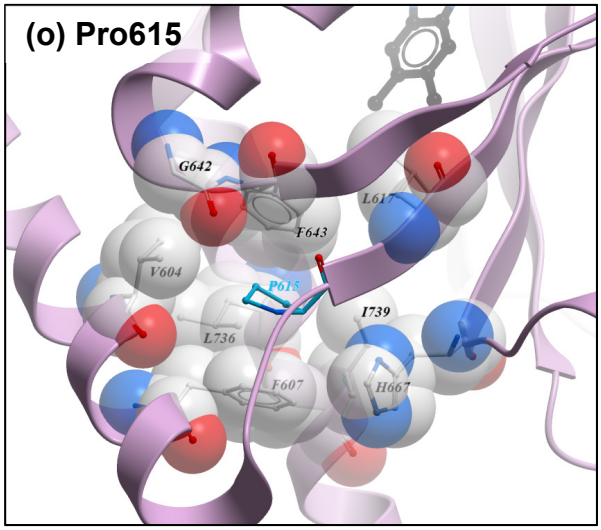
(o) Pro615
G642
L617
F643
V604
P615
I739
L736
F607
H667

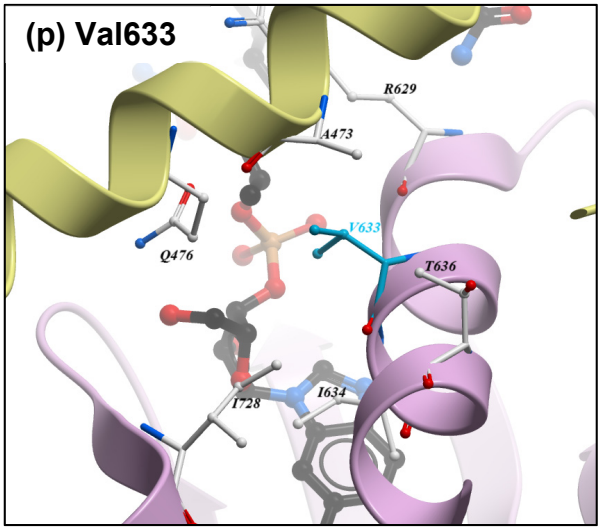
(p) Val633
R629
A473
Q476
V633
T636
I634
I728

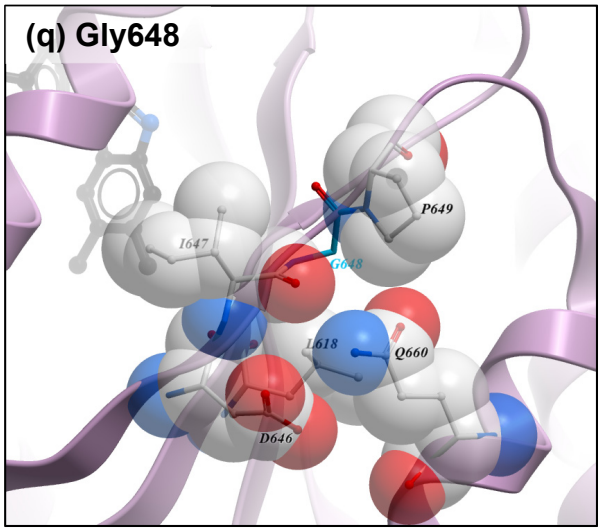
(q) Gly648
P649
I647
G648
L618
Q660
D646

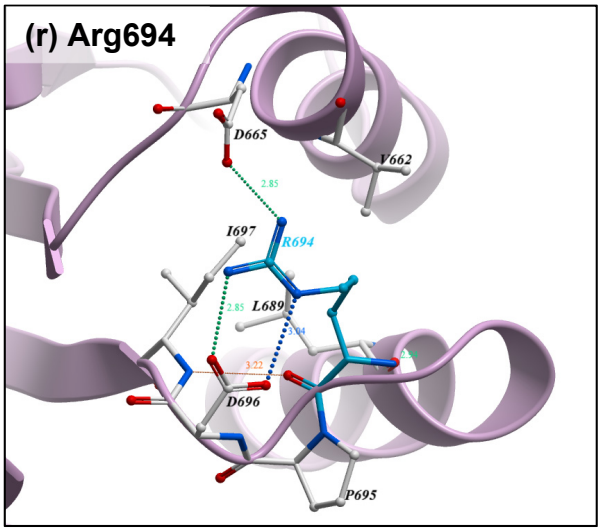
(r) Arg694
D665
V662
2.85
I697
R694
2.85
L689
3.22
D696
P695

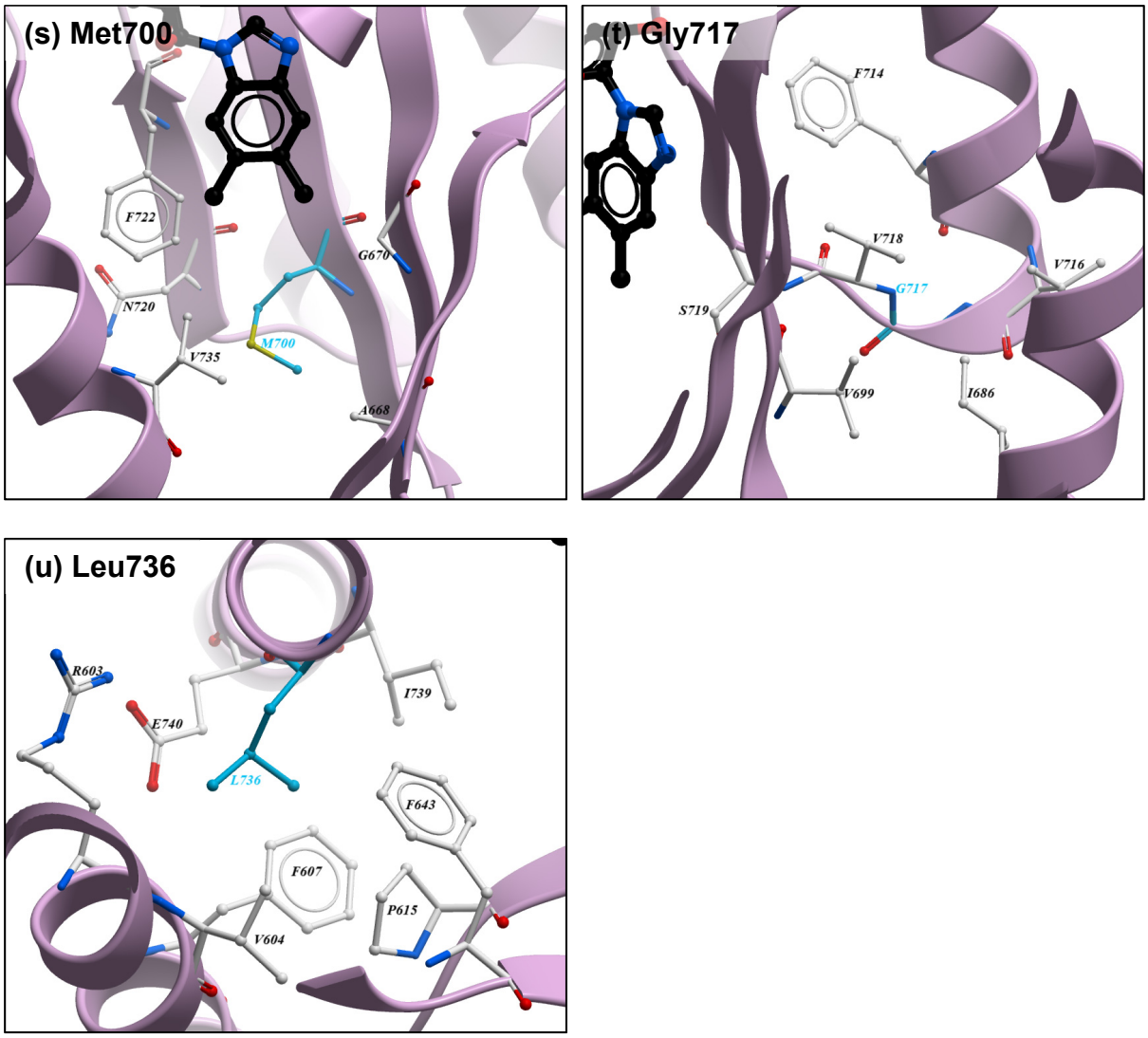

Figure S1. Structural view of the amino acid environment for each mutation in this study. For each panel, the amino acid of interest is coloured cyan. Secondary structure elements are coloured cyan for the N-terminal substrate binding domain, yellow for inter-domain linker, and magenta for C-terminal cobalamin binding domain. For panels **a, b, d, e, i** and **l**, malonyl-CoA is shown as sticks (yellow carbon atoms). For panels **d, k, p, q, s** and **t**, adenosylcobalamin is shown as sticks (black carbon atoms). For panels **a, g, k** and **m**, the neighboring subunit in the MUT dimer is shown as black cartoon. For panels **c, h, m, o** and **q**, amino acids surrounding the site of interest are also shown in spheres, to highlight the tight steric packing. Where applicable, hydrogen bonds are shown as dashed lines (distance in angstrom). An interactive version of this structural representation is available at *www.thesgc.org/MUT*.

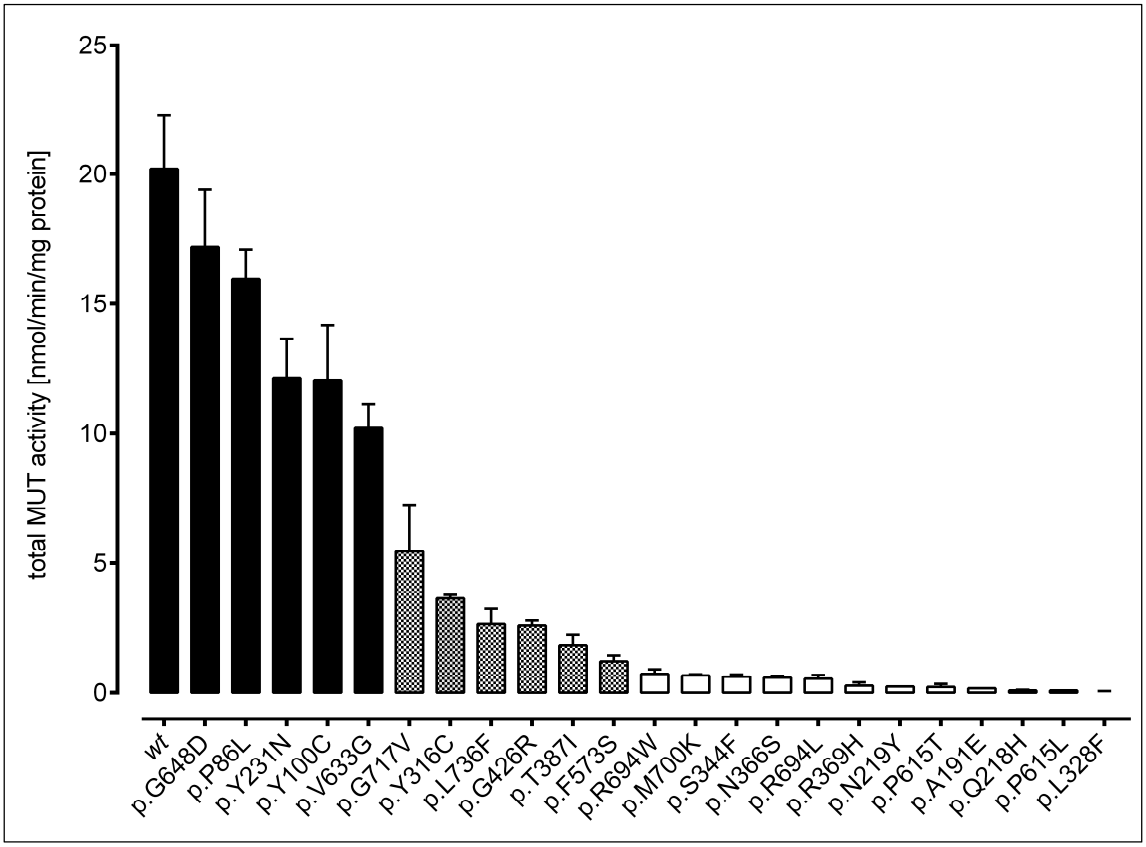

Figure S2. Enzyme activities of MUT *wt* and mutants in decreasing order. Each bar represents the mean of at least two replicate experiments (error bars depict SEM). Black bars indicate *high* (50-100% of *wt*, n=5), dotted bars *intermediate* (6-49% of *wt*, *n*=5) and white bars *low* (0-5% of *wt*, *n*=13) levels of activity.

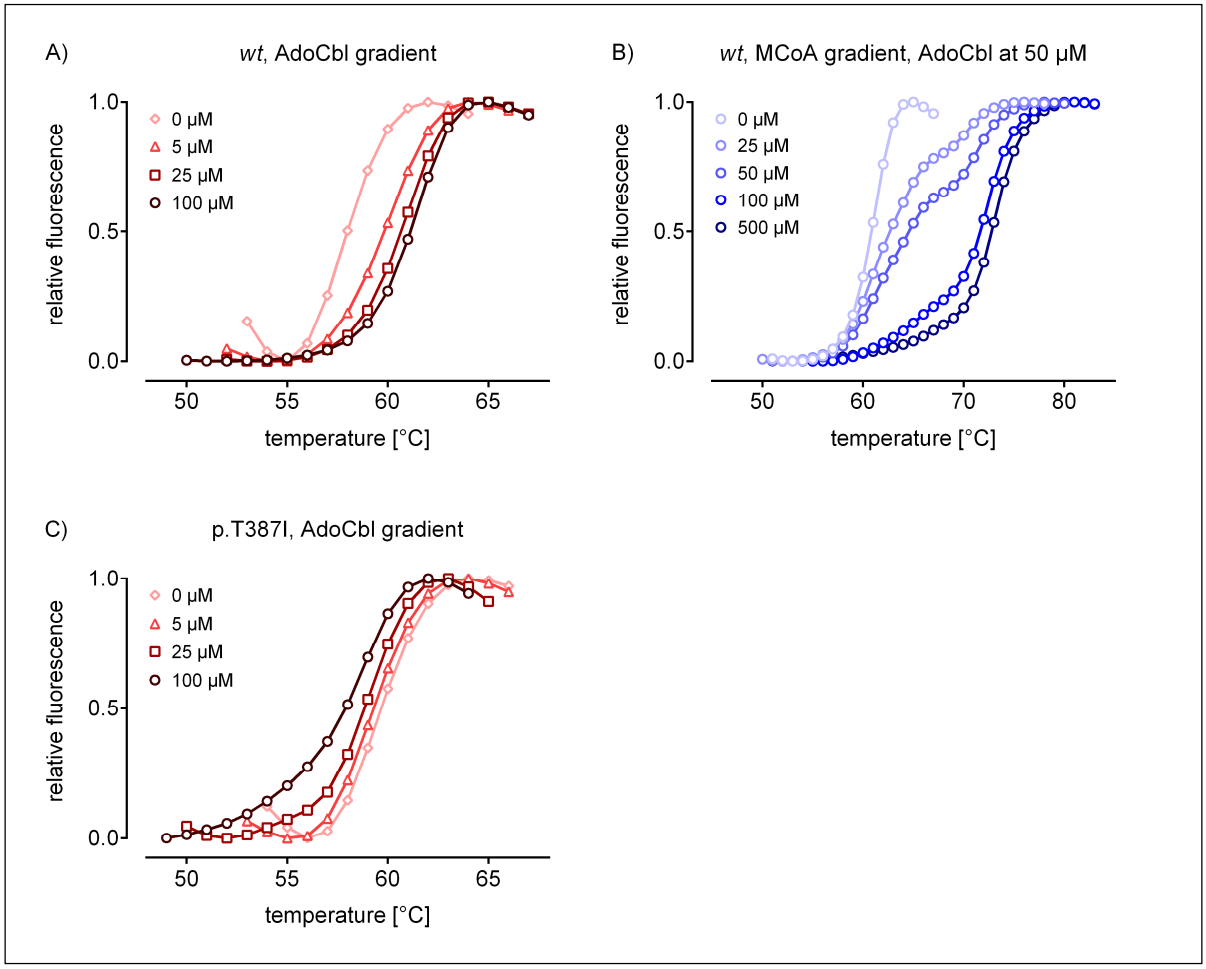

Figure S3. Ligand-dependent thermal denaturation of MUT. *wt* MUT is stabilized with increasing concentrations of AdoCbl (**A**) and malonyl-CoA (**B**). Mutant p.T387I is destabilized with increasing AdoCbl concentrations (**C**).

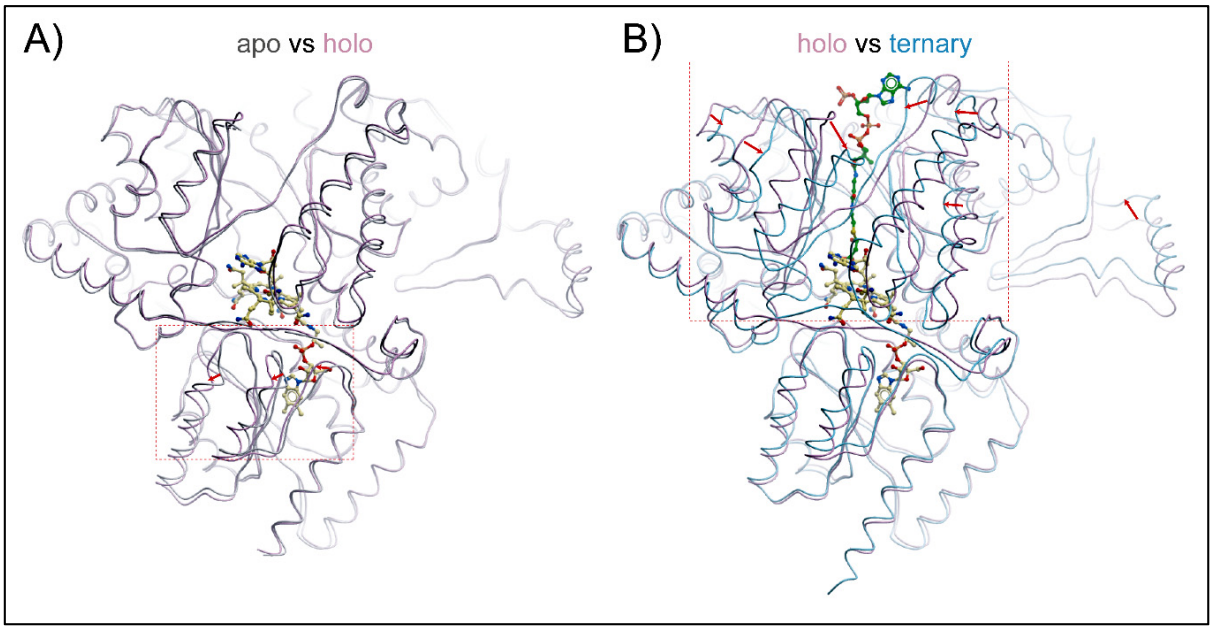

Figure S4. Substrate/cofactor-induced conformational changes in MUT. **A.** Superposition of MUT structures in the *apo* and AdoCbl-bound (*holo*) states shows modest rearrangement in the C-terminal domain (boxed) by the binding of AdoCbl alone. **B.** Superposition of MUT structures in the *holo* and ternary (AdoCbl and MCoA bound) states reveals substantial conformational changes in the N-terminal domain (boxed) by the additional binding of MCoA. Ligands are shown in sticks (AdoCbl, yellow carbon; MCoA, green carbon. (PDB codes: *apo*, 2XIQ; *holo*, 2XIJ; ternary, 2XIQ).

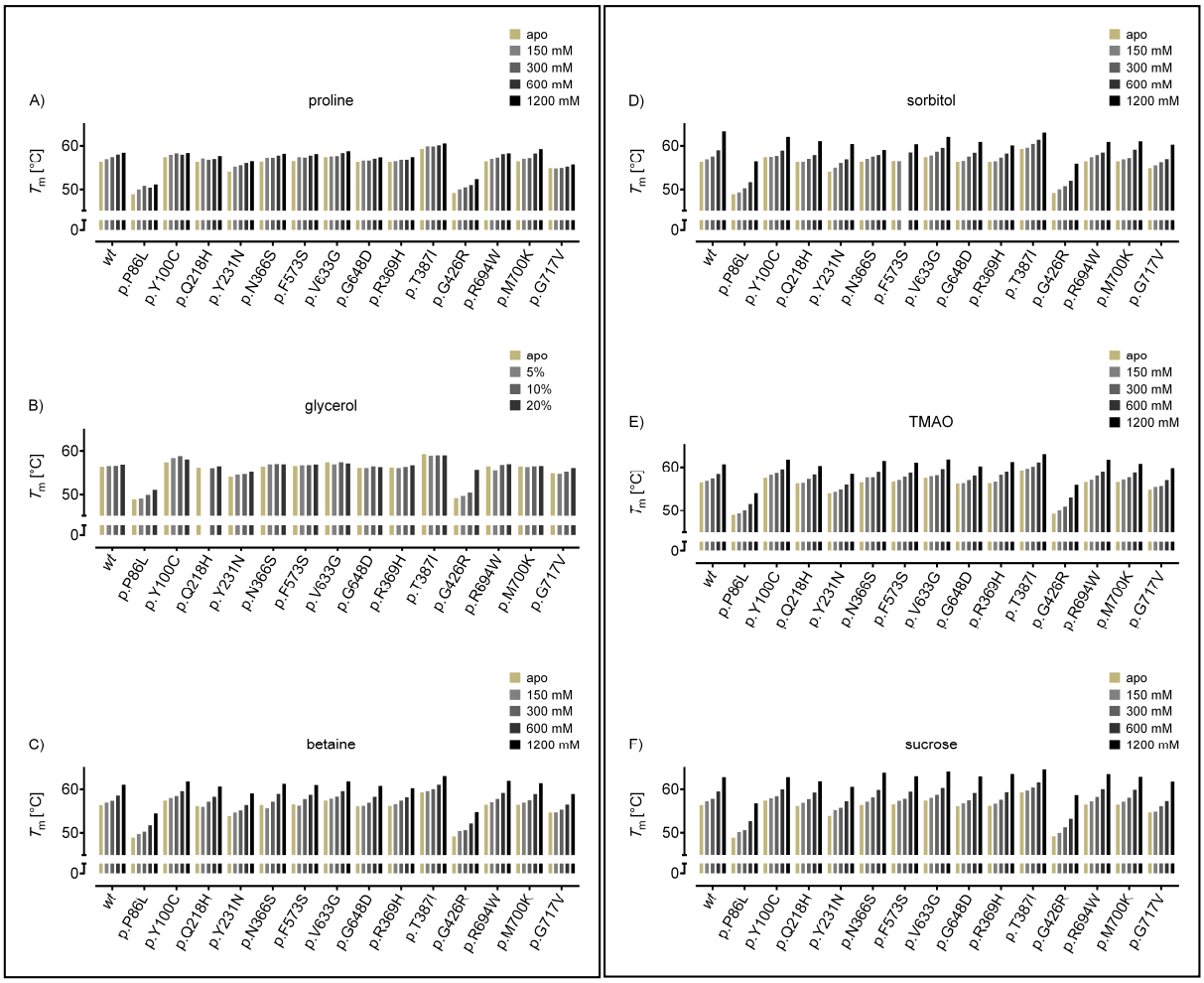

Figure S5. Concentrations-dependent thermal stabilization in wild-type and mutant MUT upon addition of chemical chaperones: **A.** proline, **B.** glycerol, **C.** betaine, **D.** sorbitol, **E.** TMAO, **F.** sucrose.

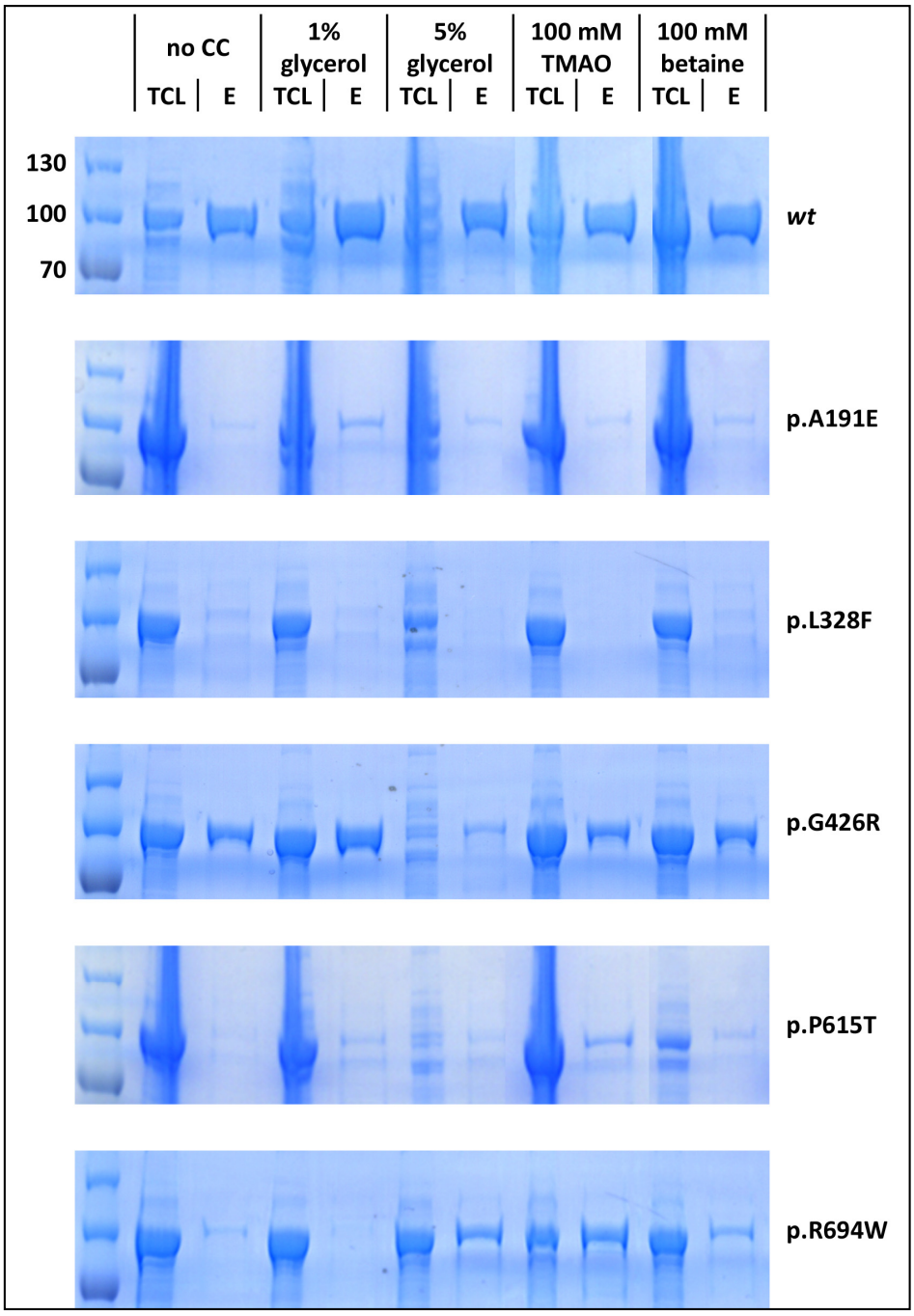

Figure S6. SDS-PAGE of test purification for wild-type, p.A191E, p.L328F, p.G426R, p.P615T and p.R694W after co-translational expression in the presence of chemical osmolytes. Glycerol (at 1% and 5%), TMAO and betaine at 100 mM were tested. For clarity, only the relevant gel section is shown. CC: chemical chaperone; TLC: total cell lysate; E: eluant after affinity purification; marker on left: sizes in kDa.

Table S1. Methylmalonyl-CoA mutase (MUT) activities and K_M values for the cofactor, adenosylcobalamin (AdoCbl). Transfection with *mut*^{0} mutations resulted in severely deficient activities of both *holo*- and total MUT whereas *mut*$^-$ mutations showed a clear response to AdoCbl with increase of MUT activity to variable levels associated with mild to highly elevated K_M for AdoCbl.

amino acid change	*mut* class	MUT activity, nmol/min/mg protein[¶]					K_M for AdoCbl, nM		
		holo-MUT (–AdoCbl)		total MUT (+AdoCbl)					
		single values	mean	single values	mean	% of *wt*	single values	mean	times *wt*
p.P86L	*mut*$^-$	0.03, 0.20	0.12	17.1, 14.8	16.0	79	3014	3014	636
p.Y100C	*mut*$^-$	0.02, 0.05, 0.07	0.05	8.49, 11.9, 15.8	12.1	60	3648	3648	770
p.A191E	*mut*^{0}	0.21	0.21	0.17	0.17	0.8	n.a.		
p.Q218H	*mut*^{0}	0.04, 0.07	0.06	0.07, 0.11	0.09	0.4	n.a.		
p.N219Y	*mut*^{0}	0.21	0.21	0.24	0.24	1.2	n.a.		
p.Y231N	*mut*$^-$	0.03, 0.24, 0.46	0.25	9.35, 12.6, 14.5	12.2	60	4759, 7280	6020	1270
p.Y316C	*mut*$^-$	0, 0.03, 0.05, 0.17	0.06	3.38, 3.48, 3.70, 3.99	3.64	18	15.5, 24.1	19.8	4
p.L328F	*mut*^{0}	0.03, 0.06	0.05	0.04, 0.06	0.05	0.2	n.a.		
p.S344F	*mut*$^-$	0, 0.01, 0.05, 0.06	0.03	0.41, 0.54, 0.74, 0.79	0.62	3.1	27.9, 44.9	36.4	8
p.N366S	*mut*$^-$	0, 0.01, 0.07	0.03	0.49, 0.56, 0.71	0.59	2.9	219	219	46
p.R369H	*mut*^{0}	0.05, 0.16, 0.16	0.12	0.04, 0.28, 0.49	0.27	1.3	n.a.		
p.T387I	*mut*$^-$	0.01, 0.05, 0.37	0.14	1.06, 2.06, 2.39	1.84	9.1	66.6	66.6	14
p.G426R	*mut*$^-$	0, 0.22	0.11	2.39, 2.79	2.59	13	9261	9261	1954
p.F573S	*mut*$^-$	0, 0.01, 0.05, 0.07	0.03	0.93, 1.02, 1.05, 1.89	1.22	6.0	6.21, 36.5	21.4	5
p.P615T	*mut*^{0}	0.06, 0.24	0.15	0.10, 0.34	0.22	1.1	n.a.		
p.P615L	*mut*^{0}	0.07	0.07	0.09	0.09	0.4	n.a.		
p.V633G	*mut*$^-$	0, 0.02, 0.04	0.02	8.73, 9.99, 11.9	10.2	51	1016	1016	214
p.G648D	*mut*$^-$	0, 0.14	0.07	15.0, 19.4	17.2	85	6503, 6720	6612	1395
p.R694W	*mut*$^-$	0.01, 0.07, 0.19	0.09	0.40, 0.80, 0.99	0.73	3.6	45.9	45.9	10
p.R694L	*mut*$^-$	0.01, 0.02, 0.06	0.03	0.26, 0.67, 0.70	0.54	2.7	84.1	84.1	18
p.M700K	*mut*$^-$	0, 0.05, 0.05	0.03	0.60, 0.66, 0.75	0.67	3.3	543, 208	376	79
p.G717V	*mut*$^-$	0.01, 0.03, 0.06	0.03	2.78, 4.69, 8.88	5.45	27	8484	8484	1790
p.L736F	*mut*$^-$	0, 0.06, 0.20	0.08	1.54, 2.96, 3.47	2.66	13	221	221	47
wt	mean range n	0.46 0.01 - 2.94 10		20.2 12.4 - 34.1 10		100	4.74 1.65-12.3 7		1
vector only[#]	mean range n	0.04 0 – 0.17 7		0.06 0 – 0.25 7					

'n.a.', not applicable.

[¶] Values are single values or the mean of duplicates from replicate experiments.

[#] Negative control: MUT activities measured after transfection with empty pTracer vector.

Table S2. Primers used for site-directed mutagenesis of pTracer-MUT *wt* and pNIC-MUT *wt* constructs.

amino acid change	F/R	primer sequence 5'-3'
p.P86L	Forward	GACTTACCTGAAGAACTTCTAGGAGTGAAGCCA
p.P86L	Reverse	TGTGAATGGCTTCACTCCTAGAAGTTCTTCAGG
p.Y100C	Forward	GGACCATATCCTACCATGTGTACCTTTAGGCC
p.Y100C	Reverse	GGTCCAGGGCCTAAAGGTACACATGGTAGGATA
p.A191E	Forward	TCCATGACTATGAATGGAGAAGTTATTCCAGTT
p.A191E	Reverse	TGCAAGAACTGGAATAACTTCTCCATTCATAGT
p.Q218H	Forward	AAACTTACTGGTACCATCCACAATGATATACTA
p.Q218H	Reverse	TTCCTTTAGTATATCATTGTGGATGGTACCAGT
p.N219Y	Forward	CTTACTGGTACCATCCAATATGATATACTAAAG
p.N219Y	Reverse	AAATTCCTTTAGTATATCATATTGGATGGTACC
p.Y231N	Forward	TTTATGGTTCGAAATACAAACATTTTTCCTCCA
p.Y231N	Reverse	TGGTTCTGGAGGAAAAATGTTTGTATTTCGAAC
p.Y316C	Forward	GGAATTGGAATGAATTTCTGTATGGAAATAGCA
p.Y316C	Reverse	CATCTTTGCTATTTCCATACAGAAATTCATTCC
p.L328F	Forward	ATGAGAGCTGGTAGAAGATTCTGGGCTCACTTA
p.L328F	Reverse	CTCTATTAAGTGAGCCCAGAATCTTCTACCAGC
p.S344F	Forward	CAGCCTAAAAACTCAAAATTTCTTCTTCTAAGA
p.S344F	Reverse	GTGTGCTCTTAGAAGAAGAAATTTTGAGTTTTT
p.N366S	Forward	GAGCAGGATCCCTACAATAGTATTGTCCGTACT
p.N366S	Reverse	TATTGCAGTACGGACAATACTATTGTAGGGATC
p.R369H	Forward	CCCTACAATAATATTGTCCATACTGCAATAGAA
p.R369H	Reverse	CATTGCTTCTATTGCAGTATGGACAATATTATT
p.T387I	Forward	GGGACTCAGTCTTTGCACATAAATTCTTTTGAT
p.T387I	Reverse	AGCTTCATCAAAAGAATTTATGTGCAAAGACTG
p.G426R	Forward	AAAGTGGCTGATCCTTGGAGAGGTTCTTAC
p.G426R	Reverse	CATCATGTAAGAACCTCTCCAAGGATCAGC
p.F573S	Forward	GATGCCCTGAAAAAGGTATCTGGTGAACATAAA
p.F573S	Reverse	ATTCGCTTTATGTTCACCAGATACCTTTTTCAG
p.P615T	Forward	GAACGTGAAGGTCGCAGAACTCGTCTTCTTGTA
p.P615T	Reverse	TTTTGCTACAAGAAGACGAGTTCTGCGACCTTC
p.P615L	Forward	GAACGTGAAGGTCGCAGACTTCGTCTTCTTGTA
p.P615L	Reverse	TTTTGCTACAAGAAGACGAAGTCTGCGACCTTC
p.V633G	Forward	CATGACAGAGGAGCAAAAGGTATTGCTACAGGA
p.V633G	Reverse	AGCAAATCCTGTAGCAATACCTTTTGCTCCTCT
p.G648D	Forward	GGTTTTGATGTGGACATAGACCCTCTTTTCCAG
p.G648D	Reverse	AGGAGTCTGGAAAAGAGGGTCTATGTCCACATC
p.R694W	Forward	GAACTTAACTCCCTTGGATGGCCAGATATT
p.R694W	Reverse	GACAAGAATATCTGGCCATCCAAGGGAGTT
p.R694L	Forward	GAACTTAACTCCCTTGGACTGCCAGATATT
p.R694L	Reverse	GACAAGAATATCTGGCAGTCCAAGGGAGTT
p.M700K	Forward	CGGCCAGATATTCTTGTCAAGTGTGGAGGGGTG
p.M700K	Reverse	TGGTATCACCCCTCCACACTTGACAAGAATATC
p.G717V	Forward	ATTTCTGTTTGAAGTTGTTGTTTCCAATGT
p.G717V	Reverse	CAAATACATTGGAAACAACAACTTCAAACA
p.L736F	Forward	AAGGCTGCCGTTCAGGTGTTTGATGATATTGAG
p.L736F	Reverse	ACACTTCTCAATATCATCAAACACCTGAACGGC

5 CHAPTER III: SCREENING AND VALIDATION OF PCS FOR MUT

This section presents the results from a screening experiment which aimed at identifying stabilizing compounds for MUT, including subsequent validation experiments. The figure and table numbering is only applicable to this section of the thesis.

5.1 BACKGROUND

In a previous publication, also presented in this thesis (Forny, et al., 2014), we have described several 'folding' mutants of MUT. These mutants were found to show very low or absent amounts of residual MUT protein on Western blotting. Therefore, they were assigned to the biochemical class of unstable mutant proteins. Since the active site is often unaffected in these mutants, resulting in a normal or sub-normal enzyme activity, they are candidates for a small molecule "chaperoning" approach in order to stabilize their native confirmation or to help the folding of a mutant polypeptide into a functional enzyme. The use of pharmacological chaperones (PCs) has been proposed as a treatment option for various protein misfolding diseases such as phenylketonuria (Nascimento, et al., 2008; Pey, et al., 2004; Pey, et al., 2008; Torreblanca, et al., 2012) or LSDs (Fan, 2008; Guce, et al., 2011; Lieberman, et al., 2007; Maegawa, et al., 2007; Suzuki, 2013).

A relatively simple and widespread method for the screening of small molecule protein stabilizers is differential scanning fluorimetry (DSF), which originated from the field of protein crystallization. The big need of such molecules required for protein stabilization in order to increase the likelihood of the formation of ordered crystals, led to the development of this method (Niesen, et al., 2007). DSF utilizes a hydrophobic fluorescent dye which binds to non-polar residues of proteins. These residues are usually buried within the core of a soluble protein and are only exposed after induced degradation, *e.g.* by heat exposure. The increasing temperature leads to the binding of the dye to the hydrophobic residues of the protein and thus the dye becomes unquenched and starts emitting a fluorescent signal. The earlier a signal can be detected, the earlier the protein degrades upon heat exposure. During a screening for stabilizers employing the DSF method, a small molecule library is randomly tested for compounds which are able to increase the melting point of the tested protein. In the presented study, MUT-*wt* protein was used to perform this screening experiment. As a proof of concept, this protein was shown to be stabilized by the natural ligands AdoCbl and malonyl-CoA (substrate analogue) (Forny, et al., 2014). After the initial screening, these compounds were validated in cell culture experiments and also tested for their effect on mutant MUT proteins. With this study, we evaluate MUT for its amenability to PC screening.

5.2 Initial Library Screening

The screening was performed in collaboration with the Department of Biomedicine at the University of Bergen in September 2012 at the lab of Prof. Aurora Martinez which has great expertise with the screening of small molecule stabilizers (Calvo, et al., 2010; Jorge-Finnigan, et al., 2013; Pey, et al., 2008; Stevens, et al., 2010; Thony, et al., 2008). For this screening, MUT-*wt* protein was purified as previously described (Forny, et al., 2014). The screened library (MyriaScreen Diversity Library) consisted of 10,000 compounds, which were all dissolved in dimethyl sulfoxide (DMSO). High-throughput screening was performed by the DSF method and each compound was evaluated for its ability to enhance thermal stability of the tested MUT-*wt* protein in comparison to the baseline condition with DMSO only.

Initially, 27 hit compounds were found to cause a positive shift of the thermal melting curve (3 examples in Fig. 1). First, false-positive compounds were excluded, *e.g.* by the pan assay interference compounds (PAINS) method (Dahlin, et al., 2015). Compounds can form aggregates or directly interfere with the signalling molecule of the assay (Baell and Holloway, 2010). Medicinal chemistry analysis allowed further reduction of the compounds to finally 14 hits which had to undergo validation experiments by biophysical methods and cell culture assays.

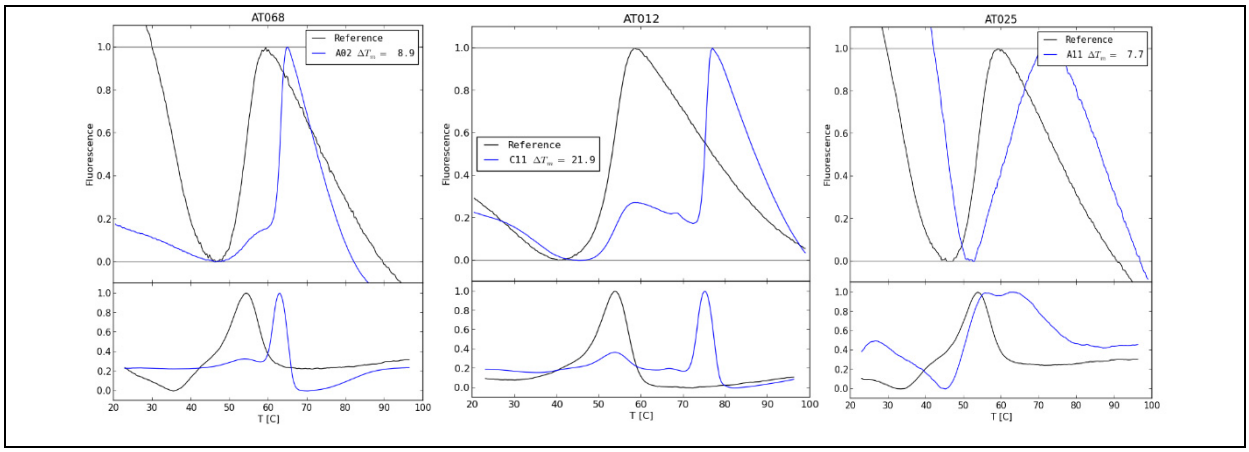

Figure 1. Three examples of compounds (F, D, C (see table 1))which were able to induce a thermal stabilization of MUT-*wt* in DSF. Upper graphs in each panel: The blue curve represents the melting curve with added compound, the black curve is the control condition with DMSO only. Lower graphs in each panel: The curves represent the slope of the curves in the upper panels.

5.3 VERIFICATION OF HIT COMPOUNDS

After the results from the high-throughput screening revealed positive hits, they were partly confirmed by surface plasmon resonance (SPR) as shown by the two examples in Fig. 2 and by repeated DSF experiments. Based on SPR and DSF results, the hits were further reduced to six compounds. For further verification of these compounds we performed experiments in cell culture in order to translate the observed stabilizing effect in DSF to a biological environment. We over-expressed MUT-*wt* and MUT mutants in an *E. coli* and a human fibroblast cell expression system to investigate the effects of the selected compounds on cell viability, residual protein levels and enzyme activity.

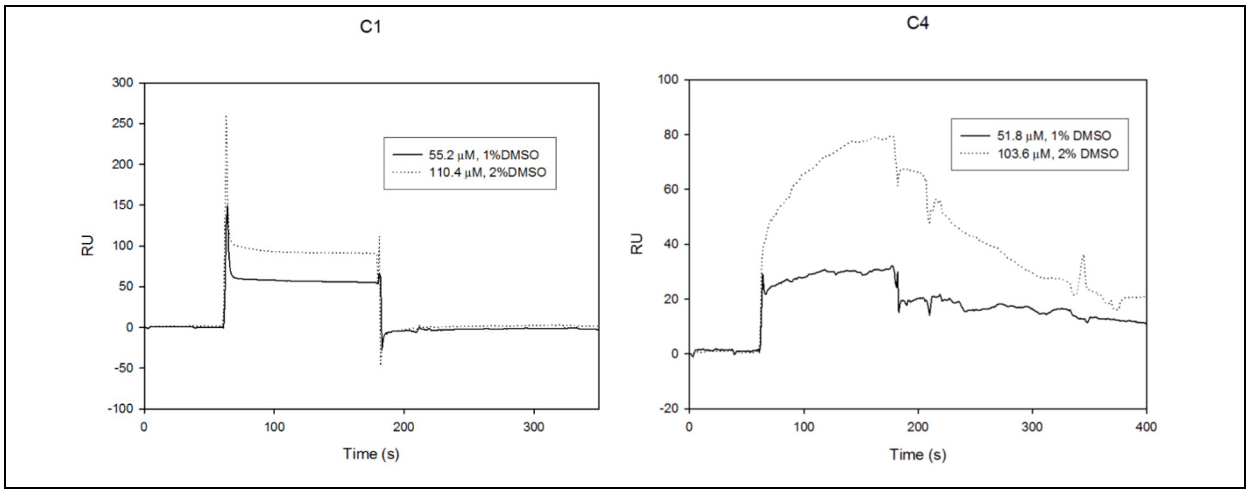

Figure 2. SPR results depict the binding curve of two exemplary compounds (A, D (see table 2)) which showed a clear binding behaviour at both concentrations tested.

5.3.1 Selection of hit compounds

Based on the first validation data, we compiled a list of compounds which were promising according to DSF and SPR. Because of a lack of overlapping results, we had to select the compounds mostly according to their individual behaviour in either DSF or SPR experiments (Table 1).

Compound number	Screening by DSF	Validation by SPR
A		X
B	X	
C	X	
D	X	X
E		X
F	X	

Table 1. The list depicts the compounds which were selected for evaluation in cell culture experiments. "X" indicates confirmation of hit compound in either the DSF or SPR experiments.

5.3.2 Evaluation of compounds in the *E. coli* expression system

To investigate the influence of compounds on the stability of MUT-*wt* and mutant MUT proteins of human and mouse, we reconstructed these alleles in a recombinant *E. coli* expression system. The proteins were assessed on their:

i. expression level relative to *wt* protein, as judged by protein amount in total cell lysate,

ii. and solubility, as judged by protein amount after affinity purification (eluant fraction). An increase in protein amount in the eluant fraction was considered a stabilization effect of the compound.

Final concentration of compounds was at 0.1 mM, final DMSO concentration was 0.5%. The respective compounds were added when protein expression was induced with IPTG before overnight cell growth as previously described (Forny, et al., 2014).

While the expression levels varied to some degree between human and mouse *wt*, and mouse mutant p.M698K respectively, the expression of each was stable (Fig. 3, left lanes) and unaffected by the growth condition (control, DMSO or compound supplemented). For human MUT-*wt* protein, no observable differences in protein stability could be identified regardless of the compound supplemented. This same protein had been used in a purified form for the library screening in the first place, where its thermostability was increased by all the tested compounds. The stabilization effect observed in the DSF experiment therefore could not be replicated with this complementary method. Although some compounds seemed to have changed the stability of mouse Mut-*wt* and mouse Mut-p.M698K, these effects might be unspecific, since DMSO increases the amount of mouse Mut-*wt* (Fig. 3, right lanes).

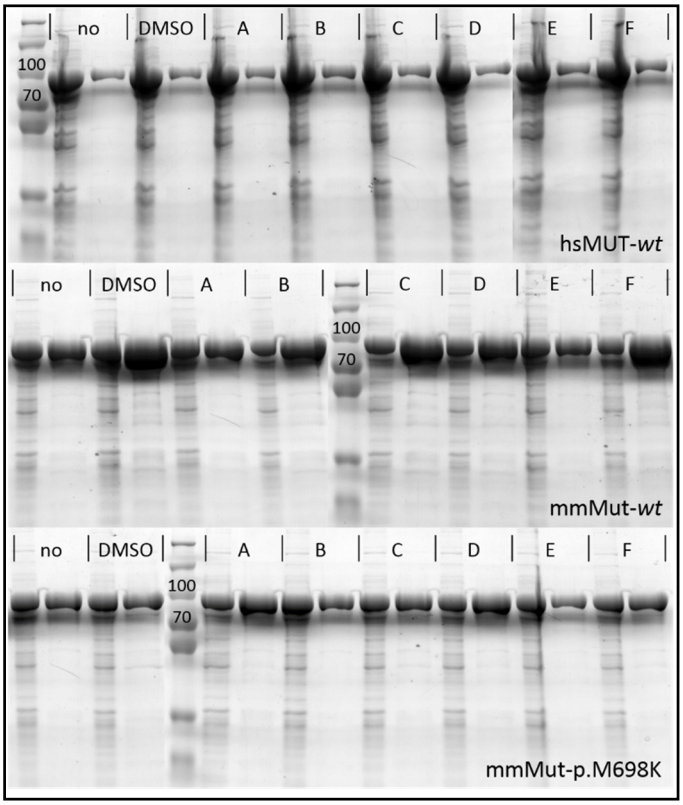

Figure 3. The influence of compounds on the stability of mutase protein after overexpression in *E. coli* system. Bacterial overnight cell growth was performed under standard conditions (two first lanes, 'no') or supplemented with either DMSO or one of the compounds A-F (lanes adjacent to the control ('no') lane). For each condition, lanes for total cell lysate (left) and eluant after one-step nickel purification (right) are shown. Calculated molecular weight of mutase: 84 kDa; hs, *homo sapiens*; mm, *mus musculus*.

Since unstable mutant proteins might be more sensitive to stability corrections mediated by a compound, we hypothesized that an increase in protein level may be better seen in an experiment with mutated translated polypeptides. Based on previous results (Forny, et al., 2014) we have selected five low-solubility MUT mutants to evaluate the effects of the compounds on their stability.

Other than compound A, which may have upregulated the soluble fraction of the human MUT mutant p.R694W, none of the compounds showed a change in the level of soluble mutant protein (Fig. 4). Compound E was not tested in this second experiment since it had shown cellular toxicity in fibroblast cell culture as further outlined in the next section (Table 2).

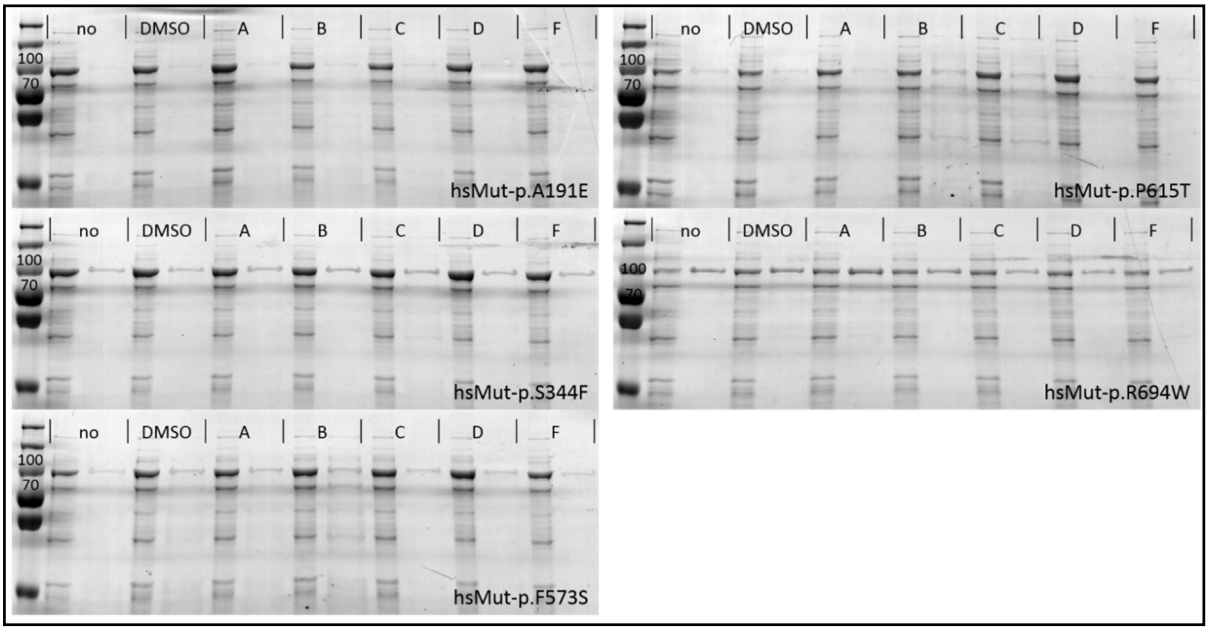

Figure 4. Compounds cannot rescue unstable MUT mutants overexpressed in *E. coli* system. *E. coli* bacteria, transformed with different hsMUT constructs, were grown under standard conditions and supplemented with either DMSO or a compound (lysates, left lanes; eluants, right lanes; details see Fig. 3); hs, *homo sapiens*; mm, *mus musculus*; no, no supplement added.

5.3.3 Evaluation of compounds in human wild-type fibroblasts

We have used a fibroblast cell culture system (human *wt* cell line PJP-T) to test the influence of compounds on MUT-*wt* stability and activity in a Eukaryotic cell environment. After cells were grown to 80% confluence, the cell culture medium was supplemented with compounds to a final concentration of 0.1 mM (0.5% DMSO). As control conditions, the culture medium was supplemented with DMSO only and non-supplemented cell culture medium was used. Cells were incubated and monitored by microscopy for 48 hours and then harvested. The cell pellet was re-suspended in 0.005 M K-phosphate lysis buffer with subsequent sonication to obtain a cell lysate which was stored at -20°C and later exposed to heat for several hours or used for MUT activity assay. To find the ideal temperature for heat exposure preliminary experiments were carried out. As a proof of principle, cells were incubated with Cbl to show the stabilization effect conferred by the endogenous ligand as previously shown in DSF.

5.3.3.1 Heat treatment of cell lysates

From DSF studies it is known that the T_m (temperature at the transition point of the melting curve) of MUT-*wt* is about 58°C (Forny, et al., 2014). Therefore, a range of temperatures from 42 to 56°C was

applied for up to six hours and MUT degradation was followed by Western blot analysis. At all temperatures tested the MUT protein was degraded over time, although at different speeds. A temperature just above 46°C resulted in useful degradation curve (Fig. 5).

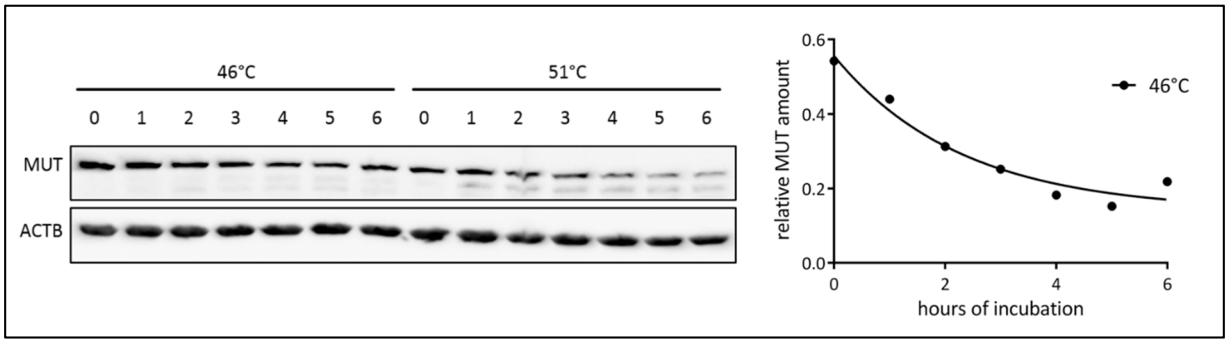

Figure 5. MUT protein degrades over time when exposed to heat. The degradation at 46°C corresponds to a non-linear fitting curve as shown on the right. ACTB = β-Actin; MUT = methylmalonyl-CoA mutase.

5.3.3.2 Proof of concept: MUT can be stabilized by the cofactor ligand

Previously we have demonstrated by the DSF assay that the cofactor AdoCbl can increase thermostability of purified MUT-*wt* protein by approximately 2.5°C *in vitro* (Forny, et al., 2014). To replicate this finding in cell culture, we supplemented the cell culture medium of fibroblasts with hydroxocobalamin (OHCbl) for two days and investigated its effect on MUT stability when the cell lysate was exposed to heat afterwards. Since OHCbl is taken up by fibroblasts and converted to the two cofactor forms MetCbl and AdoCbl, we expected OHCbl supplementation to result in the production of AdoCbl, which would then stabilize MUT.

Aliquots of cell lysates were taken during incubation at 47°C at 0 to 5 hours and Western blot analysis was performed. Degradation of MUT was slowed down when the cells had been previously incubated with OHCbl (Fig. 6).

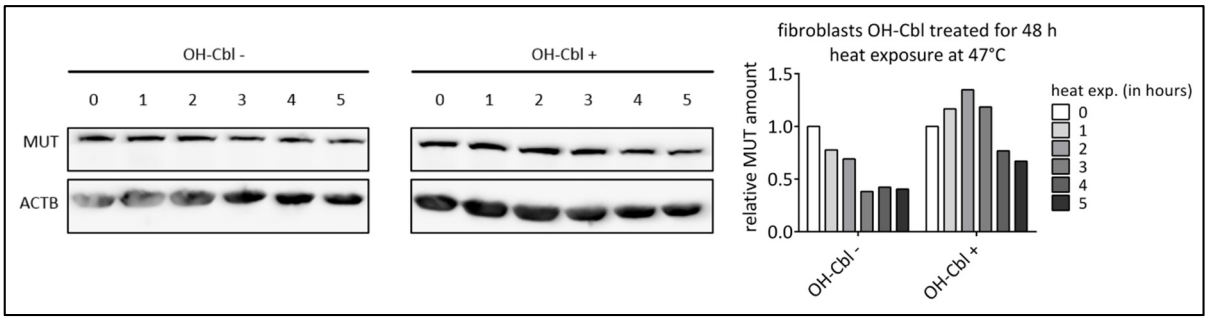

Figure 6. Mutase can be stabilized when supplemented with OHCbl for 48 hours during cell growth in human *wt* fibroblasts. Western blot images on the left show decreasing amount of MUT protein when incubated at 47°C for up to 5 hours. Quantification of the Western blot bands reveals a higher heat resistance of MUT derived from OHCbl treated cells compared to MUT from cells which were grown in non-supplemented cell culture medium. MUT band intensities were first normalized to β-Actin and then to the condition at 0 hours. ACTB = β-Actin.

5.3.3.3 Effect of compounds on cell growth

Fibroblast cell growth was monitored by microscopy during the full 48 hours following compound addition to evaluate toxicity effects. Compound E showed clear toxicity, killing all cells within 24 hours of incubation, and was therefore excluded from all further experiments. Compounds A, B and F slowed down cell proliferation, and compound F also changed the morphological appearance of the fibroblasts (Table 2).

Compound	Before incubation	After 24 hours	After 48 hours
no	80	95	>100
DMSO	80	95	>100
A	80	70	80
B	80	95	100
C	80	95	>100
D	80	95	>100
E	80	0	0
F	80	90	90

Table 2. Confluency of fibroblasts following addition of compounds. Cell viability was influenced by compounds as judged by confluence of the cell layer. Numbers indicate representative levels of confluence in percent (no cells: 0%; flask bottom is fully covered with cells: 100 %; over-confluent: >100%); no, no compound added.

5.3.3.4 MUT stability and activity after incubation with compounds

MUT protein level was determined by Western blot analysis after the cells had been incubated for 48 hours with the respective compound. None of the compounds increased MUT protein level. By contrast, some resulted in clearly reduced protein amounts (compounds A, B, F; Fig. 7i), possibly due to unspecific cell toxicity effects since these three compounds resulted in decreased cell proliferation (Table 2).

Although activity measurements are corrected for protein amount, the compounds which caused the MUT amount to decrease by Western blot analysis also showed low enzyme activity (Fig. 7ii). While DMSO has an effect on MUT protein level, it does not change the level of enzymatic activity.

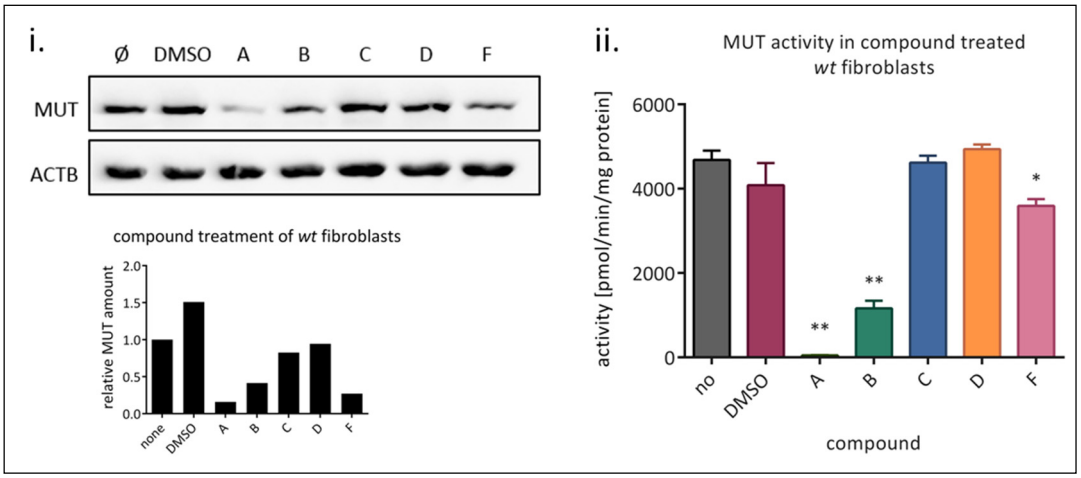

Figure 7. MUT amount and activity are influenced by the addition of compounds. (**i.**) Western blot analysis reveals different levels of detected MUT protein, suggesting an unspecific effect of the compounds on protein expression. (**ii.**) None of the compounds increased enzyme activity in lysates of incubated fibroblasts. ACTB = β-Actin. Significance levels are derived from the respective value for the compound compared to *wt* control values and were determined by ANOVA multi comparison test; *: $p < 0.05$; **: $p < 0.0001$.

5.3.3.5 Effect of heat exposure on MUT stability in incubated cells

To check the stabilization potential of compounds when they were added to cell culture medium for two days, the lysates were exposed to 48°C for 0 to 5 hours and Western blot analysis was performed. Similar to OHCbl (Fig. 6), some compounds (C, D, and F) might potentially stabilize MUT by slowing down the degradation of the protein, although this effect might be unspecific since DMSO shows a similar phenomenon (Fig. 8).

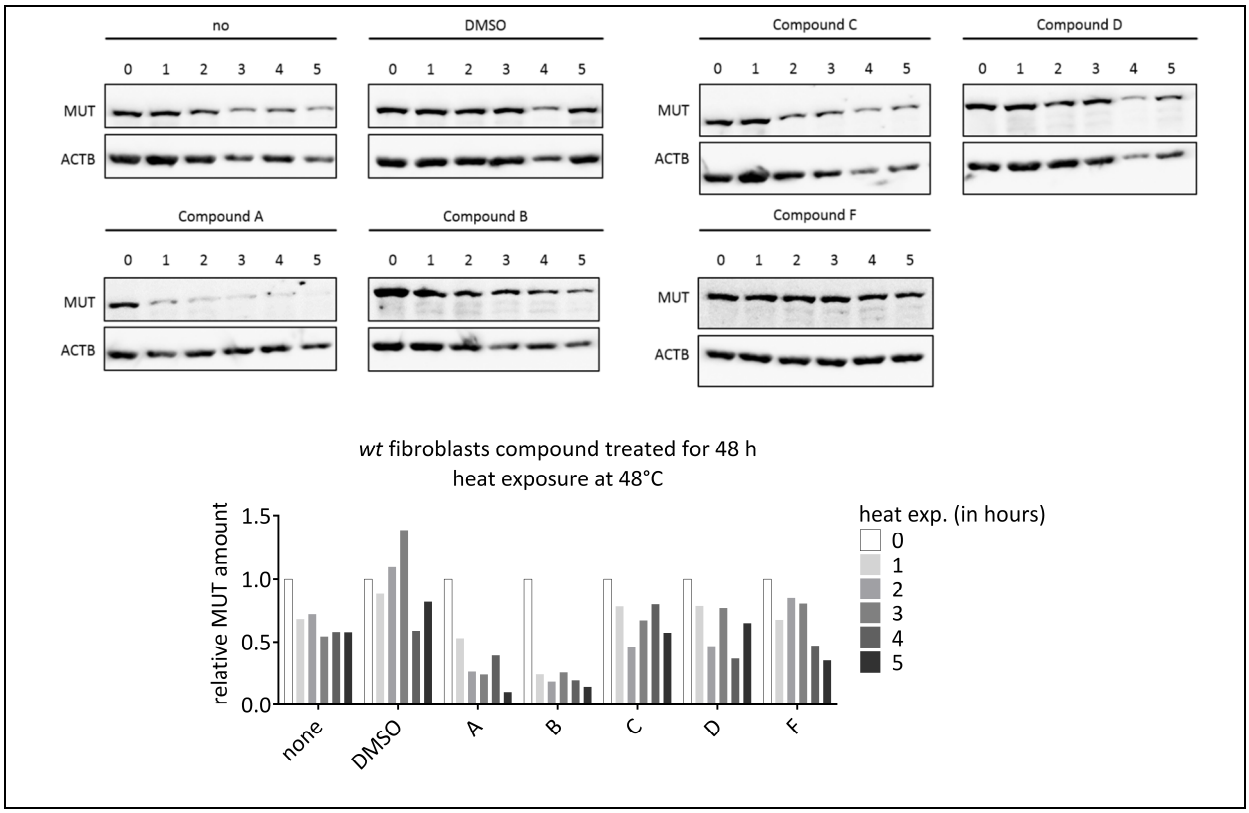

Figure 8. None of the compounds mediate a clear improvement of MUT stability. After *wt* fibroblast cells have been grown under standard conditions ('no') or incubated with DMSO or one of the compounds, its lysates were exposed to 48°C for 0 to 5 hours. Quantification of Western blot bands was normalized first to beta-actin and then to the band intensity at 0 hours for each individual condition. ACTB = β-Actin.

5.3.3.6 Compound effect on *wt* fibroblast lysates

To circumvent the effect that compounds might have during cell growth, the compounds were added at a later stage directly to lysates of *wt* fibroblasts, which were grown under normal conditions without any compound supplements. Ten minutes after the compounds were added to the lysates, one aliquot was frozen, and the second aliquot was exposed to 50°C for three hours and then frozen. Investigation of both samples after incubation to this slightly higher temperature showed two bands for MUT in Western blot with the lower one likely being derived from degraded MUT protein. This experiment aimed at checking whether the addition of compounds can (i) stabilize MUT, and (ii) decelerate the formation of degraded MUT protein.

The addition of the compounds in a later phase of the experiment did not change the outcome regarding MUT stabilization. The compounds were not capable of stabilizing the MUT protein at this higher temperature (Fig. 9). The formation of degraded MUT protein was not decelerated when the compounds were added to the cell lysate, as it was observed in the DMSO control.

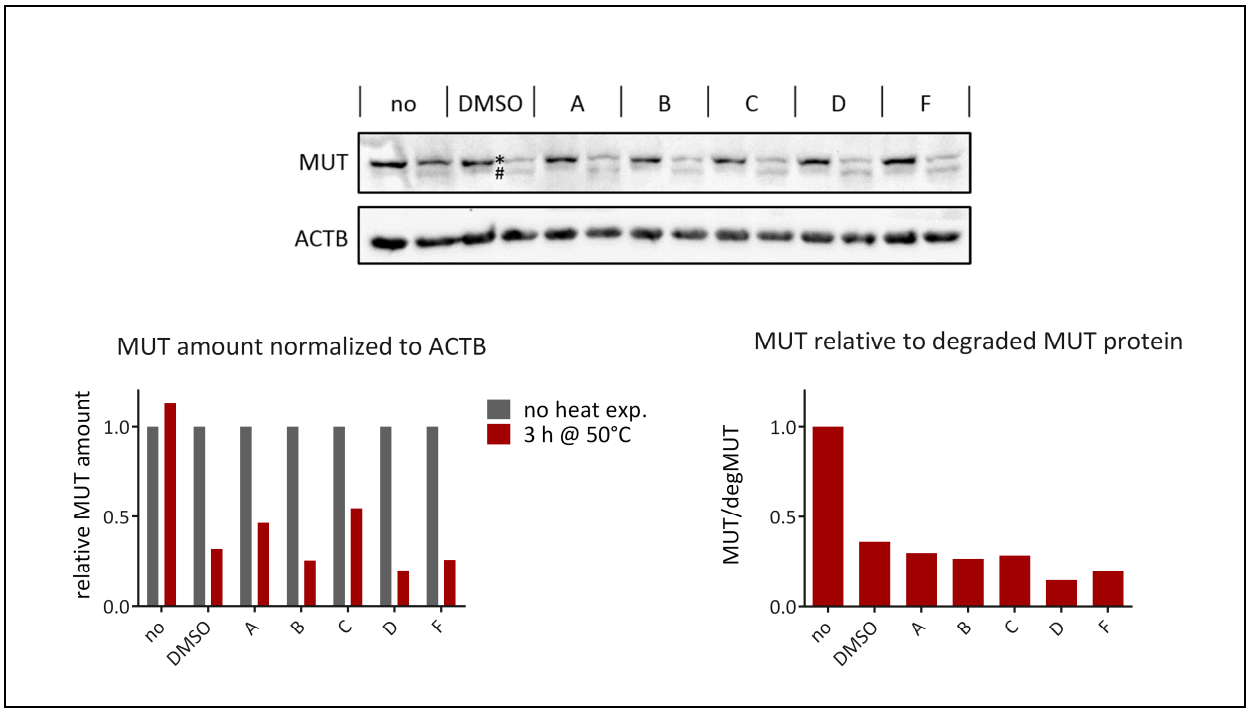

Figure 9. Compounds cannot avoid the formation of degraded MUT. Western blot on top shows two lanes for each condition: the sample on the right was exposed to 50°C for three hours after the respective compound was added while the other sample was only supplemented with compound. The heat treated sample shows two bands for MUT, with (*) the top band representing MUT protein with undisturbed integrity and (#) the lower band showing degraded MUT protein. The **left graph** depicts the quantification of the MUT bands (without considering the lower band) normalized to beta actin and relative to the sample which was not heat exposed. The **right graph** delineates the degradation of MUT protein normalized to the first sample where no compound was added ('no'). ACTB = β-Actin.

5.4 Conclusion

From the results generated in this study a clear indication, that any of the compounds increase the protein level or stability of *wt* or mutant MUT in either of the two test systems (*E. coli* or fibroblasts) applied, is not apparent. In the MUT activity assay, only unspecific (detrimental) effects were detected which may also be biased by the effects these compounds have on cell proliferation and viability. The effects which were promising (*e.g.* compound A in Fig. 4 or compound F in Fig. 9), can mostly be explained either by (i) unspecific effects which are also present in DMSO or (ii) an ambiguous impact on cell proliferation and viability.

The absence of a clear-cut MUT-specific compound effect does not directly imply an inefficacy of the selected molecules, as it remains unclear whether a change in the experimental conditions would lead to different results with different implications. Although none of these compounds have thus far shown a consistent positive effect in our validation experiments, we believe they might be worth

further time and experimental investigation (*e.g.* further verification by modified cell culture experiments or subsequent testing in mouse models).

6 CHAPTER IV: GENERATION OF A CONDITIONAL *MUT*-KO MOUSE MODEL

This chapter represents the results from a subproject which aimed at introducing a novel mouse model to study the CNS phenotype in MMAuria. The data presented will serve as a basis of future projects. The figure numbering is restricted to this section of the thesis.

6.1 BACKGROUND

One of the major long-term complications in MMAuria affects the central nervous system (CNS). Neurological disorder manifests mainly with extrapyramidal movement disorder with ataxia, diplegia and tetraparesis (Nicolaides, et al., 1998). The reason why the brain is specifically vulnerable in MMAuria remains unclear. Nevertheless, studies on glutaryl CoA dehydrogenase deficiency have investigated the role of the blood-brain barrier and how limited flux across this barrier can contribute to the CNS phenotype in this other organic aciduria (Sauer, et al., 2006). The "trapping hypothesis" conveys that the accumulating metabolites produced by cells within the blood-brain barrier cannot sufficiently be exported into the blood circulation (Morath, et al., 2008). This hypothesis is further supported by the finding of acute lesions in the brains of patients who have undergone solid organ transplantation (Chakrapani, et al., 2002; Kaplan, et al., 2006; Vernon, et al., 2014), suggesting that these patients remain at risk due to exposure of the brain to high levels of accumulating metabolites. A similar situation in line with this hypothesis can be studied in the mouse using a conditional knock-out model.

The rationale to study MMAuria neurology in rodents is given by the fact that the catabolic pathway of propionate metabolism is expressed in the rat CNS (Ballhausen, et al., 2009). To circumvent the neonatal lethality shown in homozygous ko pups (Peters, et al., 2003), we have developed a tissue-specific knock-out mouse model using the well-established Cre-Lox site-specific recombination technology (Friedel, et al., 2011). We generated a mouse model with a floxed exon 3 of the *Mut* gene, which allows the excision of the floxed DNA segment by a tissue-specifically expressed Cre recombinase. This process leads to the knock-out of the target gene (*Mut*) in this particular tissue, since deletion of exon 3 has a deleterious effect on *Mut* expression as previously shown (Peters, et al., 2003). To create a CNS-specific knock-out of *Mut* we have crossed the $Mut^{flox/flox}$ strain with a Nestin-Cre (Nes-Cre) expressing mouse line to breed $Mut^{flox/flox}$;Nes-Cre mice. Nestin is an intermediate filament protein and it is expressed at high levels in neuro-epithelial precursor cells. Hence, Nes-Cre is frequently used to induce deletion in precursor cells of the CNS (Tronche, et al., 1999). This chapter

recapitulates the basic characterization of these mice, aiming at evaluating this novel model for its suitability in the study of the neurological phenotype observed in MMAuria.

6.2 RESULTS

To verify the efficient deletion of exon 3 of *Mut* and the subsequent absence of Mut protein/activity in brain tissue, quantitative real-time PCR (RT-qPCR), Western blot analysis and enzymatic measurements were performed. To further investigate the consequence of *Mut* deletion on tissue metabolites, we determined levels of MMA and 2-methylcitrate (2-MC). For the presented experiments we used brain tissue samples harvested at 35 days of age and generated whole brain homogenates as described in chapter 7. Mice with three different genotypes were investigated: $Mut^{flox/flox}$;Nes-Cre, and wild-type (*wt*) and $Mut^{flox/flox}$ as controls. To compare brain data to values from other tissue, we used liver tissue from the same mice.

6.2.1 Downregulated *Mut* expression leads to absent Mut protein

To determine *Mut* expression in whole brain homogenates we used the RT-qPCR TaqMan method and compared Cre-positive floxed mice to *wt* and Cre-negative floxed mice. In $Mut^{flox/flox}$;Nes-Cre animals the *Mut* gene is significantly downregulated compared to the control animals (Fig. 1). The almost complete absence of *Mut* mRNA suggest an efficient deletion of exon 3 *Mut* on the genomic level by the Cre recombinase and subsequent nonsense-mediated mRNA decay of this modified mRNA molecule. To observe how these results translated to the protein level, Western blotting was used to detect the amount of residual Mut protein in the brain tissue homogenates. Consistent with RT-qPCR results, Mut is absent in $Mut^{flox/flox}$;Nes-Cre animals while it shows comparable levels in *wt* and $Mut^{flox/flox}$ mice (Fig. 2).

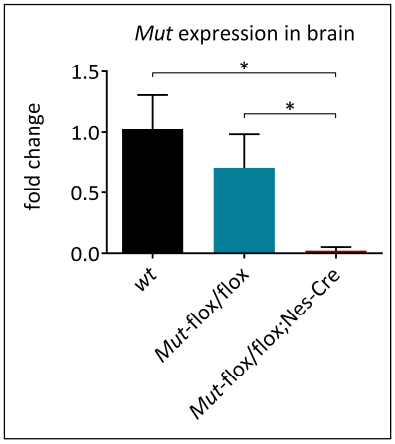

Figure 1. *Mut* expression is significantly reduced in *Mut*$^{flox/flox}$;Nes-Cre mice. Bars represent mean values (n = 5) of the fold change in *Mut* expression compared to mean *wt* expression level which is set to 1. All results have been normalized to β-actin levels in the individual samples. Error bars depict SD, *: $p < 0.01$ determined by ANOVA multiple comparison test.

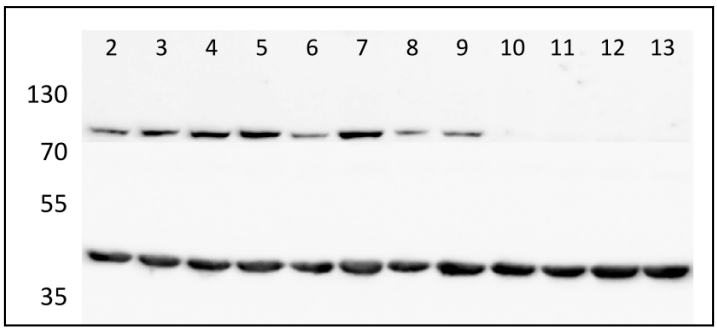

Figure 2. Western blot reveals the absence of the Mut protein in the brains of *Mut*$^{flox/flox}$;Nes-Cre mice. Lane **1**, ladder (not shown); lanes **2-5**, *wt* samples; lanes **6-9**, *Mut*$^{flox/flox}$ samples; lanes **10-13**, *Mut*$^{flox/flox}$;Nes-Cre samples. Lower band depicts β-actin (41 kDa), upper band represents the Mut protein (84 kDa).

6.2.2 Decreased Mut activity leads to elevated MMA and 2-MC levels

To determine the tissue-specificity of the Cre knock-down, we measured Mut activity in brain and liver tissue as described (Forny, et al., 2014). While Mut activity was clearly down-regulated below detection limit of the assay in brain tissue of *Mut*$^{flox/flox}$;Nes-Cre mice, activity levels in brains of control mice (*Mut*$^{flox/flox}$ and *wt* mice) was normal (Fig. 3, left panel). In liver the genotype of the mice did not affect the activity levels (Fig. 3, right panel), suggesting that Nes-Cre is not active in liver cells. This finding points to a tissue specificity of Cre activity in the brain, where it led to the knock-out of *Mut*. As a consequence of the absent Mut activity in brains of *Mut*$^{flox/flox}$;Nes-Cre mice, MMA and 2-MC were elevated in this tissue but not in the brain of control mice (Fig. 4), while metabolites were low or below detection limit of the assay in *wt* and *Mut*$^{flox/flox}$ mice. Liver tissue showed constant levels of MMA and 2-MC (Fig. 4) which is in line with the normal enzyme activity found in this organ (Fig. 3).

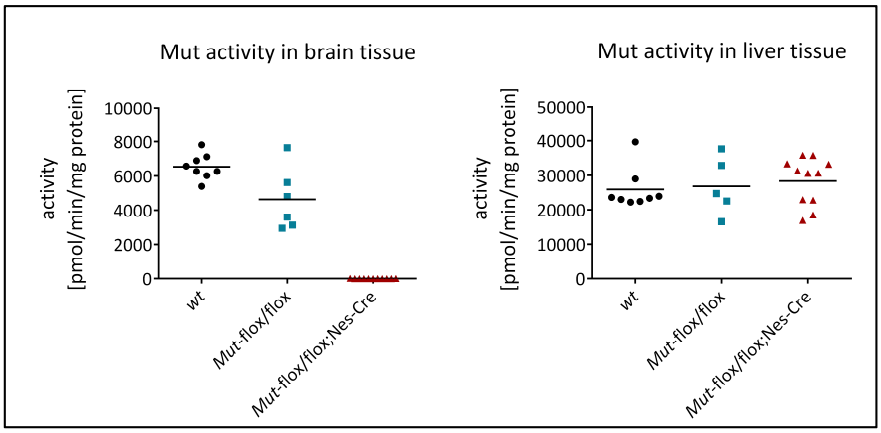

Figure 3. The activity assay shows no residual mutase activity in the brain homogenates of *Mut*$^{flox/flox}$;Nes-Cre mice. Data points represent single animals; horizontal lines represent the mean values of the respective group.

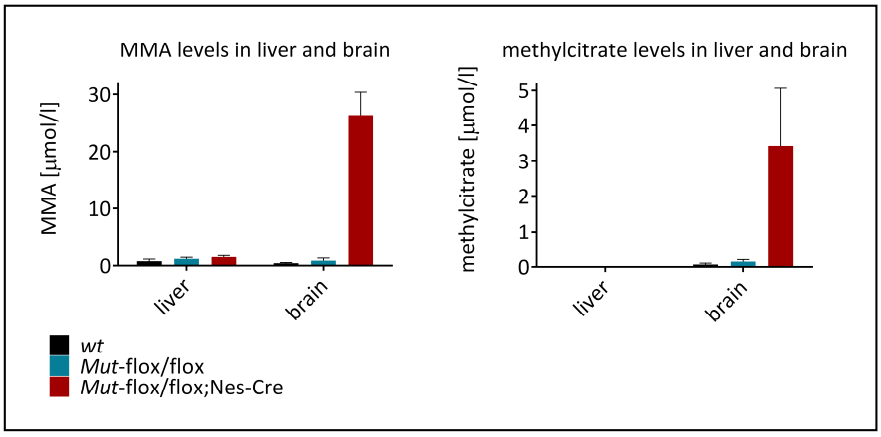

Figure 4. MMA (left panel) and 2-MC (right panel) values were determined in brain and liver homogenates by LC-MS. MMA levels were only increased in brains of *Mut*$^{flox/flox}$;Nes-Cre mice. 2-MC showed the same pattern while in liver this metabolite was not detectable.

6.3 Discussion

Mut activity is down-regulated below detection limit in the brain, but normal in liver of *Mut*$^{flox/flox}$;Nes-Cre mice. This indicates that Cre deletion of exon 3 of *Mut* is tissue-specific and efficient at the same time. Although the enzyme assay has a detection limit, the real activity of Mut in the brain of *Mut*$^{flox/flox}$;Nes-Cre mice seems to be lowered enough in order to lead to increased metabolites derived from the substrate of the Mut catalysed reaction. Although the application of Nes-Cre transgenic mice is regarded as reliable (Dubois, et al., 2006), one has to bear in mind the pitfalls of the Cre-Lox site-specific recombination system (Harno, et al., 2013). In our experiments we could show that

Mut$^{flox/flox}$ did not show any effects of Cre-induced deletion of *Mut*, indicating a robust system without epigenetic Cre transmission during breeding as described previously (Harno, et al., 2013).

Overall, these preliminary results confirm the conditional-ko model and its tissue-specific nature. They encourage further studies in which the neurological phenotype in mice can be investigated. In fact, the "trapping hypothesis" as described in (Morath, et al., 2008) could be confirmed with these results, since metabolites which are produced in the brain of *Mut*$^{flox/flox}$;Nes-Cre mice due to Mut deficiency are only found to be accumulated in brain homogenates but not in the liver.

7 CHAPTER V: BASIC CHARACTERIZATION OF NOVEL MMAURIA MOUSE MODELS

This section represents an article which is prepared to be submitted for publication. Citations in this chapter correlate to the bibliography at the end of the thesis. Figure and table numbering is only applicable to this section of the thesis.

NOVEL MOUSE MODELS OF METHYLMALONIC ACIDURIA RECAPITULATE PHENOTYPIC TRAITS WITH A GENETIC DOSAGE EFFECT

Patrick Forny[a,b,c], Anke Schumann[a,b,c], Merima Mustedanagic[a], Deborah Mathis[d], Marie-Angela Wulf[e], Claus-Dieter Langhans[f], Assem Zhakupova[g], Joerg Heeren[h] , Ludger Scheja[h], Ralph Fingerhut[i], Heidi L Peters[j], Thorsten Hornemann[g], Beat Thony[a], Stefan Koelker[f], Patricie Burda[a], D Sean Froese[a,b], Olivier Devuyst[b,c,k], Matthias R Baumgartner[a,b,c,1]

[a] Division of Metabolism and Children's Research Center, University Children's Hospital Zurich, 8032 Zurich, Switzerland

[b] radiz – Rare Disease Initiative Zurich, Clinical Research Priority Program for Rare Diseases, University of Zurich, 8006 Zurich, Switzerland

[c] Zurich Center for Integrative Human Physiology, University of Zurich, 8057 Zurich, Switzerland

[d] Division of Clinical Chemistry, University Children's Hospital Zurich, 8032 Zurich, Switzerland

[e] Institute of Neuropathology, University Hospital Zurich, Zurich, Switzerland

[f] Division of Inherited Metabolic Diseases, University Children's Hospital, 69120 Heidelberg, Germany

[g] Institute of Clinical Chemistry, University of Zurich and University Hospital Zurich, 8006 Zurich, Switzerland

[h] Department of Biochemistry and Molecular Cell Biology, University Medical Center Hamburg-Eppendorf, 20246 Hamburg, Germany

[i] Swiss Newborn Screening Laboratory, University Children's Hospital Zurich, 8032 Zurich, Switzerland

[j] Metabolic Research, Murdoch Childrens Research Institute, Royal Children's Hospital, Parkville Victoria 3052, Australia

[k] Institute of Physiology, University of Zurich, 8057 Zurich, Switzerland

[1] To whom correspondence may be addressed:

Matthias R Baumgartner, matthias.baumgartner@kispi.uzh.ch

The authors declare no conflict of interest.

7.1 ABSTRACT

Methylmalonic aciduria (MMAuria), caused by deficiency of methylmalonyl-CoA mutase (MUT), usually presents in the newborn period with failure to thrive and metabolic crisis leading to coma or even death. Survivors remain at risk for further metabolic decompensations (e.g. due to infection or increased protein load) and often suffer severe long-term complications, most notably renal failure and neurological impairment. *Mut* knock-out (ko) mice display neonatal lethality, limiting their value as a disease model. To create surviving mouse models closely mimicking human MMAuria, we have generated a constitutive *Mut* knock-in (ki) based on the p.M700K patient mutation, which can be used homozygously (ki/ki) or combined with a ko allele (ko/ki). Transgenic $Mut^{ki/ki}$ and $Mut^{ko/ki}$ mice survive post-weaning, show decreased weight gain, increased methylmalonic acid levels in blood, urine and tissues, and increased blood propionylcarnitine, odd-chain fatty acid and sphingoid bases, compared to littermate controls. Consistent with a genetic dosage effect, $Mut^{ko/ki}$ mice show lower residual Mut activity, less weight gain, and higher levels of metabolites than $Mut^{ki/ki}$. Further, $Mut^{ko/ki}$ mice exhibit manifestations of kidney and brain damage, as illustrated by increased plasma urea, impaired diuresis and changes in brain weight. When fed a high protein diet, $Mut^{ki/ki}$ and $Mut^{ko/ki}$ mice have further elevated metabolite levels, including blood ammonia, and show catastrophic weight loss, which, in $Mut^{ki/ki}$ mice, is rescued by treatment with hydroxocobalamin. Together, these two new mouse models provide an accurate clinical and biochemical recapitulation of human MMAuria, and contribute a platform from which further pathogenesis and treatments studies can be performed.

7.2 INTRODUCTION

Methylmalonyl-CoA mutase (MUT) is a homodimeric enzyme that catalyzes the reversible isomerization of L-methylmalonyl-CoA to succinyl-CoA by using vitamin B_{12} (cobalamin; Cbl) in the cofactor form (5'-deoxyadenosylcobalamin; AdoCbl). In this anaplerotic reaction, several metabolic pathways, including the breakdown of branched chain amino acids, odd-chain fatty acids, and the side chain of cholesterol, converge on the propionate pathway. The vital importance of this enzyme is demonstrated by the severe inborn error of metabolism methylmalonic aciduria (MMAuria), which is caused by mutations in the *MUT* gene (*mut*-type MMAuria, OMIM #251000) or by defects of AdoCbl synthesis. Dysfunction of MUT leads to an accumulation of methylmalonic acid (MMA), 2-methylcitrate (2-MC), propionylcarnitine (C3) and other metabolites in body fluids and tissues. *mut*-type MMAuria patients often present in the newborn period with ketoacidosis, lethargy, failure to thrive, coma or even death. In surviving patients, the chronic course manifests with organ-specific complications, the most common being neurological impairment and renal dysfunction. End stage

renal disease, occurring as early as the 2nd decade of life in patients with severe MMAuria, is frequently seen (Baumgartner, et al., 2014; Cosson, et al., 2009; Horster, et al., 2007; Horster, et al., 2009). Besides symptomatic care, there are a few rational treatment approaches, including reduction of protein intake in order to decrease the flux through the propionate pathway, as well as carnitine and Cbl supplementation (Baumgartner, et al., 2014). Although this treatment appears to partly improve metabolic control in some cases, most patients still suffer severe long-term complications.

Since the mouse *Mut* gene shows a high homology to human *MUT*, several attempts to generate a mouse model of *mut*-type MMAuria have been undertaken. The first such effort was made in 2003, when a *Mut* knock-out (ko) model resulted in neonatal lethality of all homozygous (ko/ko) pups (Peters, et al., 2003). In 2007, Chandler et al. generated their own *Mut*-ko mouse by the same method (Chandler, et al., 2007). Their switch to a different genetic background resulted in a semi-penetrant neonatal lethality with some ko/ko mice surviving the neonatal period (Chandler, et al., 2009), although nearly all died within 25 days (Chandler and Venditti, 2010). Using their own ko model, the same group applied AAV-mediated gene therapy (Chandler and Venditti, 2008; Chandler and Venditti, 2010) and stable transgenic *Mut* expression in the liver (Manoli, et al., 2013) to provide a long-term rescue of lethality. However, despite these efforts, no model to date has been able to provide an accurate depiction of the patient situation. Neonatal or early lethality disallow studies of the chronic development of disease, while transgenic rescue of *Mut* does not represent the natural situation, where a patient carries the same genetic defect in all cells.

In order to devise a model of MMAuria reflective of the patient situation and amenable to the study of the long-term disease course, we opted to knock-in (ki) a hypomorphic allele based on a patient missense mutation. From our previous in depth *MUT* missense mutation characterization (Forny, et al., 2014), we identified p.Met700Lys (c.2099T>A human cDNA; p.Met698Lys in mouse) as an ideal candidate for this allele due to the residual enzymatic activity and *in vitro* response to hydroxocobalamin (OHCbl) found in MUT protein carrying this mutation. p.Met700Lys has been detected heterozygously in 4 MMAuria patients in conjunction with severe mutations (Acquaviva, et al., 2005; Forny, et al., 2016), but at least 3 of these patients have had an intermediate disease course with a relatively late age of onset (between 14 days and 6 months) (Forny, et al., 2016), supporting the potential of this mutation to cause moderate MMAuria. To assess the effect of genetic dosage on the phenotype and to generate a more severe disease model, the new ki mutation was combined with a ko mutation (Peters, et al., 2003). Here we present a thorough characterization of these newly generated $Mut^{ki/ki}$ and $Mut^{ko/ki}$ mouse models, which survive long-term and recapitulate the key biochemical and clinical features of MMAuria.

7.3 RESULTS

7.3.1 *In vitro* characterization of the p.Met698Lys knock-in allele

To characterize the selected ki mutation, we tested the biochemical properties of the human mutation p.Met700Lys (*hs*-p.Met700Lys) and the equivalent mutation in mouse (*mm*-p.Met698Lys). Separate constructs incorporating each allele were overexpressed in human fibroblasts carrying a homozygous null allele of *MUT* in order to determine enzyme activity and kinetics. In both, the residual activity was reduced to a few percent of wild-type (*wt*) (Fig. 1A) with an almost 100-fold increased K_M for AdoCbl (Fig. 1B). These nearly identical biochemical results for the human and mouse equivalent mutations led us to conclude that the *mm*-p.Met698Lys mutation would be expected to produce an intermediate phenotype of MMAuria, similar to its *hs*-p.Met700Lys counterpart.

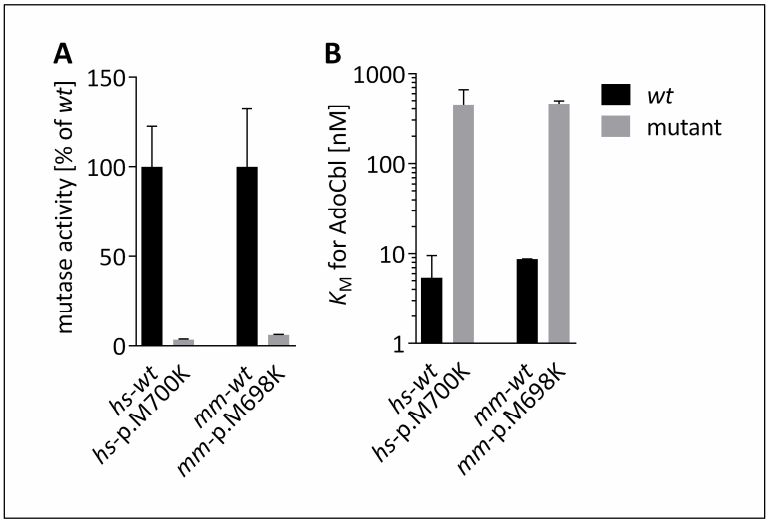

Fig. 1. Human (*hs*) and mouse (*mm*) mutant proteins show similar enzyme parameters when expressed in a *mut*^{0} patient cell line. (**A**) Bar chart depicts mean enzyme activities measured in fibroblast homogenates after overexpression of the respective constructs. Mutant values were calculated in relation to their *wt* counterparts and normalized to percent residual activity of *wt*. (**B**) Bars are absolute K_M values for AdoCbl determined by measuring MUT activity with increasing concentrations of AdoCbl ranging from 0.0025 to 50 µM. Error bars in both panels depict SD; means were calculated from at least two independent experiments; *wt*, black; mutant, grey.

7.3.2 Generation of ki allele and initial characterization

To generate the knock-in p.Met698Lys mutation, a targeting vector was designed to replace the thymine with an adenine at position c.2093 of *Mut* (based on NM_008650.3). The construct contained a long arm of homology of 4.5 kilobases (kb) (spanning the sequence of intron 8 to exon 12), a short

homology arm of 1.4 kb covering most of intron 12, and an insert comprised of the point mutation in exon 12 and a neomycin cassette flanked by flippase recognition target (FRT) sites (Fig. 2A). Upon embryonic stem cell (C57BL/6-derived) targeting, the clone 12H5 was confirmed to be positive by Southern hybridization (Fig. 2B) and was used for blastocyst injections to generate chimeric mice. Pups of chimeras and flippase (Flp)-deleter mice were screened for germ-line transmission of the targeted allele by detection of the remaining FRT-site after Flp recombination via PCR genotyping (Fig. 2C, upper panel). Additionally, *Mut*$^{ko/ki}$ mice were generated as a second disease model by crossing the previously established *Mut*$^{ko/wt}$ mice (Peters, et al., 2003) with our *Mut*$^{ki/ki}$ mice, and followed by PCR genotyping of the ko allele (Fig. 2C, lower panel).

To determine the direct consequences of the missense change on Mut transcript, stability and function, we investigated Mut expression and activity in various tissues. In *wt* mice, we found *Mut* expression to be lower in brain than in liver or kidney (Fig. 2D), similar to previously published results (Ballhausen, et al., 2009). The ki allele did not result in an appreciable decrease of Mut transcript levels in all tissues tested, however, mice with one ko allele had ~50% of *Mut* transcript levels compared to *wt* (Fig. 2E), likely indicative of nonsense mediated decay. At the protein level, the amount of the homozygous *Mut*$^{ki/ki}$ protein was massively reduced compared to controls, suggesting an unstable mutant protein, while ko/ki Mut protein showed similar massive reduction (Fig. 2F). Mut activity from *wt* mice significantly varied among tissue types, with highest activities in kidney, liver and heart (Fig. 2G). Activities from ki/ki and ko/ki mice were greatly decreased in all tissues tested (Fig. 2H), comparable to the *in vitro* measurements (Fig. 1A). Furthermore, a gene dosage-dependent decrease of enzyme activity was identified, with *Mut*$^{ko/ki}$ activity slightly lower than *Mut*$^{ki/ki}$ in most tissues (Fig. 2H). As expected, ~50% percent of residual activity was maintained in the *Mut*$^{ki/wt}$ and *Mut*$^{ko/wt}$ animals, reflecting the activity of the remaining *wt* allele (Fig. 2H).

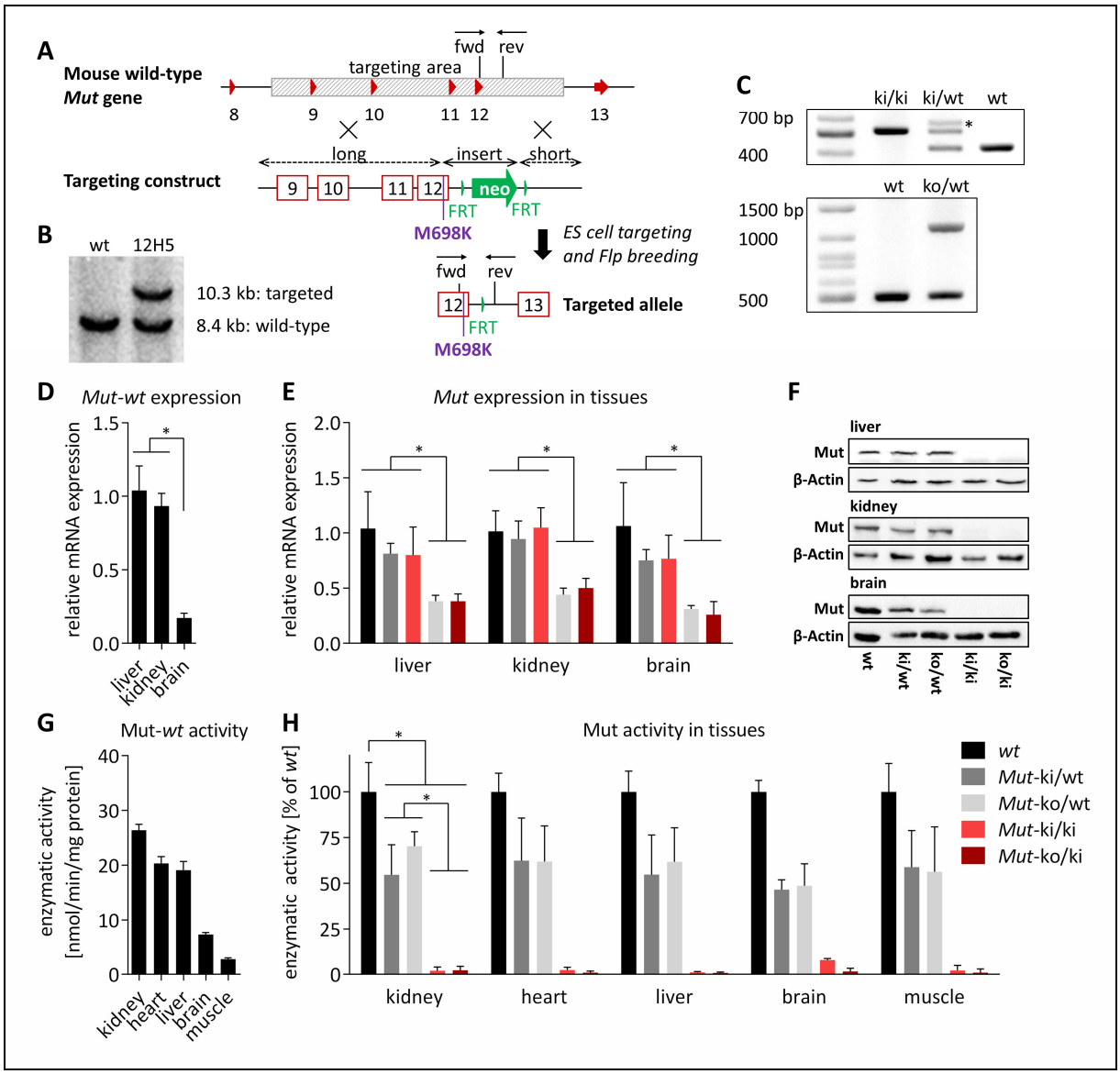

Fig. 2. Generation of ki allele and initial characterization. (**A**) Based on the *wt* mouse *Mut* gene, a targeting construct was generated to replace the *Mut* gene region spanning from intron 8 to intron 12 (shaded in grey), consisting of a long and short arm of homology as well as an insert with the missense mutation (p.Met698Lys) and a neomycin cassette (neo, green arrow) flanked by FRT sites (vertical green triangles). Homologous recombination and Flp-deletor breeding resulted in the final targeted ki allele with the mutation and one remaining FRT site. Exons are represented by red triangles or boxes, arrows "fwd" and "rev" indicate forward and reverse genotyping primers, respectively. (**B**) Southern blotting of targeted clone 12H5. (**C**) Upper panel: genotyping PCR of ear biopsy DNA for the ki allele with fwd and rev primers depicted in panel **A**. Asterisk indicates an additional heterodimer band as confirmed by Sanger sequencing. Lower panel: genotyping PCR of ko allele. (**D**) *Mut* expression among *wt* tissues (error bars are SEM; $n = 4$; *: $p < 0.01$) and (**E**) ko allele dependent loss of *Mut* expression (bars are means normalized to *wt* in each tissue; error bars depict SEM; $n \geq 4$; *: $p < 0.05$). (**F**) Western blot analysis of Mut protein levels using β-actin as loading control. (**G**) Mut activity varies by tissue and (**H**) by genotype (bars are mean values and in each tissue normalized to the *wt* value; error bars are SEM; $n \geq 4$; *: $p < 0.0001$). Significance levels are the same in all five tissues (not depicted for clarity).

7.3.3 Gene dosage-dependent clinical/biochemical features in *Mut*$^{ki/ki}$ and *Mut*$^{ko/ki}$ mice

Mice homozygous for the targeted point mutation (*Mut*$^{ki/ki}$) were viable and, when crossed with heterozygous *Mut*$^{ki/wt}$ mice, reproduced at the expected Mendelian ratio of 50% percent per genotype (Table 1A). Breeding of *Mut*$^{ko/ki}$ also resulted in viable animals and displayed the expected Mendelian distribution of the genotypes (50% *Mut*$^{ko/ki}$ and 50% *Mut*$^{ki/wt}$; Table 1B). Mice of both genotypes survived long-term (> 1 year), allowing us to monitor long-term development. At early stages of life, *Mut*$^{ki/ki}$ and *Mut*$^{ko/ki}$ mice were largely indistinguishable from their heterozygous littermates (*Mut*$^{ki/wt}$) and *wt* control mice. However, after the age of about 100 days in females (Fig. 3A) and about 150 days in males (Supp. Fig. S1A), mice of both genotypes showed signs of significant growth retardation. The difference between littermate control (*Mut*$^{ki/wt}$) and *Mut*$^{ko/ki}$ female mice was 30% after ~1 year (Fig. 3A), while food intake and weight loss (when single-caged overnight) remained constant (Supp. Fig. S1B). In this cohort, C3 (normalized to acetylcarnitine, C2) in blood and MMA in urine were constantly elevated over the entire time span investigated (Fig. 3B and C). Survival was the same in all three groups (all mice still alive after one year except for 1 *Mut*$^{ki/ki}$ and 1 *Mut*$^{ko/ki}$, both of which died during blood collection).

A

Breeding pair	**Genotype of animals**		
Mut-ki/wt × *Mut*-ki/ki	*Mut*-ki/wt	*Mut*-ki/ki	total
litters: 33*	96	94	190
	51%	49%	100%

*All animals (except 1 with unclear genotype) survived post-weaning

B

Breeding pair	**Genotype of animals**		
Mut-ko/wt × *Mut*-ki/ki	*Mut*-ki/wt	*Mut*-ko/ki	total
litters: 36*	100	104	204
	49%	51%	100%

*All animals (except 5 with unclear genotype) survived post-weaning

Table 1. Breeding patterns of pairs to generate *Mut*$^{ki/ki}$ and *Mut*$^{ko/ki}$ mice.

To gain further insight into the consequences of massively reduced Mut enzymatic activity, we performed a cross-sectional analysis of hallmark metabolites of MMAuria (Kolker and Okun, 2005) at 35 days of age. The eponymous compound MMA was found elevated in a genetic dosage-dependent manner in tissues, urine and dried blood, with the highest levels found in *Mut*$^{ko/ki}$ mice (Fig. 3D). Alt-

hough *Mut*$^{ki/ki}$ animals showed considerably lower levels, they were still significantly elevated compared to controls (Fig. 3D). Propionylcarnitine (C3) levels (normalized to C2) showed the same trend (Fig. 3E). *Mut*$^{ki/wt}$ and *Mut*$^{ko/wt}$ did not show any elevations, suggesting that one functional *wt* allele is sufficient to cope with the demands of the propionate pathway (Fig. 3D and E). Ammonia levels, which are elevated during metabolic crisis in patients, were normal (Fig. 3F), suggesting these animals did not suffer from acute crises on normal chow. Similar to patients (Kolker, et al., 2015; Matsui, et al., 1983b; Perry, et al., 1977), both *Mut*$^{ko/ki}$ and *Mut*$^{ki/ki}$ showed elevated glycine levels (Fig. 3G), while other amino acid levels were mostly unchanged (Supp. Fig. 2).

In addition to classic metabolites, we performed a comprehensive analysis of fatty acids and sphingoid bases. We found increased levels of odd-chain fatty acids (Fig. 3H), including the 17-carbon chain length fatty acid, which has recently been proposed as a biomarker of MMAuria (Malvagia, et al., 2015), with normal levels of even-chain fatty acids (Supp. Fig. S3A; Supp. Table 1). Further, we show here for the first time an elevation in odd-chain length sphingoid bases in plasma (Fig. 3I) and tissues (Fig. 3J), possibly as a consequence of the increased odd-chain fatty acids, while levels of even-chain sphingoids remained normal (Supp. Fig. S3B; Supp. Table 2).

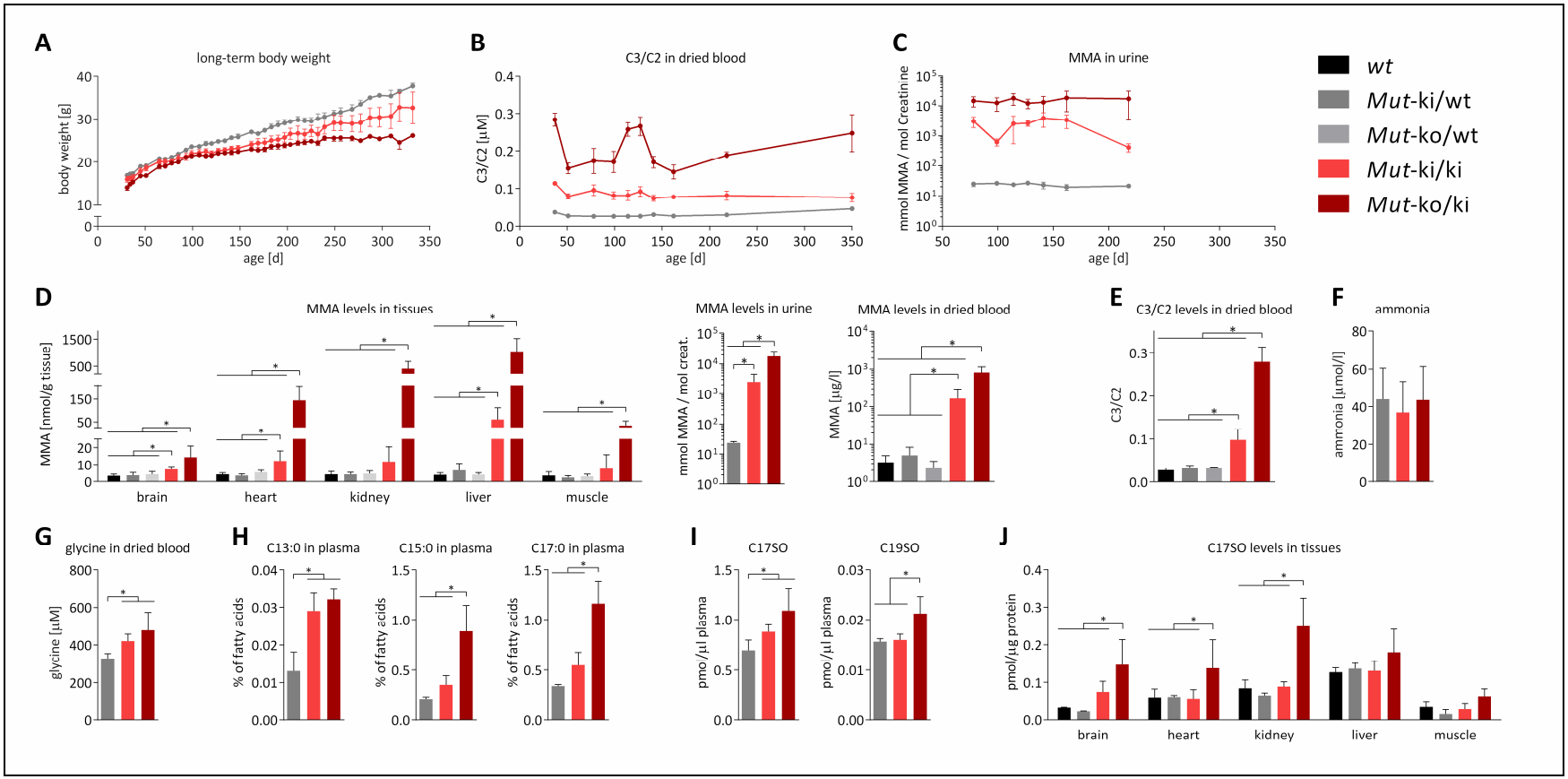

Fig. 3. Clinical and biochemical phenotype of *Mut*$^{ki/ki}$ and *Mut*$^{ko/ki}$ mice. (**A**) Monitoring of body weight of female mice over time (male data in Supp. Fig. S1A). Decreased body weight in *Mut*$^{ki/ki}$ mice is significant compared to *Mut*$^{ki/wt}$ from day 162, and in *Mut*$^{ko/ki}$ significant compared to *Mut*$^{ki/wt}$ from day 114. For both: $p < 0.05$. (**B**) C3 levels in dried blood spots normalized to acetylcarnitine (C2). (**C**) MMA levels measured by LC-MS/MS in urine collected overnight in metabolic cages. In panels A-C points represent mean values, error bars depict SEM and $n = 5$ per group. (**D**) MMA levels in tissues (left panel), urine (middle) and dried blood (right), determined by tandem mass spectrometry. (**E**) C3 levels normalized to C2 in dried blood. (**F**) Ammonia levels measured in whole blood. (**G**) Glycine concentration determined in dried blood by tandem mass spectrometry. (**H**) Fatty acid levels determined in plasma and expressed as percent of total fatty acids. (**I**) Plasma levels of sphingoid bases (expressed as pmol per µl plasma). (**J**) 17-carbon chain sphingoid base levels in different tissues expressed as pmol per µg protein. Panels D-J: bars represent mean values from 35 days old mice (error bars depict SD; $n \geq 4$; *: $p < 0.05$).

7.3.4 Initial characterization of the renal and neurological phenotypes

We investigated whether *Mut*$^{ko/ki}$ mice suffer from similar long-term complications as patients with MMAuria, e.g. renal dysfunction. When normalized to body weight, *Mut*$^{ko/ki}$ mice consistently produced less urine during adulthood than littermate controls (*Mut*$^{ki/wt}$) (Fig. 4A), although water intake was not significantly different between the two groups (Fig. 4B). Consistent with renal dysfunction, these mice also had increased plasma urea throughout the time course measured (Fig. 4C), suggestive of a decreased glomerular filtration rate (Schwartz, et al., 2009). Renal tubular dysfunction in these animals was further underlined by disturbed excretion of several electrolytes in urine (Fig. 4D). These signs of kidney dysfunction were further supported by the finding of increased levels of the biomarker Lipocalin-2 (Lcn2) in kidney tissue (Fig. 4E). However, no gross changes in weight (Supp. Fig. S1B) in the *Mut*$^{ki/ki}$ and *Mut*$^{ko/ki}$ kidneys were detected, suggesting that the source of these renal defects are likely at the (sub)cellular level.

Neurological dysfunction is the other important long-term complication of MMAuria (Nicolaides, et al., 1998), often manifesting as movement disorder due to lesions in the basal ganglia caused by metabolic stroke, which may also induce brain edema in the acute phase. In the *Mut*$^{ko/ki}$ mice we observed an increase in brain weight at the age of one month as well as one year (Fig. 4F), which may be suggestive of brain edema. Although brain histology was normal in the basal ganglia (Supp. Fig. S4), we also identified an upregulation in Lcn2 at the mRNA and protein level (Fig. 4G).

Together, the initial characterization of both the brain and kidney, in combination with the metabolites already identified in these organs, suggest an initial dysfunction in each, which has not yet manifested at the gross level.

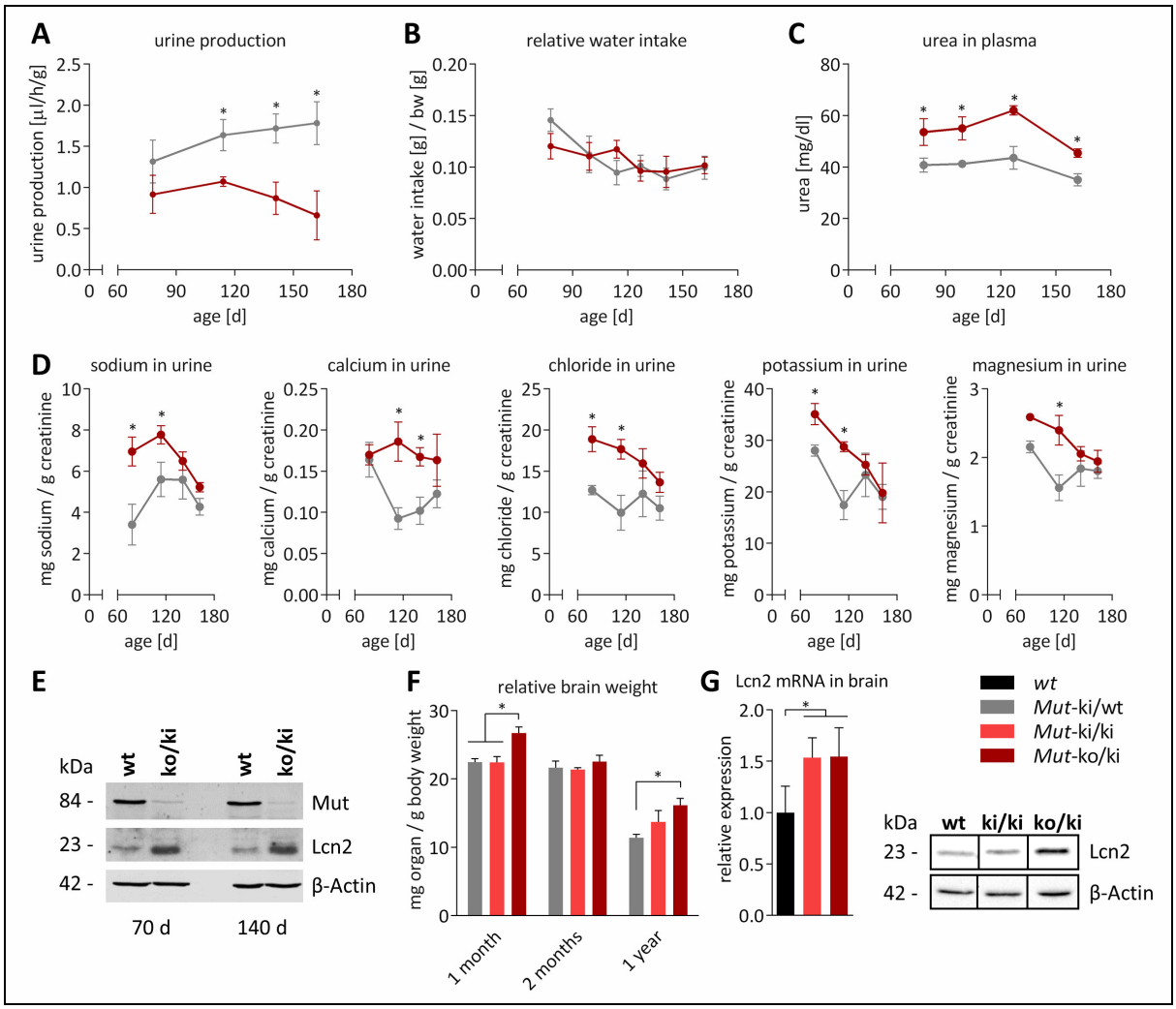

Fig. 4. Renal and neurological phenotype. (**A**) Urine production measured in metabolic cages overnight and expressed as microliters of urine per hour normalized to body weight. (**B**) Overnight water intake measured in grams of water normalized to body weight. (**C**) Urea in plasma expressed in mg per deciliter. (**D**) Electrolytes measured in urine and normalized to grams of creatinine. (**E**) Western blot of Mut and Lcn2 at two different time points. (**F**) Kidney histology. (**G**) Brain weight normalized to body weight at three different time points. (**H**) Expression of Lcn2 in brain tissue on mRNA level normalized to β-actin and on protein level (β-actin as loading control). In panels A-D and G-H, points and bars represent mean values; error bars depict SEM; *: $p < 0.05$.

7.3.5 Diet-induced metabolic decompensation

An increased throughput of the propionate pathway in patients with MMAuria, e.g. due to a catabolic state or an augmented protein intake, often results in metabolic decompensation (crisis). In order to replicate this state in our MMAuria mouse models and exacerbate their clinical phenotype, we used dietary challenge. Mice were fed a high protein (HP) diet, as used previously (Manoli, et al., 2013), or a precursor-enriched (PE) diet comprised of increased levels of amino acids directly relevant to the propionate pathway (isoleucine, valine, threonine; for formulations see Supp. Table 3). Upon

initiation of both diets at the age of 2 months, both *Mut*$^{ko/ki}$ and *Mut*$^{ki/ki}$ mice experienced rapid weight loss, which was so severe that the study had to be terminated after 3 days (Fig. 5A; Supp. Fig. S5). The effect exerted by the PE diet appeared to be stronger than the HP diet, as shown by the more pronounced weight loss (Fig. 5A), likely reflecting the two-fold higher isoleucine, valine and threonine content in the PE diet (Supp. Table 3). Brain weight (normalized to body weight) was increased in *Mut*$^{ko/ki}$ mice under both diets, which was not the case on reference chow (RC) at this age (Fig. 5B). Investigation of the sacrificed animals revealed, from both diets, elevated levels (2.5-3.5 times) of plasma MMA, C3, and for the first time in these mice, ammonia (~4-7 times; Fig. 5C, D and E), consistent with the induction of metabolic crisis. Further investigation of MMA and C3 in brain, kidney and liver demonstrated a gene dosage-dependent increase in both metabolites for mice on either diet compared to those on the control diet (RC) in all tissues tested (Fig. 5F, G and H; Supp. Fig. S6). Indeed, while these metabolites were already elevated in *Mut*$^{ko/ki}$ and *Mut*$^{ki/ki}$ mice on RC (*e.g.* brain levels of MMA in *Mut*$^{ko/ki}$ are 4.4 times higher than *Mut*$^{ki/wt}$, Fig. 5F), they were further increased up to 53-times when the diet was changed to HP or PE (Fig. 5F).

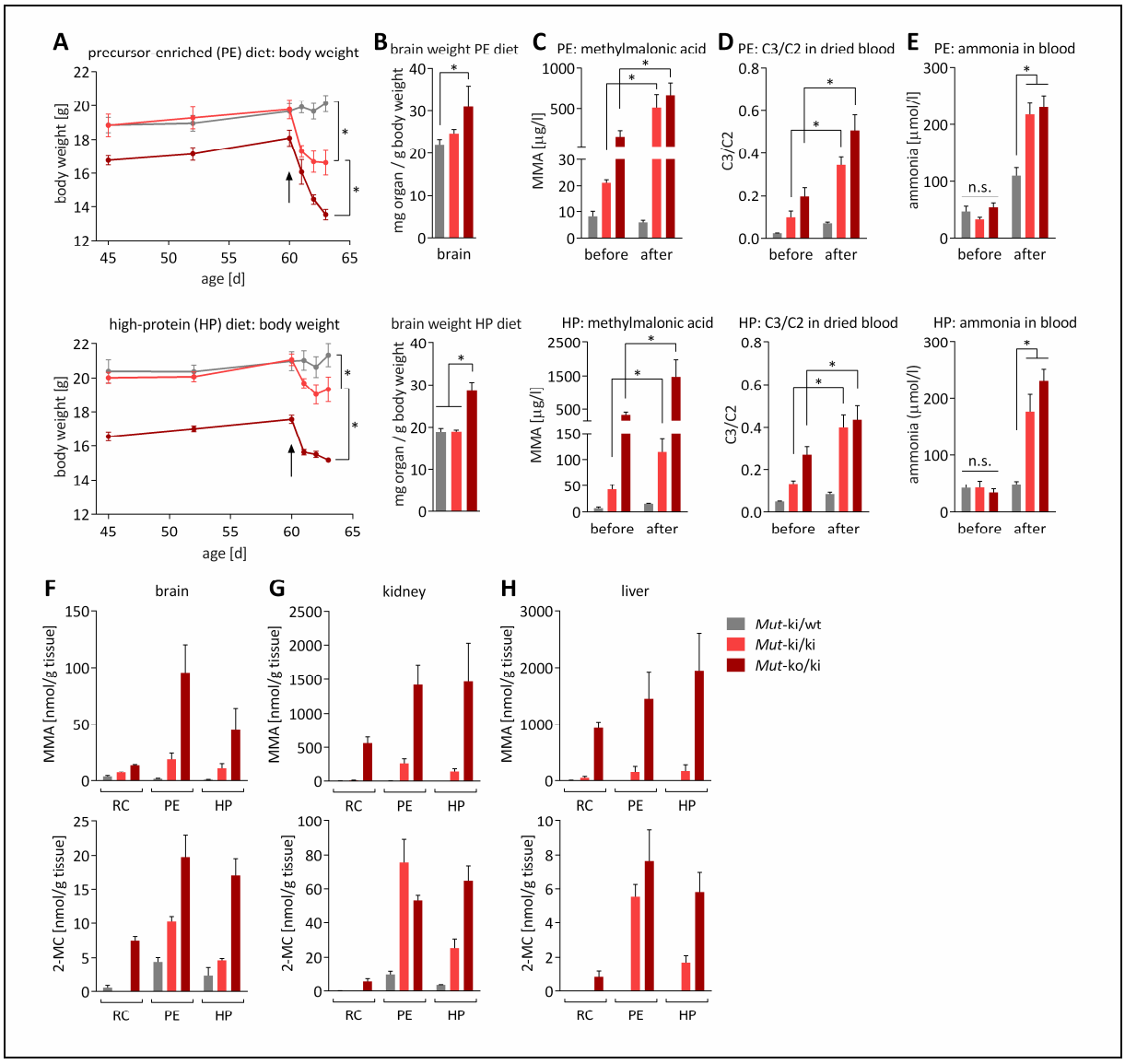

Fig. 5. Modified diet leads to disease acceleration. **A**) Start of both modified diets (upper panel: PE, precursor-enriched; lower panel: HP, high protein) at 60 days of age is indicated by the black arrows. Monitoring of body weight showed significant differences among the three groups on day 63 for both diets. (**B**) Weight of kidney and brain whole organs normalized to body weight after determination of diet study. (**C**) MMA in dried blood. (**D**) C3 (normalized to C2) in dried blood. (**E**) Whole blood ammonia before and after diet modification. (**F-H**) MMA and 2-MC values in homogenates of (**F**) brain, (**G**) kidney, and (**H**) liver tissue on reference chow (RC), high protein (HP) and precursor-enriched (PE) as determined by GC-MS. For all panels, from 5 animals for each genotype bars and points represent means; error bars are SEM; *: $p < 0.01$; n.s., not significant.

7.3.6 Cobalamin treatment partly rescues diet induced metabolic crisis

To attempt to mitigate the effects exerted by the HP diet, we treated the mice with daily intraperitoneal (*i.p.*) injections of hydroxocobalamin (OHCbl, 0.3 µg/g) for a week before and continuously during the dietary challenge. These injections resulted in nearly doubled levels of plasma Cbl (Fig. 6A),

indicating efficient uptake of the vitamin into the blood stream. *Mut*$^{ki/ki}$ mice appeared to be at least partially protected by this treatment, as, in contrast to mice on the HP diet alone (Fig. 5A), OHCbl treated *Mut*$^{ki/ki}$ mice did not show significant weight loss (Fig. 6B). Further, elevations in C3 and ammonia were markedly delayed, although they increased considerably, along with MMA, by the study's end (Fig. 6C-E). *Mut*$^{ko/ki}$ mice showed a less obvious, but still slight protective effect. They lost less weight compared to their untreated counterparts (compare Fig. 5A HP and Fig. 6B), and did not have the significantly increased brain weight (Fig. 6F) seen previously (Fig. 5B). However, they did show immediate and striking increases in metabolite levels (Fig. 6C-E) suggesting they remained metabolically compromised.

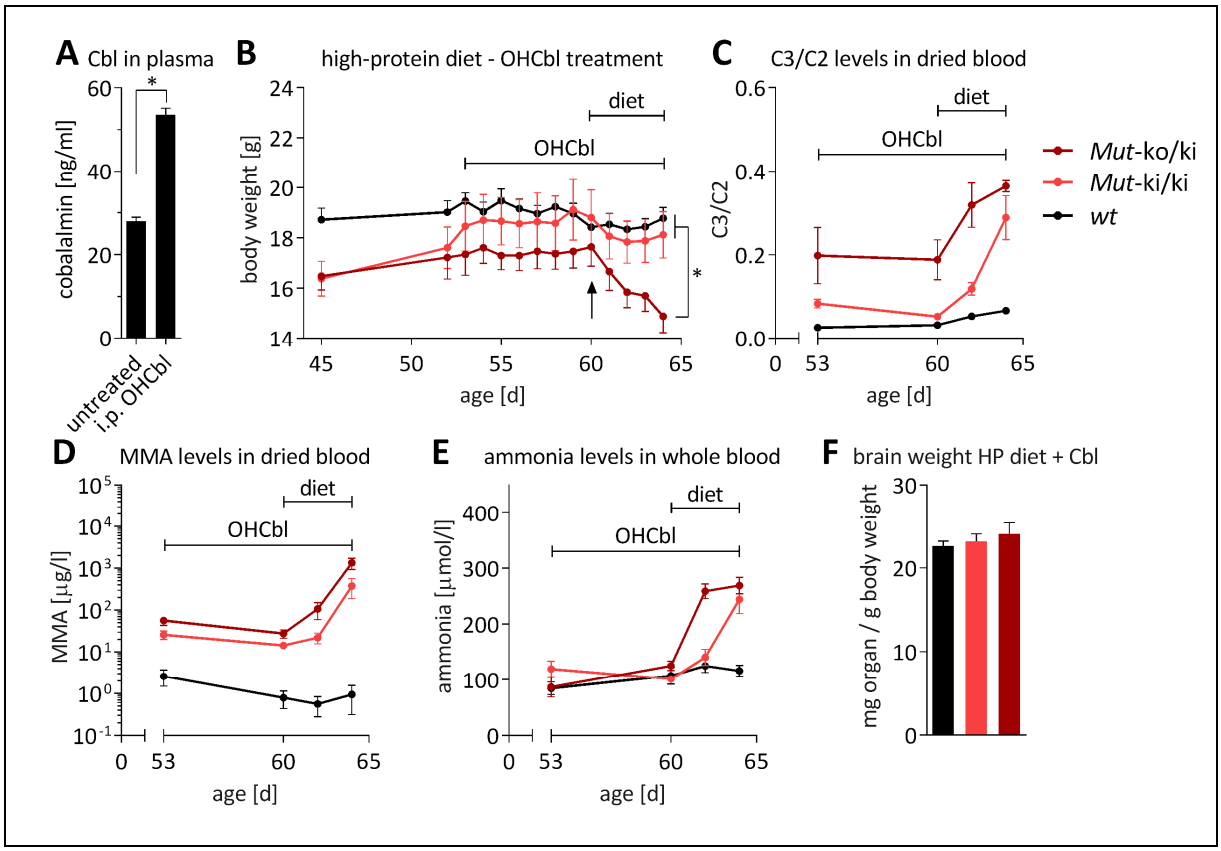

Fig. 6. Treatment of HP diet-induced phenotype by OHCbl. (**A**) Cobalamin levels in plasma of untreated mice and OHCbl treated mice; *: $p < 0.0001$. (**B**) Time course of body weight. Black arrow indicates start of HP diet on day 60. Differences of body weight on day 64 were significant between *Mut*$^{ko/ki}$ and the other two genotypes (*Mut*$^{ki/ki}$ and *wt*) which did not differ significantly. (**C**) C3 (normalized to C2), (**D**) MMA levels in dried blood and (**E**) whole blood ammonia levels were measured on the day before diet start and on day 62 and day 64 following diet commencement. (**F**) Weights of brain whole organs in sacrificed animals at the end of the study. In panels B-E duration of HP diet was from day 60 to day 64 and OHCbl treatment from day 53 to day 64 as indicated by capped horizontal lines. Points and bars represent mean values; error bars in all panels depict SEM.

7.4 DISCUSSION

In this study, we aimed to generate a novel mouse model of MMAuria which survives through adulthood but shows clear biochemical and clinical signs of disease. To achieve this model, we knocked in a missense mutation to the mouse *Mut* gene. This constitutive ki allele causes Mut deficiency, which is further aggravated by combination with a ko allele. The success of this approach is demonstrated by the successful production of ki/ki and ko/ki mouse pups, which survive into adulthood, but show growth retardation, elevated metabolites in blood and tissues, and signs of renal and neurological dysfunction. Further, these biochemical and clinical signs of disease follow a gene dosage-dependent increase, where mice with one ko allele are clearly more affected than those homozygous for the ki allele. Thus, these novel mouse models recapitulate the biochemical and clinical features of MMAuria.

7.4.1 Novel mouse models recapitulate clinical and biochemical phenotype of MMAuria

The most striking phenotypic sign in our mice was growth retardation, which is likely a correlate of failure to thrive described in human patients (Baumgartner, et al., 2014). This lack of weight gain is not readily explained by reduced energy intake, as we identified no difference in overnight food consumption between the mutant mice and controls, suggesting that other, possibly subcellular, processes are affected. Previous studies point towards inhibited tricarboxylic acid cycle enzymes and interference with oxidative phosphorylation in MMAuria (de Keyzer, et al., 2009; Morath, et al., 2008). It will be important to assess these potential mechanisms in future studies.

Further clinical signs could be observed when the disease was accelerated by means of a high protein challenge. The success of this approach was demonstrated by the massive elevation of metabolites and immediate loss of weight in both diets (HP and PE) for both mouse genotypes ($Mut^{ko/ki}$ and $Mut^{ki/ki}$), suggesting that the propionate pathway was unable to process the additional metabolic load contributed by the modified diets. As indicated by the significantly elevated ammonia levels, this induced situation is consistent with acute metabolic crisis, where aggressive treatment is required to prevent encephalopathy when ammonia levels rise above a threshold of 200 µmol/l (Brismar and Ozand, 1994; Haberle, et al., 2012).

Along with these general organism-wide symptoms, we were able to identify organ-specific disturbances in the kidney and the brain. Under normal diet conditions, adult $Mut^{ko/ki}$ mice showed manifestations of kidney dysfunction, as evidenced by increased plasma urea, impaired diuresis and changes in the urinary excretion of electrolytes. These changes mirror the dysfunction found in MMAuria, in which chronic renal failure is observed in almost half of all cases (Baumgartner, et al.,

2014; Cosson, et al., 2009; Horster, et al., 2007; Horster, et al., 2009). In our mice, these changes were accompanied by increased renal levels of Lcn2, a protein which has been suggested to be an early biomarker of chronic kidney damage (Fassett, et al., 2011; Malyszko, et al., 2008), including in MMAuria (Manoli, et al., 2013). Further, we found increased brain weight in the *Mut*$^{ko/ki}$ mice at 1 month and 1 year of age, potentially indicative of edema as a sign of cytotoxic stress. Interestingly, we also found increased Lcn2 mRNA and protein levels in the brain of these mice. In contrast to its potential role as a kidney specific marker, upregulation of Lcn2 in the brain has been suggested to be a biomarker in multiple sclerosis (Berard, et al., 2012), and was found to be upregulated in animal models of brain-specific diseases (Ferreira, et al., 2015; Marques, et al., 2012; Naude, et al., 2012). Hence, the specific role of Lcn2 as an organ-specific biomarker remains unclear, however, the finding of upregulation in affected tissues suggests at least a general role in dysfunctional cells.

Biochemically, the phenotype of human patients was accurately emulated, as illustrated by the types of metabolites which were increased and the extent of their elevation. For example, MMA levels in the urine were detected in a range comparable to human *mut*$^{-}$ patients (Fowler, et al., 2008), while glycine, speculated to increase via inhibition of the intra-mitochondrial glycine cleavage enzyme due to accumulated organic acids or their CoA esters (Hillman and Otto, 1974), was found at high levels in our mice, similar to the description in the first MMAuria patients (Oberholzer, et al., 1967). Further, we found elevated levels of odd-chain fatty acids, in line with their proposed role as an additional aid to monitoring MMAuria in patients (Baumgartner, et al., 2014; Coker, et al., 1996; Merinero, et al., 2008; Wendel, et al., 1991). In addition, we present for the first time elevations of odd-numbered chain sphingoid bases in plasma and tissue. Their elevation may be explained by the disturbed fatty acid metabolism, i.e. serine palmitoyltransferase, a key enzyme in sphingoid base synthesis, may more often utilize 17- or 19-carbon fatty acid-CoAs as substrate, instead of the normally preferred 14- or 18-chain length fatty acids. The pathophysiological significance of this newly discovered phenomenon remains unknown.

Overall, these novel models of MMAuria recapitulate many of the biochemical and clinical hallmarks of MMAuria patients and thus are excellent tools to study the pathogenesis of disease. Application of a long-term dietary challenge with less potent diets will potentially allow monitoring of chronic disease progression, leading to more pronounced impacts on brain and kidney tissue.

7.4.2 Gene dose-dependence allows titration of disease severity

Patients carrying the p.Met700Lys mutation show an intermediate phenotype with relatively late onset and residual enzyme and pathway activity in fibroblast cell homogenates (Acquaviva, et al., 2005; Forny, et al., 2016; Lempp, et al., 2007). Based on these observations, the measurable residual enzyme activity *in vitro* and the missense type of the variant used for the generation of the ki allele,

we expected that the ki allele would result in a milder phenotype than the ko allele, which is in fact a truncating mutation. Indeed, a gene dose-dependent effect was corroborated by all observed data: the *Mut*$^{ko/ki}$ mice displayed higher levels of MMA, 2-MC, and C3, more pronounced growth retardation, and a stronger reaction to dietary challenge than homozygous *Mut*$^{ki/ki}$ animals. Therefore, the gene dose effect detected in our study may be reflective of the phenotypic differences in patients and has benefitted our study, allowing us to assess milder and more severe forms of MMAuria.

7.4.3 Response to cobalamin treatment

It is recommended to evaluate every *mut*-type MMAuria patient for responsiveness to cobalamin treatment (Baumgartner, et al., 2014; Fowler, et al., 2008). However, no systematic study has thus far investigated the effectiveness of cofactor treatment in *mut*-type MMAuria. If effective, the cofactor would be expected to ameliorate disease by supporting the enzyme's activity and/or stability, similar to the cofactor response displayed by phenylalanine hydroxylase (Christ, et al., 2013; Ziesch, et al., 2012). The human mutant p.Met700Lys is an excellent candidate to test cobalamin responsiveness, as patient fibroblasts compound heterozygous for this and a premature stop mutation showed ~4.5 times increased incorporation of ^{14}C propionate into acid precipitable material when supplemented with OHCbl (Lempp, et al., 2007), and biochemically this mutation was found to affect the K_M of MUT for AdoCbl (Forny, et al., 2014). Indeed, in our HP diet study, *Mut*$^{ki/ki}$ mice appear to have been at least partly protected by pre-administration of OHCbl. These mice did not show the immediate weight loss associated with the initiation of the HP diet, and showed delayed accumulation of metabolites. The reduced degree of protection for *Mut*$^{ko/ki}$ mice suggests that with the level of Cbl achieved by these injections, both mutant alleles are required to be potentially Cbl-responsive. An even better rescue may be facilitated by the application of higher Cbl doses in these mice, potentially reaching levels suggested for treatment in human patients (Fowler, et al., 2008). Nevertheless, our results set the stage for further exploration of cofactor response – a concept which may be applicable to many other missense mutations, since about one quarter of all *mut*-type mutations show an *in vitro* response to cobalamin (Horster, et al., 2007; Worgan, et al., 2006).

7.5 Materials and Methods

7.5.1 *In vitro* cell culture and enzyme activity assay

Immortalized fibroblast cells of a *mut*^{0} patient (carrying the homozygous mutation p.Gln30*) were cultivated in cell culture medium (DMEM, Ref. 31966-021, Gibco, Thermo Fisher Scientific) supplemented with 10% fetal bovine serum (FBS, Ref. 10270-106, Gibco, Thermo Fisher Scientific) and antibiotics (Ref. 15240-062, Gibco, Thermo Fisher Scientific). Constructs of human (hs) MUT wild-type

and mouse (mm) Mut wild-type and the mutants hs-p.M700K and mm-p.M698K were made by site-directed mutagenesis in the pTracer-CMV2 vector (Invitrogen, Thermo Fisher Scientific). Electroporation was used to transiently transfect constructs into the immortalized fibroblasts. Cells were harvested 48 hours after electroporation by trypsinization. The cell pellet was washed with phosphate buffered saline and stored at -80°. Lysates were obtained by sonication of the frozen pellet in 5 mM potassium phosphate buffer (pH 7.4) and used for MUT activity assay as described in (Forny, et al., 2014). To determine K_M for AdoCbl in the cell lysates, the concentration of AdoCbl was varied between 0.0025 and 50 µM. Instead of cell lysates, homogenates from mouse tissues were also used for the activity assay (preparation see below).

7.5.2 Mouse tissue preparation

Liver, kidney, brain, heart, and muscle tissues were removed immediately after the mice were euthanized in a CO_2 chamber. Blood was collected in heparin tubes (Microvette 200 LH, Sarstedt) and centrifuged for 5 minutes at 2000 xg; supernatant was removed and plasma stored at -80°C. Lysates of tissues were prepared as follows: Approximately 50 mg of tissue was homogenized in the tissue lyser (TissueLyser II, Qiagen) in 300-600 µl of a lysis buffer dependent on the subsequent usage of the sample: Buffer A (TritonX-100 0.5% (v/v), 10 mM HEPES at pH 7.4, 2 mM DTT, 1 tablet of Complete Protease Inhibitor Cocktail Tablets (Cat # 11 697 498 001, Roche) per 50 ml of buffer) was used for Western blot and activity assay; buffer B (250 mM sucrose, 50 mM KCl, 5 mM MgCl2, 20 mM Tris base, adjusted to pH 7.4) for determination of MMA and 2-MC levels The homogenate was centrifuged at 14'000 rpm for 10 minutes at 4°C. The supernatant was used for protein determination by Bradford assay (Cat. #500-0205, BioRad).

7.5.3 Housing of mice and generation of knock-in allele

Animal experiments were performed in accordance with policies of the Veterinary Office of the State of Zurich and Swiss law on animal protection. Animal studies were approved by the Cantonal Veterinary Office Zurich under the license number 202/2014. Animals were kept in single-ventilated cages and under controlled humidity and temperature (21-23°C). Whenever possible littermate controls were used to compare experimental groups.

To generate (in collaboration with Polygene AG, Rümland, Switzerland) mice homozygous for the mutation Mut-p.Met698Lys (c.2093T>A on RefSeq NM_008650.3) (C57BL/6 *Mut*$^{ki/ki}$), a vector was generated to be used for embryonic stem cell targeting. The neomycin resistance cassette helped to select cells for screening by PCR and Southern blotting. Positive clones were used for blastocyst injections and generation of chimeric animals. Backcrossing to C57BL/6 mice allowed the testing of the pups for germline transmission. The breeding of the germline-positive animals to Flp-deletor

mice lead to the deletion of the FRT-flanked neomycin cassette via recombination. Mutational analysis by Sanger sequencing confirmed the mutation c.2093T>A. To maintain the knock-in allele, female *Mut*$^{ki/wt}$ mice were crossed with *Mut*$^{ki/ki}$males. To generate *Mut*$^{ko/ki}$ mice, female *Mut*$^{ko/wt}$ (Peters, et al., 2003) were crossed to *Mut*$^{ki/ki}$males.

Mouse genotyping was performed on genomic DNA from ear punch biopsies after previous extraction (DNAeasy Blood & Tissue Kit, Cat. No. 69506, Qiagen). The primers 5'-GTGGGTGTCAGCACACTTG-3' (forward) and 5'-CGTATGACTGGGATGCCT-3' (reverse) amplified (HotStarTaq DNA Polymerase, Cat. No. 203205, Qiagen) a PCR segment which differed in size because of the remaining FRT site after recombination. An amplicon of 432 base pairs (bp) corresponded to a wild-type allele, 531 bp indicated a knock-in allele. For the genotyping of the knock-out allele, the primers 5'-ACAACTCCTT-GTGTAGGTC-3' (forward) and 5'-CCTTTAGGATGTCATTCTG-3' (reverse primer binding to exon 3) were used to generate an amplicon of 507 bp in size. If exon 3 was replaced by a neomycin cassette as demonstrated in (Peters, et al., 2003) the same forward primer together with the the reverse primer 5'-GAATGAACTGCAAGACGAG-3' resulted in an amplicon of 1138 bp. For the breeding of *Mut*$^{ko/ki}$ mice, both genotyping protocols were performed to determine the genotype of the weaned pups at the age of 3 weeks.

7.5.4 Long-term studies and metabolic cage studies

Long-term monitoring of mice entailed weekly weight measurements and regular blood collections as well as urine collections. Animals were single caged overnight to collect urine and measure individual chow and water intake. Urine was collected in the morning, the sediment removed and frozen at -80°C.

7.5.5 Quantitative real time PCR analysis

Total RNA was extracted from frozen tissue using the QIAmp RNA Blood Mini Kit (Cat. No. 52304, Qiagen). Reverse transcription of 300 µg of RNA was performed with the 1st Strand cDNA Synthesis Kit (Takara). TaqMan gene expression assays were done in the 7900HT Fast Real-Time PCR System (Thermo Fisher Scientific) using TaqMan Gene Expression Master Mix (Thermo Fisher Scientific). Specific probes (all Thermo Fisher Scientific) for Mut (Mm00485312_m1), Lcn2 (Mm01324470_m1), p62 (Mm00448091_m1) and Lc3 (Mm00458724_m1) were used. Experiments were performed in triplicates and results were normalized to beta-actin (Mm00607939_s1). Relative gene expression was expressed as fold change compared to baseline and was calculated with the $2^{-\Delta\Delta CT}$ method.

7.5.6 Western blot

Tissue samples were prepared as described above. 30 µg of protein was loaded onto the gel and subsequently analyzed by Western blotting using the following antibodies for methylmalonyl-CoA mutase (ab67869, 1:500, Abcam) and Lcn2 (ab63929, 1:1000, Abcam). Beta-actin (A2228, Sigma-Aldrich) was used as loading control at a dilution of 1:4000. Secondary antibodies were horseradish peroxidase (HRP)-labelled goat anti-mouse (sc-2302, Santa Cruz) or goat anti-rabbit (sc-2301, Santa Cruz) IgG at a dilution of 1:5000. HRP activity was visualized by applying electrochemical luminescence (RPN2109, GE Healthcare). Bands were quantified by normalization to internal beta-actin control bands.

7.5.7 Metabolite measurements

MMA in mice urine was analysed by liquid chromatography mass spectrometry (LC-MS/MS) on a Thermo Scientific UltiMate 3000 Rapid Separation LC coupled to an AB Sciex 5500 TripleQuad mass spectrometer using a commercial Kit (Recipe ClinMass® advanced). In brief, the urine probes were first diluted with Milli-Q water (18.2 MΩ·cm at 25 °C) at different levels (factor 10 to 20'000) to which internal standard (d3-MMA) was added. The samples were vortexed, centrifuged, transferred to HPLC vials and 2 µl were injected into the instrument.

For determination of the concentrations of amino acids, acylcarnitines (C2 and C3) as well as MMA in dried blood spots, blood was collected from tail vein onto a filter card and dried. Punches from filter cards were analysed by tandem mass spectrometry similar to (Turgeon, et al., 2010).

For MMA and 2-MC determinations in tissue, 250-300 µl of homogenate were used for liquid–liquid extraction. Briefly, 10 µl of 1 mM stable isotope-labeled d3-MMA (Cambridge Isotope Laboratories, Inc., Andover, USA) and 100 µl of 1.25 mM d4-nitrophenol (d4-NP; euriso-top GmbH, Saarbrucken, Germany) were added as internal standards. Samples were acidified with 300 µl of 5 M HCl and after addition of solid sodium chloride extracted twice with 5 ml ethyl acetate each. The combined ethyl acetate fractions were dried over sodium sulfate and then evaporated at 40°C under a stream of nitrogen. Samples were then derivatized with N-methyl-N-(trimethylsilyl)heptafluorobutyramide (MSHFBA, Macherey-Nagel, Düren, Germany) for 1 h at 60°C. For GC/MS analysis, the quadrupole mass spectrometer MSD 5975A (Agilent Technologies, USA) was run in the selective ion-monitoring mode with electron impact ionization. Gas chromatographic separation was achieved on a capillary column (DB-5MS, 30 m x 0.25 mm; film thickness: 0.25 µm; Agilent J&W Scientific, USA) using helium as a carrier gas. A volume of 1 µl of the derivatized sample was injected in splitless mode. GC temperature parameters were 80°C for 2 minute, ramp 50°C/minute to 150 °C, then ramp 10°C/minute to 300°C. Injector temperature was set to 260°C and interface temperature to 260°C. Fragment ions

for quantification were m/z 247 (MMA), m/z 250 (d3-MMA), m/z 200 (d4-NP) and m/z 361 (MCA). A dwell time of 50 ms was used for MCA and d4-NP and 100 ms for MMA and d3-MMA.

Total fatty acid profiles from plasma/serum were determined by direct methylation and gas chromatography, as described (Scheja, et al., 2008). Sphingoid base were analysed in tissue homogenates prepared in buffer A (see above) or directly in heparin plasma (100 µl). Proteins were precipitated by adding 500 µl MeOH (Honeywell), including 200 pmol internal standards (d7-SA and d7-SO, Avanti Polar Lipids, Alabaster CA) and lipids extracted under constant agitation (1h, 1400rpm @ 37°C; Eppendorf Thermomixer Comfort; Eppendorf, Hamburg, Germany). Precipitated proteins were removed by centrifugation (5 min at 16'100 rcf, 22°C; Model 5415, Eppendorf, Hamburg, Germany) and the supernatant (500 µl) transferred followed by the addition of 75 µl HCl (32%, Sigma). This mixture was incubated at 65°C for 16 h and finally neutralized by the addition of 100 µl KOH [10 M]. Hydrolyzed lipids were re-extracted by adding 125 µl $CHCl_3$, followed by the stepwise addition of another 500 µl $CHCl_3$, 100 µl NH_4OH [2 N] and 500 ul alkaline H_2O. Phases were separated by centrifugation at room temperature (13'000 x*g* for 5 min). The upper phase was removed and the lower phase washed twice with alkaline H_2O (1 ml). The remaining $CHCl_3$ phase was evaporated under a flow of N_2 (Techne Sample Concentrator, Bibby Scientific Ltd, Staffordshire, UK) and lipids stored under N_2 at -20°C. For LC-MS analysis, lipids were re-dissolved in 75 µl derivatization mix (56.7% MeOH, 33.3% EtOH, 10% H_2O) and derivatized with 5 µl of OPA working solution (990 µl boric acid [3%] + 10 µl o-Phthalaldehyde [50 mg/ml in EtOH] + 0.5 µl 2-Mercaptoethanol). Samples were separated for 30min on a reverse phase C18 column (Uptispere 120 Å, 5µm, 125x2 mm, Interchim, France) with an isocratic mobile phase (50% MeOH + 5 mM Ammonium Acetate (Sigma) at a flowrate of 400 µl/min. After each run the column was regenerated for 10 min with 100%MeOH. Spectra were recorded on a triple quad MassSpec (TSQ quantum ultra, Thermo scientific) in positive mode using APCI ionization.

Ammonia levels in whole blood were measured by the PocketChem blood ammonia meter (PA-4140, Arkray) after validating the device by certified photometric endpoint measurement.

Electrolytes in urine were measured by a timed endpoint method (SYNCHRON System kit, Beckman Coulter). Kit references are: Magnesium (445360), Sodium (467935), Potassium, Chloride and Calcium (467935 & 467915). For urea determination in plasma the SYNCHRON CX3 Delta System was used (Beckman Coulter, Nyon), kit no. 443350.

7.5.8 Histology and immunohistochemistry

Stainings were performed on sections from brain tissues fixed in formalin and embedded in paraffin. After deparaffinization through xylol and graded alcohols, sections were stained with the following antibodies: GFAP (1:13000; Dako), IBA1 (1:1000; WAKO) and active Caspase3 (1:200; BD Biosciences).

Stainigs for GFAP and IBA1 were performed on an automated BenchMarkTX platform (Ventana) using the I-View Kit according to the manufacturer's protocol. Stainings for active Caspase3 were done on an automated BOND III platform (Leica) using the RefineDetection Kit according to the manufacturer's protocol. Hematoxylin counterstain was subsequently applied. Images were acquired using the NanoZoomer scanner (Hamamatsu Photonics) and NanoZoomer digital pathology software (NDPview;Hamamatsu Photonics). Images were analyzed with Adobe Photoshop and Adobe Illustrator.

7.5.9 Diet and cobalamin therapy

Two different diets were used and fed to the mice ad libitum. A high protein diet with 70% casein (weight per weight) or 61% protein (TD.140830, Harlan) and a precursor-enriched diet (35.4% protein, of which 20% derived from casein; TD.140829, Harlan) were applied. The precursor-enriched diet had specific amino acid levels increased: isoleucine (total of 70 g/kg, 700% compared to reference diet), valine (84 g/kg, 700%) and threonine (53 g/kg, 700%) because they are precursors of the propionate pathway; leucine (19 g/kg, 119%) since its uptake might compete with the update of the other amino acids which are increased in the diet; cystine (3.5 g/kg, 700%) to elevate the overall sulfur content; methionine was not elevated because of its atherogenic potential and possible effect on brain function when applied in excess (McCampbell, et al., 2011; Troen, et al., 2003).

For the cobalamin treatment studies, mice were pre-treated for one week with daily intraperitoneal injections of 0.3 µg hydroxocobalamin (OHCbl) (Streuli Pharma AG) per gram body weight starting at the age of 53 days. At day 60 the high protein diet was initiated and *i.p.* OHCbl treatment continued.

7.5.10 Statistical analyses

All data were analyzed with Prism 6.0 (GraphPad) software. Statistical comparison tests used are ANOVA multiple comparisons test and Student's *t* test. In sample groups always a minimum of four animals was used and the data were calculated as means ±SD or ±SEM, respectively. A *p* value below 0.05 was considered significant.

7.6 Acknowledgments

This work was supported by the Rare Disease Initiative Zurich (radiz), a clinical research priority program for rare diseases of the University of Zurich, Switzerland, the Swiss National Science Foundation (SNSF 31003A_138521) and the Wolferman-Nägeli foundation. P.F. was supported by an SNSF MD-

PhD fellowship (SNSF 323530_145248). P.F. would like to thank Adam Guenzel for discussion, Elisabeth Rushing and the Institute of Neuropathology, University Hospital Zurich for brain histology, and Museer Lone for analysis of sphingoid bases.

7.7 SUPPLEMENTARY MATERIAL

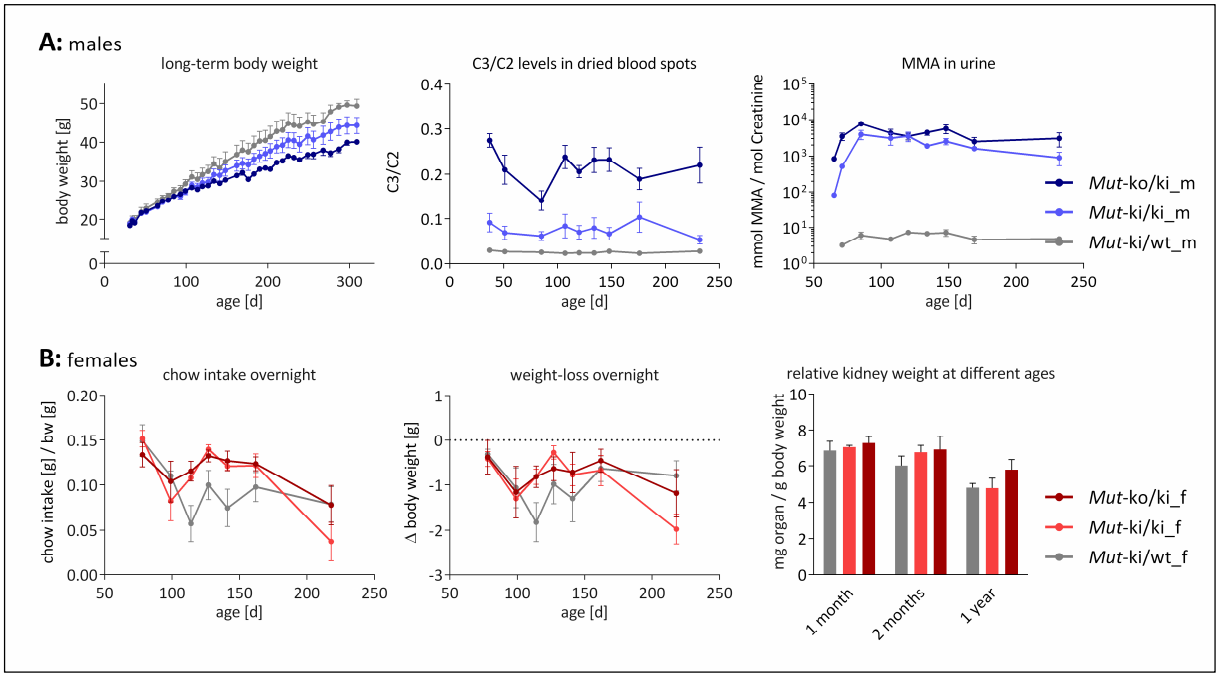

Supp. Figure S1. Long-term data in male and female mice. (**A**) Left panel: Body weight of male mice is monitored over time; middle panel: Elevated C3 levels normalized to C2 in *Mut*$^{ki/ki}$ and *Mut*$^{ko/ki}$ mice determined in dried blood spots by tandem mass spectrometry; right panel: MMA urine levels measured by LC-MS/MS. (**B**) Left panel: Chow intake in female mice determined by overnight measurements in metabolic cages; middle panel: Weight loss in mice when single-caged overnight; right panel: Weights of whole kidney (1 organ) normalized to body weight at different time points.

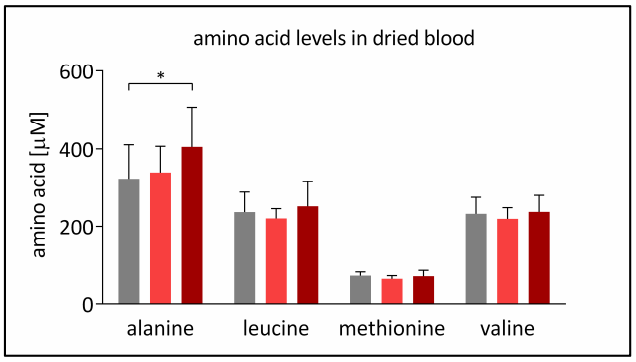

Supp. Figure S2. Amino acid levels expressed in µM at the age of 35 days. Dried blood spots of three different genotypes (*Mut*$^{ki/wt}$, grey; *Mut*$^{ki/ki}$, red; *Mut*$^{ko/ki}$, dark red) were used for tandem mass spectrometry measurements of amino acid levels. Bars represent mean values; error bars depict SD; $n = 5$ per group; *: $p < 0.05$.

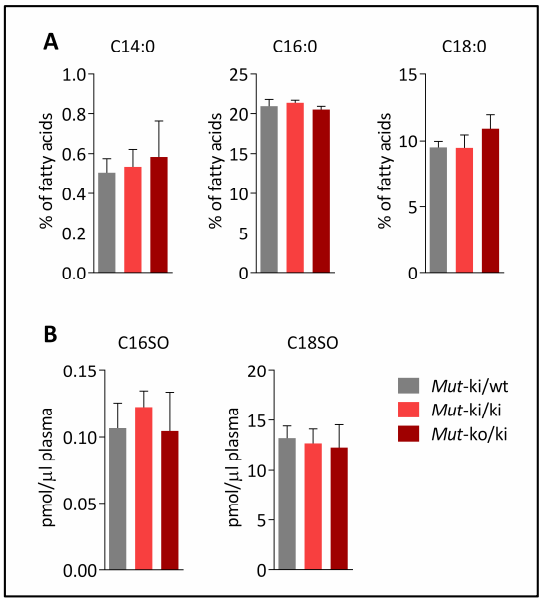

Supp. Figure S3. (**A**) Levels of even-chain fatty acids determined in plasma and expressed as percentage of total amount of fatty acids. (**B**) Even-chain sphingoid bases determined in plasma and expressed as pmol per microliter of plasma.

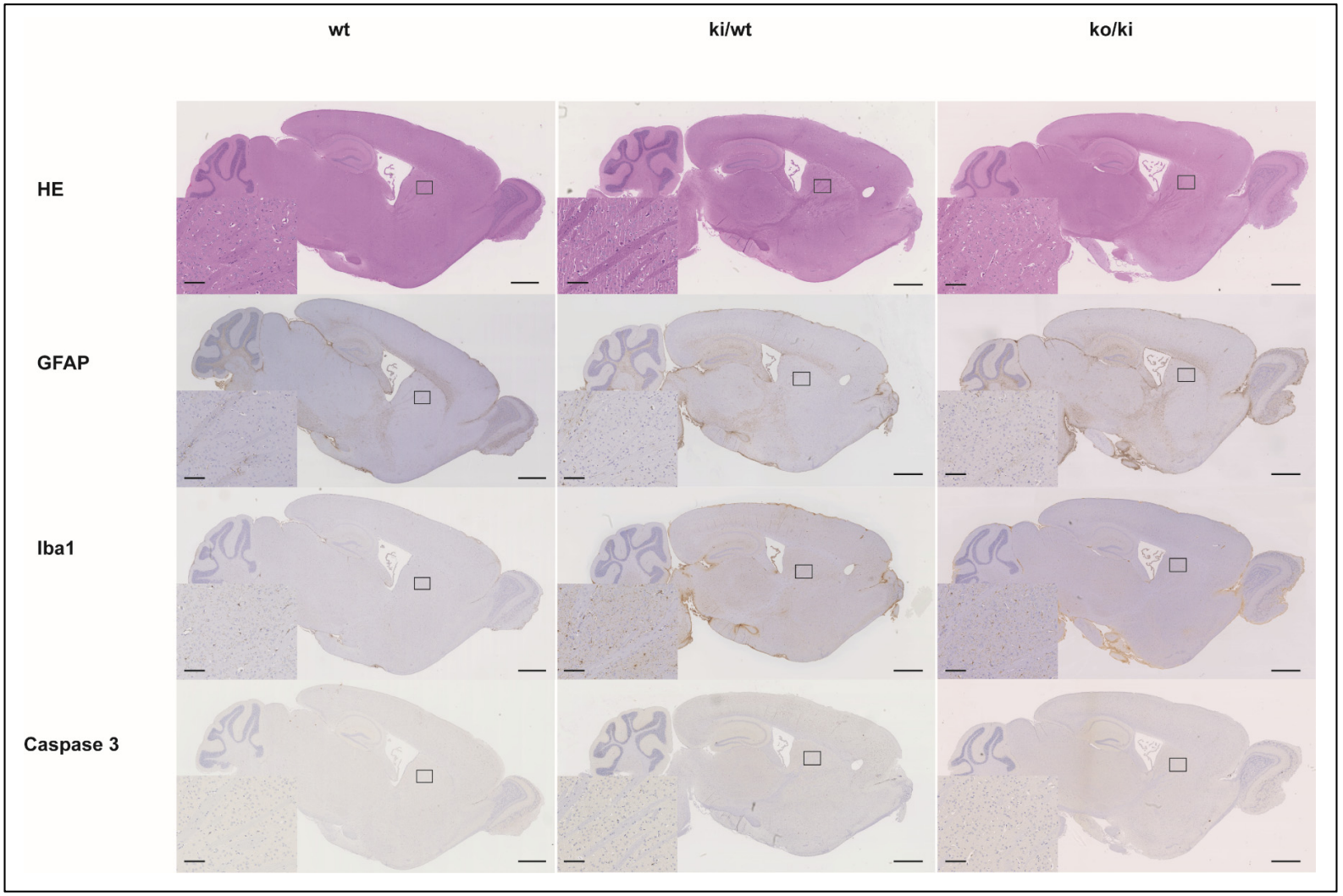

Supp. Figure S4. Brain histology of *Mut*$^{ko/ki}$ mice and control mice (*wt* and *Mut*$^{ki/wt}$). *Mut*$^{ki/wt}$ and *Mut*$^{ko/ki}$ brains are from animals at the age of 1 year, *wt* control is 140 days old. Apart from traditional haematoxylin-eosin staining, slices were stained for glial fibrillary acidic protein (GFAP), ionized calcium-binding adapter molecule 1 (Iba1), and Caspase 3. Scale bars on overview pictures are 1 mm, scale bars of insets in the basal ganglia are 100 µm.

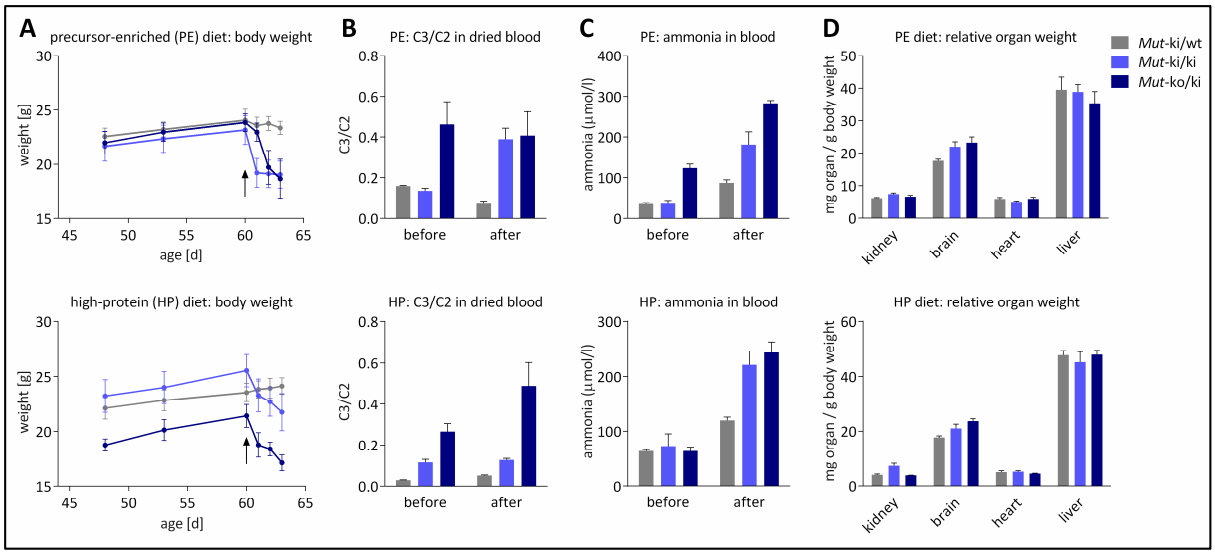

Supp. Figure 5. Diet modification in male mice at the age of 60 days leads to a severe exacerbation of the phenotype. (**A**) Weight loss induced by high protein (HP) or precursor-enriched (PE) diets in *Mut*$^{ki/ki}$ and *Mut*$^{ko/ki}$ mice. Black arrows indicate start of respective diet. Levels of (**B**) C3 normalized to C2 and (**C**) ammonia in whole blood before and after the diet was initiated. (**D**) Weight of whole organs normalized to body weight. Bars and points represent means; error bars are SEM.

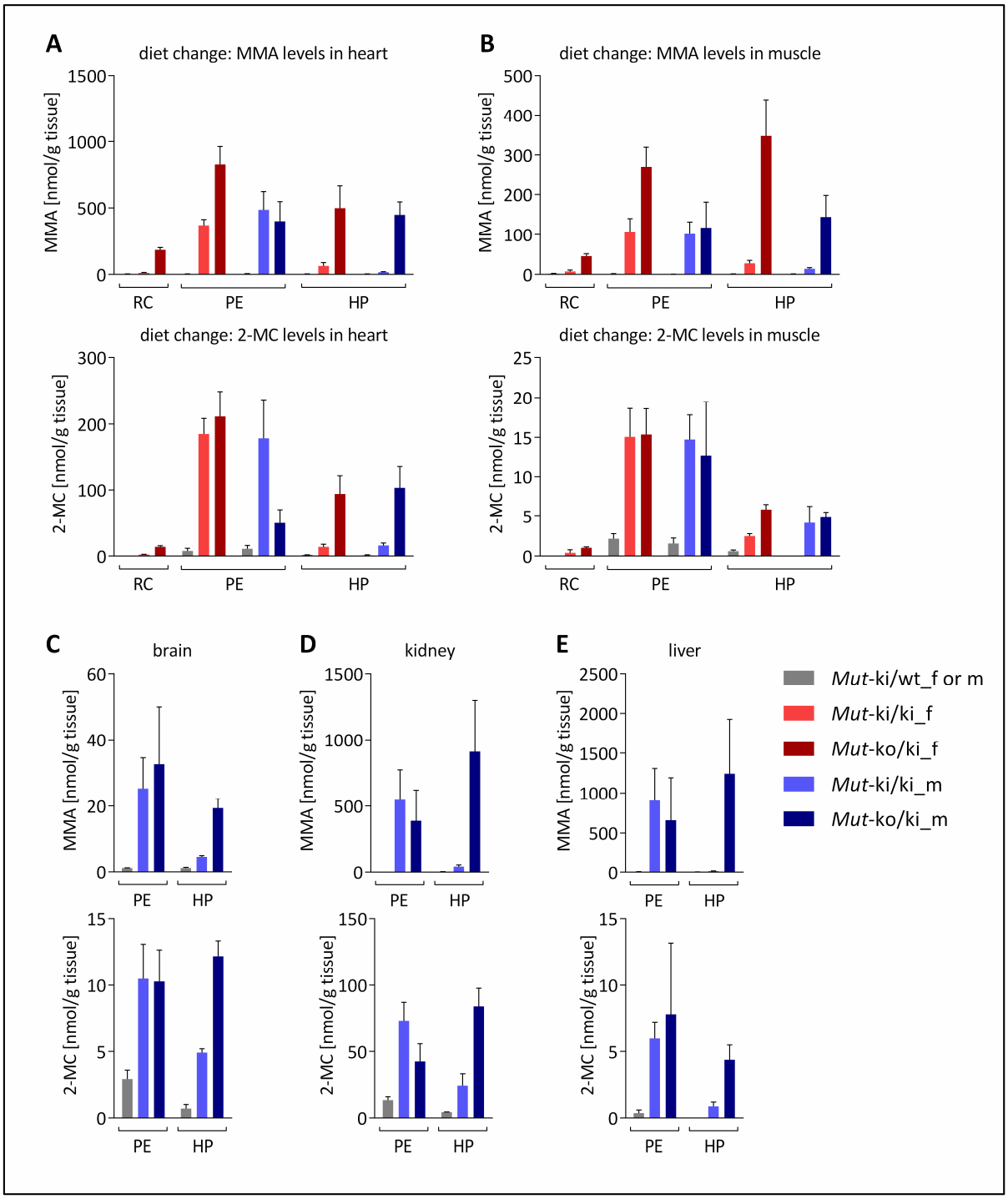

Supp. Figure S6. MMA and 2-MC levels in tissues from mice on high protein (HP) and precursor-enriched (PE) diet compared to levels on reference chow (RC). MMA and 2-MC values in nmol are normalized to wet weight of tissues in gram. The panels represent data from (**A**) heart, (**B**) muscle, (**C**) brain, (**D**) kidney and (**E**) liver tissues. The female data, which is not displayed in panels C, D and E, are shown in Fig. 5F, G and H. Bars are means of $n = 5$; error bars depict SEM. Groups with red bars represent data from female mice, blue bars originate from data on male mice. Genotype according to the following colour code: *Mut*$^{ki/wt}$, grey; *Mut*$^{ki/ki}$, red or blue; *Mut*$^{ko/ki}$, dark red or dark blue. If a grey bar is grouped with red bars it represents a female control, with blue bars it is a male control.

Fatty acid name	*Mut*-ki/wt	*Mut*-ki/ki	*Mut*-ko/ki
Linoleic acid	25.84	27.72	28.61
Palmitic acid	20.90	21.33	20.51
Oleic acid	18.52	17.65	15.31
Arachidonic acid	10.57	9.90	10.49
Stearic acid	9.47	9.43	10.91
Vaccenic acid	3.13	2.66	2.21
Palmitoleic acid	2.68	2.41	1.55
Docosahexaenoic acid	2.49	2.13	2.27
alpha-Linolenic acid	1.02	1.20	1.31
Dihomo-gamma-linolenic acid	1.02	0.86	0.84
d-7-Hexadecane	0.61	0.59	0.58
Eicosapentaenoic acid	0.55	0.49	0.39
Myristic acid	0.51	0.53	0.58
Eicosenoic acid	0.43	0.43	0.45
Heptadecanoic acid	0.34	0.55	1.16
Nervonic acid	0.32	0.33	0.34
gamma-Linolenic acid	0.26	0.31	0.28
Docosapentaenoic acid	0.21	0.21	0.25
Pentadecanoic acid	0.21	0.35	0.89
Eicosadienoic acid	0.20	0.17	0.18
Behenic acid	0.19	0.21	0.27
Eicosatrienoic acid	0.17	0.18	0.21
Lignoceric acid	0.11	0.13	0.18
Eicosatetraenoic acid	0.11	0.09	0.08
Heneicosylic acid	0.05	0.05	0.05
Erucic acid	0.05	0.05	0.06
Myristoleic acid	0.03	0.03	0.02
Tridecylic acid	0.01	0.03	0.03

Supp. Table 1. Specific fatty acids in plasma in percent of total amount of fatty acids.

sphingoid base	*wt*	*Mut*-ki/wt	*Mut*-ki/ki	*Mut*-ko/ki
C19SO				
brain	0.015	0.011	0.047	0.020
heart	0.002	0.002	0.002	0.002
kidney	0.007	0.007	0.008	0.010
liver	0.006	0.007	0.007	0.006
muscle	0.001	0.000	0.002	0.001
C16SO				
brain	0.023	0.026	0.060	0.022
heart	0.018	0.025	0.019	0.017
kidney	0.022	0.018	0.023	0.018
liver	0.023	0.028	0.022	0.017
muscle	0.005	0.002	0.004	0.006
C18SO				
brain	13.968	13.053	32.065	13.956
heart	2.573	2.463	2.502	2.021
kidney	8.373	8.430	8.380	9.673
liver	3.615	4.327	4.212	3.212
muscle	0.795	1.037	1.402	1.551
C20SO				
brain	0.677	0.570	1.300	0.665
heart	0.012	0.005	0.003	0.004
kidney	0.022	0.034	0.035	0.035
liver	0.014	0.021	0.012	0.012
muscle	0.001	0.002	0.001	0.008

Supp. Table 2. Sphingoid bases in tissues in pmol/µg protein.

	Reference chow (RC)	High protein (HP)	Precursor-enriched (PE)
Isoleucine, g/Kg	10	35	70
Leucine, g/Kg	16	56	19
Valine, g/Kg	12	42	84
Threonine, g/Kg	7.6	27	53
Cystine, g/Kg	0.5	1.8	3.5
Methionine, g/Kg	4.6	16	4.6
Protein, g/Kg	177	609	354
Casein, g/Kg	200	700	200
Cbl, mg/Kg	0.0375	0.0375	0.0375

Supp. Table 3. Composition of reference chow, high protein and precursor-enriched chow. Cbl, cobalamin.

8 CONCLUSION AND OUTLOOK

8.1 MMAURIA PATIENT COHORT ANALYSIS

We were able to analyse 151 patients and to stratify them according to their genotype, biochemical data, and age of onset. We provide information on genotype-phenotype correlation and present 41 novel mutations in the *MUT* gene. This study shows that patients of the *mut*$^-$ subclass have a later age of disease onset which is in line with the previously shown milder disease course in this subgroup compared to *mut*^{0} (Horster, et al., 2007). Responsiveness to cobalamin was evaluated *in vitro* and a detectable response correlated to the genotype of patients with missense mutations, making this mutations type more likely to be responsive compared to other mutation types. Nevertheless, we conclude that the prediction of disease severity and responsiveness to cobalamin treatment based on biochemical assays and mutations type is not certain. Since a reliable prognosis would be very helpful for the health management of the patient and also the patient itself, we suggest further studies to improve the understanding of cobalamin responsiveness from a clinical point of view and also from a molecular/mechanistic perspective.

Additionally, we analysed the missense mutations in more detail and performed Western blot analysis to determine residual protein amount as a surrogate marker of protein stability. We identified only a handful of missense mutations which resulted in a considerable amount of residual protein. In fact, most missense mutations lead to a destabilized MUT mutant protein, adding *mut*-type MMAuria to the growing list of misfolding disorders. Based on this phenomenon we suggest future studies which may involve investigations of specific small molecules in order to improve the stability of unstable mutant proteins with these compounds.

8.2 MUT MUTANTS CHARACTERIZATION

In addition to the detailed update on all *MUT* mutations detected in our patient cohort, we selected 23 missense mutants to perform an in-depth characterization of their biochemical properties. Each of the 23 mutants was assigned to a category of biochemical defects: K_M defect, catalytic defect, thermolabile mutant, or unstable mutant. This categorization improves the understanding of possible defects conferred by missense mutations on the MUT protein and can guide future investigations of missense changes in *MUT*. We have shown that MUT is amenable to analysis of temperature stability tests by DSF and that it can be used as a target protein in large scale screenings applying this methodology. Therefore, our study establishes MUT as a potential target for chaperone-based therapy, constituting a promising novel therapeutic approach in MMAuria.

8.3 Pharmacological Chaperone Screening for MUT

In previous investigations (Forny, et al., 2014) MUT was established as a suitable candidate for high throughput screening by DSF . Such screening was performed in order to find stabilizing molecules for MUT-*wt* which may be later also applied to mutants of MUT. In screening of a library, consisting of 10,000 compounds, about two dozen molecules were identified to have a stabilizing effect on the MUT-*wt* protein. Validation experiments by biophysical and cell culture experiments could inconsistently confirm some of the hit compounds from the screening. Since some of the orthogonal validation methods did not support the original screening results, we suggest the following future directions in PC screening for MUT:

i. The conditions used in the verification methods should be varied to test different concentrations of the tested compounds and various times of incubation. *E.g.* cell cultures could be incubated with higher concentrations of the compounds and for a longer time. These changes of the experimental conditions could lead to other results in the validation experiments. Additionally, careful monitoring of the compounds with regard to their uptake into the cell, intracellular localisation, and intracellular or even intra-mitochondrial concentration is essential.

ii. The screened library of 10,000 compounds is rather small compared to existing libraries available to the drug industry, which often consist of 10-50 fold more compounds per library. If the number of compounds screened would be increased, the likelihood of finding specific binders of MUT will dramatically rise.

iii. The screening was performed based on MUT-*wt* protein. This might be problematic since the protein targets in patients are MUT mutants and not wild-type proteins. As illustrated by the *E. coli* expression experiments, unstable MUT mutants were not rescued by the hit compounds. Despite the convenience of using the wild-type protein, which can be purified at high amounts, it might be necessary to use several different mutant proteins as targets of the screening process. The difficulty of the instability of MUT mutant proteins could be overcome by large-scale growth of large amounts of bacterial cultures and the application of chemical chaperones, such as glycerol, during the purification process.

iv. The screening approach applies the DSF method which is based on the stability of the MUT protein. Alternative screening approaches, based on read-out criteria different from structural protein integrity, might be more precise and reveal more promising hit compounds. Since the final aim of a potential PC therapy in MMAuria is the increase of enzyme activity at

the correct location, future screening methods could be based on enzyme activity and/or subcellular distribution and thereby result in identification of more effective hit compounds.

v. Potential evaluation in mouse models should be monitored carefully. The route of administration has to be selected based on pilot studies which investigate the uptake and delivery of the compounds to the target protein in different organs. Special emphasis should be put on the uptake of compounds into brain tissue, since satisfactory MMAuria treatment would include therapy of the neurological phenotype.

8.4 Novel Mouse Models of MMAuria

8.4.1 Conclusions on current studies

In this study novel mouse models of MMAuria were generated and evaluated for their value as tools in MMAuria research.

The conditional brain knock-out of *Mut* showed that the Cre/loxP recombination system can be robustly applied in our model. The results presented include basic investigations on the validity of the brain-knockout and sets the stage for further characterization of this model with a special emphasis on the CNS phenotype.

The novel $Mut^{ki/ki}$ and $Mut^{ko/ki}$ models were evaluated regarding the accurate mimicking of human MMAuria and found to recapitulate the disease in many biochemical and clinical aspects with a gene-dose effect. The severity of the disease can be modulated by a modified protein diet, which allows the titration of disease symptoms. Additionally, we could evaluate the responsiveness of these models to classical Cbl treatment and found some parameters, which were ameliorated upon this treatment, suggesting that evaluation of Cbl response is crucial in MMAuria patients. Taken together, the results generated in this study encourage further studies on pathomechanisms in kidney and CNS, novel treatment approaches, and cofactor response.

8.4.2 Potential future studies

Future studies should focus on the exploration of the phenotype, especially organ manifestations, of MMAuria with a focus on the pathomechanisms. The following methods allow disease acceleration in both models (conditional brain knock-out and constitutive knock-in):

i. As exemplified in our study, a protein increase in the diet leads to a stress situation in the animals, resulting in massive weight loss after only a couple of days on this modified diet. This severe impact of a high-protein or precursor-enriched diet can be titrated to a level, where weight loss is not so severe but the disease manifestations are still enhanced.

ii. The diet modification approach leads to an increase in the throughput of the propionate pathway. The same effect can be achieved by fasting. The absence of food intake leads to the breakdown of endogenous protein resources and thus to an elevated production of propionate. This stress situation, which can also be observed in patients, can induce a metabolic crisis which enhances MMAuria symptoms.

iii. Mice can be observed over a longer time, so phenotypic changes can accumulate and are therefore easier to be observed. Aging experiments also allow the study of the dynamics of certain processes, *e.g.* changes of pathomechanistic markers over time.

When the conditions are determined under which a maximal acceleration of the phenotype can be expected, CNS and kidney should be investigated in-depth. In our study, Lcn2 and brain weight was elevated in the *Mut*$^{ko/ki}$ mice, indicating phenotypic changes in the brain of those animals. Despite these results, brain histology remained unchanged, suggesting that the molecular changes did not translate to the macroscopic level of the cell. To observe changes such as basal ganglia lesions or white matter disease, additional methods are required to monitor these phenotypic phenomena such as magnetic resonance imagining, behavioural studies including gait analysis, and electron microscopy. Renal investigations may include measurement of glomerular filtration rate and ultrastructural analysis by electron microscopy in order to monitor the potential development of end stage renal disease. Moreover, the kidney can be investigated with the conditional knock-out model, when *Mut*$^{flox/flox}$ mice are crossed with a kidney-specific Cre expressing mouse line, generating a similar model to the brain-specific conditional *Mut*-ko model. In order to study specific tissues, primary cell cultures derived from organs of *Mut*$^{flox/flox}$ mice with subsequent *in vitro* Cre-mediated deletion of *Mut* can also be developed.

In addition, metabolomics (and also transcriptomics) approaches may be helpful to identify affected pathways in the pathology of MMAuria. Although whole metabolome approaches are getting increasing attention in the field of IEMs, they are often targeted (Janeckova, et al., 2012) or not disease-specific (Mussap, et al., 2013). In MMAuria knowledge about the metabolome of patients is sparse. One study on MMAuria and propionic aciduria patient plasma identified propionylcarnitine as the best biomarker of disease (Wikoff, et al., 2007). Non-targeted metabolite profiling is usually carried out as comparative analysis between control and patient groups (Miller, et al., 2015). Our mouse models serve as an ideal tool for such an approach, allowing the definition of a clearer picture of the metabolite pattern in MMAuria. The homogenous genetic background of the samples should allow the measurement of a robust data set with little individual variation. The identification of novel biomarkers would elucidate so far unknown pathways involved in MMAuria pathogenesis.

8.4.2.1 Pharmacological chaperones

As described in this thesis, the search for PCs is complicated and requires a step-wise procedure in order to screen, verify and implement PCs. I suggest the following future studies/improvements:

i. Screening processes can be improved by using several methods at once, based on different features of the target protein such as structural integrity or enzymatic activity.

ii. *In silico* screenings (*e.g.* by molecular docking methods) may be considered in order to take advantage of the available knowledge of the protein structure of MUT.

iii. Since many disease-causing mutations in the *MUT* gene are known, different mutant proteins should be used as a substrate of screening, allowing the development of mutation-tailored molecules.

iv. Different verification methods should be applied:

    a. Methods which are based on the same feature of the protein as the initial screening method (*e.g.* thermal stability in DSF) in order to confirm the results from the screening.

    b. Orthogonal verification methods should be based on features of the protein which are different from the features used in the initial screening, *i.e.* if the screening method is based on stability (*e.g.* DSF), the verification method should evaluate the effect of the compound on activity (*e.g.* enzyme assay) or other aspects.

    c. Verification methods should employ different concentrations and incubation times of PC molecules.

    d. Verification methods may include studies on the uptake of the compounds into cells and their subcellular localisation.

v. Once candidate PCs for MUT are validated by verification methods, such as cell culture testing or activity assays, they can be tested in the mouse models introduced in this thesis. As a proof of principle, molecules should be tailored to the p.Met698Lys mutation in case of the ki mouse model introduced here. Further studies may include other mutations which require the generation of additional mouse models, carrying different mutations.

8.4.2.2 Gene therapy

To replace the defective *MUT* gene with a healthy copy in all cells of the organism (including the CNS) would be the ideal treatment for every *mut*-type MMAuria patient. Gene therapy in MMAuria has been successfully applied in mice (Chandler and Venditti, 2008; Chandler and Venditti, 2010) but

human trials have not been initiated yet. In fact, successful gene therapy would be the holy grail for all single-gene disorders (including MMAuria) but has seen significant opposition since its effectiveness needs to be improved and its safety is uncertain at this point.

REFERENCES

Acquaviva C, Benoist JF, Callebaut I, Guffon N, Ogier de Baulny H, Touati G, Aydin A, Porquet D, Elion J. 2001. N219Y, a new frequent mutation among mut(degree) forms of methylmalonic acidemia in Caucasian patients. Eur J Hum Genet 9(8):577-82.

Acquaviva C, Benoist JF, Pereira S, Callebaut I, Koskas T, Porquet D, Elion J. 2005. Molecular basis of methylmalonyl-CoA mutase apoenzyme defect in 40 European patients affected by mut(o) and mut- forms of methylmalonic acidemia: identification of 29 novel mutations in the MUT gene. Hum Mutat 25(2):167-76.

Adjalla CE, Hosack AR, Gilfix BM, Lamothe E, Sun S, Chan A, Evans S, Matiaszuk NV, Rosenblatt DS. 1998. Seven novel mutations in mut methylmalonic aciduria. Hum Mutat 11(4):270-274.

Adzhubei IA, Schmidt S, Peshkin L, Ramensky VE, Gerasimova A, Bork P, Kondrashov AS, Sunyaev SR. 2010. A method and server for predicting damaging missense mutations. Nat Methods 7(4):248-9.

Ando T, Rasmussen K, Nyhan WL, Hull D. 1972. 3-hydroxypropionate: significance of -oxidation of propionate in patients with propionic acidemia and methylmalonic acidemia. Proc Natl Acad Sci U S A 69(10):2807-11.

Applegarth DA, Toone JR, Lowry RB. 2000. Incidence of inborn errors of metabolism in British Columbia, 1969-1996. Pediatrics 105(1):e10.

Arakawa T, Timasheff SN. 1985. The stabilization of proteins by osmolytes. Biophys J 47(3):411-4.

Ashkenazy H, Erez E, Martz E, Pupko T, Ben-Tal N. 2010. ConSurf 2010: calculating evolutionary conservation in sequence and structure of proteins and nucleic acids. Nucleic Acids Res 38(Web Server issue):W529-33.

Baell JB, Holloway GA. 2010. New Substructure Filters for Removal of Pan Assay Interference Compounds (PAINS) from Screening Libraries and for Their Exclusion in Bioassays. J Med Chem 53(7):2719-2740.

Baker EH, Sloan JL, Hauser NS, Gropman AL, Adams DR, Toro C, Manoli I, Venditti CP. 2014. MRI Characteristics of Globus Pallidus Infarcts in Isolated Methylmalonic Acidemia. AJNR Am J Neuroradiol.

Ballhausen D, Mittaz L, Boulat O, Bonafé L, Braissant O. 2009. Evidence for catabolic pathway of propionate metabolism in CNS: expression pattern of methylmalonyl-CoA mutase and propionyl-CoA carboxylase alpha-subunit in developing and adult rat brain. Neuroscience 164(2):578-587.

Banerjee R, Ragsdale S. 2003. The many faces of vitamin B12: catalysis by cobalamin-dependent enzymes. Annual review of biochemistry 72(45b65db4-a303-a95f-1e4a-27d987256e0d):209-256.

Baumgartner MR, Almashanu S, Suormala T, Obie C, Cole RN, Packman S, Baumgartner ER, Valle D. 2001. The molecular basis of human 3-methylcrotonyl-CoA carboxylase deficiency. J Clin Invest 107(4):495-504.

Baumgartner MR, Horster F, Assoun M, Ballhausen D, Burlina A, Chapman KA, Dionisi-Vici C, Fowler B, Grunert S, Grunewald S and others. 2014. Proposed guidelines for the diagnosis and management of methylmalonic and propionic acidemia. Orphanet J Rare Dis 9(1):130.

Baumgartner R. 1983. Activity of the cobalamin-dependent methylmalonyl-CoA mutase. In: Hall CA, editor. The Cobalamins - Volume 10 of Methods in Hematology: Churchill Livingstone. p 181-193.

Beadle GW, Tatum EL. 1941. Genetic Control of Biochemical Reactions in Neurospora. Proc Natl Acad Sci U S A 27(11):499-506.

Berard JL, Zarruk JG, Arbour N, Prat A, Yong VW, Jacques FH, Akira S, David S. 2012. Lipocalin 2 is a novel immune mediator of experimental autoimmune encephalomyelitis pathogenesis and is modulated in multiple sclerosis. Glia 60(7):1145-59.

Bikker H, Bakker HD, Abeling NG, Poll-The BT, Kleijer WJ, Rosenblatt DS, Waterham HR, Wanders RJ, Duran M. 2006. A homozygous nonsense mutation in the methylmalonyl-CoA epimerase gene (MCEE) results in mild methylmalonic aciduria. Hum Mutat 27(7):640-3.

Boyd RE, Lee G, Rybczynski P, Benjamin ER, Khanna R, Wustman BA, Valenzano KJ. 2013. Pharmacological Chaperones as Therapeutics for Lysosomal Storage Diseases. J Med Chem.

Brassier A, Boyer O, Valayannopoulos V, Ottolenghi C, Krug P, Cosson MA, Touati G, Arnoux JB, Barbier V, Bahi-Buisson N and others. 2013. Renal transplantation in 4 patients with methylmalonic aciduria: a cell therapy for metabolic disease. Mol Genet Metab 110(1-2):106-10.

Brismar J, Ozand PT. 1994. CT and MR of the brain in disorders of the propionate and methylmalonate metabolism. AJNR Am J Neuroradiol 15(8):1459-73.

Britten RJ. 2002. Divergence between samples of chimpanzee and human DNA sequences is 5%, counting indels. Proc Natl Acad Sci U S A 99(21):13633-5.

Calvo AC, Scherer T, Pey AL, Ying M, Winge I, McKinney J, Haavik J, Thony B, Martinez A. 2010. Effect of pharmacological chaperones on brain tyrosine hydroxylase and tryptophan hydroxylase 2. J Neurochem 114(3):853-63.

Carleton SM, Peck DS, Grasela J, Dietiker KL, Phillips CL. 2010. DNA carrier testing and newborn screening for maple syrup urine disease in Old Order Mennonite communities. Genet Test Mol Biomarkers 14(2):205-8.

Causey AG, Bartlett K. 1984. A radio-HPLC assay for the measurement of methylmalonyl-CoA mutase. Clin Chim Acta 139(2):179-86.

Chace DH, DiPerna JC, Kalas TA, Johnson RW, Naylor EW. 2001. Rapid diagnosis of methylmalonic and propionic acidemias: quantitative tandem mass spectrometric analysis of propionylcarnitine in filter-paper blood specimens obtained from newborns. Clin Chem 47(11):2040-4.

Chakrapani A, Sivakumar P, McKiernan PJ, Leonard JV. 2002. Metabolic stroke in methylmalonic acidemia five years after liver transplantation. J Pediatr 140(2):261-3.

Chandler RJ, Sloan J, Fu H, Tsai M, Stabler S, Allen R, Kaestner KH, Kazazian HH, Venditti CP. 2007. Metabolic phenotype of methylmalonic acidemia in mice and humans: the role of skeletal muscle. BMC Med Genet 8:64.

Chandler RJ, Venditti CP. 2008. Adenovirus-mediated gene delivery rescues a neonatal lethal murine model of mut(0) methylmalonic acidemia. Hum Gene Ther 19(1):53-60.

Chandler RJ, Venditti CP. 2010. Long-term rescue of a lethal murine model of methylmalonic acidemia using adeno-associated viral gene therapy. Mol Ther 18(1):11-6.

Chandler RJ, Zerfas PM, Shanske S, Sloan J, Hoffmann V, DiMauro S, Venditti CP. 2009. Mitochondrial dysfunction in mut methylmalonic acidemia. FASEB J 23(4):1252-61.

Chaudhuri TK, Paul S. 2006. Protein-misfolding diseases and chaperone-based therapeutic approaches. FEBS J 273(7):1331-49.

Chemelli AP, Schocke M, Sperl W, Trieb T, Aichner F, Felber S. 2000. Magnetic resonance spectroscopy (MRS) in five patients with treated propionic acidemia. J Magn Reson Imaging 11(6):596-600.

Chimpanzee-Sequencing-Consortium. 2005. Initial sequence of the chimpanzee genome and comparison with the human genome. Nature 437(7055):69-87.

Choi Y, Chan AP. 2015. PROVEAN web server: a tool to predict the functional effect of amino acid substitutions and indels. Bioinformatics 31(16):2745-7.

Christ SE, Moffitt AJ, Peck D, White DA. 2013. The effects of tetrahydrobiopterin (BH4) treatment on brain function in individuals with phenylketonuria. Neuroimage Clin 3:539-47.

Church DM, Goodstadt L, Hillier LW, Zody MC, Goldstein S, She X, Bult CJ, Agarwala R, Cherry JL, DiCuccio M and others. 2009. Lineage-specific biology revealed by a finished genome assembly of the mouse. PLoS Biol 7(5):e1000112.

Clothier JC, Chakrapani A, Preece MA, McKiernan P, Gupta R, Macdonald A, Hulton SA. 2011. Renal transplantation in a boy with methylmalonic acidaemia. J Inherit Metab Dis 34(3):695-700.

Coelho D, Kim JC, Miousse IR, Fung S, du Moulin M, Buers I, Suormala T, Burda P, Frapolli M, Stucki M and others. 2012. Mutations in ABCD4 cause a new inborn error of vitamin B(12) metabolism. Nat Genet.

Coelho D, Suormala T, Stucki M, Lerner-Ellis JP, Rosenblatt DS, Newbold RF, Baumgartner MR, Fowler B. 2008. Gene identification for the cblD defect of vitamin B12 metabolism. N Engl J Med 358(14):1454-64.

Cohen FE, Kelly JW. 2003. Therapeutic approaches to protein-misfolding diseases. Nature 426(6968):905-9.

Coker M, de Klerk JB, Poll-The BT, Huijmans JG, Duran M. 1996. Plasma total odd-chain fatty acids in the monitoring of disorders of propionate, methylmalonate and biotin metabolism. J Inherit Metab Dis 19(6):743-51.

Cooper DN, Youssoufian H. 1988. The CpG dinucleotide and human genetic disease. Hum Genet 78(2):151-5.

Corpet F. 1988. Multiple sequence alignment with hierarchical clustering. Nucleic Acids Res 16(22):10881-90.

Cosson MA, Benoist JF, Touati G, Dechaux M, Royer N, Grandin L, Jais JP, Boddaert N, Barbier V, Desguerre I and others. 2009. Long-term outcome in methylmalonic aciduria: a series of 30 French patients. Mol Genet Metab 97(3):172-8.

Crane AM, Ledley FD. 1994. Clustering of mutations in methylmalonyl CoA mutase associated with mut- methylmalonic acidemia. Am J Hum Genet 55(1):42-50.

Crane AM, Martin LS, Valle D, Ledley FD. 1992. Phenotype of disease in three patients with identical mutations in methylmalonyl CoA mutase. Hum Genet 89(3):259-64.

D'Adamo E, Caprio S. 2011. Type 2 diabetes in youth: epidemiology and pathophysiology. Diabetes Care 34 Suppl 2:S161-5.

Dahlin JL, Nissink JW, Strasser JM, Francis S, Higgins L, Zhou H, Zhang Z, Walters MA. 2015. PAINS in the assay: chemical mechanisms of assay interference and promiscuous enzymatic inhibition observed during a sulfhydryl-scavenging HTS. J Med Chem 58(5):2091-113.

de Keyzer Y, Valayannopoulos V, Benoist JF, Batteux F, Lacaille F, Hubert L, Chretien D, Chadefeaux-Vekemans B, Niaudet P, Touati G and others. 2009. Multiple OXPHOS deficiency in the liver, kidney, heart, and skeletal muscle of patients with methylmalonic aciduria and propionic aciduria. Pediatr Res 66(1):91-5.

Deme JC, Hancock MA, Xia X, Shintre CA, Plesa M, Kim JC, Carpenter EP, Rosenblatt DS, Coulton JW. 2014. Purification and interaction analyses of two human lysosomal vitamin B12 transporters: LMBD1 and ABCD4. Mol Membr Biol 31(7-8):250-61.

Desmet FO, Hamroun D, Lalande M, Collod-Beroud G, Claustres M, Beroud C. 2009. Human Splicing Finder: an online bioinformatics tool to predict splicing signals. Nucleic Acids Res 37(9):e67.

Dickson P, McEntee M, Vogler C, Le S, Levy B, Peinovich M, Hanson S, Passage M, Kakkis E. 2007. Intrathecal enzyme replacement therapy: successful treatment of brain disease via the cerebrospinal fluid. Mol Genet Metab 91(1):61-8.

Dobson CM, Gradinger A, Longo N, Wu X, Leclerc D, Lerner-Ellis J, Lemieux M, Belair C, Watkins D, Rosenblatt DS and others. 2006. Homozygous nonsense mutation in the MCEE gene and siRNA suppression of methylmalonyl-CoA epimerase expression: a novel cause of mild methylmalonic aciduria. Mol Genet Metab 88(4):327-33.

Dobson CM, Wai T, Leclerc D, Kadir H, Narang M, Lerner-Ellis JP, Hudson TJ, Rosenblatt DS, Gravel RA. 2002a. Identification of the gene responsible for the cblB complementation group of vitamin B12-dependent methylmalonic aciduria. Hum Mol Genet 11(26):3361-9.

Dobson CM, Wai T, Leclerc D, Wilson A, Wu X, Dore C, Hudson T, Rosenblatt DS, Gravel RA. 2002b. Identification of the gene responsible for the cblA complementation group of vitamin B12-responsive methylmalonic acidemia based on analysis of prokaryotic gene arrangements. Proc Natl Acad Sci U S A 99(24):15554-9.

Dubois NC, Hofmann D, Kaloulis K, Bishop JM, Trumpp A. 2006. Nestin-Cre transgenic mouse line Nes-Cre1 mediates highly efficient Cre/loxP mediated recombination in the nervous system, kidney, and somite-derived tissues. Genesis 44(8):355-60.

Dundar H, Ozgul RK, Guzel-Ozanturk A, Dursun A, Sivri S, Aliefendioglu D, Coskun T, Tokatli A. 2012. Microarray based mutational analysis of patients with methylmalonic acidemia: identification of 10 novel mutations. Mol Genet Metab 106(4):419-23.

Fan JQ. 2008. A counterintuitive approach to treat enzyme deficiencies: use of enzyme inhibitors for restoring mutant enzyme activity. Biological Chemistry 389(1):1-11.

Fassett RG, Venuthurupalli SK, Gobe GC, Coombes JS, Cooper MA, Hoy WE. 2011. Biomarkers in chronic kidney disease: a review. Kidney Int 80(8):806-21.

Fenton WA, Hack AM, Willard HF, Gertler A, Rosenberg LE. 1982. Purification and properties of methylmalonyl coenzyme A mutase from human liver. Arch Biochem Biophys 214(2):815-23.

Ferreira AC, Da Mesquita S, Sousa JC, Correia-Neves M, Sousa N, Palha JA, Marques F. 2015. From the periphery to the brain: Lipocalin-2, a friend or foe? Prog Neurobiol 131:120-36.

Filippi L, Gozzini E, Cavicchi C, Morrone A, Fiorini P, Donzelli G, Malvagia S, la Marca G. 2009. Insulin-resistant hyperglycaemia complicating neonatal onset of methylmalonic and propionic acidaemias. J Inherit Metab Dis 32 Suppl 1:S179-86.

Forny P, Froese DS, Suormala T, Yue WW, Baumgartner MR. 2014. Functional characterization and categorization of missense mutations that cause methylmalonyl-CoA mutase (MUT) deficiency. Hum Mutat 35(12):1449-58.

Forny P, Schnellmann A-S, Buerer C, Lutz S, Fowler B, Froese DS, Baumgartner MR. 2016. Molecular genetic characterization of 151 mut-type methylmalonic aciduria patients and identification of 41 novel mutations in MUT. Manuscript in preparation.

Fowler B, Leonard JV, Baumgartner MR. 2008. Causes of and diagnostic approach to methylmalonic acidurias. J Inherit Metab Dis 31(3):350-60.

Friedel RH, Wurst W, Wefers B, Kuhn R. 2011. Generating conditional knockout mice. Methods Mol Biol 693:205-31.

Froese DS, Gravel RA. 2010. Genetic disorders of vitamin B metabolism: eight complementation groups--eight genes. Expert Rev Mol Med 12:e37.

Froese DS, Healy S, McDonald M, Kochan G, Oppermann U, Niesen FH, Gravel RA. 2010a. Thermolability of mutant MMACHC protein in the vitamin B12-responsive cblC disorder. Mol Genet Metab 100(1):29-36.

Froese DS, Kochan G, Muniz JR, Wu X, Gileadi C, Ugochukwu E, Krysztofinska E, Gravel RA, Oppermann U, Yue WW. 2010b. Structures of the human GTPase MMAA and vitamin B12-dependent methylmalonyl-CoA mutase and insight into their complex formation. J Biol Chem 285(49):38204-13.

Fuchshuber A, Mucha B, Baumgartner ER, Vollmer M, Hildebrandt F. 2000. mut0 methylmalonic acidemia: eleven novel mutations of the methylmalonyl CoA mutase including a deletion-insertion mutation. Hum Mutat 16(2):179.

Garrod AE. 1902. About Alkaptonuria. Med Chir Trans 85:69-78.

Gekko K, Timasheff SN. 1981. Mechanism of protein stabilization by glycerol: preferential hydration in glycerol-water mixtures. Biochemistry 20(16):4667-76.

Gersting SW, Kemter KF, Staudigl M, Messing DD, Danecka MK, Lagler FB, Sommerhoff CP, Roscher AA, Muntau AC. 2008. Loss of function in phenylketonuria is caused by impaired molecular motions and conformational instability. Am J Hum Genet 83(1):5-17.

Gloyn AL, Braun M, Rorsman P. 2009. Type 2 diabetes susceptibility gene TCF7L2 and its role in beta-cell function. Diabetes 58(4):800-2.

Gomes CM. 2012. Protein misfolding in disease and small molecule therapies. Curr Top Med Chem 12(22):2460-9.

Gravel RA, Mahoney MJ, Ruddle FH, Rosenberg LE. 1975. Genetic complementation in heterokaryons of human fibroblasts defective in cobalamin metabolism. Proc Natl Acad Sci U S A 72(8):3181-5.

Gregersen N. 2006. Protein misfolding disorders: Pathogenesis and intervention. J Inherit Metab Dis 29(2-3):456-470.

Guce AI, Clark NE, Rogich JJ, Garman SC. 2011. The molecular basis of pharmacological chaperoning in human alpha-galactosidase. Chem Biol 18(12):1521-6.

Gunter C, Dhand R. 2002. Human biology by proxy. Nature 420(6915):509-509.

Haberle J, Boddaert N, Burlina A, Chakrapani A, Dixon M, Huemer M, Karall D, Martinelli D, Crespo PS, Santer R and others. 2012. Suggested guidelines for the diagnosis and management of urea cycle disorders. Orphanet J Rare Dis 7:32.

Harmatz P. 2015. Enzyme Replacement Therapies and Immunogenicity in Lysosomal Storage Diseases: Is There a Pattern? Clin Ther 37(9):2130-4.

Harno E, Cottrell EC, White A. 2013. Metabolic pitfalls of CNS cre-based technology. Cell Metab 18(1):21-8.

Hillman RE, Otto EF. 1974. Inhibition of glycine-serine interconversion in cultured human fibroblasts by products of isoleucine catabolism. Pediatr Res 8(12):941-5.

Horowitz NH, Berg P, Singer M, Lederberg J, Susman M, Doebley J, Crow JF. 2004. A centennial: George W. Beadle, 1903-1989. Genetics 166(1):1-10.

Horster F, Baumgartner MR, Viardot C, Suormala T, Burgard P, Fowler B, Hoffmann GF, Garbade SF, Kolker S, Baumgartner ER. 2007. Long-term outcome in methylmalonic acidurias is influenced by the underlying defect (mut0, mut-, cblA, cblB). Pediatr Res 62(2):225-30.

Horster F, Garbade SF, Zwickler T, Aydin HI, Bodamer OA, Burlina AB, Das AM, De Klerk JB, Dionisi-Vici C, Geb S and others. 2009. Prediction of outcome in isolated methylmalonic acidurias: combined use of clinical and biochemical parameters. J Inherit Metab Dis 32(5):630-9.

Hutchesson AC, Bundey S, Preece MA, Hall SK, Green A. 1998. A comparison of disease and gene frequencies of inborn errors of metabolism among different ethnic groups in the West Midlands, UK. J Med Genet 35(5):366-70.

Janata J, Kogekar N, Fenton WA. 1997. Expression and kinetic characterization of methylmalonyl-CoA mutase from patients with the mut- phenotype: evidence for naturally occurring interallelic complementation. Human Molecular Genetics 6(9):1457-1464.

Janeckova H, Hron K, Wojtowicz P, Hlidkova E, Baresova A, Friedecky D, Zidkova L, Hornik P, Behulova D, Prochazkova D and others. 2012. Targeted metabolomic analysis of plasma samples for the diagnosis of inherited metabolic disorders. J Chromatogr A 1226:11-7.

Jansen R, Ledley FD. 1990. Heterozygous mutations at the mut locus in fibroblasts with mut0 methylmalonic acidemia identified by polymerase-chain-reaction cDNA cloning. Am J Hum Genet 47(5):808-14.

Jorge-Finnigan A, Brasil S, Underhaug J, Ruíz-Sala P, Merinero B, Banerjee R, Desviat LR, Ugarte M, Martinez A, Pérez B. 2013. Pharmacological chaperones as a potential therapeutic option in methylmalonic aciduria cblB type. Hum Mol Genet.

Jung JW, Hwang IT, Park JE, Lee EH, Ryu KH, Kim SH, Hwang JS. 2005. Mutation analysis of the MCM gene in Korean patients with MMA. Mol Genet Metab 84(4):367-70.

Jusufi J, Suormala T, Burda P, Fowler B, Froese DS, Baumgartner MR. 2014. Characterization of functional domains of the cblD (MMADHC) gene product. J Inherit Metab Dis.

Kaplan P, Ficicioglu C, Mazur AT, Palmieri MJ, Berry GT. 2006. Liver transplantation is not curative for methylmalonic acidopathy caused by methylmalonyl-CoA mutase deficiency. Mol Genet Metab 88(4):322-6.

Kolker S, Cazorla AG, Valayannopoulos V, Lund AM, Burlina AB, Sykut-Cegielska J, Wijburg FA, Teles EL, Zeman J, Dionisi-Vici C and others. 2015. The phenotypic spectrum of organic acidurias and urea cycle disorders. Part 1: the initial presentation. J Inherit Metab Dis 38(6):1041-57.

Kolker S, Okun JG. 2005. Methylmalonic acid--an endogenous toxin? Cell Mol Life Sci 62(6):621-4.

Kolker S, Sauer SW, Hoffmann GF, Muller I, Morath MA, Okun JG. 2008. Pathogenesis of CNS involvement in disorders of amino and organic acid metabolism. J Inherit Metab Dis.

Kolker S, Sauer SW, Surtees RA, Leonard JV. 2006. The aetiology of neurological complications of organic acidaemias--a role for the blood-brain barrier. J Inherit Metab Dis 29(6):701-4; discussion 705-6.

Krissinel E, Henrick K. 2007. Inference of macromolecular assemblies from crystalline state. J Mol Biol 372(3):774-97.

Kumar P, Henikoff S, Ng PC. 2009. Predicting the effects of coding non-synonymous variants on protein function using the SIFT algorithm. Nat Protoc 4(7):1073-81.

Leandro J, Leandro P, Flatmark T. 2011a. Heterotetrameric forms of human phenylalanine hydroxylase: co-expression of wild-type and mutant forms in a bicistronic system. Biochim Biophys Acta 1812(5):602-12.

Leandro J, Simonsen N, Saraste J, Leandro P, Flatmark T. 2011b. Phenylketonuria as a protein misfolding disease: The mutation pG46S in phenylalanine hydroxylase promotes self-association and fibril formation. Biochim Biophys Acta 1812(1):106-20.

Ledley FD, Lumetta M, Nguyen PN, Kolhouse JF, Allen RH. 1988a. Molecular cloning of L-methylmalonyl-CoA mutase: gene transfer and analysis of mut cell lines. Proc Natl Acad Sci U S A 85(10):3518-21.

Ledley FD, Lumetta MR, Zoghbi HY, VanTuinen P, Ledbetter SA, Ledbetter DH. 1988b. Mapping of human methylmalonyl CoA mutase (MUT) locus on chromosome 6. Am J Hum Genet 42(6):839-46.

Ledley FD, Rosenblatt DS. 1997. Mutations in mut methylmalonic acidemia: clinical and enzymatic correlations. Hum Mutat 9(1):1-6.

Leinekugel P, Michel S, Conzelmann E, Sandhoff K. 1992. Quantitative correlation between the residual activity of beta-hexosaminidase A and arylsulfatase A and the severity of the resulting lysosomal storage disease. Hum Genet 88(5):513-23.

Lempp TJ, Suormala T, Siegenthaler R, Baumgartner ER, Fowler B, Steinmann B, Baumgartner MR. 2007. Mutation and biochemical analysis of 19 probands with mut0 and 13 with mut- methylmalonic aciduria: identification of seven novel mutations. Mol Genet Metab 90(3):284-90.

Leonard JV. 1995. The management and outcome of propionic and methylmalonic acidaemia. J Inherit Metab Dis 18(4):430-4.

Leonard JV, Walter JH, McKiernan PJ. 2001. The management of organic acidaemias: The role of transplantation. J Inherit Metab Dis 24(2):309-311.

Lerner-Ellis JP, Tirone JC, Pawelek PD, Dore C, Atkinson JL, Watkins D, Morel CF, Fujiwara TM, Moras E, Hosack AR and others. 2006. Identification of the gene responsible for methylmalonic aciduria and homocystinuria, cblC type. Nat Genet 38(1):93-100.

Lieberman RL, Wustman BA, Huertas P, Powe AC, Jr., Pine CW, Khanna R, Schlossmacher MG, Ringe D, Petsko GA. 2007. Structure of acid beta-glucosidase with pharmacological chaperone provides insight into Gaucher disease. Nat Chem Biol 3(2):101-7.

Litzkas P, Jha KK, Ozer HL. 1984. Efficient transfer of cloned DNA into human diploid cells: protoplast fusion in suspension. Mol Cell Biol 4(11):2549-52.

Liu MY, Liu TT, Yang YL, Chang YC, Fan YL, Lee SF, Teng YT, Chiang SH, Niu DM, Lin SJ and others. 2012. Mutation Profile of the MUT Gene in Chinese Methylmalonic Aciduria Patients. JIMD Rep 6:55-64.

Loferer MJ, Webb BM, Grant GH, Liedl KR. 2003. Energetic and stereochemical effects of the protein environment on substrate: a theoretical study of methylmalonyl-CoA mutase. J Am Chem Soc 125(4):1072-8.

Lubrano R, Elli M, Rossi M, Travasso E, Raggi C, Barsotti P, Carducci C, Berloco P. 2007. Renal transplant in methylmalonic acidemia: could it be the best option? Report on a case at 10 years and review of the literature. Pediatr Nephrol 22(8):1209-14.

Lubrano R, Scoppi P, Barsotti P, Travasso E, Scateni S, Cristaldi S, Castello MA. 2001. Kidney transplantation in a girl with methylmalonic acidemia and end stage renal failure. Pediatr Nephrol 16(11):848-51.

Machaczka M, Hast R, Dahlman I, Lerner R, Klimkowska M, Engvall M, Hagglund H. 2012. Substrate reduction therapy with miglustat for type 1 Gaucher disease: a retrospective analysis from a single institution. Ups J Med Sci 117(1):28-34.

Maegawa GH, Tropak M, Buttner J, Stockley T, Kok F, Clarke JT, Mahuran DJ. 2007. Pyrimethamine as a potential pharmacological chaperone for late-onset forms of GM2 gangliosidosis. J Biol Chem 282(12):9150-61.

Majtan T, Liu L, Carpenter JF, Kraus JP. 2010. Rescue of cystathionine beta-synthase (CBS) mutants with chemical chaperones: purification and characterization of eight CBS mutant enzymes. J Biol Chem 285(21):15866-73.

Malvagia S, Haynes CA, Grisotto L, Ombrone D, Funghini S, Moretti E, McGreevy KS, Biggeri A, Guerrini R, Yahyaoui R and others. 2015. Heptadecanoylcarnitine (C17) a novel candidate biomarker for newborn screening of propionic and methylmalonic acidemias. Clin Chim Acta 450:342-8.

Malyszko J, Bachorzewska-Gajewska H, Sitniewska E, Malyszko JS, Poniatowski B, Dobrzycki S. 2008. Serum neutrophil gelatinase-associated lipocalin as a marker of renal function in non-diabetic patients with stage 2-4 chronic kidney disease. Ren Fail 30(6):625-8.

Mancia F, Keep NH, Nakagawa A, Leadlay PF, McSweeney S, Rasmussen B, Bosecke P, Diat O, Evans PR. 1996. How coenzyme B12 radicals are generated: the crystal structure of methylmalonyl-coenzyme A mutase at 2 A resolution. Structure 4(3):339-50.

Manoli I, Sysol JR, Li L, Houillier P, Garone C, Wang C, Zerfas PM, Cusmano-Ozog K, Young S, Trivedi NS and others. 2013. Targeting proximal tubule mitochondrial dysfunction attenuates the renal disease of methylmalonic acidemia. Proc Natl Acad Sci U S A.

Marques F, Mesquita SD, Sousa JC, Coppola G, Gao F, Geschwind DH, Columba-Cabezas S, Aloisi F, Degn M, Cerqueira JJ and others. 2012. Lipocalin 2 is present in the EAE brain and is modulated by natalizumab. Front Cell Neurosci 6:33.

Martinez MA, Rincon A, Desviat LR, Merinero B, Ugarte M, Perez B. 2005. Genetic analysis of three genes causing isolated methylmalonic acidemia: identification of 21 novel allelic variants. Mol Genet Metab 84(4):317-25.

Matsui S, Mahoney M, Rosenberg L. 1983a. The natural history of the inherited methylmalonic acidemias. N Engl J Med 308(83e33799-d1c2-9794-33b1-ec4532987e5b):857-918.

Matsui SM, Mahoney MJ, Rosenberg LE. 1983b. The natural history of the inherited methylmalonic acidemias. N Engl J Med 308(15):857-61.

Mayer AN, Dimmock DP, Arca MJ, Bick DP, Verbsky JW, Worthey EA, Jacob HJ, Margolis DA. 2011. A timely arrival for genomic medicine. Genet Med 13(3):195-6.

McCampbell A, Wessner K, Marlatt MW, Wolffe C, Toolan D, Podtelezhnikov A, Yeh S, Zhang R, Szczerba P, Tanis KQ and others. 2011. Induction of Alzheimer's-like changes in brain of mice expressing mutant APP fed excess methionine. J Neurochem 116(1):82-92.

Merinero B, Perez B, Perez-Cerda C, Rincon A, Desviat LR, Martinez MA, Sala PR, Garcia MJ, Aldamiz-Echevarria L, Campos J and others. 2008. Methylmalonic acidaemia: examination of genotype and biochemical data in 32 patients belonging to mut, cblA or cblB complementation group. J Inherit Metab Dis 31(1):55-66.

Miller MJ, Kennedy AD, Eckhart AD, Burrage LC, Wulff JE, Miller LA, Milburn MV, Ryals JA, Beaudet AL, Sun Q and others. 2015. Untargeted metabolomic analysis for the clinical screening of inborn errors of metabolism. J Inherit Metab Dis 38(6):1029-39.

Mitchell JJ, Trakadis YJ, Scriver CR. 2011. Phenylalanine hydroxylase deficiency. Genet Med 13(8):697-707.

Montagutelli X. 2000. Effect of the genetic background on the phenotype of mouse mutations. J Am Soc Nephrol 11 Suppl 16:S101-5.

Morath MA, Okun JG, Muller IB, Sauer SW, Horster F, Hoffmann GF, Kolker S. 2008. Neurodegeneration and chronic renal failure in methylmalonic aciduria--a pathophysiological approach. J Inherit Metab Dis 31(1):35-43.

Morrow G, 3rd, Revsin B, Clark R, Lebowitz J, Whelan DT. 1978. A new variant of methylmalonic acidemia-defective coenzyme-apoenzyme binding in cultured fibroblasts. Clin Chim Acta 85(1):67-72.

Morrow G, Mahoney MJ, Mathews C, Lebowitz J. 1975. Studies of Methylmalonyl Coenzyme-a Carbonylmutase Activity in Methylmalonic Acidemia .1. Correlation of Clinical Hepatic, and Fibroblast Data. Pediatr Res 9(8):641-644.

Muntau AC, Gersting SW. 2010. Phenylketonuria as a model for protein misfolding diseases and for the development of next generation orphan drugs for patients with inborn errors of metabolism. J Inherit Metab Dis 33(6):649-658.

Muntau AC, Leandro J, Staudigl M, Mayer F, Gersting SW. 2014. Innovative strategies to treat protein misfolding in inborn errors of metabolism: pharmacological chaperones and proteostasis regulators. J Inherit Metab Dis 37(4):505-23.

Mussap M, Antonucci R, Noto A, Fanos V. 2013. The role of metabolomics in neonatal and pediatric laboratory medicine. Clin Chim Acta 426:127-38.

Nascimento C, Leandro J, Tavares de Almeida I, Leandro P. 2008. Modulation of the activity of newly synthesized human phenylalanine hydroxylase mutant proteins by low-molecular-weight compounds. Protein J 27(6):392-400.

Naude PJ, Nyakas C, Eiden LE, Ait-Ali D, van der Heide R, Engelborghs S, Luiten PG, De Deyn PP, den Boer JA, Eisel UL. 2012. Lipocalin 2: novel component of proinflammatory signaling in Alzheimer's disease. FASEB J 26(7):2811-23.

Newman CG, Wilson BD, Callaghan P, Young L. 1967. Neonatal death associated with isovalericacidaemia. Lancet 2(7513):439-42.

Nicolaides P, Leonard J, Surtees R. 1998. Neurological outcome of methylmalonic acidaemia. Arch Dis Child 78(6):508-12.

Niesen FH, Berglund H, Vedadi M. 2007. The use of differential scanning fluorimetry to detect ligand interactions that promote protein stability. Nat Protoc 2(9):2212-21.

Nyhan WL, Gargus JJ, Boyle K, Selby R, Koch R. 2002. Progressive neurologic disability in methylmalonic acidemia despite transplantation of the liver. Eur J Pediatr 161(7):377-9.

Oberholzer VG, Levin B, Burgess EA, Young WF. 1967. Methylmalonic aciduria. An inborn error of metabolism leading to chronic metabolic acidosis. Arch Dis Child 42(225):492-504.

Ohashi T. 2012. Enzyme replacement therapy for lysosomal storage diseases. Pediatr Endocrinol Rev 10 Suppl 1:26-34.

Ostergaard E, Wibrand F, Orngreen MC, Vissing J, Horn N. 2005. Impaired energy metabolism and abnormal muscle histology in mut- methylmalonic aciduria. Neurology 65(6):931-3.

Parenti G, Andria G, Valenzano KJ. 2015. Pharmacological Chaperone Therapy: Preclinical Development, Clinical Translation, and Prospects for the Treatment of Lysosomal Storage Disorders. Mol Ther 23(7):1138-48.

Parenti G, Moracci M, Fecarotta S, Andria G. 2014. Pharmacological chaperone therapy for lysosomal storage diseases. Future Med Chem 6(9):1031-45.

Parenti G, Pignata C, Vajro P, Salerno M. 2013. New strategies for the treatment of lysosomal storage diseases (review). Int J Mol Med 31(1):11-20.

Pekkala S, Martinez AI, Barcelona B, Yefimenko I, Finckh U, Rubio V, Cervera J. 2010. Understanding carbamoyl-phosphate synthetase I (CPS1) deficiency by using expression studies and structure-based analysis. Hum Mutat 31(7):801-8.

Pennisi E. 2012. Genomics. ENCODE project writes eulogy for junk DNA. Science 337(6099):1159, 1161.

Perez B, Desviat LR, Rodriguez-Pombo P, Clavero S, Navarrete R, Perez-Cerda C, Ugarte M. 2003. Propionic acidemia: identification of twenty-four novel mutations in Europe and North America. Mol Genet Metab 78(1):59-67.

Perry TL, Urquhart N, Hansen S. 1977. Studies of the glycine cleavage enzyme system in brain from infants with glycine encephalopathy. Pediatr Res 11(12):1192-7.

Peters H, Nefedov M, Sarsero J, Pitt J, Fowler KJ, Gazeas S, Kahler SG, Ioannou PA. 2003. A knock-out mouse model for methylmalonic aciduria resulting in neonatal lethality. J Biol Chem 278(52):52909-13.

Peters HL, Nefedov M, Lee LW, Abdenur JE, Chamoles NA, Kahler SG, Ioannou PA. 2002. Molecular studies in mutase-deficient (MUT) methylmalonic aciduria: identification of five novel mutations. Hum Mutat 20(5):406.

Pey AL, Perez B, Desviat LR, Martinez MA, Aguado C, Erlandsen H, Gamez A, Stevens RC, Thorolfsson M, Ugarte M and others. 2004. Mechanisms underlying responsiveness to tetrahydrobiopterin in mild phenylketonuria mutations. Hum Mutat 24(5):388-99.

Pey AL, Stricher F, Serrano L, Martinez A. 2007. Predicted effects of missense mutations on native-state stability account for phenotypic outcome in phenylketonuria, a paradigm of misfolding diseases. Am J Hum Genet 81(5):1006-24.

Pey AL, Ying M, Cremades N, Velazquez-Campoy A, Scherer T, Thony B, Sancho J, Martinez A. 2008. Identification of pharmacological chaperones as potential therapeutic agents to treat phenylketonuria. J Clin Invest 118(8):2858-67.

Raff ML, Crane AM, Jansen R, Ledley FD, Rosenblatt DS. 1991. Genetic characterization of a MUT locus mutation discriminating heterogeneity in mut0 and mut- methylmalonic aciduria by interallelic complementation. J Clin Invest 87(1):203-7.

Ravn K, Chloupkova M, Christensen E, Brandt NJ, Simonsen H, Kraus JP, Nielsen IM, Skovby F, Schwartz M. 2000. High incidence of propionic acidemia in greenland is due to a prevalent mutation, 1540insCCC, in the gene for the beta-subunit of propionyl CoA carboxylase. Am J Hum Genet 67(1):203-6.

Redon R, Ishikawa S, Fitch KR, Feuk L, Perry GH, Andrews TD, Fiegler H, Shapero MH, Carson AR, Chen W and others. 2006. Global variation in copy number in the human genome. Nature 444(7118):444-54.

Robert X, Gouet P. 2014. Deciphering key features in protein structures with the new ENDscript server. Nucleic Acids Res 42(Web Server issue):W320-4.

Rosenberg LE, Lilljeqvist A, Hsia YE. 1968. Methylmalonic aciduria: metabolic block localization and vitamin B 12 dependency. Science 162(3855):805-7.

Ross LF, Saal HM, David KL, Anderson RR, American Academy of P, American College of Medical G, Genomics. 2013. Technical report: Ethical and policy issues in genetic testing and screening of children. Genet Med 15(3):234-45.

Rutsch F, Gailus S, Miousse IR, Suormala T, Sagne C, Toliat MR, Nurnberg G, Wittkampf T, Buers I, Sharifi A and others. 2009. Identification of a putative lysosomal cobalamin exporter altered in the cblF defect of vitamin B12 metabolism. Nat Genet 41(2):234-9.

Santos-Sierra S, Kirchmair J, Perna AM, Reiss D, Kemter K, Roschinger W, Glossmann H, Gersting SW, Muntau AC, Wolber G and others. 2012. Novel pharmacological chaperones that correct phenylketonuria in mice. Hum Mol Genet 21(8):1877-87.

Saudubray JM, Van den Berghe G, Walter J. 2012. Inborn metabolic diseases : diagnosis and treatment. Berlin: Springer.

Sauer SW, Okun JG, Fricker G, Mahringer A, Muller I, Crnic LR, Muhlhausen C, Hoffmann GF, Horster F, Goodman SI and others. 2006. Intracerebral accumulation of glutaric and 3-hydroxyglutaric acids secondary to limited flux across the blood-brain barrier constitute a biochemical risk factor for neurodegeneration in glutaryl-CoA dehydrogenase deficiency. J Neurochem 97(3):899-910.

Scheja L, Toedter K, Mohr R, Niederfellner G, Michael MD, Meissner A, Schoettler A, Pospisil H, Beisiegel U, Heeren J. 2008. Liver TAG transiently decreases while PL n-3 and n-6 fatty acids are persistently elevated in insulin resistant mice. Lipids 43(11):1039-51.

Schwartz GJ, Munoz A, Schneider MF, Mak RH, Kaskel F, Warady BA, Furth SL. 2009. New equations to estimate GFR in children with CKD. J Am Soc Nephrol 20(3):629-37.

Shchelochkov OA, Li FY, Geraghty MT, Gallagher RC, Van Hove JL, Lichter-Konecki U, Fernhoff PM, Copeland S, Reimschisel T, Cederbaum S and others. 2009. High-frequency detection of deletions and variable rearrangements at the ornithine transcarbamylase (OTC) locus by oligonucleotide array CGH. Mol Genet Metab 96(3):97-105.

Shi Z, Sellers J, Moult J. 2012. Protein stability and in vivo concentration of missense mutations in phenylalanine hydroxylase. Proteins 80(1):61-70.

Shigematsu Y, Hirano S, Hata I, Tanaka Y, Sudo M, Sakura N, Tajima T, Yamaguchi S. 2002. Newborn mass screening and selective screening using electrospray tandem mass spectrometry in Japan. Journal of Chromatography B 776(1):39-48.

Sloan JL, Manoli I, Venditti CP. 2015. Liver or combined liver-kidney transplantation for patients with isolated methylmalonic acidemia: who and when? J Pediatr 166(6):1346-50.

Sniderman LC, Lambert M, Giguere R, Auray-Blais C, Lemieux B, Laframboise R, Rosenblatt DS, Treacy EP. 1999. Outcome of individuals with low-moderate methylmalonic aciduria detected through a neonatal screening program. Journal of Pediatrics 134(6):675-680.

Spada M, Calvo PL, Brunati A, Peruzzi L, Dell'Olio D, Romagnoli R, Porta F. 2015. Liver transplantation in severe methylmalonic acidemia: The sooner, the better. J Pediatr 167(5):1173.

Stevens RC, Sancho J, Martinez A. 2010. Rescue of misfolded proteins and stabilization by small molecules. Methods Mol Biol 648:313-24.

Stucki M, Coelho D, Suormala T, Burda P, Fowler B, Baumgartner M. 2012. Molecular mechanisms leading to three different phenotypes in the cblD defect of intracellular cobalamin metabolism. Hum Mol Genet 21(59943daa-a8c7-0cb2-20cc-0e19c576b461):1410-1418.

Suormala T, Baumgartner MR, Coelho D, Zavadakova P, Kozich V, Koch HG, Berghauser M, Wraith JE, Burlina A, Sewell A and others. 2004. The cblD defect causes either isolated or combined deficiency of methylcobalamin and adenosylcobalamin synthesis. J Biol Chem 279(41):42742-9.

Suzuki Y. 2013. Chaperone therapy update: Fabry disease, GM1-gangliosidosis and Gaucher disease. Brain Dev 35(6):515-23.

Tanaka K, Budd MA, Efron ML, Isselbacher KJ. 1966. Isovaleric acidemia: a new genetic defect of leucine metabolism. Proc Natl Acad Sci U S A 56(1):236-42.

Theobald DL. 2010. A formal test of the theory of universal common ancestry. Nature 465(7295):219-22.

Thomas PM, Cote GJ, Wohllk N, Haddad B, Mathew PM, Rabl W, Aguilar-Bryan L, Gagel RF, Bryan J. 1995. Mutations in the sulfonylurea receptor gene in familial persistent hyperinsulinemic hypoglycemia of infancy. Science 268(5209):426-9.

Thompson GN, Chalmers RA. 1990. Increased urinary metabolite excretion during fasting in disorders of propionate metabolism. Pediatr Res 27(4 Pt 1):413-6.

Thony B, Calvo AC, Scherer T, Svebak RM, Haavik J, Blau N, Martinez A. 2008. Tetrahydrobiopterin shows chaperone activity for tyrosine hydroxylase. J Neurochem 106(2):672-81.

Torreblanca R, Lira-Navarrete E, Sancho J, Hurtado-Guerrero R. 2012. Structural and mechanistic basis of the interaction between a pharmacological chaperone and human phenylalanine hydroxylase. Chembiochem 13(9):1266-9.

Traber G, Baumgartner MR, Schwarz U, Pangalu A, Donath MY, Landau K. 2011. Subacute bilateral visual loss in methylmalonic acidemia. J Neuroophthalmol 31(4):344-6.

Troen AM, Lutgens E, Smith DE, Rosenberg IH, Selhub J. 2003. The atherogenic effect of excess methionine intake. Proc Natl Acad Sci U S A 100(25):15089-94.

Tronche F, Kellendonk C, Kretz O, Gass P, Anlag K, Orban PC, Bock R, Klein R, Schutz G. 1999. Disruption of the glucocorticoid receptor gene in the nervous system results in reduced anxiety. Nat Genet 23(1):99-103.

Turgeon CT, Magera MJ, Cuthbert CD, Loken PR, Gavrilov DK, Tortorelli S, Raymond KM, Oglesbee D, Rinaldo P, Matern D. 2010. Determination of total homocysteine, methylmalonic acid, and 2-methylcitric acid in dried blood spots by tandem mass spectrometry. Clin Chem 56(11):1686-95.

Valdar WS. 2002. Scoring residue conservation. Proteins 48(2):227-41.

Van Calcar SC, Harding CO, Lyne P, Hogan K, Banerjee R, Sollinger H, Rieselbach RE, Wolff JA. 1998. Renal transplantation in a patient with methylmalonic acidaemia. J Inherit Metab Dis 21(7):729-37.

Vedadi M, Niesen FH, Allali-Hassani A, Fedorov OY, Finerty PJ, Wasney GA, Yeung R, Arrowsmith C, Ball LJ, Berglund H and others. 2006. Chemical screening methods to identify ligands that promote protein stability, protein crystallization, and structure determination. Proc Natl Acad Sci U S A 103(43):15835-15840.

Vernon HJ, Sperati CJ, King JD, Poretti A, Miller NR, Sloan JL, Cameron AM, Myers D, Venditti CP, Valle D. 2014. A detailed analysis of methylmalonic acid kinetics during hemodialysis and after combined liver/kidney transplantation in a patient with mut (0) methylmalonic acidemia. J Inherit Metab Dis 37(6):899-907.

Welch WJ, Brown CR. 1996. Influence of molecular and chemical chaperones on protein folding. Cell Stress Chaperones 1(2):109-15.

Wendel U, Baumgartner R, van der Meer SB, Spaapen LJ. 1991. Accumulation of odd-numbered long-chain fatty acids in fetuses and neonates with inherited disorders of propionate metabolism. Pediatr Res 29(4 Pt 1):403-5.

Wikoff WR, Gangoiti JA, Barshop BA, Siuzdak G. 2007. Metabolomics identifies perturbations in human disorders of propionate metabolism. Clin Chem 53(12):2169-76.

Wilcken B, Kilham HA, Faull K. 1977. Methylmalonic aciduria: a variant form of methylmalonyl coenzyme A apomutase deficiency. J Pediatr 91(3):428-30.

Wildman DE, Uddin M, Liu G, Grossman LI, Goodman M. 2003. Implications of natural selection in shaping 99.4% nonsynonymous DNA identity between humans and chimpanzees: enlarging genus Homo. Proc Natl Acad Sci U S A 100(12):7181-8.

Wilkemeyer MF, Crane AM, Ledley FD. 1991. Differential diagnosis of mut and cbl methylmalonic aciduria by DNA-mediated gene transfer in primary fibroblasts. J Clin Invest 87(3):915-8.

Willard HF, Ambani LM, Hart AC, Mahoney MJ, Rosenberg LE. 1976. Rapid prenatal and postnatal detection of inborn errors of propionate, methylmalonate, and cobalamin metabolism: a sensitive assay using cultured cells. Hum Genet 34(3):277-83.

Willard HF, Mellman IS, Rosenberg LE. 1978a. Genetic Complementation among Inherited Deficiencies of Methylmalonyl-Coa Mutase Activity - Evidence for a New Class of Human Cobalamin Mutant. American Journal of Human Genetics 30(1):1-13.

Willard HF, Mellman IS, Rosenberg LE. 1978b. Genetic Complementation among Inherited Deficiencies of Methylmalonyl-Coa Mutase Activity - Evidence for a New Class of Human Cobalamin Mutant. Am J Hum Genet 30(1):1-13.

Willard HF, Rosenberg LE. 1977. Inherited deficiencies of human methylamlonyl CoA mutase activity: Reduced affinity of mutant apoenzyme for adenosylcobalamin. Biochem Biophys Res Commun 78(3):927-934.

Willard HF, Rosenberg LE. 1980. Inherited methylmalonyl CoA mutase apoenzyme deficiency in human fibroblasts: evidence for allelic heterogeneity, genetic compounds, and codominant expression. J Clin Invest 65(3):690-8.

Williams ZR, Hurley PE, Altiparmak UE, Feldon SE, Arnold GL, Eggenberger E, Mejico LJ. 2009. Late onset optic neuropathy in methylmalonic and propionic acidemia. Am J Ophthalmol 147(5):929-33.

Wilson JM, Jungner YG. 1968. Principles and practice of mass screening for disease. Bol Oficina Sanit Panam 65(4):281-393.

Worgan LC, Niles K, Tirone JC, Hofmann A, Verner A, Sammak A, Kucic T, Lepage P, Rosenblatt DS. 2006. Spectrum of mutations in mut methylmalonic acidemia and identification of a common Hispanic mutation and haplotype. Hum Mutat 27(1):31-43.

Yang X, Sakamoto O, Matsubara Y, Kure S, Suzuki Y, Aoki Y, Yamaguchi S, Takahashi Y, Nishikubo T, Kawaguchi C and others. 2004. Mutation spectrum of the PCCA and PCCB genes in Japanese patients with propionic acidemia. Mol Genet Metab 81(4):335-42.

Yi Q, Lv J, Tian F, Wei H, Ning Q, Luo X. 2011. Clinical characteristics and gene mutation analysis of methylmalonic aciduria. J Huazhong Univ Sci Technolog Med Sci 31(3):384-9.

Yue WW, Froese DS, Brennan PE. 2014. The role of protein structural analysis in the next generation sequencing era. Top Curr Chem 336:67-98.

Ziesch B, Weigel J, Thiele A, Mutze U, Rohde C, Ceglarek U, Thiery J, Kiess W, Beblo S. 2012. Tetrahydrobiopterin (BH4) in PKU: effect on dietary treatment, metabolic control, and quality of life. J Inherit Metab Dis 35(6):983-92.

Zsengeller ZK, Aljinovic N, Teot LA, Korson M, Rodig N, Sloan JL, Venditti CP, Berry GT, Rosen S. 2014. Methylmalonic acidemia: a megamitochondrial disorder affecting the kidney. Pediatr Nephrol 29(11):2139-46.

Zurfluh MR, Zschocke J, Lindner M, Feillet F, Chery C, Burlina A, Stevens RC, Thony B, Blau N. 2008. Molecular genetics of tetrahydrobiopterin-responsive phenylalanine hydroxylase deficiency. Hum Mutat 29(1):167-75.